Population Synthesis of Compact Object Binaries

Xing, Zepei

UNIVERSITÉ DE GENÈVE FACULTÉ DES SCIENCES

Département d'Astronomie Professeur Anastasios Fragkos

Population Synthesis of Compact Object Binaries

THÈSE

Présentée à la Faculté des sciences de l'Université de Genève,

Pour obtenir le grade de Docteur ès sciences,

mention astronomie et astrophysique

Par

Zepei Xing

de Xi'an (China)

Thèse N°5906

GENÈVE

Observatoire Astronomique de l'Université de Genève

2025

ABSTRACT

Compact objects, such as Neutron stars (NSs) and black holes (BHs), are the remnants of massive stars and play a central role in some of the most energetic phenomena in the Universe. Through accretion and merger processes, they power X-ray binaries and gravitational-wave (GW) sources, respectively. These systems are key to probing the physics of extreme gravity, dense matter, and relativistic astrophysics. The ever-growing samples from GW observations provide an unprecedented opportunity to advance our understanding of stellar and binary evolution through population studies in the era of multi-messenger astronomy.

This thesis presents binary population synthesis (BPS) studies of compact-object binaries containing BHs and NSs, focusing on wind-fed BH high-mass X-ray binaries and merging NS–BH (NSBH) systems. Through these studies, we investigate several open questions, including the origin of BH spins, distinguishable channel-wise characteristics of merging NSBHs, and the existence of lower mass-gap BHs.

These populations are investigated using the next-generation BPS code `POSYDON`, which combines detailed binary evolution models, computed using the stellar evolution code `MESA`, with a self-consistent population framework. It includes full stellar structure, rotation, and realistic modeling of mass transfer, enabling more physically accurate simulations of binary interactions and compact object formation.

The results of this thesis highlight that accurately modeling key physical processes, using physically motivated approaches is essential for interpreting current and future multi-messenger observations, and for deepening our understanding of stellar and binary evolution. As gravitational-wave and electromagnetic observations continue to grow, their integration with advanced BPS studies will be crucial for probing the underlying physics of compact object binaries. This thesis establishes a foundation for more reliable and unified population modeling in the era of multi-messenger astronomy.

RÉSUMÉ

Les objets compacts, tels que les étoiles à neutrons (NS) et les trous noirs (BH), sont les vestiges d'étoiles massives et jouent un rôle central dans certains des phénomènes les plus énergétiques de l'Univers. Par les processus d'accrétion et de fusion, ils alimentent respectivement les binaires X et les sources d'ondes gravitationnelles (GW). Ces systèmes constituent des laboratoires clés pour explorer la physique de la gravité forte, de la matière dense et de l'astrophysique relativiste. L'augmentation rapide du nombre de détections d'ondes gravitationnelles offre une opportunité sans précédent de faire progresser notre compréhension de l'évolution stellaire et binaire à travers des études de population dans l'ère de l'astronomie multi-messager.

Cette thèse présente des études de synthèse de population binaire (BPS) portant sur des systèmes binaires à objets compacts contenant des BH et des NS, en se concentrant sur les binaires X à haute masse alimentées par vent avec des BH et sur les systèmes en coalescence NS–BH (NSBH). À travers ces études, nous abordons plusieurs questions ouvertes, notamment l'origine du spin des BH, les caractéristiques distinctes selon les canaux de formation des NSBH en fusion, ainsi que l'existence de BH dans la lacune de masse basse.

Ces populations sont étudiées à l'aide du code de BPS de nouvelle génération `POSYDON`, qui combine des modèles détaillés d'évolution binaire, calculés avec le code d'évolution stellaire `MESA`, à un cadre de population cohérent. Il intègre la structure stellaire complète, la rotation, et un traitement réaliste du transfert de masse, permettant des simulations plus fidèles des interactions binaires et de la formation des objets compacts.

Les résultats de cette thèse montrent que la modélisation précise des processus physiques clés à l'aide d'approches fondées sur des principes physiques est essentielle pour interpréter les observations multi-messager actuelles et futures, et pour approfondir notre compréhension de l'évolution stellaire et binaire. À mesure que les observations gravitationnelles et électromagnétiques se multiplient, leur intégration avec des études BPS avancées sera cruciale pour sonder la physique sous-jacente des systèmes binaires à objets compacts. Cette thèse pose ainsi les bases d'une modélisation de population plus fiable et unifiée dans l'ère de l'astronomie multi-messager.

CONTENTS

LIST OF ILLUSTRATIONS

LIST OF TABLES

Chapter 1

INTRODUCTION

Neutron stars (NSs) and black holes (BHs) are among the most fascinating and mysterious objects in our Universe, driving some of the most extreme cosmic phenomena. These compact objects are the remnants of massive stars, with their origins often linked to supernova (SN) explosions or gamma-ray bursts.[1] Through accretion from other stellar objects, NSs and BHs form X-ray binaries that appear as the brightest X-ray sources in the sky. The mergers of double compact objects, such as binary BHs (BBHs), double NSs (DNSs), and NS–BH binaries (NSBHs), lead to the most powerful energetic bursts in the Universe, producing gravitational waves (GW) that can be captured by the ground-based GW detectors, including LIGO (LIGO Scientific Collaboration et al., 2015), Virgo (Acernese et al., 2015), and Kagra (Aso et al., 2013) (LVK network). DNS mergers, and potentially some NSBH mergers, give rise to electromagnetic counterparts (EMCs), such as kilonovae and short gamma-ray bursts.

The study of compact objects is intrinsically intertwined with various aspects of fundamental physics. The extreme environments around compact objects serve as excellent laboratories for probing general relativity in the strong-field regime. The nature of NSs, particularly the equation of state (EoS), holds the key to understanding high-density nuclear physics and quantum mechanics. Moreover, the presence of intense magnetic fields and the occurrence of extreme accretion processes around them provide critical insights into particle physics and radiation mechanisms.

The investigation of these compact objects is closely tied to binary stars. Not only are these energetic phenomena strongly related to binary interactions, but massive stars, the origin of compact objects, often form in pairs. Sana et al. (2012) investigated the multiplicity properties of the type O star population in nearby open stellar clusters, finding about 70% of these massive stars have companions. Offner et al. (2023) computed bias-corrected multiplicity fraction based on various surveys on the multiplicity of brown dwarfs and main-sequence (MS) stars. The results, shown in the right panel of Figure 1.1, indicate that binary fractions are particularly high for massive stars.

In the introduction, I first introduce BHs and NSs from an observational perspective, covering

[1] In this context, the focus is on stellar-mass BHs, excluding supermassive BHs whose formation and evolution follow distinct pathways.

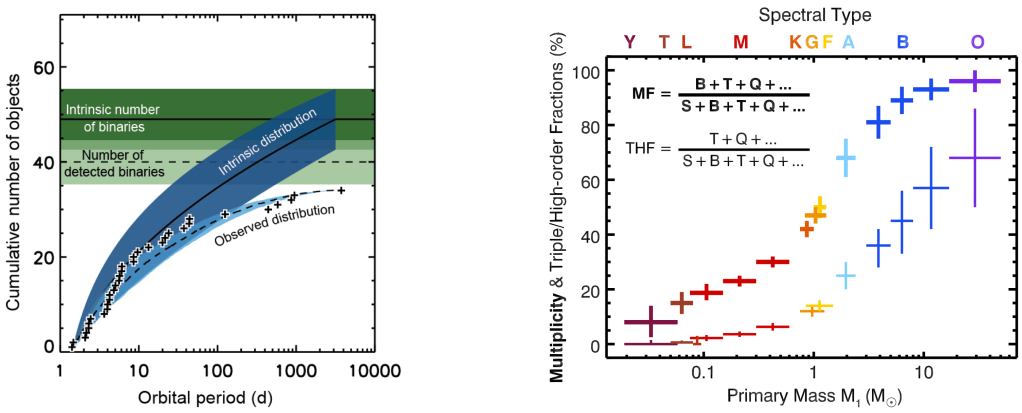

Figure 1.1: Left: cumulative number distribution of logarithmic orbital periods for 71 O-type objects. The intrinsic number of binaries indicates an intrinsic binary fraction of 0.69 ± 0.09. Credit: Sana et al. (2012). Right: bias-corrected multiplicity fraction as a function of primary star mass. Credit: Offner et al. (2023).

both isolated systems and binaries containing them, as revealed through electromagnetic and GW observations in Section 1.1. In Section 1.2, I present the essential framework of single-star and binary evolution. This is followed by an overview of the theoretical formation pathways of compact object binaries within the classic framework in Section 1.3. Finally, I introduce the binary population synthesis technique in Section 1.4, which serves as the primary method used throughout this thesis.

1.1 Observational landscape of neutron stars and black holes

In the first section, I provide an overview of the observational perspective on NSs and BHs. I describe the fundamental observational characteristics and classifications of NS and BH systems, spanning isolated objects, detached binaries, interacting systems, and GW sources.

1.1.1 Neutron stars and black holes: isolated and binary observations

Isolated neutron stars

The signals from radio pulsars provided the first direct confirmation of the existence of NSs. These rapidly rotating, highly magnetized NSs emit radio radiation that is captured as periodic pulses, with periods defined by their spin rates. For radio pulsars, their emission is mainly powered by their rotational energy. Rotating radio transients (RRATs) represent a class of isolated NSs characterized by sporadic radio bursts with intervals ranging from seconds to hours (McLaughlin et al., 2006). Unlike standard pulsars, whose periodicity allows for continuous monitoring, RRATs are only detectable when they emit a burst. NSs

with extremely high magnetic fields are known as magnetars (see Woods et al., 2006, for a review). These young NSs exhibit a variety of X-ray and gamma-ray activity, driven by the decay of their magnetic fields.

Another class of young NSs, known as central compact objects (CCOs) (De Luca, 2017), are found at the centers of SN remnants and are characterized by the absence of strong pulsations but the presence of thermal X-ray emissions. These isolated NSs possess weak magnetic fields and are primarily powered by thermal energy. Their weak magnetic fields are believed to result from the barrier of fallback material from the SN. X-ray dim isolated NS (XDINS) is another type of isolated NS, characterized by their soft X-ray emission powered by thermal cooling (Haberl, 2007). XDINSs are older than CCOs and show no clear association with SN remnants. Despite their distinct observed behaviors, these various types of isolated NSs are understood within a unified evolutionary framework, shaped by initial conditions such as intrinsic magnetic field strength and the properties of fallback disks from their progenitor SNe.

Isolated black holes: microlensing

Isolated BHs are challenging to detect because they do not emit detectable electromagnetic radiation on their own. Aside from potential accretion in dense environments, the most promising method for detecting an isolated BH and measuring its mass is astrometric microlensing. To date, one strong candidate has been identified: OGLE-2011-BLG-046, with a measured mass of $7.1 \pm 1.3\, M_{\odot}$ (Sahu et al., 2022).

Compact objects in binary systems

Compact objects are more frequently observed within binary systems, particularly BHs, which mostly reveal themselves indirectly in binaries. Interactions within binary systems not only confirm the presence of compact objects but also offer additional information, such as enabling mass measurements through analysis of the motion of the binary components. The following subsection summarizes the fundamental concepts of measuring binary orbits and determining the masses of compact objects through electromagnetic observations.

A binary system in which both stars are visible and their motions can be tracked is known as a visual binary. When the distance to the binary system is known, it is possible to estimate the masses of the individual components by directly measuring the orbital parameters and their motions. However, interacting binaries are typically too tight to be resolved as separate stars. One way to capture their orbital motion is by analyzing Doppler shifts in their spectral lines; such systems are known as spectroscopic binaries. If the orbital plane is

nearly edge-on, the system may also be an eclipsing binary, allowing us to extract additional information from periodic eclipses. In the case of a spectroscopic binary, provided that the distance is accurately estimated, the primary observable is the radial velocity, $v_{\rm rad}$, which is proportional to the semi-amplitude K, defined as:

$$K = \frac{2\pi a \sin i}{P_{\rm orb}\sqrt{1-e^2}}, \tag{1.1}$$

where a is the semi-major axis, i is the orbital inclination angle with respect to the plane of the sky, $P_{\rm orb}$ is the orbital period, and e is the eccentricity. For each component, we can obtain its semi-amplitude as a function of the semi-major axis in the center mass reference frame, $K_1(a_1)$ and $K_2(a_2)$. If one spectra is observed, the so-called mass function can be determined as (e.g., Tauris et al., 2006):

$$f(m_1, m_2, i) \equiv \frac{(m_2 \sin i)^3}{(m_1+m_2)^2} = \frac{1}{2\pi G} M_\odot K_1^3 P_{\rm orb}(1-e^2)^{3/2}, \tag{1.2}$$

where m_1 and m_2 are the binary component masses. One expects to find $m_1 \sin^3 i$ and $m_2 \sin^3 i$, equivalent to the mass ratio, if both spectra are available. Accurate estimates of individual masses necessitate knowing the inclination angle i, which can be obtained if the binary is also observed as an eclipsing binary.

Various combinations of binary components and interaction conditions give rise to a wide diversity of compact object binaries. The following subsections introduce various types of these compact object binaries.

1.1.2 X-ray binaries

The first indirect measurements of stellar-mass BHs came from the detection of the X-ray binary Cygnus X-1, where the accretion of hot material onto an invisible, compact object revealed its presence (Webster et al., 1972). X-ray binaries are systems consisting of a compact object, either an NS or a BH, that accretes material from a companion star. Through efficient accretion around NSs or BHs, the gravitational energy is converted into the heat of the accreted material, resulting in emission that is predominantly in X-rays. Based on the donor star mass, X-ray binaries (XRBs) can be generally classified as high-mass X-ray binaries (HMXBs) with donor stars $\gtrsim 10\,M_\odot$, and low-mass X-ray binaries (LMXBs) with donor stars $\lesssim 2\,M_\odot$. Typically, in HMXBs, the compact object accretes material from the strong stellar winds of the massive companion star, whereas in LMXBs, the compact object accretes matter via Roche-lobe overflow (RLOF). Galactic HMXBs are distributed along the Galactic plane, indicating a young population. In contrast, Galactic LMXBs are concentrated near the Galactic center and exhibit a broader distribution around the Galactic

plane, suggesting an older population. For an NS accretor, HMXBs and LMXBs exhibit distinct X-ray variability and spectral hardness, as the NS magnetic field strength decreases with age. If the donor star mass is within the two thresholds of $\sim 2-10\,M_{\odot}$, they are called intermediate-mass XRBs (IMXBs). On one hand, intermediate-mass donor stars do not possess stellar winds as strong as those of massive stars in HMXBs to initiate significant wind accretion. On the other hand, if they undergo RLOF, the mass transfer timescale is typically too short, or the process becomes unstable more rapidly compared to LMXBs. As a result, they are rarely observed.

1.1.2.1 High-mass X-ray binaries

From recent catalogs, about 150−170 HMXBs and candidates have been found in our Galaxy (Fortin et al., 2023; Neumann et al., 2023). 40 HMXBs have been identified in the Large Magellanic Cloud (Antoniou et al., 2016) and 121 HMXBs in the Small Magellanic Cloud (Haberl et al., 2016). Within all HMXBs, a large fraction of them has been confirmed to host an NS, while only $\lesssim 10$ are candidates that contain a BH. Based on their donor star types and transient behaviors, HMXBs can be classified into two main types: supergiant XRBs (SGXBs) and Be-XRBs. More subclasses have been proposed including highly obscured HMXBs, supergiant fast X-ray transients (SFXTs), Wolf-Rayet XRBs (WR-XRBs), and ultraluminous X-ray sources (ULXs).

Supergiant X-ray binaries

Classical SGXBs are typically wind-fed systems with a supergiant O or B type donor star, mostly with an orbital period of $\lesssim 20\,\mathrm{d}$. They produce persistent X-ray emissions, with flux variations caused by the clumpy structure of the stellar winds. Some SGXBs show persistent high obscuration and can only be detected in hard X-rays, which have been classified as highly obscured HMXBs. One explanation for the high obscuration is that the short-period systems are in the transition between wind-fed phase and RLOF phase. (Walter et al., 2015). In contrast to classical SGXBs, SFXTs exhibit transient properties. They show short flares lasting for tens of minutes to a few hours during outbursts, with a sudden increase in X-ray luminosity by several magnitudes. SFXTs have been suggested to be in the earlier stages of SGXBs. In general, the spectral types of the supergiants in SFXTs are earlier than those in SGXBs. The stars are more compact and well within their Roche lobe, exhibiting different wind properties that lead to a less dense accretion environment compared to classical SGXBs (see Kretschmar et al., 2019, for a review). Several systems have been found showing intermediate behaviors between SFXTs and SGXBs (e.g. Sidoli et al., 2018). The transient behavior of SFXTs can be explained by transitions between

different wind accretion regimes (Bozzo et al., 2016) or between wind and disk accretion (Romano et al., 2015). A few SGXBs are believed to undergo RLOF rather than wind accretion, characterized by the presence of accretion disks and notably high averaged X-ray luminosities. Examples of NS accreting SGXBs include SMC X-1 (Leong et al., 1971; Wojdowski et al., 1998), LMC X-4 (White et al., 1983), and Cen X-3 (Giacconi et al., 1971), while SS433 (Fabrika, 2004), which may host a BH, is another prominent candidate.

Be X-ray binaries

Be-XRBs form the largest subclass of HMXBs. They consist of a rapidly rotating MS star and an NS (with one BH Be-XRB candidate, AS 386 (Khokhlov et al., 2018)) in an eccentric orbit, typically with orbital periods $\gtrsim 20\,\mathrm{d}$. Classical Be stars refer to spectral type B stars that show Balmer emission lines. However, the Be phenomenon occurs in broader populations from early A ($\gtrsim 3\,M_\odot$) to late O-type stars (Rivinius et al., 2013). Nevertheless, in the observational sample of Be-XRBs, the Be stars have masses $\gtrsim 6\,M_\odot$. The emission lines are attributed to the presence of a viscous decretion disk around the star, whose formation has been linked to the rapid rotation of the star. Most of these systems are transient sources, with active phases occurring when the NS accretes material from the decretion disk, and quiescent phases occurring when the NS is not actively accreting. Regarding the rotation rate of Be stars, previous studies suggested that Be stars are rapidly rotating stars with an average rate $\overline{W} \gtrsim 80\%$ (see Rivinius et al., 2013, and references in there). The rate W is defined as $W = v_{\rm rot}/v_{\rm eq}$, where $v_{\rm rot}$ is the linear rotation velocity at the equator and $v_{\rm eq}$ is the Keplerian velocity at the equatorial radius. Some recent studies found that Be stars have a wider rotation rate $30\% \lesssim W \lesssim 95\%$, and exhibit a single peak $W \simeq 65\% - 75\%$ (Zorec et al., 2016; Cochetti et al., 2019; Balona et al., 2021).

Wolf-Rayet X-ray binaries

WR stars are massive, highly evolved stars characterized by their strong optically thick stellar winds ($\sim 10^{-5}\,M_\odot\,\mathrm{yr}^{-1}$), high luminosities, and unique spectral features dominated by emission lines. Seven candidates containing a WR star paired with a compact object have been identified (Esposito et al., 2015), namely WR-XRBs. The strong winds from WR stars hinder precise dynamical mass measurements of the compact objects, making it challenging to determine their nature. Theoretically, it has been proposed that only BH WR-XRBs can exist, as NSs are unlikely to survive the spiral-in phase during mass transfer between the compact object and the massive WR progenitor star due to large orbital energy required (van den Heuvel et al., 2017).

Ultraluminous X-ray sources

More than a thousand ULX point sources have been observed outside the Milky Way (Walton et al., 2022). Their isotropic-equivalent X-ray luminosity can reach above $10^{39}-10^{41}$ erg s^{-1}, which is higher than the typical Eddington luminosity of NSs and stellar mass BHs. They have been proposed to be candidates for accreting intermediate-mass BHs ($100-1000\,M_{\odot}$) at sub-Eddington luminosities (Colbert et al., 1999; Maccarone et al., 2007), but very limited evidence has been found to support this origin (e.g., Mann et al., 2019). Now, it is widely accepted that most of these bright sources are XRBs, in which a non-degenerate star transfers mass onto an NS or a stellar-mass BH. ULXs are observed to be super-Eddington, either due to super-Eddington accretion or significant geometrical beaming (King et al., 2001). The observation of X-ray pulsations in some ULXs has suggested that at least a fraction of them contain an NS (Bachetti et al., 2014). Tauris et al. (2017) and Misra et al. (2020) proposed that ULXs that host NSs can be explained by IMXBs, which contain donor stars with masses between those of LMXBs and HMXBs, because IMXBs are more likely to sustain a longer rapid stable RLOF phase than HMXBs. However, several pulsating ULXs with measured donor masses fall within the HMXB regime. It is possible that ULXs are RLOF HMXBs, as their short theoretical lifetimes align with their observed rarity.

Wind-fed black hole high-mass X-ray binaries

As mentioned previously, most HMXBs host an NS. To date, only three wind-fed BH-HMXBs have been dynamically confirmed. They are Cygnus X-1 (Orosz et al., 2011) in the Milky Way, LMC X-1 (Orosz et al., 2009), and M33 X-7 (Pietsch et al., 2006). Their donor stars are thought to be MS stars, rather than supergiants. All three systems share several notable features: their donors nearly fill their Roche lobes, they have relatively short orbital periods, and the BHs appear to have high spin parameters.

Observations of Cygnus X-1 clearly reveal features that deviate from the classical wind accretion Bondi–Hoyle–Lyttleton model (Hoyle et al., 1939; Bondi et al., 1944). Instead, it has been suggested that disk accretion must be present for these systems to be X-ray bright, since purely spherical accretion onto black holes can be relatively inefficient (Sen et al., 2021; Hirai et al., 2021). In practice, the total number of black hole–massive star binaries is likely not small; however, many such systems are X-ray faint and thus difficult to detect.

1.1.2.2 Low-mass X-ray binaries

According to recent catalogs, about 340 – 350 LMXBs have been identified in our Galaxy (Avakyan et al., 2023; Fortin et al., 2024) and the populations of LMXBs are limited in the Magellanic Clouds. Approximately 23 LMXBs have been confirmed to host a BH,

outnumbered by NS LMXBs by a factor of ~ 2 (Bahramian et al., 2023).

Canonical low-mass X-ray binaries

Canonical LMXBs typically involve a MS, subgiant, or red giant star that transfers mass onto a compact object through RLOF. Most of these canonical LMXBs exhibit transient behavior. The quiescent phase is crucial for accurate measurements of the compact object's mass, as good radial velocity measurements can be obtained only in the quiescent phase of LMXBs.

Ultracompact X-ray binaries

Systems containing a white dwarf (WD), a helium star, or a H-deficient evolved star as the donor star, in a tight orbit with an orbital period $\lesssim 80$ min, are referred to as ultracompact X-ray binaries (UCXBs). The recent catalog includes 49 UCXBs or candidates, with 45 of them confirmed to contain an NS and 2 having been proposed to contain a BH through indirect evidence (Armas Padilla et al., 2023).

Symbiotic X-ray binaries

Just as some HMXBs deviate from the typical wind accretion scenario, certain atypical LMXBs containing giant stars transfer mass through stellar winds rather than RLOF. They are called symbiotic X-ray binaries (SyXBs). No BH-SyXB has been observed so far. SyXBs have wide orbital periods, ranging from hundreds to thousands of days, and are characterized by relatively low X-ray luminosities.

The lower mass gap

Bailyn et al. (1998) conducted a Bayesian analysis on the BH mass distribution in LMXBs. At that time, only seven sources were included in their study. They found that six out of seven BHs clustered near $7\,M_\odot$. If excluding the one system that appears belonging to a different population (characterized by a longer orbital period and a more evolved donor star compared with other systems), there is a significant mass gap between these BH masses and NS masses. Later, Özel et al. (2010) extended the sample to 16 transient LMXBs and found that the BH masses can be best described by a narrow distribution of $7.8 \pm 1.2\,M_\odot$. They confirmed the implication from Bailyn et al. (1998) that a mass gap of $\sim 2-5\,M_\odot$ exists between BHs and NSs. Then, Farr et al. (2011) performed a Bayesian analysis on the BH masses with the data from 15 LMXBs and 5 HMXBs. They found a low boundary of the BH masses around $4-5\,M_\odot$ and again confirmed the existence of the gap.

1.1.3 Pulsar binaries

Millisecond pulsars

Unlike X-ray binaries, where accretion dominates the observational characteristics, in systems with inactive mass transfer, the NS emits may emit radio signals, making the system identifiable as a pulsar binary. Most pulsars in such binaries are millisecond pulsars (MSPs), also called recycled pulsars. Typically, they have a short spin period of $1 - 10$ ms. MSPs are believed to have been spun up during a prior phase of mass transfer, where material and angular momentum were accreted from their companion stars, leading to their 'recycled' nature. Naturally, they are generally considered a later evolutionary phase of LMXBs. LMXBs and recycled pulsars are over-represented in observational samples due to their significantly longer lifetimes, compared to those of typical young pulsars. MSP binaries typically have a WD as the companion star. MSPs can also pair with helium stars, representing an earlier evolutionary stage of MSP-WD binaries. Those with a low-mass MS or subgiant companion ($0.1 - 0.7\,M_{\odot}$) are known as redback pulsars, while those with a brown dwarf or planetary-mass companion $\lesssim 0.05\,M_{\odot}$ are referred to as black widow pulsars (Roberts, 2013). The name of these spider pulsars comes from the fact that they stripped their companion stars down to very low masses. The evolutionary path from LMXBs to MSP binaries can be well connected through transitional systems including accreting millisecond X-ray pulsars (AMXPs) (Patruno et al., 2021), where an NS exhibits both accretion-driven X-ray pulsations and rapid spin, and transitional millisecond pulsars (tMSPs) (Archibald et al., 2009), which oscillate between accretion-powered X-ray states and rotation-powered radio states.

Non-recycled pulsars

Certainly, some young, non-recycled pulsars have been found in binary systems as well. For example, PSR J1755-2550 is a young pulsar with a slow spin period of 315 ms, paired with an unseen companion that is either an NS or a WD (Ng et al., 2018). In general, non-recycled pulsars have much shorter radio lifetimes compared to recycled pulsars, making such discoveries rare.

Pulsars in double neutron star binaries

Besides systems hosting MS, subgiant, or red giant companions, around 25 double NS (DNS) systems have been identified. Typically, one of the NSs is a recycled pulsar–spun up through accretion during a previous binary phase–making it easier to detect. The other one is a younger non-recycled NS, with a slower spin and stronger magnetic field. The first-born NS is typically only mildly recycled rather than a MSP. Observed DNS orbital periods in

the Milky Way span from just a few hours to several years, and some systems will merge within a Hubble time, making them progenitors of GW events.

Pulsar black hole systems

No MSP-BH binary has been confirmed to date. According to the recent study of Liotine et al. (2024), forming an MSP–BH system through isolated binary evolution is particularly challenging. First, the inefficient mass transfer between non-degenerate stars makes it difficult for the system to undergo a mass reversal that would allow the NS to form first. Second, once the NS has formed, the BH progenitor tends to stay compact, largely avoiding further mass transfer and thus bypassing the recycling process.

1.1.4 Detached invisible compact object binaries

Invisible black holes

In practice, most BHs in binaries do not interact with their companion stars and therefore do not appear as X-ray binaries. It has been proposed that $\sim 10^8$ BHs reside in our galaxy (Olejak et al., 2020; Sweeney et al., 2022). Population synthesis studies predict thousands to tens of thousands of BHs in binaries in the Milky Way (Shao et al., 2019; Shao et al., 2020; Breivik et al., 2017) and only a small fraction of them are interacting binaries. In total, ~ 60 BHs have been identified through X-ray detection (Corral-Santana et al., 2016). Finding detached BH binaries can be achieved through high-precision astrometric, photometric, and spectroscopic measurements, leveraging current missions and telescopes such as Gaia, TESS, LAMOST, and others.

Recently, dedicated programs utilizing Gaia DR3 data have been carried out to search for unseen objects in the Milky Way. A few BHs have been found, including Gaia BH1, with a mass of $9.62 \pm 0.18\,M_\odot$ and a sun-like companion star of $0.9\,M_\odot$ (Chakrabarti et al., 2023; El-Badry et al., 2023b), Gaia BH2, with a mass of $8.94 \pm 0.34\,M_\odot$ and a red giant companion of $1\,M_\odot$ (El-Badry et al., 2023a; Tanikawa et al., 2023), and Gaia BH3, with a mass of $32.7 \pm 0.82\,M_\odot$ and a low-mass giant star of $0.76\,M_\odot$ (Gaia Collaboration et al., 2024). Additionally, a potential lower mass-gap BH with a mass of $3.6^{+0.8}_{-0.5}\,M_\odot$ has been recently reported in a wide circular orbit with an orbital period of 880 days. (Wang et al., 2024). Among these Gaia BHs, Gaia BH3 stands out as particularly peculiar due to its extreme mass ratio and its long orbital period of 11.6 yr. It has been proposed to be likely formed within a tidally disrupted globular cluster in a low-metallicity environment (Balbinot et al., 2024; Marín Pina et al., 2024).

Invisible neutron stars

Some NSs remain invisible themselves, either due to their emission beams not pointing towards the Earth or because they have aged and spun down, making their pulsar radiation undetectable. Some potential unseen NSs have been identified using Gaia DR3 data. El-Badry et al. (2024a) reported a potential $1.9 \pm 0.04\,M_\odot$ NS in a two-year orbit around a G-type MS star. The system has a low eccentricity of $e = 0.122 \pm 0.002$. Subsequently, a sample of 21 candidate NS and solar-like star binaries have been identified (El-Badry et al., 2024b). Those unseen NSs have estimated masses ranging from 1.25 to $1.90\,M_\odot$ and most of these systems exhibit orbital periods spanning 400 to 1000 days.

1.1.5 Gravitational-wave sources

In 1916, Einstein predicted the existence of GWs in his general theory of relativity. His theory showed that massive accelerating objects like NSs and BHs would generate ripples in space-time, traveling at the speed of light. Undoubtedly, GWs represent a fundamentally different approach to detecting compact objects compared to electromagnetic observations. Nearly 60 years later, the first indirect evidence supporting the existence of GWs emerged from observing the orbital evolution of a double pulsar system. In 2015, LIGO captured the first GW signal directly, originating from the merger of two BHs, an event known as GW150914. This milestone marked the beginning of GW astronomy as a crucial avenue for studying compact object binaries. Since then, GW transient catalogs have been continuously expanding, including GWTC-1 (Abbott et al., 2019), GWTC-2 (Abbott et al., 2021a), GWTC-2.1 (Abbott et al., 2024), GWTC-3 (Abbott et al., 2023a), and upcoming GWTC-4. Nowadays, in the middle of the fourth observing run, the LVK collaboration has observed more than 200 events. Figure 1.2 shows the mean inferred component masses of 76 published double compact object mergers, with several noteworthy events highlighted. With the upcoming fifth observing run of LVK network and the next-generation GW observatories, including the ground-based Einstein Telescope (Hild et al., 2011) and Cosmic Explorer (Reitze et al., 2019), and space-based LISA (Amaro-Seoane et al., 2017) and TianQi (Luo et al., 2016), the detection of numerous GW events is anticipated, heralding a new era of population studies.

A double compact object can be described by the following intrinsic parameters: the mass of the more massive component M_1, the mass of the less massive component M_2, two dimensionless spin vectors $\vec{\chi}_1$ and $\vec{\chi}_2$, and the orbital angular momentum vector $\vec{L}$. Figure 1.3 is a schematic illustration of a double compact object and the parameters that can describe the system. The angles between the spin vectors and the orbit, which are tilt angles, are denoted as θ_1 and θ_2. When extracting these quantities from GW signals, large

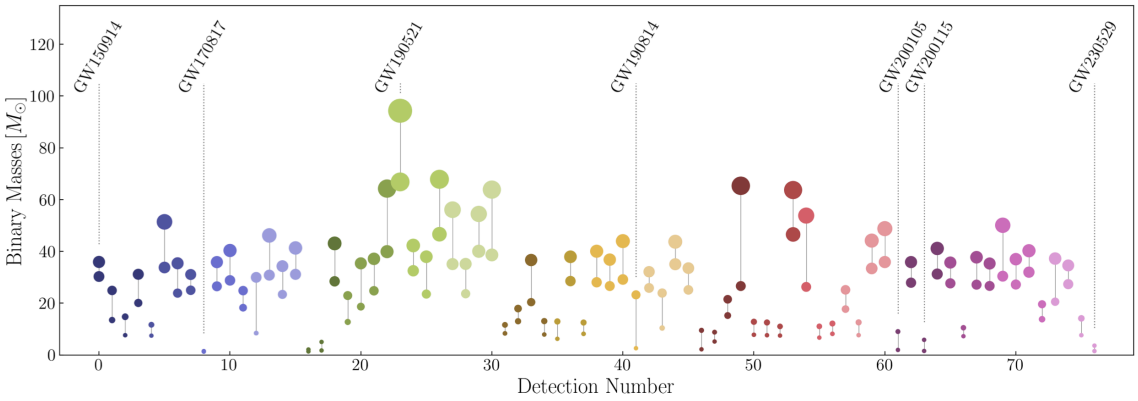

Figure 1.2: Mean inferred component masses for 76 published double compact object mergers. Credit: Callister (2024).

uncertainties can arise, and some source parameters are strongly correlated, even partially degenerate. In comparison to individual component masses that suffer from degeneracies, the chirp mass $M_{\rm chirp}$ is typically measured with higher precision that can be directly obtained from the GW wave frequency:

$$M_{\rm chirp} = \frac{(M_1 M_2)^{3/5}}{(M_1 + M_2)^{1/5}}. \tag{1.3}$$

For the spin, the effective inspiral spin $\chi_{\rm eff}$, which encapsulates the aligned component of the spins, can be better measured:

$$\chi_{\rm eff} = \frac{M_1 \vec{\chi}_1 + M_2 \vec{\chi}_2}{M_1 + M_2} \cdot \vec{L}. \tag{1.4}$$

For a merger event, the luminosity distance and extrinsic parameters that describe the sky location and the orientation are needed to characterize the source. Additionally, for specific types of sources, measuring the eccentricity in eccentric mergers and the tidal deformabilities of NSs in NS binary systems is necessary.

Table 1.1 summarizes the properties of several noteworthy events, including component masses, chirp masses, and effective inspiral spins.

Binary black holes

As illustrated in Figure 1.2, the majority of GW detections so far arise from BBHs. This predominance stems from two key factors: first, high-mass BHs produce strong signals; second, BBH inspirals emit signals in the frequency band where LIGO and Virgo are most sensitive. These conditions also result in severe selection effects that favor systems with

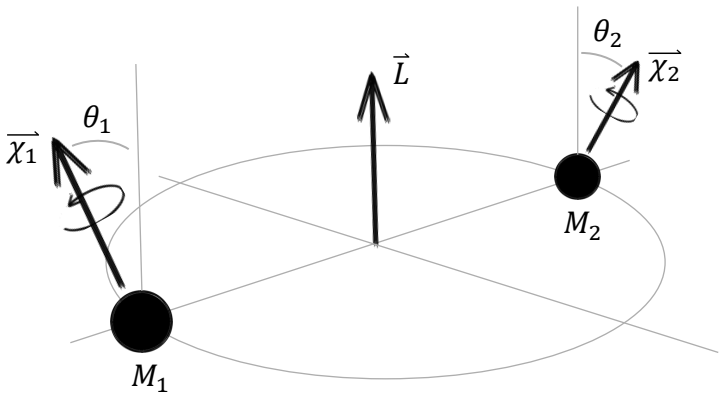

Figure 1.3: Schematic illustration of a double compact object system.

large component masses. Certainly, GW detections have biases related to other parameters, including mass ratios, spins, and source locations. To uncover the underlying population of GW sources, these selection effects must be carefully taken into account. Figure 1.4 shows the inferred primary mass distribution of BBH mergers.

Several notable features of the BH mass distribution in BBH mergers are summarized below. First, a vast majority of BBHs have primary masses concentrated around $10\,M_\odot$. Second, an excess appears around $35\,M_\odot$ in the distribution. An analysis on the secondary masses suggests that this feature is also present or even only significant in the secondary mass distribution (Farah et al., 2024). Third, BHs are observed in the region of the theoretically predicted pair-instability gap. In the theory, for massive stars that develop a massive helium core ($64-133\,M_\odot$) (Heger et al., 2002; Stevenson et al., 2019), the core temperature becomes sufficiently high during the post-carbon-burning phase to produce electron-positron pairs. As a consequence, the pressure is diminished and a runaway thermonuclear reaction is triggered, leading to complete disruption of the star with no remnant left. This process is known as a pair-instability SN (PISN; Fowler et al., 1964; Woosley et al., 2002; Heger et al., 2002). For even more massive stars, direct collapse to form BHs is expected. Due to PISN, a mass gap of $\sim 45-150\,M_\odot$ is anticipated (Woosley, 2017; Woosley et al., 2021), with the boundaries being sensitive to the $^{12}\mathrm{C}(\alpha,\gamma)^{16}\mathrm{O}$ reaction rate (Farmer et al., 2019). The BHs

Table 1.1: Median and 90% symmetric credible intervals for the one-dimensional marginal posterior distributions on component masses, chirp masses, effective inspiral spins, and redshifts of several noteworthy events.

Events	$M_1\ [M_\odot]$	$M_2\ [M_\odot]$	$M_{\rm chirp}\ [M_\odot]$	$\chi_{\rm eff}$	z
GW150914[1]	$35.8^{+5.3}_{-3.9}$	$29.1^{+3.8}_{-4.3}$	$28.0^{+2.0}_{-1.7}$	$-0.07^{+0.16}_{-0.17}$	$0.09^{+0.03}_{-0.03}$
GW170817[2]	$1.46^{+0.12}_{-0.10}$	$1.27^{+0.09}_{-0.09}$	$1.186^{+0.001}_{-0.001}$	$-0.00^{+0.02}_{-0.01}$	$0.01^{+0.00}_{-0.00}$
GW190412[4]	$27.7^{+6.0}_{-6.0}$	$9.0^{+2.0}_{-1.4}$	$13.3^{+0.5}_{-0.5}$	$0.21^{+0.12}_{-0.13}$	$0.15^{+0.04}_{-0.04}$
GW190425[3]	$2.0^{+0.6}_{-0.3}$	$1.4^{+0.3}_{-0.3}$	$1.44^{+0.02}_{-0.02}$	$0.06^{+0.11}_{-0.05}$	$0.03^{+0.01}_{-0.02}$
GW190521[4]	$98.4^{+33.6}_{-21.7}$	$57.2^{+27.1}_{-30.1}$	$63.3^{+19.6}_{-14.6}$	$-0.14^{+0.50}_{-0.45}$	$0.56^{+0.36}_{-0.27}$
GW190814[4]	$23.3^{+1.4}_{-1.4}$	$2.6^{+0.1}_{-0.1}$	$6.11^{+0.06}_{-0.05}$	$0.00^{+0.07}_{-0.07}$	$0.05^{+0.01}_{-0.01}$
GW191219[5]	$31.1^{+2.2}_{-2.8}$	$1.17^{+0.07}_{-0.06}$	$4.31^{+0.12}_{-0.17}$	$0.00^{+0.07}_{-0.09}$	$0.11^{+0.05}_{-0.03}$
GW200105[5]	$9.1^{+1.7}_{-1.7}$	$1.91^{+0.33}_{-0.24}$	$3.42^{+0.08}_{-0.08}$	$0.00^{+0.13}_{-0.18}$	$0.06^{+0.02}_{-0.02}$
GW200115[5]	$5.9^{+2.0}_{-2.5}$	$1.44^{+0.85}_{-0.28}$	$2.43^{+0.05}_{-0.07}$	$0.15^{+0.23}_{-0.42}$	$0.06^{+0.03}_{-0.02}$
GW200210[5]	$24.1^{+7.5}_{-4.6}$	$2.83^{+0.47}_{-0.42}$	$6.56^{+0.38}_{-0.40}$	$0.02^{+0.22}_{-0.21}$	$0.19^{+0.08}_{-0.06}$

[1] Abbott et al. (2016)
[2] Abbott et al. (2019)
[3] Abbott et al. (2021a)
[4] Abbott et al. (2024)
[5] Abbott et al. (2023a)

within the pair-instability gap could potentially be explained by hierarchical mergers (e.g., Kimball et al., 2021).

Regarding BH spins, GW observations indicate that most BHs have small spins. As shown in the left panel of Figure 1.5, most individual BHs in BBH mergers have spins less than ~ 0.4, with only a small fraction exhibiting high spins. The distribution of the better-measured quantity $\chi_{\rm eff}$ is shown in the right panel of Figure 1.5. $\chi_{\rm eff}$ are concentrated around 0.05 and are mostly below ~ 0.2, which is consistent with the small spins of individual BHs. Moreover, this is consistent with the notion that BH spins are preferentially aligned with the orbital angular momentum, although some systems exhibit significant misalignment angles, as indicated by the extension to negative $\chi_{\rm eff}$.

Up to GWTC-3, the BBH merger rate $\mathcal{R}_{\rm BBH}$ has been estimated to be $17.9 - 44\,{\rm Gpc^{-3}\,yr^{-1}}$ at a fiducial redshift of $z = 0.2$ (Abbott et al., 2023b). It has been found that the BBH merger rate density increases with redshift (Fishbach et al., 2018; Abbott et al., 2023b).

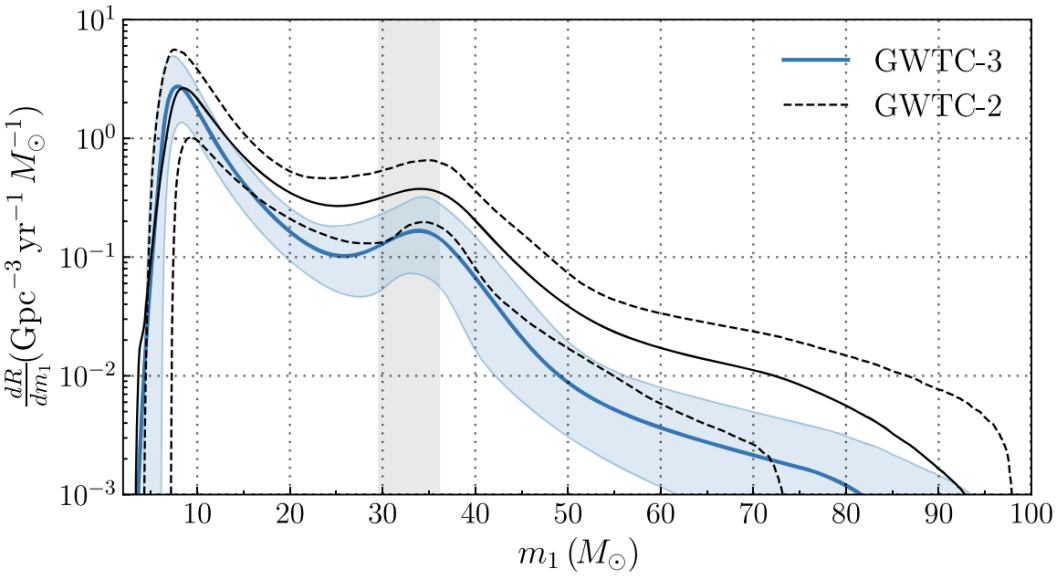

Figure 1.4: The underlying BBH primary mass distribution for the fiducial population model analysis performed in Abbott et al. (2023b). The plot shows the merger rate per primary mass as a function of primary mass. The vertical gray band shows 90% credible intervals on the location of the mean of the Gaussian peak for the fiducial model.

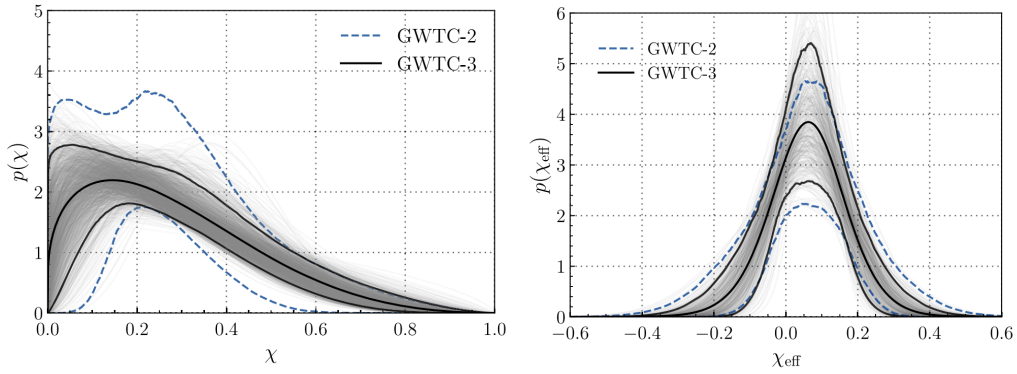

Figure 1.5: Distributions of component spins (left) and effective inspiral spin (right) of merging BBHs. Credit: Abbott et al. (2023b).

This is expected because the formation rate of massive stellar progenitors peaks near $z \approx 2$. In principle, the redshift evolution of the BBH merger rate density should be connected to the cosmic star formation history convolved with the distribution of merger delay times-the time between the double compact object formation and coalescence.

Double neutron stars

Currently, two merger events that are very likely DNSs have been detected, which are GW170817 (Abbott et al., 2017b) and GW190425 (Abbott et al., 2020a). GW170817, the first DNS merger, is famous for the followed observations of electromagnetic emissions. A two-second delayed short gamma-ray burst GRB 170817A was captured immediately after the detection of GW170817 (Abbott et al., 2017a) and was followed by optical, radio, and X-ray emissions (Abbott et al., 2017c). Most importantly, a kilonova counterpart (Eichler et al., 1989) was detected. This event establishes a firm link between short GRBs and DNS mergers, and provides firm evidence for the kilonova theory (Li et al., 1998). GW190425 was detected during the third observing run. Its total mass is $3.4^{+0.3}_{-0.1}\,M_\odot$, which is much higher than the Galactic DNS mass range of $2.5 - 2.89\,M_\odot$ (Abbott et al., 2020a). The mass discrepancy has been investigated through population synthesis studies (Kruckow, 2020). Identifying both GW170817 and GW190425 as DNSs, the merger rate $\mathcal{R}_{\rm DNS}$ has been estimated to be $10 - 1700\,{\rm Gpc^{-3}\,yr^{-1}}$. No new DNSs have been discovered so far during the fourth observing run, resulting in an estimated merger rate toward the lower end.

Neutron star–black holes

Merging NSBH systems are the most recently detected group of double compact objects. There are a handful of NSBH candidates, which are GW200105, GW200115 (Abbott et al., 2021b), GW190426, GW190917 (Abbott et al., 2024), GW191219 (Abbott et al., 2023a), GW230529 (Abac et al., 2024). Additionally, GW190814 (Abbott et al., 2020b) and GW200210 contain a secondary near the boundary between NS and BH masses, but they are more likely to be BBHs. The lately detected event GW230529 has a primary with a mass of $3.6^{+0.8}_{-1.2}\,M_\odot$, falling within the lower mass gap. Its discovery has shifted the BH mass distribution of merging NSBHs toward lower masses. Figure 1.6 displays the inferred BH mass distribution in merging NSBH populations, including only GW200105 and GW200115 or GW200105, GW200115, and GW230529. As shown, the BH mass distribution peaks within the lower mass gap after adding GW230529 to the population. Moreover, with the detection of GW230529, the merger rate of merging NSBHs increases from $\mathcal{R}_{\rm NSBH} = 45^{+75}_{-33}\,{\rm Gpc^{-3}yr^{-1}}$ to $\mathcal{R}_{\rm NSBH} = 94^{+109}_{-64}\,{\rm Gpc^{-3}yr^{-1}}$.

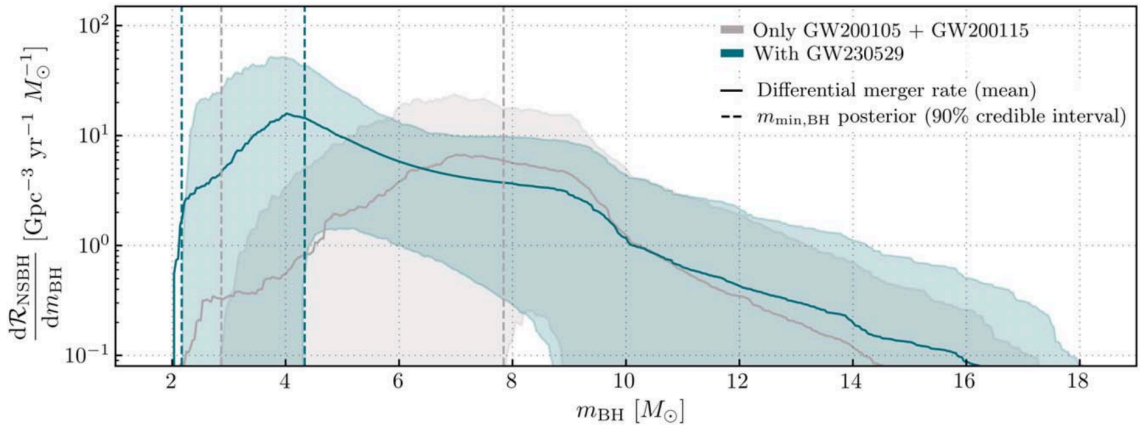

Figure 1.6: The BH mass distribution in merging NSBHs, shown as the differential merger rate. The solid curves represent the mean and the shaded regions indicate the 90% credible intervals. Credit: Abac et al. (2024).

1.2 Frameworks of stellar and binary evolution

To understand the formation and evolution of NS and BH binaries, it is essential to first learn the theoretical frameworks underlying single-star and binary physics. In this section, I introduce the most critical aspects of the physics involved in describing the evolution of single stars and binaries.

1.2.1 Single stars

A star is a self-gravitating gaseous object, producing energy through nuclear fusion in its core. The evolutionary path of a single star is primarily determined by its mass and metallicity at zero-age main sequence (ZAMS). Massive stars with initial mass above $\sim 7-9\,M_\odot$ will form an NS or a BH at the end of their lives. Less massive stars will end their lives as WDs. Figure 1.7 shows the evolution of single stars with varying initial masses and metallicities on the Hertzsprung–Russell diagram.

1.2.1.1 Timescales in stellar physics

In the framework of single-star evolution, three relevant timescales are crucial. One such timescale is the dynamical timescale, also known as the free-fall timescale, which represents the time over which a star would collapse under its own gravity if its internal pressure were suddenly removed. This timescale characterizes how rapidly a star can adjust to an imbalance in hydrostatic equilibrium. The dynamical timescale τ_{dyn} is given by:

$$\tau_{\mathrm{dyn}} \approx \sqrt{\frac{R^3}{GM}}, \tag{1.5}$$

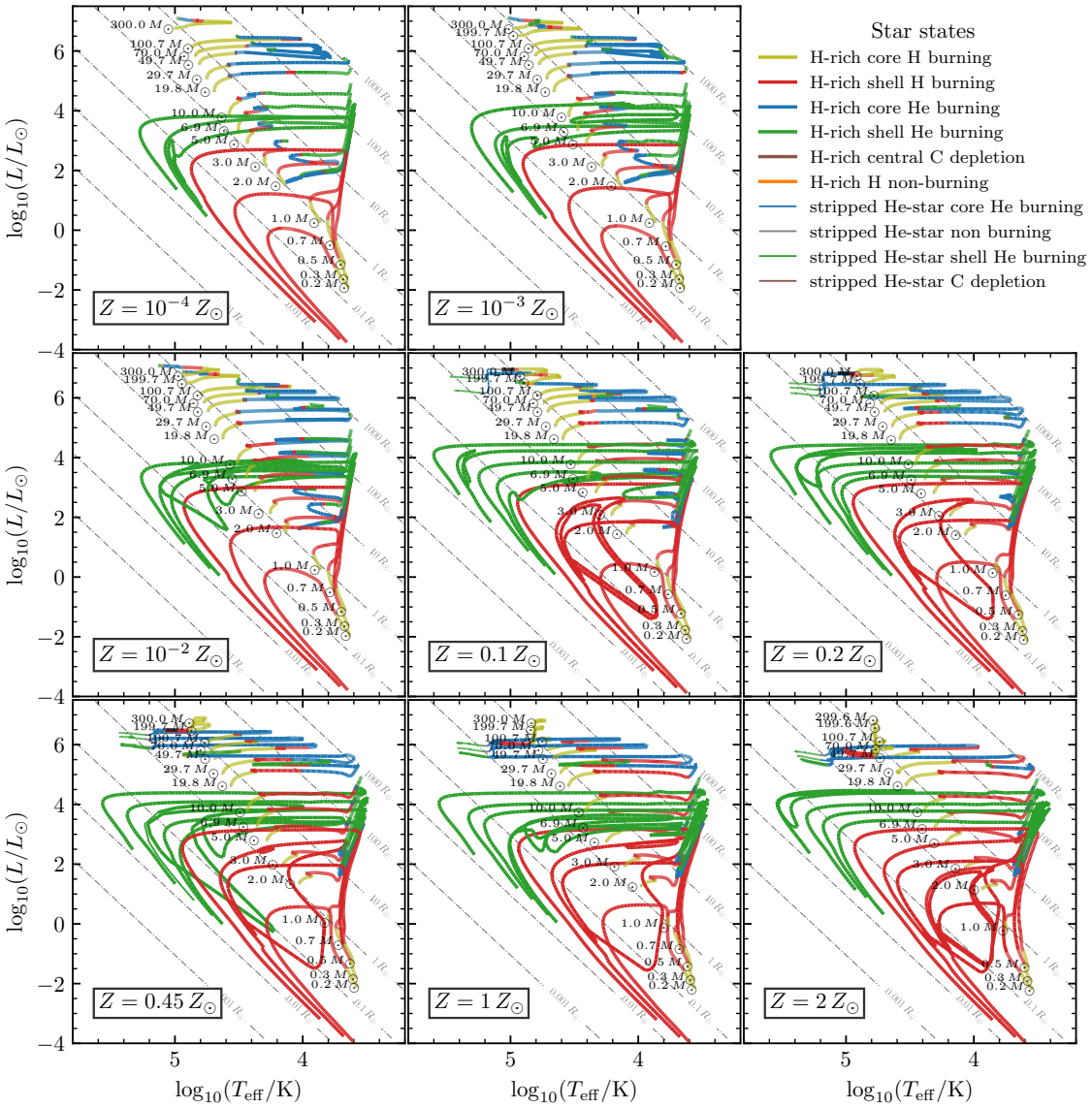

Figure 1.7: Hertzsprung–Russell diagrams for the POSYDON v2 grids of H-rich single-star tracks at 8 metallicities. Line colors indicate the evolutionary states of the stars. Credit: Andrews et al. (2024).

where G is the gravitational constant, and R and M are the radius and mass of the star. Another key timescale is the thermal timescale, or Kelvin–Helmholtz timescale, which describes how rapidly the star adjusts to any changes in its thermal structure. The thermal timescale $\tau_{\rm th}$ can be estimated as the time required for the star to radiate away its gravitational binding energy $E_{\rm g}$ at its current luminosity L:

$$\tau_{\rm th} = \frac{E_{\rm g}}{L} \approx \frac{GM^2}{RL}. \tag{1.6}$$

The last timescale is the nuclear timescale $\tau_{\rm nuc}$, which is defined as the time it would take for a star to exhaust its nuclear energy reservoir $E_{\rm nuc}$ at its current energy loss rate L:

$$\tau_{\rm nuc} = \frac{E_{\rm nuc}}{L}. \tag{1.7}$$

1.2.1.2 From main sequence to core collapse

A star spends the majority of its life on the MS, during which hydrogen in its core is fused into helium. During this phase, the nuclear timescale provides a rough estimate of the star's MS lifetime, assuming constant luminosity. Because the star is in hydrostatic equilibrium, an important implication is provided by the virial theorem, which connects two important primary energy reservoirs within a star. Under the assumption of a simplified perfect gas model for the star, the virial theorem can be expressed as:

$$E_{\rm g} = -2E_{\rm i}, \tag{1.8}$$

where $E_{\rm i}$ is the internal energy of the star.

During the MS stage, a helium core forms in the star as a result of central hydrogen burning. The star then transitions into a phase of hydrogen shell burning. In this post-MS stage, the core contracts and heats up, while the envelope expands and cools. This behavior can be simply explained by the virial theorem, coupled with the assumption of energy conservation. The contraction of the core, accompanied by the release of gravitational energy and an increase in internal energy, drives the opposite behavior in the envelope, causing it to expand and cool. In practice, the total energy does not remain constant. The energy generated by shell burning is largely absorbed by the expanding envelope, resulting in a drop in luminosity. This structural adjustment is governed by the thermal timescale. Since this timescale is relatively short, stars spend little time in this phase, making them difficult to observe and resulting in the so-called Hertzsprung gap between the MS and the red giant stage for most intermediate-mass stars. At a certain point, the helium core ignites, and the stars transition into the helium-burning phase to gradually form a carbon-oxygen core.

The stars move from the horizontal branch to the asymptotic giant branch (AGB), where the stars have hydrogen and helium shell burning. Being different from intermediate-mass stars, massive stars ($\gtrsim 8\,M_\odot$) exhibit smoother transitions during the ignition of successive core-burning phases. They will undergo a red supergiant or a blue supergiant phase. At a high metallicity, these stars will eventually deplete the H envelope completely via stellar winds, becoming a WR star (a stripped helium star). The most massive stars will experience all nuclear-burning phases until the formation of the iron core. The iron core continues to grow as a result of silicon shell burning. When the electron degeneracy pressure is no longer sufficient to support the core or photodisintegration is triggered to break the support, it undergoes a catastrophic collapse. This runaway process can result in either a SN explosion or the direct formation of a BH and is referred to as a core-collapse supernova (CCSN).

1.2.1.3 Convection

Mixing-length theory

The seemingly straightforward evolution of stars becomes increasingly complex when examined in greater detail. Convection is one of the critical physical processes in stars that requires careful consideration. It is vital for energy transfer and chemical mixing throughout the entire evolution of a star. Convection in stars can be triggered by various conditions, such as high opacity, which makes radiative transport inefficient in low-mass stars and the outer envelopes of solar-type stars, or a steep temperature gradient caused by intense fusion in the cores of massive stars. In the post-MS stage of massive stars, both factors contribute to convection in their inflated outer envelopes. For simplicity, convection is commonly treated using the mixing-length theory (MLT). It describes how energy is transported by moving bubbles of gas within the convective regions by defining a local mean free path as the mixing length l_m:

$$l_m = \alpha_{\rm MLT} H_{\rm p}, \tag{1.9}$$

where $\alpha_{\rm MLT}$ is the mixing length parameter and $H_{\rm p}$ is the pressure scale height.

Overshooting

When convective bubbles reach the boundary of a convective region, they can cross it due to their residual momentum. This mechanism is called overshooting. Core overshooting can be crucial for determining the core size in massive stars, as it influences the available fuel for core burning. Overshooting can be treated as a diffusive process, assuming that the

mixing efficiency decays exponentially with distance from the convective boundary:

$$D(r) = D_0 \exp \frac{-r}{f_{\rm ov} H_{\rm p}}, \tag{1.10}$$

where D_0 is the diffusion coefficient at the boundary, r is the distance from the boundary, and $f_{\rm ov}$ is a free parameter that needs to be calibrated using observational data.

1.2.1.4 Stellar winds

Stellar winds are a complex yet critical aspect of stellar evolution, especially for massive stars. They depend strongly on stellar surface properties, such as temperature, density, and chemical abundance. Currently, no comprehensive theoretical model for stellar winds exists. Instead, empirical wind-loss prescriptions, based on observations of various star types, are used in stellar modeling (e.g., Nugis et al., 2000; Vink et al., 2001). For massive stars, stellar winds play a crucial role because the mass loss rates affect the evolution of envelope properties, modify evolutionary timescales, and ultimately affect the mass of the remnant compact object.

1.2.1.5 Stellar rotation and angular momentum transport

Stellar rotation has several significant effects on stars, profoundly influencing their evolution. One of the most prominent impacts is the enhancement of chemical mixing within the stellar interior. Heavier elements can be transported outward to the surface, while additional hydrogen is mixed into the core, thereby extending the duration of the MS core-burning phase. Moreover, rotation influences the internal redistribution of angular momentum and can enhance mass loss. Rotation is particularly important in binary systems, as interactions such as mass transfer and tidal effects can spin up the stars, making it more significant.

To investigate the rotational profiles of stars, understanding the mechanisms of angular momentum transport within their interiors is crucial. As a star evolves off the MS, its core contracts and spins up while its envelope expands and slows down. Angular momentum transport efficiency determines the rotation rate of the final core, which in turn influences the rotation properties of the remnants. Thanks to asteroseismology observations that provide access to the internal rotation of stars with mass $\lesssim 3\,M_\odot$, we can further refine our understanding of angular momentum transport within stellar interiors. Observations generally point to the need for highly efficient angular momentum transport mechanisms. The Tayler-Spruit (TS) dynamo (Spruit, 2002) is one of the most widely considered theories as it is more effective than most known hydrodynamic mechanisms. It posits that the Tayler instability (Spruit, 1999), amplified by differential rotation in radiative zones, is a promising mechanism. This mechanism successfully explains the rotational profile of

the Sun (Eggenberger et al., 2005). However, the observed low core rotation rates in subgiant and red giant stars suggest that the TS dynamo alone is not sufficiently efficient. Consequently, revised prescriptions have been proposed to better match observations (Fuller et al., 2019; Eggenberger et al., 2022). Despite these efforts, no existing model fully explains the rotational profiles of all types of stars, indicating that our understanding of angular momentum transport remains incomplete.

1.2.1.6 Core collapse

Electron capture supernovae

Stars at the lower end of the initial mass range capable of forming an NS develop an oxygen–neon–magnesium (ONeMg) core, rather than an iron core, prior to collapse. If the core grows sufficiently to approach mass close to the Chandrasekhar mass limit of $\sim 1.44\,M_{\odot}$ and enough Mg is present, electron capture on Mg and Ne nuclei can lead to a loss of electron degeneracy pressure and initiate a core collapse (Miyaji et al., 1980). This so-called electron capture supernova (ECSN) is thought to bridge the transition between the formation of massive ONe WDs and NSs. The precise initial mass range or the corresponding helium core mass range that leads to ECSNe remains uncertain, primarily due to ambiguities in mass loss rates, reaction rates, and convective mixing during the final stages of stellar evolution (see Poelarends et al., 2017, and references therein). Furthermore, the complexities introduced by binary evolution further contribute to this uncertainty (Podsiadlowski et al., 2004; Woosley et al., 2015; Tauris et al., 2015).

Core collapse supernovae

More massive stars eventually develop an iron core. When the core temperature becomes high enough to trigger photodisintegration of iron nuclei, the pressure are no longer sufficient to support the core, leading to its collapse.

CCSNe remain an active area of research. The birth of an NS is widely believed to be accompanied by a CCSN explosion. The delayed neutrino-heating explosion mechanism has been developed for decades (Colgate et al., 1966; Bethe et al., 1985; Burrows et al., 1993) and has been recognized as the standard model. However, whether the formation of BHs is accompanied by an energetic explosion remains debated. Three-dimensional (3D) hydrodynamical simulations have been extensively conducted to study CCSNe, and diverse behaviors of CCSNe in the context of BH formation have been observed (Burrows et al., 2024). The fallback explosion scenario has been shown to be able to explain the formation of lower mass-gap BHs (Chan et al., 2020; Vigna-Gómez et al., 2021; Burrows et al.,

2024). However, these 3D simulations are typically conducted on a limited set of models, and no comprehensive simulation-based framework has yet been established to determine the amount of fallback mass that can be accreted by the proto-NS. In addition to various uncertainties, the relationship between the pre-collapse core properties and the remnant properties remains poorly constrained. The implication we have is that a smooth transition between NS and BH formation may not exist. The final remnant types and properties are suggested to depend on both explosion physics and the final core structure, represented by the compactness parameter (e.g., Sukhbold et al., 2016; Patton et al., 2020; Laplace et al., 2024). Due to the immature state of the field and computational limitations, most studies on compact object populations have employed simplified linear prescriptions for remnant masses and types based on the pre-collapse core masses, such as the widely used Fryer et al. (2012) prescription, or stochastic recipes (Mandel et al., 2020b) that draw insights from 3D simulations and parametrized 1D models.

Natal kicks

As the SN explosions that give birth to NSs are often asymmetric in mass ejection or neutrino emission (Bisnovatyi-Kogan, 1993; Burrows et al., 1996; Janka, 2017), NSs are expected to receive a natal kick at birth. These kicks can lead to the ejection of NSs from their host environments or the disruption of their binary systems. Observations of isolated radio pulsars have been used to infer kick velocities $v_{\rm k}$ (Hobbs et al., 2005; Faucher-Giguère et al., 2006; Verbunt et al., 2017; Igoshev, 2020). The kicks imparted to these young NSs can be estimated by calculating their current space velocities and correcting the effects of Galactic rotation and the Sun's motion relative to the system. From a population perspective, NS kick velocities are typically modeled using Maxwellian distributions:

$$f(v_{\rm k}) = \sqrt{\frac{2}{\pi}} \frac{v_{\rm k}^2}{\sigma^3} \exp\left(-\frac{v_{\rm k}^2}{2\sigma^2}\right), \tag{1.11}$$

where σ is the velocity dispersion. Hobbs et al. (2005) estimated a dispersion for CCSNe of $\sigma_{\rm CCSN} = 265\,{\rm km\,s^{-1}}$, a value that has been widely adopted in population studies. Recent studies suggest that the kick velocity distribution may be bimodal (Verbunt et al., 2017; Igoshev, 2020). It has been proposed that NSs formed through ECSNe receive weaker kicks, contributing to the low-velocity component. Consequently, a smaller $\sigma_{\rm ECSN} = 20\,{\rm km\,s^{-1}}$ (Giacobbo et al., 2019) is often assumed. However, observations indicate that not all NSs inferred to have received low kicks fall within the expected mass range for ECSNe. This discrepancy suggests that our understanding of natal kicks and their connection to NS formation channels remains incomplete.

Since massive stars are often born in binaries, the kick velocities inferred from isolated NSs may be overestimated, as they likely represent a population that received strong kicks sufficient to disrupt their binary systems. (Igoshev et al., 2021) combined data from Be-XRBs and isolated radio pulsars, finding a bimodal velocity distribution. More recently, (O'Doherty et al., 2023) estimated NS kicks in binary systems using their orbital properties and found a significantly lower equivalent Maxwellian dispersion of $\sigma = 61.6\,\mathrm{km\,s^{-1}}$. This lower dispersion is consistent with the expectation that NSs bound in binaries receive weaker kicks. This study suggests that kick velocities inferred from isolated radio pulsars underestimate the fraction of NSs that receive low kicks. To fully understand NS kicks, a comprehensive study incorporating all populations, including both isolated NSs and those in binaries, is essential.

Unlike NS kicks, which have been extensively studied, BH kicks are less well understood. The study on the isolated BH OGLE-2011-BLG-0462 suggests that the natal kick is $\lesssim 100\,\mathrm{km\,s^{-1}}$ if it was formed within the kinematic thin disk (Andrews et al., 2022). Studies of the BH-LMXB population have been used to infer BH natal kicks. Repetto et al. (2012) found that natal kicks of BHs appear to be similar to that of NSs. (Repetto et al., 2015) found several binaries exhibit evidence for significant natal kicks, but Mandel (2016) argued that observations solely of the spatial locations of LMXBs are not sufficient to confidently infer strong BH natal kicks. Later, (Atri et al., 2019) suggested a unimodal Gaussian model with a mean of $107 \pm 16\,\mathrm{km\,s^{-1}}$ for the potential kick velocity of BH-XRBs. Nagarajan et al. (2024) revisited constraints on BH natal kicks using Gaia DR3 data and found at least four BHs has kicks $\gtrsim 100\,\mathrm{km\,s^{-1}}$, six BHs exhibit low kicks, and two BHs, V404 Cyg and VFTS 243, have very weak kicks $\lesssim 10\,\mathrm{km\,s^{-1}}$, which is consistent with previous studies Vigna-Gómez et al. (2024) and Burdge et al. (2024). Individual studies on BH binary natal kicks suggest a varied range of velocities. For instance, a kick velocity of $\sim 45 - 115\,\mathrm{km\,s^{-1}}$ has been suggested for GRO J1655-40 (Willems et al., 2005). Fragos et al. (2009) found the kick for XTE J1118+480 must be between 80 and $310\,\mathrm{km\,s^{-1}}$. Wong et al. (2014) determined that the kick of IC10 X-1 was smaller than $130\,\mathrm{km\,s^{-1}}$. Kimball et al. (2023) found that the natal kick of MAXI J1305-704 was at least $70\,\mathrm{km\,s^{-1}}$ if it formed via isolated binary evolution in the thick Galactic disk. Dashwood Brown et al. (2024) reported a high kick of $\sim 296\,\mathrm{km\,s^{-1}}$ for H 1705-250. In conclusion, the fact that some BHs are suggested to receive no kick and some BHs appear to have strong kicks may indicate that there are different formation pathways for BHs, and that varying BH natal kicks are imprinted by these channels.

1.2.1.7 Compact stars

To fully characterize an NS, the key is to understand the dense-matter physics that governs its interior. In particular, the EoS (Lattimer, 2021) of NSs determines both the mass-radius relation and the maximum mass they can support before collapsing into a BH. Lattimer et al. (2001) and Lattimer et al. (2007) provided a general summary of the EoS, which remains subject to significant uncertainties. Recent progress in constraining the EoS has been driven by an expanding set of NS observations. Key contributions come from precise measurements of NS masses via Shapiro delay (Demorest et al., 2010; Fonseca et al., 2016; Arzoumanian et al., 2018; Cromartie et al., 2020; Fonseca et al., 2021), simultaneous determinations of masses and radii derived from `NICER` X-ray observations (Riley et al., 2019; Miller et al., 2019; Baym et al., 2019; Riley et al., 2021; Kojo et al., 2022), and the analysis of GW signals from DNS mergers. Within the framework of general relativity, the EoS sets a fundamental limit on the mass of non-rotating NSs, referred to as the Tolman–Oppenheimer–Volkoff limit $M_{\rm TOV}$ (Tolman, 1939; Oppenheimer et al., 1939). $M_{\rm TOV}$ has been constrained to be $\sim 2-3\,M_\odot$ (Rhoades et al., 1974; Kalogera et al., 1996; Lattimer et al., 2001; Pang et al., 2021). The most massive NSs from electromagnetic observations, including PSR J0740 + 6620 with a mass of $2.08\pm0.07\,M_\odot$ (Fonseca et al., 2021), and the recently estimated rapidly rotating black widow pulsar PSR J0952-0607 with a mass of $2.35\pm0.17\,M_\odot$ (Romani et al., 2022), have provided insights into the determination of the maximum mass of NSs. Recent studies have inferred the TOV mass to be $M_{\rm TOV} = 2.25^{+0.08}_{-0.07}$ (Fan et al., 2024), $2.27^{+0.08}_{-0.09}$ (Biswas et al., 2024), and $2.28^{+0.41}_{-0.21}$ (Golomb et al., 2025).

Unlike NSs, Kerr BHs are fully described by just two parameters: their mass and spin. This means that all other details about the matter that formed the BH are concealed behind the event horizon, leaving only mass and angular momentum as observable characteristics. The spin of a BH is typically characterized by the dimensionless spin parameter, defined as $\chi_{\rm BH} = cJ/GM_{\rm BH}^2$, where c is the speed of light, J is the angular momentum of the BH, G is the gravitational constant, and $M_{\rm BH}$ is the mass of the BH. $\chi_{\rm BH}$ is theoretically constrained to be within $0-1$. As discussed in Zajacek et al. (2019), the electric charge of astrophysical BHs is commonly assumed to be zero. However, the charge may play a role when cosmic rays are involved. Additionally, the presence of charge could potentially shift the position of the innermost stable circular orbit (ISCO) of a BH. ISCO represents the smallest radius around a BH at which a particle can maintain a stable circular orbit before plunging into the event horizon. It defines the inner edge of a thin accretion disk.

1.2.2 Binary systems

The evolution of stars in a binary system can differ from that of an isolated star due to various binary interactions. The evolution of a binary system not only depends on the evolution of its individual components, but also on its orbit. In the following, I introduce the orbital evolution of a binary system and discuss key aspects of binary evolution, including tidal interactions, mass transfer, and SN kicks in binaries.

1.2.2.1 Tidal effects

Two stars in a binary system are bound by gravitational force. Because stars are not point masses, the gravitational force varies across their extended structures, leading to the formation of tidal bulges. As a result of rotation and orbital motion, these tidal bulges on the stars are often misaligned with the line connecting their centers. Tidal torques are exerted on the stars due to the misalignment, resulting in the exchange of energy and angular momentum. These effects become significant when the orbital separation is small.

In the classic tidal theory, tidal effects can be decomposed into two parts: the equilibrium tides and the dynamical tides. Equilibrium tides involve the global distortion of the star, with energy dissipated through viscous friction, predominantly in convective regions. Dynamical tides arise from internal oscillations, with energy dissipated primarily via radiative damping in radiative zones (Zahn, 1977). Tides in binary systems primarily result in two effects: synchronization of each star's rotational period with the orbital period, and the circularization of the orbit. Tidal interactions in binary systems are widely regarded as a crucial mechanism that influences the orbital evolution, stellar rotation, and internal structure of the stars in close binaries.

1.2.2.2 Orbital angular momentum evolution

During the binary evolution, several factors contribute to the change of the orbital angular momentum $\dot{J}_{\rm orb}$:

$$\dot{J}_{\rm orb} = \dot{J}_{\rm ml} + \dot{J}_{\rm mb} + \dot{J}_{\rm ls} + \dot{J}_{\rm gr}, \tag{1.12}$$

$\dot{J}_{\rm ml}$ represents the contribution from mass loss from the system. This term dominates when high-mass stars exhibit strong stellar winds and when the binary undergoes mass transfer. $\dot{J}_{\rm mb}$ denotes the angular momentum change due to magnetic braking. Magnetic braking is a fundamental mechanism that governs the angular momentum evolution of stars, particularly for low-mass stars with substantial convective envelopes. The underlying mechanism is the coupling of the stellar winds to the magnetic field, which exerts a torque and gradually spins down the star. The effect in the individual stars is then transferred to the orbital

evolution of binary systems via tidal interactions. In binary systems, especially in close binaries where tidal effects are efficient, this mechanism can efficiently drain orbital angular momentum, tightening the orbit (Mestel, 1968; Verbunt et al., 1981). The orbital evolution of LMXBs are typically driven by magnetic braking. $\dot{J}_{\rm ls}$ refers to the angular momentum transport between stellar spins and the orbit. Finally, $\dot{J}_{\rm gr}$ is the angular momentum loss due to gravitational wave radiation.

1.2.2.3 Mass transfer

As a star evolves and expands, or as a binary orbit contracts during its evolution, mass transfer between the two stars may commence. This process, a fundamental interaction mechanism in binary systems, is traditionally described using the Roche approximation. In the Roche approximation, the two stars are treated as point masses co-rotating in a circular orbit. The equipotential surfaces are defined by the sum of their gravitational potentials and the centrifugal potential in the co-rotating frame. The Roche lobe is the region around each star enclosed by a specific equipotential surface, within which material remains gravitationally bound to that star. Figure 1.8 illustrates the equipotential surfaces in two binary configurations, where the donor star is either more or less massive than the accretor. The Lagrangian points L1 to L3 are the points where the gravitational forces and the centrifugal force are balanced. When the donor star fills its Roche lobe due to the expansion of the star or the shrinkage of the orbit, material can flow through the L1 point to the accretor. This mass transfer process is known as RLOF. To better characterize the Roche lobe, the Roche lobe radius $R_{\rm L}$, defined as the radius of a sphere with the same volume as the Roche lobe, is commonly used. A widely adopted approximation for $R_{\rm L}$ is given by Eggleton's formula (Eggleton, 1983):

$$R_{\rm L} = \frac{0.49q^{2/3}}{0.6q^{2/3} + \ln(1 + {\rm q}^{1/3})}a, \tag{1.13}$$

where $R_{\rm L}$ is the Roche lobe radius of the donor star, a is the binary separation, and q is the mass ratio (defined as the ratio of the donor star's mass to that of the accretor star). Based on the evolutionary stages of the donor star, RLOF is classified into different cases: case A mass transfer occurs while the donor star is on the MS with core hydrogen burning; case B mass transfer takes place during the shell hydrogen-burning phase as the donor expands after leaving the MS; and case C mass transfer occurs when the donor star has exhausted core helium. Additionally, it can be further divided into additional subclasses. For instance, if a star becomes a stripped helium star and later re-expands to overflow its Roche lobe, thereby initiating mass transfer, this phase is referred to as case BB mass transfer.

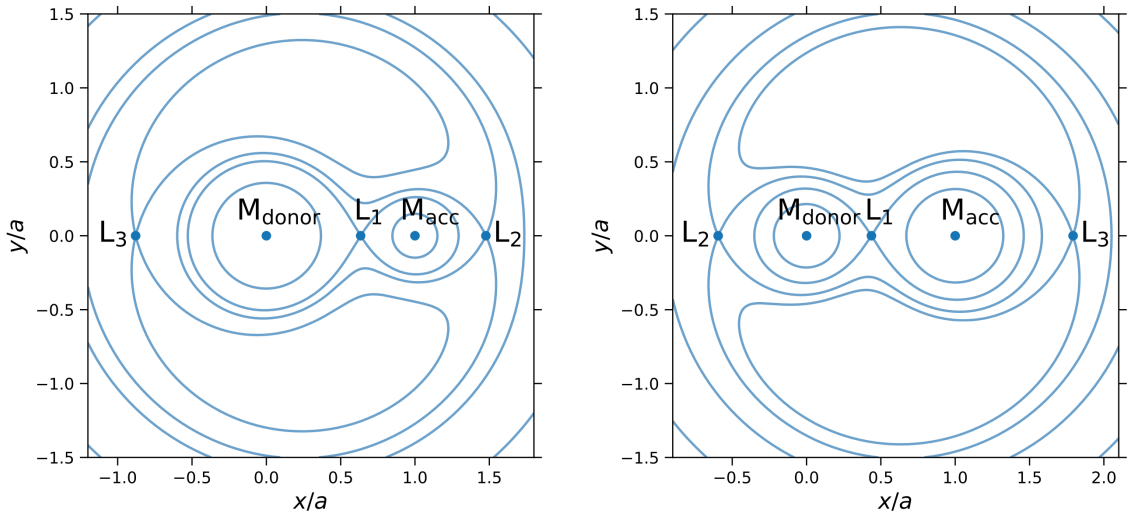

Figure 1.8: Equipotential surfaces for two binaries. In the left panel, the donor star is more massive than the accretor, whereas in the right panel, the accretor is more massive than the donor. Credit: Misra et al. (2020)

To estimate the mass transfer rate through RLOF, Ritter (1988) has provided a model in the case of $R < R_{\rm L}$, assuming that stars have extended atmospheres to initiate RLOF:

$$\dot{M}_{\rm RLOF} = -\dot{M}_0 \exp\left(\frac{R - R_{\rm L}}{H_{\rm p}/\gamma(q)}\right), \tag{1.14}$$

where R is the donor star's radius, $H_{\rm p}$ is the pressure scale height of the atmosphere of the donor star, and $\gamma(q)$ is a fitting function. $\dot{M}_0$ depends on the effective cross section of the flow, the isothermal sound speed at L1, and the density of the donor star's photosphere. Later, Kolb et al. (1990) extended the Ritter scheme to the case of $R > R_{\rm L}$ with an updated prescription.

When the mass stream flows across L1, it either impacts the accretor directly, leading to direct accretion, or orbits around the star and interacts with itself, forming a Keplerian accretion disk. The minimum radius for the accretor to avoid direct accretion has been introduced in Lubow et al. (1975) and de Mink et al. (2013) (see an updated treatment in Sepinsky et al. (2010)). If a disk forms, the star is assumed to accrete from the inner radius of the Keplerian

disk. It has been suggested that even a small amount of accreted mass is able to spin up the accretor to critical rotation, provided that the accreted material carries the Keplerian specific angular momentum at the accretor's surface (Packet, 1981). In this case, mass transfer will be surpassed afterwards, resulting in a very low accretion efficiency. However, some studies have suggested that the accretor star can continue to accrete at critical rotation, since the accretion disk can regulate angular momentum transport without hindering mass accretion (Popham et al., 1991; Paczynski, 1991). How much mass the accretor can accrete and the mechanisms of angular momentum transport during mass transfer remain unresolved questions.

1.2.2.4 Orbital evolution due to mass transfer and mass loss

When binaries undergo mass transfer or mass loss, their binary orbital configuration changes rapidly due to angular momentum loss or redistribution. In this subsection, I systematically examine the orbital evolution resulting from mass transfer and mass loss in binary systems under various scenarios.

Let us consider a binary with a donor star $M_{\rm d}$, an accretor star $M_{\rm a}$, and an orbital separation of a in a circular orbit. The total angular momentum of the binary, $J_{\rm orb}$, is:

$$J_{\rm orb} = M_{\rm d} M_{\rm a} \sqrt{\frac{Ga}{M_{\rm d} + M_{\rm a}}}. \tag{1.15}$$

Taking the time derivative of both sides, we obtain the rate of change in orbital separation:

$$\frac{\dot{a}}{a} = -2\frac{\dot{M}_{\rm d}}{M_{\rm d}} - 2\frac{\dot{M}_{\rm a}}{M_{\rm a}} + \frac{\dot{M}_{\rm d} + \dot{M}_{\rm a}}{M_{\rm d} + M_{\rm a}} + 2\frac{\dot{J}_{\rm orb}}{J_{\rm orb}}. \tag{1.16}$$

Now, we define the mass ratio, $q = \frac{M_{\rm d}}{M_{\rm a}}$, and assume that a fraction β of the transferred mass is accreted by the accretor. Then, we get $\dot{M}_{\rm a} = -\beta \dot{M}_{\rm d}$. Equation 1.16 can be written as:

$$\frac{\dot{a}}{a} = 2\frac{\dot{M}_{\rm d}}{M_{\rm d}}\left(-1 + q\beta + \frac{1}{2}(1-\beta)\frac{q}{1+q}\right) + 2\frac{\dot{J}_{\rm orb}}{J_{\rm orb}}. \tag{1.17}$$

In the simplest case of conservative mass transfer, which means $\beta = 1$ and $\dot{J}_{\rm orb} = 0$, equation 1.17 simplifies to $\frac{\dot{a}}{a} = 2\frac{\dot{M}_{\rm d}}{M_{\rm d}}(q-1)$. Because the donor star is losing mass, meaning $\dot{M}_{\rm d} < 0$, it is clear that the orbit shrinks when the donor star is more massive and the orbital expands when the donor star is less massive.

We consider another straightforward scenario where the mass lost from the donor star does not interact with the accretor but leaves the binary system entirely. This is referred to as the Jeans mode, typically assuming that one star is losing mass through fast isotropic winds. For simplicity, here we ignore the angular momentum change of the stars themselves and assume

that the lost mass carries away the orbital angular momentum at the vicinity of the donor star. In this case, we have $\beta = 0$, $\dot{M}_{\rm a} = 0$, and $\dot{J}_{\rm orb} = \dot{M}_{\rm d}\frac{J_{\rm d}}{M_{\rm d}} = \frac{\dot{M}_{\rm d}}{M_{\rm d}}(\frac{M_{\rm a}}{M_{\rm d}+M_{\rm a}})J_{\rm orb} = \frac{\dot{M}_{\rm d}}{M_{\rm d}}(\frac{1}{q+1})J_{\rm orb}$. Equation 1.17 becomes:

$$\frac{\dot{a}}{a} = 2\frac{\dot{M}_{\rm d}}{M_{\rm d}}\left(-1 + \frac{1}{2}\frac{q}{1+q} + \frac{1}{1+q}\right). \tag{1.18}$$

From equation 1.18, we can get

$$\frac{\dot{a}}{a} = -\frac{\dot{M}_{\rm d}}{M_{\rm d} + M_{\rm a}}, \tag{1.19}$$

which indicates that in the Jeans mode, the orbit always expands. Furthermore, equation 1.19 tells us that the orbital change can be calculated by the total mass change:

$$\frac{a_{\rm f}}{a_{\rm i}} = \frac{M_{\rm i}}{M_{\rm f}}, \tag{1.20}$$

where $a_{\rm i}$ and $a_{\rm f}$ are the initial and final orbital separations, and $M_{\rm i}$ and $M_{\rm f}$ are the initial and final total masses, respectively.

At last, we consider a more general case, where the mass transfer is non-conservative. The expelled mass is lost from the vicinity of the accretor and usually assumed to be lost as isotropic winds (isotropic re-emission mode), which means the specific angular momentum lost from the system is equal to the specific orbital angular momentum of the accretor star. Now, $\dot{J}_{\rm orb} = (1-\beta)\dot{M}_{\rm d}\frac{J_{\rm a}}{M_{\rm a}} = \frac{\dot{M}_{\rm d}}{M_{\rm d}}[(1-\beta)\frac{q^2}{q+1})]J_{\rm orb}$. Equation 1.17 becomes:

$$\frac{\dot{a}}{a} = 2\frac{\dot{M}_{\rm d}}{M_{\rm d}}\left[(1-\beta)\frac{q^2}{q+1} - (1-q\beta) + \frac{1}{2}(1-\beta)\frac{q}{1+q}\right]. \tag{1.21}$$

We define the function $f(q)$ as the right-hand side of equation 1.21, excluding the term $2\frac{\dot{M}_{\rm d}}{M_{\rm d}}$ but taking the negative sign of $\dot{M}_{\rm d}$. $f(q)$ determines the sign of the orbital derivative, where $f(q) > 0$ indicates orbital expansion and $f(q) < 0$ means orbital shrinkage. The same applies to equation 1.18. Figure 1.9 shows $f(q)$, representing the orbital behavior, under different mass transfer modes. In the non-conservative model, the mass accretion efficiency is set to $\beta = 0.5$. Fully non-conservative model and fully conservative model correspond to $\beta = 0$ and 1, respectively. It is clear that for fully conservative mass transfer, the transition between orbital expansion and shrinkage occurs at $q = 1$. In the Jeans mode, the orbit always expands regardless of q. For non-conservative mass transfer, the transition occurs at $q > 1$, moving further to larger q as the accretion efficiency decreases, with the maximum transition point reached under fully non-conservative mass transfer.

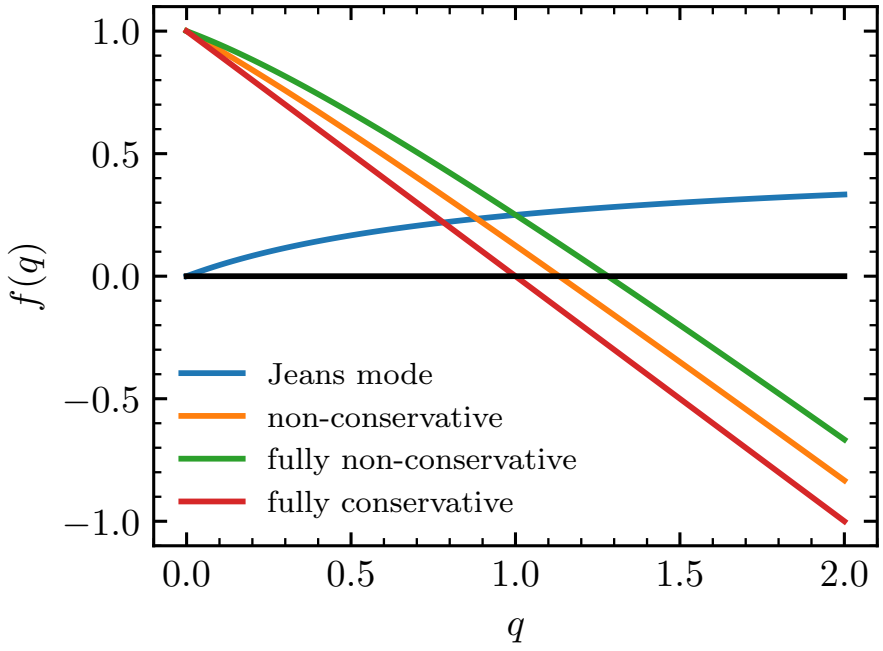

Figure 1.9: Orbital behavior as a function of mass ratio q for different mass transfer modes. The black line marks the boundary between orbital expansion and contraction.

1.2.2.5 Mass transfer stability

Regarding RLOF, a vital question to consider is the stability of mass transfer. The classical approach to analyzing the stability involves comparing of a serials of radial responses resulting from mass loss, which can be expressed as the mass-radius exponents $\zeta = \partial \ln R / \partial \ln M$, with the Roche lobe radial response $\zeta_{\rm L}$. When the donor star loses mass, it responds on the dynamical timescale to retain hydrostatic equilibrium. This process is nearly adiabatic and the donor star's radial response is denoted as $\zeta_{\rm ad}$. On top of this, the star responds on the thermal timescale to reestablish thermal equilibrium and the change in the radius can be expressed as $\zeta_{\rm th}$. If $\zeta_{\rm L}$ is smaller than both $\zeta_{\rm ad}$ and $\zeta_{\rm th}$, which means the new stellar radius will be well within the Roche lobe radius, the mass transfer is stable, driven by the evolutionary expansion of the star and the orbital shrinkage on the nuclear timescale. If $\zeta_{\rm ad} \geq \zeta_{\rm L} > \zeta_{\rm th}$, the mass transfer is stable, driven by the thermal readjustment of the star on the thermal timescale. Finally, if $\zeta_{\rm L} > \zeta_{\rm ad}$, which means the adiabatic response of the star cannot keep the star within its Roche lobe radius, mass transfer proceeds on the dynamical timescale in a runaway process, resulting in unstable mass transfer. ζ may depend on the nature of the donor star's envelope. For stars with a radiative envelope, they initially shrink in response to mass loss to maintain hydrostatic equilibrium (with $\zeta_{\rm ad}$ much greater than zero) and later expand to restore thermal equilibrium. In contrast, for stars with a deep

convective envelope, the stars expand in response to mass loss on the dynamical timescale, meaning $\zeta_{\rm ad} < 0$. As a result, mass transfer is usually expected to be dynamically unstable for these stars.

1.2.2.6 Common envelope

When mass transfer becomes unstable, the system undergoes a runaway process that leads to the formation of a common envelope (CE). Subsequently, drag forces acting on the companion star drive it to spiral inward, transferring orbital energy and angular momentum into the envelope. This transferred energy is then converted into kinetic energy that helps expel the envelope. The entire process typically occurs on a very short timescale. CE evolution results in either the merger of the two stars or the successful ejection of the envelope, leaving behind a close binary consisting of the core of the donor star and the companion.

CE evolution is widely regarded as one of the most intricate and uncertain processes in binary evolution. The classical approach to modeling CE evolution relies on the energy formalism, commonly referred to as the $\alpha - \lambda$ prescription (Webbink, 1984; de Kool et al., 1987; Livio et al., 1988). The CE efficiency parameter, $\alpha_{\rm CE}$, is defined to describe how efficiently the released orbital energy can be converted to eject the CE:

$$E_{\rm bind} = \alpha_{\rm CE} \Delta E_{\rm orb}, \tag{1.22}$$

where $E_{\rm bind}$ is the binding energy of the CE, and $\Delta E_{\rm orb}$ is the orbital energy released during the inspiral. In principle, if orbital energy is the sole energy source, $\alpha_{\rm CE}$ cannot be larger than unity. However, additional energy sources, such as accretion energy from the companion star and recombination energy, may be involved to justify an $\alpha_{\rm CE}$ greater than unity. Nonetheless, the amount of energy that can be converted remains uncertain and may depend on the binary configuration. For instance, the energy released from accretion onto the companion star can be relatively large for an NS accretor, but less so for a BH or a MS star. Conversely, $\alpha_{\rm CE}$ may be lower if there are unaccounted energy dissipation mechanisms like radiation. In reality, the value of $\alpha_{\rm CE}$ is highly uncertain and not constant, as it may depend on the both the nature and the mass of the accretor star.

The efficiency $\alpha_{\rm CE}$ alone is not sufficient to describe CE evolution. The parameter $\lambda_{\rm CE}$ was introduced to express the binding energy:

$$E_{\rm bind} = -\frac{G M_{\rm d} M_{\rm env}}{\lambda_{\rm CE} R_{\rm d}}, \tag{1.23}$$

where $M_{\rm env}$ is the mass of the donor star's envelope and $R_{\rm d}$ is the donor star's radius at the onset of CE evolution. $\lambda_{\rm CE}$ depends on the evolutionary stage of the donor star, or the inner

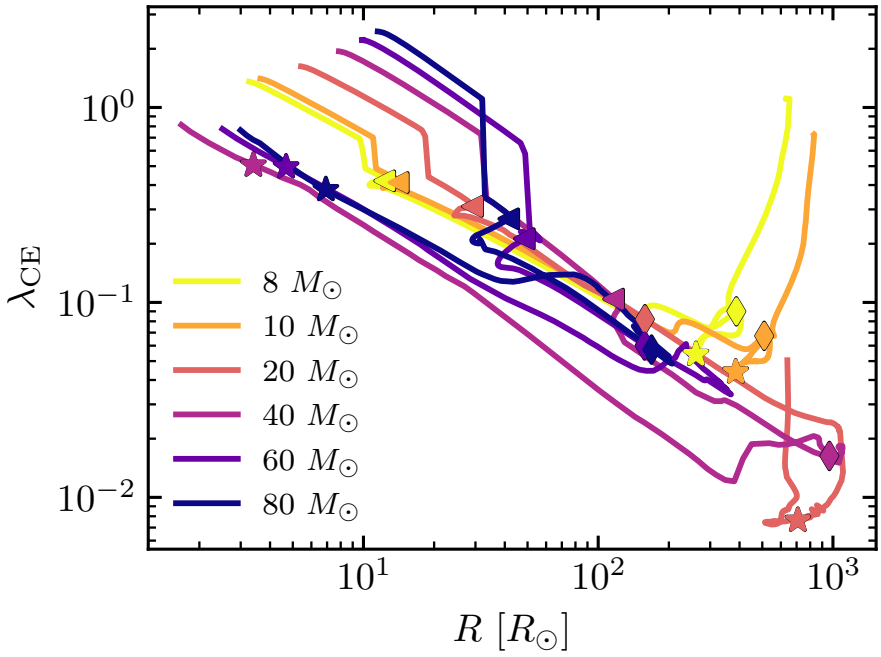

Figure 1.10: Evolution of the $\lambda_{\rm CE}$ parameter for different initial masses. The triangle, diamond, and star markers represent the start of shell hydrogen burning, the start of core helium burning, and the end of core helium burning, respectively. Credit: Fragos et al. (2023).

structure of the donor star, and may be related to the prior mass transfer history (Renzo et al., 2023). Figure 1.10 illustrates the evolution of $\lambda_{\rm CE}$ with the stellar evolution stage, represented by the stellar radii, for a set of single star simulations. The most prominent uncertainty for $\lambda_{\rm CE}$ is the definition of the boundary of the envelope. The binding energy is sensitive to this because the deeper envelope layers are more tightly bound.

1.2.2.7 Supernova kicks in binaries

SN kicks are crucial in binary modeling, as they can drastically alter the orbital configuration or even disrupt the system. Meanwhile, binary interactions can also influence the SN itself. For example, the initial mass range for ECSNe is broader in binaries than in single stars. In addition, prior mass transfer can strip the progenitor star, leading to an ultra-stripped supernova (USSN). USSNe are thought to impart smaller natal kicks and thus increase the chances of the binary surviving.

SN kicks can significantly modify the orbital semi-major axis, induce eccentricity, and tilt the orbit. The orbital tilt is particularly important for GW sources because the effective spin, a key observable directly constrained by GW data, depends sensitively on any misalignment

between the compact objects' spins and orbital angular momentum vector. Here, I illustrate the impact of SN kicks on orbit tilt using the example of a double compact object that experiences two SN kicks.

When the first SN occurs, the component of the kick perpendicular to the orbital plane tilts the orbit. It is commonly assumed that the compact object's spin remains unchanged by this kick. Another simplifying assumption is that the non-degenerate star reorients itself to align with the tilted orbit through tidal effects or subsequent mass-transfer phases. In contrast, the compact object's spin angle may change during mass transfer but not necessarily become fully aligned with the orbit. I denote the angle between the first compact object's spin and the second pre-SN orbit by θ_1'. Then, when the secondary star explodes, the second kick tilts the orbit again, creating a tilt angle θ_2 for the second compact object. Figure 1.3 presents a schematic illustration on the two tilt angles.

One can imagine that the final tilt θ_1 for the first compact object arises from the vector combination of θ_2 and θ_1'. θ_1 is not simply the sum or difference of the two angles (as would be the case if two kicks occurred at the same or the opposite relative position along the orbit), but is instead defined by the trihedral angle resulting from the two kicks (see the calculation in Chapter 3).

1.2.3 Stellar and binary evolution codes

Detailed calculations of stellar interiors matured in the 1970s, when it became computationally feasible to solve the full set of stellar structure equations. Eggleton's `STARS` (Eggleton, 1971; Eggleton, 1972; Pols et al., 1995; Eldridge et al., 2004; Stancliffe et al., 2009) code was one of the first major codes developed to model both single and binary star evolution. Single star 1D codes, such as `GENEC` (Schaller et al., 1992; Eggenberger et al., 2008; Georgy et al., 2013b; Georgy et al., 2013a)(famous for its inclusion of rotation physics), `PARSEC` (Bressan et al., 2012), and `GARSTEC` (Weiss et al., 2008), have been created and developed to specialize in different aspects of stellar evolution. Evolution codes supporting binary evolution have also emerged, such as `BEC` (Heger et al., 2000b; Heger et al., 2000a), `BINSTAR` (Siess et al., 2013), and `TWIN` (Nelson et al., 2001; Eggleton et al., 2002). Modules for Experiments in Stellar Astrophysics (`MESA`, Paxton et al., 2011; Paxton et al., 2013; Paxton et al., 2015; Paxton et al., 2018; Paxton et al., 2019; Jermyn et al., 2023) stands out as an open-source, flexible, and comprehensive tool for modeling both single and binary stars. It has been used by researchers worldwide, enabling them to contribute to and benefit from ongoing advancements. Detailed binary evolution codes simultaneously solve the stellar structure equations for individual stars while calculating RLOF and orbital evolution.

The limitations of 1D simulation codes lie in the simplified treatment of 3D convection, the absence of large-scale instabilities, and the reliance on semi-empirical prescriptions for physical processes such as rotation, mixing, and mass loss. Moreover, binary processes like mass transfer and CE evolution can only be treated in a simplified manner. 3D simulations provide a new perspective by offering a realistic treatment of convection and turbulence, as well as by simulating non-spherical processes. The code `CO5BOLD` (Freytag et al., 2012) is effective at modeling convection, while hydrodynamic codes such as `AREPO` (Springel, 2010) and `FLASH` (Fryxell et al., 2000) have been employed to simulate CE evolution, and magnetohydrodynamics (MHD) codes like `Athena++` (Stone et al., 2020) have the potential to simulate disks and accretion processes. Because 3D simulations are computationally expensive and typically focus on a short evolutionary timescale, it is imperative to combine 3D and 1D simulations to obtain insights into the physics of single and binary star evolution.

1.3 Formation of neutron star/black hole binaries

In this section, I present a general picture of the evolutionary pathways in isolated binary systems that lead to the formation of NS/BH binaries. Following a classic binary evolution path in which two stars are assumed to form together on the ZAMS, various possible evolutionary bifurcations are described, and different types of binaries emerge at certain phases along the evolutionary path. Generally speaking, for two stars, there are three possibilities regarding mass transfer: the system may undergo stable mass transfer, unstable mass transfer–CE evolution–or avoid mass transfer via RLOF. The specific evolutionary mode of a binary is primarily determined by its initial component masses, metallicity, and orbital properties. During evolution, a SN explosion can occur as a stochastic process that influences the subsequent evolution and the fate of the binary. Nevertheless, the effects of SN kick also depend on the pre-SN orbits. In simulations, the specific assumptions made regarding single-star physics and binary interactions can lead to different outcomes. Among them, the prescriptions for single star mass loss, the overshooting parameter, prescriptions for SN remnants, and binary mass transfer efficiency, stability, and CE parameters are the most important and uncertain factors.

1.3.1 High-mass X-ray binaries and double compact objects

Only a small fraction of HMXBs will ultimately form double compact objects, because they are very likely to merge during subsequent CE evolution or be disrupted at the second SN. Among those that do form double compact objects, only a small subset will merge within a Hubble time. Along their evolutionary path, these binaries necessarily pass through HMXB phases at certain stages. However, these phases can be short-lived, making them

difficult to observe. Furthermore, differences in observational scales and selection effects imply that electromagnetic and gravitational-wave detectors probe distinct subsets of binary populations, often under different redshifts, metallicities, component masses, and other properties. Consequently, the goal of this section is not to unify all observed compact object binaries into a single evolutionary sequence. Instead, it is to propose a general framework in which certain evolutionary stages may correspond to the observed populations.

Another important point is that the evolutionary path proposed in this section is based on specific assumptions regarding binary interaction physics. The most prominent one is the mass transfer efficiency. High efficiency may lead to mass rejuvenation commonly, which substantially alters the overall evolution. In the framework discussed in this section, the binary evolution is described based on low accretion efficiency, as indicated by detailed 1D binary evolution (See Chapter 3 for a discussion).

1.3.1.1 The classic formation channel

I present a general schematic of binary evolution that encompasses a broad range of HMXBs and double compact objects in Figure 1.11. This illustration demonstrates the potential outcomes at each stage of evolution, taking into account the varied orbits, masses, and metallicities of different systems. In this classic evolutionary path, two nondegenerate stars initiate RLOF that either leads to a CE phase with a high possibility of merger or a stable mass transfer phase. Following mass transfer, the primary star's envelope is stripped. Some wide binaries can avoid mass transfer. Such avoidance can also occur in very close orbits for high-metallicity stars, as their strong stellar winds help stripping the envelope, preventing the expansion during the post MS phase. Finally, the primary star evolves to core collapse, forming an NS or a BH. The SN kick can either disrupt the binary completely or alter its orbital configuration.

If the primary star forms an NS, and the binary survives the SN, then it may potentially evolve into an NS-HMXB. Depending on the previous mass transfer phase and the orbital period, the secondary star can spin fast enough to form a Be star with a decretion disk. Specifically, this requires that the secondary accretes enough mass adding angular momentum, and that tidal effects are not sufficient to significantly spin down the star. Then, the binary may appear as a Be-XRB, provided it is in an appropriate orbit where the NS can interact with the decretion disk. If the secondary star does not form a Be star, the binary may instead evolve into a SGXB, with the NS accreting from intense stellar winds. Alternatively, if the NS does not interact strongly with the companion star, it may be observed as a pulsar binary containing a massive secondary star. As the secondary star evolves, it fills its Roche lobe and

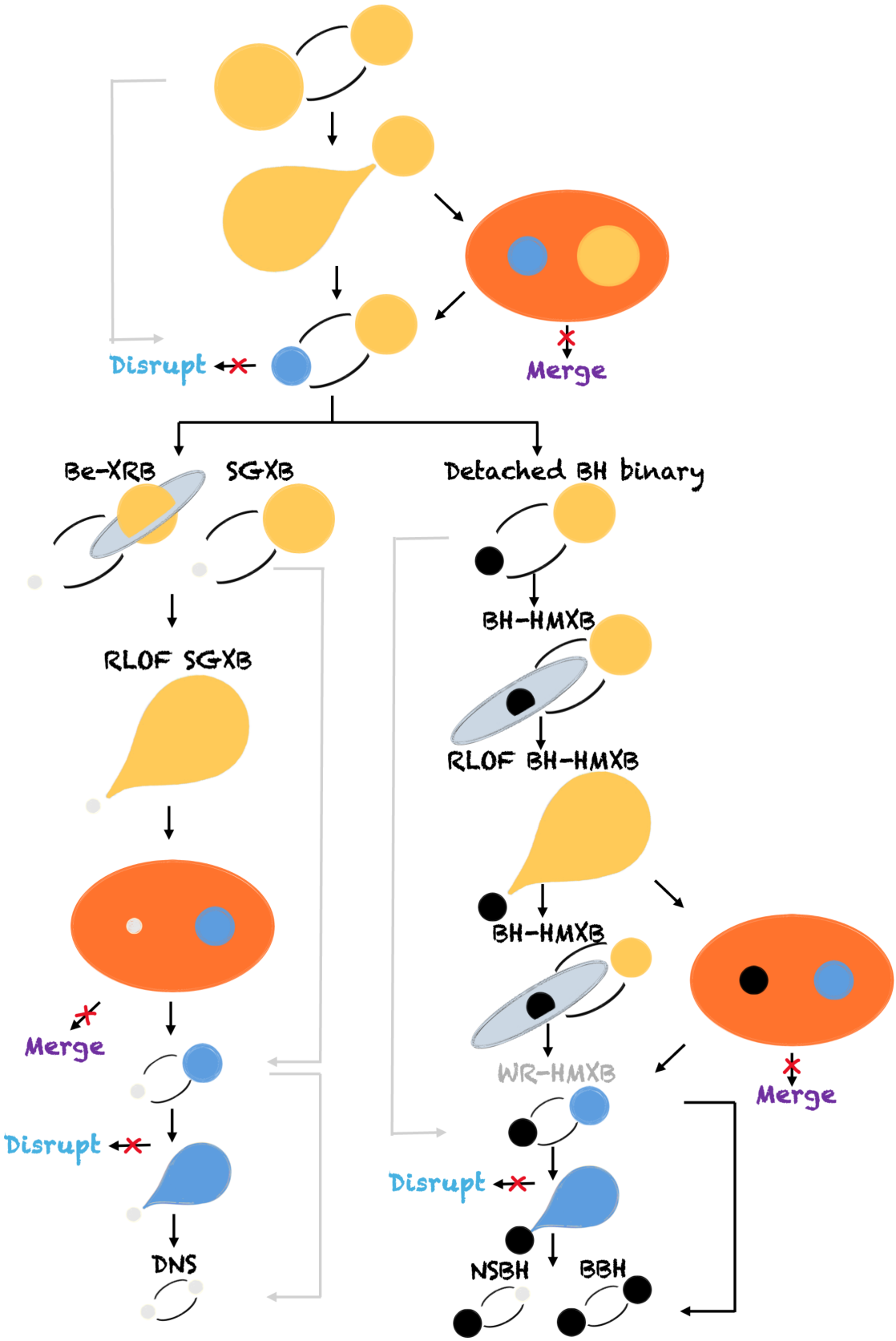

Figure 1.11: Schematic diagram of the evolutionary paths of massive binaries that form HMXBs and double compact object systems. Yellow and blue indicate H-rich stars and He-rich stars, respectively. White and black represent NSs and BHs, respectively.

initiates mass transfer onto the NS. At this stage, the binary appears as a RLOF NS-HMXB. Because the secondary star is massive, the binary very likely enters a CE evolution due to its high mass ratio. Again, most of them merge during CE evolution and some systems successfully eject the CE, leaving behind the helium core of the secondary star and the NS being in a close orbit. Then, the helium star expands to fill the Roche lobe as it enters the helium shell-burning stage, initiating a stable case BB mass transfer. If the helium star is massive enough, it finally explodes to form an NS. If the second SN does not disrupt the binary, it becomes a DNS. As the first-born NS has experienced mass transfer, it may be detected as a mildly recycled pulsar. Furthermore, if the orbit is tight enough, the system could eventually merge as a GW source.

Now, let us assume that the primary star forms a BH after the core collapse. In this case, the binary could in principle form a BH Be-XRB. Observationally, BH Be-XRBs are rare, and there is only one potential candidate. It has been discussed in Rocha et al. (2024) that the rarity of BH progenitors, the lower formation rate of Be stars with BH progenitors, and a possible accretion luminosity selection effect are responsible for the dearth of BH Be-XRBs. In reality, most BH binaries are in the detached phase. Depending on the orbital separation and metallicity, the binary may remain detached till the second core collapse. Apart from this population, most BH binaries become X-ray faint, and a small fraction of them form an accretion disk through wind accretion, appearing as wind-fed BH-HMXBs. Then, RLOF occurs and the binary becomes a RLOF BH-HMXB. If the mass transfer is stable and in case A, the secondary star may be partially stripped, allowing it to shrink back within its Roche lobe, appearing again as a wind-fed BH-HMXB. If the secondary star evolves off the MS during this whole phase, it could appear as a bright X-ray source as well. However, the short duration of post-MS evolution makes it hard to capture, explaining its rarity. Certainly, the RLOF phase can be unstable and develop to CE evolution. After stable RLOF or CE evolution, depending on the mass and metallicity, the secondary star may become a WR star and the binary appears as a WR HMXB. Afterwards, as an NS progenitor, the helium star is more likely to initiate a case BB mass transfer, while it is more likely to keep being detached as a BH progenitor. Ultimately, the second core collapse occurs, and if the binary is not disrupted, it forms either an NSBH or a BBH.

1.3.1.2 Other formation channels

Apart from the classic channel discussed in the last section, there exist several alternative formation channels and additional evolutionary phases that, although less common, may play a significant role in the formation of double compact objects.

Reverse mass transfer

If two stars have masses close to each other, their MS evolutionary timescales are close. As a result, the secondary star could evolve off the MS before the primary star goes to core collapse. After the first mass transfer from the primary star onto the secondary star, the secondary initiates a reverse mass transfer phase, transferring mass back to the primary star. Reverse mass transfer can be either stable or unstable. Figure 1.12 shows the evolution of two example binaries that experience stable and unstable reverse mass transfer at solar metallicity. These two binaries have initial parameters of $M_1 = 28.2\,M_\odot, q = 0.95, P_{\rm orb} = 268\,{\rm d}$, and $M_1 = 22.3\,M_\odot, q = 0.95, P_{\rm orb} = 139\,{\rm d}$. The plot, from top to bottom, shows the two component masses, the mass transfer rate, the component radii, the surface rotation angular velocity over the critical value, and the spin parameters. Reverse MT is more likely to be unstable as metallicity decreases. This occurs because, at low metallicity, the initially more massive star does not fully detach and can maintain stable mass transfer until carbon exhaustion. In addition, this star may not be completely stripped during the mass-transfer phase, and the residual thin hydrogen layer influences its radial response. A prominent effect of reverse mass transfer is on the rotation of the stars, and thus on the spin of the potentially formed BHs. In the stable case, the reverse mass transfer directly spins up the primary progenitor star. In the CE case, the two stars can experience tidal spin-up in the post-CE orbit.

Double common envelope

Another pathway for binaries that have mass ratios close to unity is the so-called double CE evolution. In this scenario, two stars both evolve off the MS and both fill their Roche lobes, forming a CE composed of the envelopes of both stars. If the CE evolution is successful, two helium cores are left in a close orbit. The helium stars subsequently form NSs or BHs. This channel was proposed as a formation pathway for DNSs and BBHs (Brown, 1995; Dewi et al., 2006; Neijssel et al., 2019). Interestingly, because the tidal effects make the progenitors spin rapidly, the BH formed via this channel can exhibit high natal spin. Additionally, Liotine et al. (2024) found this channel is the dominant channel for the formation of NSBH systems that NS forms first, under the framework of inefficient mass transfer between non-degenerate stars.

Chemically homogeneous evolution

If a massive star rotates rapidly, it may undergo strong internal mixing, leading to nearly homogeneous composition. Consequently, the star can retain a high surface temperature and remain compact . This is referred to as chemically homogeneous evolution (CHE) (Maeder,

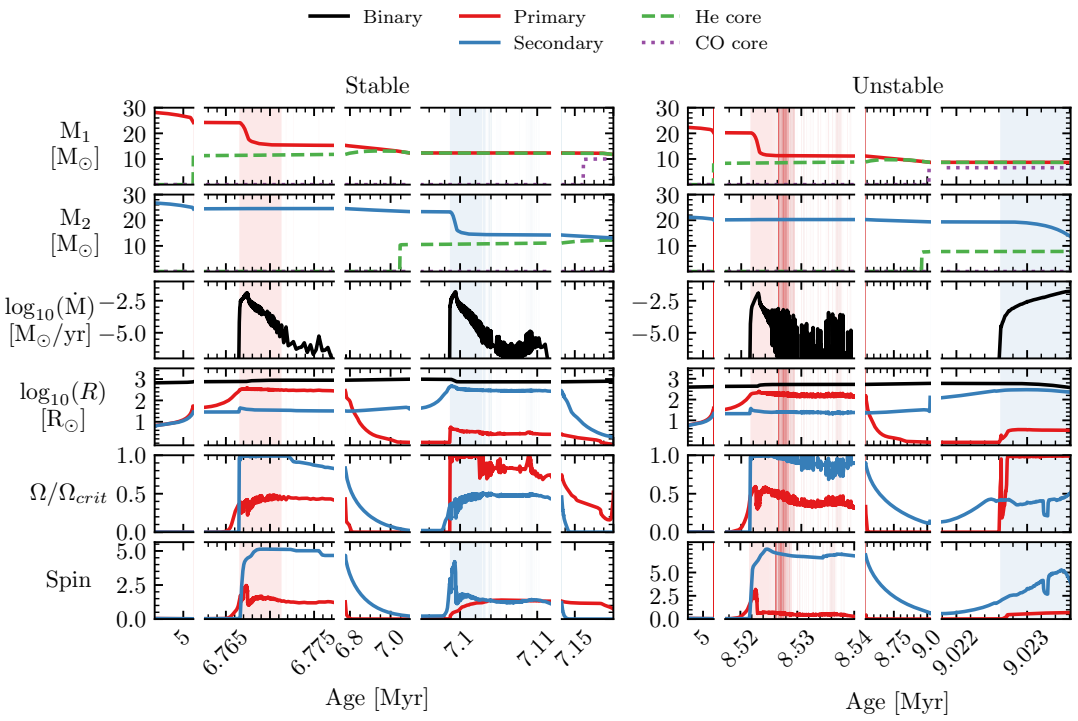

Figure 1.12: Evolution of two binary systems undergoing reverse mass transfer. The left panels show a stable reverse mass transfer and the right panels show an unstable case. Credit: Andrews et al. (2024)

1987; Heger et al., 2000a). CHE occurs for stars with sub-solar metallicity because they can avoid significant angular momentum loss via strong stellar winds. Rapid rotation can be induced by mass transfer or tidal interactions. If two massive stars with nearly equal masses form in a close orbit with an orbital period of less than ~ 2 days, tides can drive the stars to undergo CHE. This channel has been proposed as an important channel for the formation of merging BBHs (de Mink et al., 2016; Mandel et al., 2016; Marchant et al., 2016). Through the CHE channel, the BHs can acquire relatively high natal spins, and their spin directions tend to be nearly aligned if not considering high kicks during the formation of these massive BHs.

1.3.2 Low-mass X-ray binaries and pulsar binaries

The nuclear mass transfer timescale for low-mass stars is much longer than that for high-mass stars, making the lifetime of LMXBs very long. However, the observed LMXBs do not outnumber HMXBs in proportion to their lifetimes, which indicates that their formation rate is lower than that of HMXBs. From a binary evolution perspective, this is expected

because the progenitor binaries of LMXBs tend to have more extreme mass ratios, which frequently lead to CE evolution, and the SN kicks are more likely to disrupt these systems. An open question regarding the formation of LMXBs is why the low-mass companion stars are able to expel the CE and prevent mergers. This may suggest that our understanding of CE evolution is incomplete. Throughout their evolution, detached NS systems may form either before or after mass transfer, potentially appearing as pulsar binaries.

1.3.2.1 The classic formation channel

In Figure 1.13, I present a general schematic of binary evolution that encompasses LMXBs and pulsar binaries. In this schematic, the primary star is the progenitor of an NS or a BH, while the secondary star is a low-mass star. Consequently, the first mass transfer phase between two non-degenerate stars is expected to be unstable, leading to CE evolution. It has been suggested that the LMXB progenitor binaries are in wide orbits so that when CE initiates, the donor star has evolved substantially and the binding energy of the CE is low. In particular, for BH-LMXBs, it has been proposed that BH progenitors in wide orbits initiate case C mass transfer. In this situation, the stellar core has grown massive enough at the onset of the mass transfer phase to form a BH.

Before the core collapse that forms NSs, the helium stars very likely undergo case BB mass transfer in the post-CE orbit. After the SN explosion, if the binary remains bound, a non-recycled pulsar accompanied by a low-mass MS star may form. As the secondary star evolves, it may fill its Roche lobe either during its MS, subgiant, or red giant phase, thereby appearing as an LMXB. If the orbit is so wide that RLOF is not initiated when the secondary star becomes a red giant, the NS can accrete the stellar winds from the red giant , resulting in the formation of a SyXB. Finally, SyXB may evolve into a very wide MSP binary. Following the LMXB stage, if the orbit is very tight, it may evolve directly to a UCXB. If the orbit period is a little bit longer but still below the so-called bifurcation period, the LMXBs could evolve to spider binaries, including redbacks and black widows. If the orbit is wide enough, after the mass transfer phase, a recycled MSP binary can form, with the companion being a helium star or a WD, depending on the secondary star's mass. Subsequently, the orbit shrinks due to GW emission. If the binary becomes close enough to initiate RLOF, it appears as a UCXB. Finally, UCXB form a recycled pulsar either being isolated or in a tight orbit with a very low-mass object.

1.3.2.2 Accretion induced collapse

Another important formation channel for LMXBs is related to the accretion-induced collapse (AIC) process (Canal et al., 1990; Nomoto et al., 1991; Woosley et al., 1992). An ONeMg

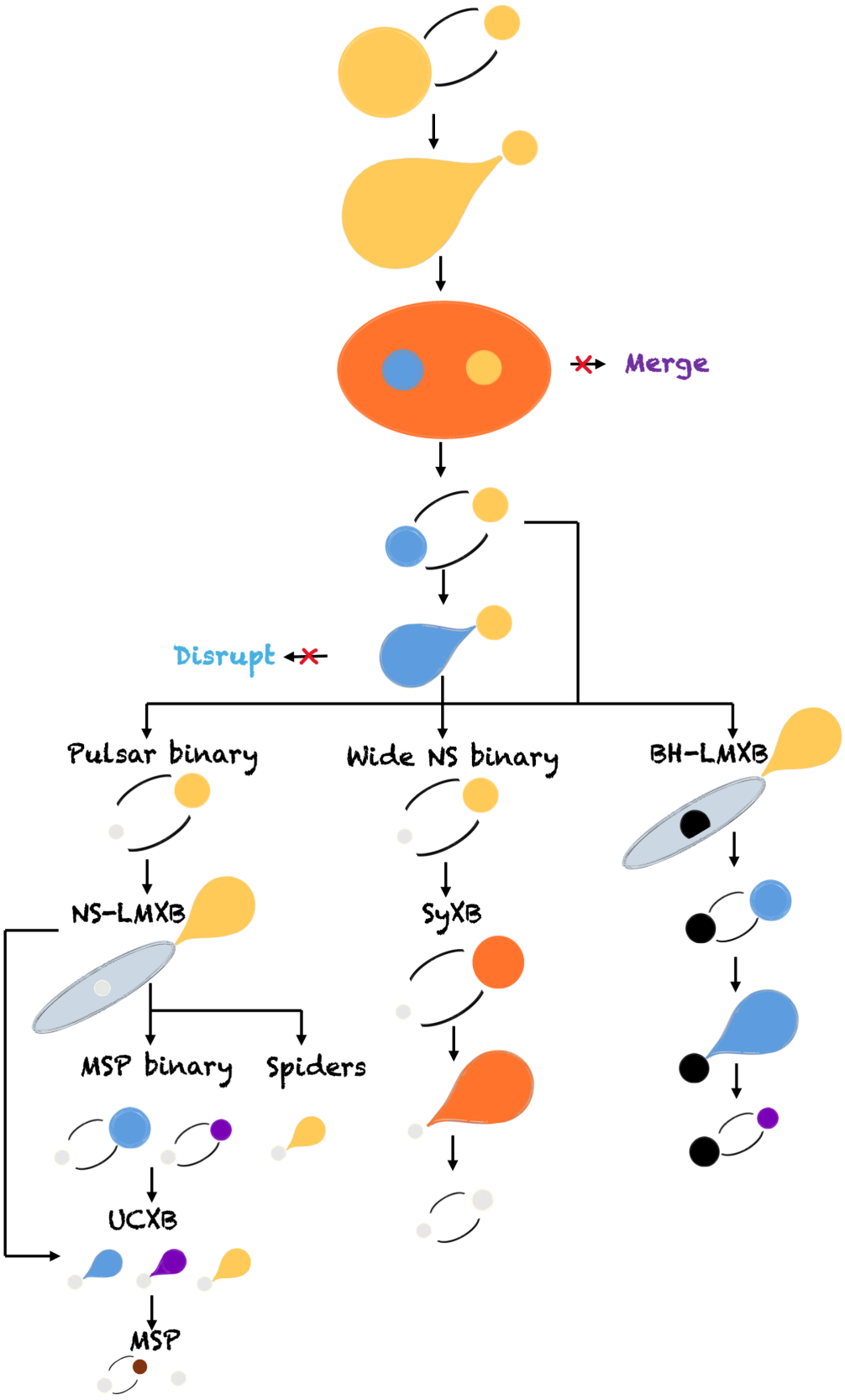

Figure 1.13: Schematic diagram of the evolutionary paths of LMXBs and pulsar binaries. Yellow and orange indicate H-rich stars in MS and post-MS stage. Blue, purple, and brown represent He-rich stars, WDs, and planetary objects, respectively.

WD or under certain circumstances, a massive CO WD, can collapse to form an NS provided that a reasonable mass transfer rate is maintained. In many ways, the AIC is not very different from ECSN. In this scenario, the primary star is not massive enough to initiate core collapse, but instead forms a massive ONeMg WD. Then, the WD accretes mass from the secondary star and triggers an AIC to form an NS. Because the orbit is tight and the kick is relatively weak, the binary remains bound. Then, RLOF is initiated again, and the binary becomes an LMXB (see Tauris et al., 2013, for a review). Moreover, it has been proposed that the formation of SyXBs can be explained by AIC in the wind-fed phase (Ablimit, 2023). The evidence for AIC includes young pulsars in old globular clusters and non-recycled, strong magnetic-field pulsars in binaries that should have experienced mass transfer.

1.4 Binary population synthesis

1.4.1 Principles of binary population synthesis

As discussed in section 1.2, stellar and binary evolution codes allow us to simulate their evolutionary path, by solving the equations of stars along with the evolution of the orbit. As the sample size of observed binaries grows, a population perspective is imperative for gaining deeper insights into stellar and binary evolution theories as well as galaxy and cosmology studies, since individual simulations have a limited scope. Astrophysicists have developed the so-called BPS technique, which aims at creating and evolving a large number of binary systems to model their populations. BPS techniques have proven invaluable for interpreting diverse binary systems within the framework of fundamental theories of stellar and binary evolution. They serve as a tool for exploring critical physical processes, such as mass transfer, CE evolution, and SN explosions, by revealing trends in model predictions and identifying limitations of the theories. Additionally, they can be used to predict population properties in systems with limited observational samples, providing guidance for future observations.

The initialization mainly includes setting up the initial mass function (IMF), the parameter space for binary properties, and the star formation history. To obtain an initial mass distribution for the primary component, an IMF–for example, those proposed by Salpeter (1955), Kroupa et al. (1993), or Kroupa (2001)–is usually adopted. The specific mass range can be tailored based on the types of binaries under investigation. The mass ratio is usually assumed to follow a flat distribution ranging from the minimum up to equal masses (Mazeh et al., 1992; Duchêne et al., 2013). Alternatively, the mass ratio may be applied with observationally guided distribution (e.g., Moe et al., 2017). The binary orbital distribution

can be described by a power-law distribution in log-space in period (Sana et al., 2013), or by a log-flat distribution in orbital separation (Abt, 1983). The initial orbital eccentricity is often assumed to be zero. Since orbital circularization is typically assumed when mass transfer occurs in most BPS codes, the initial eccentricity can be regarded as an alternation of the orbital separation distribution.

With the initialized binary parameters, BPS codes evolve a large number of binaries until the end conditions are met. The computational cost is an important factor, and BPS codes must remain computationally efficient. There are different strategies for simulating binaries. The most commonly used approach is through approximating stars with fitting formulae based on single stellar tracks (e.g., `BSE`, Hurley et al., 2002) or look-up tables (e.g.,`ComBinE`, Kruckow et al., 2018), and modeling most binary interactions with parametric methodologies. The code `BSE` was developed based on the single-star evolution (`SSE`, Hurley et al., 2000) formulae, which are derived from the stellar models computed by Pols et al. (1998). The models cover a mass range from 0.5 $M_\odot$ to 50 $M_\odot$, and are extrapolated up to 100 $M_\odot$ for `SSE`. As a result, one of the major systematic errors in `BSE` arises from the inaccuracy of massive star models. Bavera et al. (2023) has shown that `SSE` predicts the radial expansion of massive stars at solar metallicity differently than detailed models, resulting in an overestimation of mass loss from stellar winds. Since the creation of `BSE`, many BPS codes have been developed based on `SSE` and/or within the framework of `BSE` with improved input physics and customized functions. These codes include `COMPAS` (Stevenson et al., 2017; Riley et al., 2022), `COSMIC` (Breivik et al., 2020), `MOBSE` (Giacobbo et al., 2018b), and `StarTrack` (Belczynski et al., 2002; Belczynski et al., 2008). Other BPS codes include `SEVN` (Spera et al., 2015; Iorio et al., 2023), `binary_c` (Izzard et al., 2004; Izzard et al., 2006; Izzard et al., 2009), `BPASS` (Eldridge et al., 2017), `SeBa` (Portegies Zwart et al., 1996; Toonen et al., 2012), and `TRES` (Toonen et al., 2016). Among these codes, `SEVN` allows incorporating customized stellar tracks while leveraging binary physics recipes closely based on `BSE`. `BPASS` utilizes comprehensive grids of binary evolution simulations generated with a modified version of the `STARS` code. Within these `BPASS` grids, both the primary and secondary stars are tracked in detail, but they are evolved separately for computational efficiency. While the primary is evolving, the secondary star's properties are approximated using formulae based on single-star models (Hurley et al., 2000). After the primary's evolution has been fully modeled, the code then calculate the secondary's evolution.

Most of these codes model binary interaction using approximate prescriptions and parameterizations. For example, mass transfer rates are typically calculated using an approximate prescription that is a function of the mass, radius and Roche-lobe radius of the star. The

stability of mass transfer is usually determined by certain critical mass ratios that are derived from comparisons of the radial response to mass loss or directly adopting empirical radial responses for different types of stars (Vigna-Gómez et al., 2018). CE evolution is treated using the $\alpha - \lambda$ prescription. Because of the lack of detailed interior information for the stars, the $\lambda_{\rm CE}$ parameter is adopted as a constant or through fitting formulae obtained from single stars (Xu et al., 2010).

After a large set of binaries has been evolved, and following appropriate selection criteria, synthetic populations can be obtained. The population properties, including formation rates, numbers, distributions of component masses and orbital properties, can be used for predictions or compared with observations.

1.4.2 The novel binary population synthesis code – `POSYDON`

`POSYDON` (POpulation SYnthesis with Detailed binary-evolution simulatiONs) stands out among BPS codes by incorporating detailed single- and binary-star evolution models. Within the `POSYDON` framework, two single-star grids and three binary-star grids, each pre-calculated with the detailed stellar evolution code `MESA`, serve as foundational datasets. Classification and interpolation algorithms then leverage these grids, making it possible to conduct comprehensive BPS studies.

`POSYDON` grids

The `POSYDON` binary grids include three types of binary configurations: two hydrogen (H)-rich ZAMS stars (HMS-HMS), a compact object and an H-rich star at the onset of RLOF (CO-HMS), and a compact object with a helium (He)-rich ZAMS star (CO-HeMS). All modeled binaries are initially in circular orbits, and their stellar spins are assumed to be synchronized with the orbits. In addition to these three binary grids, two single-star grids, H–rich (HMS) and He-rich (HeMS), are integrated into `POSYDON`. `POSYDON` v1 (Fragos et al., 2023) contains only solar-metallicity grids. By contrast, `POSYDON` v2 (Andrews et al., 2024) expands to eight metallicities, namely $10^{-4}, 10^{-3}, 10^{-2}, 0.1, 0.2, 0.45, 1, 2\,Z_{\odot}$. Detailed information about the grids in these two versions is provided in Table 1.2, which displays the mass ranges and intervals, mass ratios, orbital period ranges and intervals, and the numbers of models.

Treatments of common envelope and core collapse

The detailed simulations stop under one of the following termination conditions: a star evolves to a late evolutionary stage, unstable mass transfer occurs, or the simulation reaches a specified maximum time. Specifically, if the central degeneracy parameter $\Gamma_{\rm c}$ of a star

Table 1.2: Summary of the single- and binary-star model grids in POSYDON v1 and v2.

Grids (v1/v2)	M_1 [$M_\odot$]	$\Delta\log_{10}(M_1/M_\odot)$	M_2 [$M_\odot$]	$\Delta\log_{10}(M_2/M_\odot)$	$P_{\rm orb}$ [days]	$\Delta\log_{10}(P_{\rm orb}/{\rm days})$	N
HMS	0.5-300	0.014	-	-	-	-	200
HeMS	0.5-80	0.055	-	-	-	-	40
HMS-HMS	6.23-120	0.025	$q = 0.05 - 0.99$	$\Delta q = 0.05$	0.7-6150	0.07	58,240
CO-HMS	0.5-120	0.12	1-35.88	0.074	1.26-3162	0.13	25,200
CO-HeMS	0.5-80	0.055	1-35.88	0.074	0.02-1117.2	0.09	39,480
HMS	0.1-300	0.0093	-	-	-	-	375
HeMS	0.5-151	0.0093	-	-	-	-	268
HMS-HMS	5.55-286	0.05	$q = 0.05 - 0.99$	$\Delta q = 0.05$	0.1-5179	0.14	23,596
CO-HMS	0.5-321	0.12	1-307	0.077	0.1-9236	0.31	13,464
CO-HeMS	0.5-192	0.15	1-307	0.077	0.02-1147	0.207	14,256

exceeds 10 (Choi et al., 2016), the star is assumed to become a WD, and the simulation is terminated. If a star reaches core depletion, defined as the helium and carbon abundances in the core respectively dropping below 10^{-6} and 10^{-2}, it is considered to be in a late stage. At that point, the star's core masses and abundances are passed to the SN step to determine the properties of the resulting remnant.

The following conditions are used to identify unstable mass transfer. First, the mass transfer rate reaches 0.1 $M_\odot$ yr^{-1}. It is expected that if the transfer rate reaches this value, it further increases to a value corresponding to a dynamical limit on the mass-loss rate for giant stars. Second, we assume unstable mass transfer when a star expands beyond L2. The material lost from L2 removes the orbital angular momentum efficiently, shrinking the orbit and triggering a runaway process (Tylenda et al., 2011; Nandez et al., 2014). Third, if both stars simultaneously fill their Roche lobes and at least one has left the MS, the system is assumed to enter a CE evolution. Fourth, for a compact-object accretor, when its photon-trapping radius (Begelman, 1979; King et al., 1999) reaches its Roche-lobe radius, mass transfer is also considered unstable. If any of these conditions is met, the binary simulation ends and the system transitions to a CE step. The CE evolution is then treated using the $\alpha - \lambda$ prescription. A key advantage of POSYDON in this context is that the binding energy parameter $\lambda_{\rm CE}$, which depends on the stellar structure and the boundary between the core and the envelope, is computed self-consistently from the star's internal structure at the onset of CE evolution, rather than relying on pre-computed fits derived from single-star models.

Detached step

After the SN step, the orbit may become eccentric due to natal kicks. Eccentricity adds another dimension, complicating the picture. Nevertheless, because the two stars are detached, there is no need to run additional MESA binary grids in eccentric orbits where no mass transfer occurs. The detached step was introduced to simulate the binaries as single stars after SN or CE in a detached phase, in order to connect different MESA binary grids

where circular orbits are assumed and mass transfer is simulated.

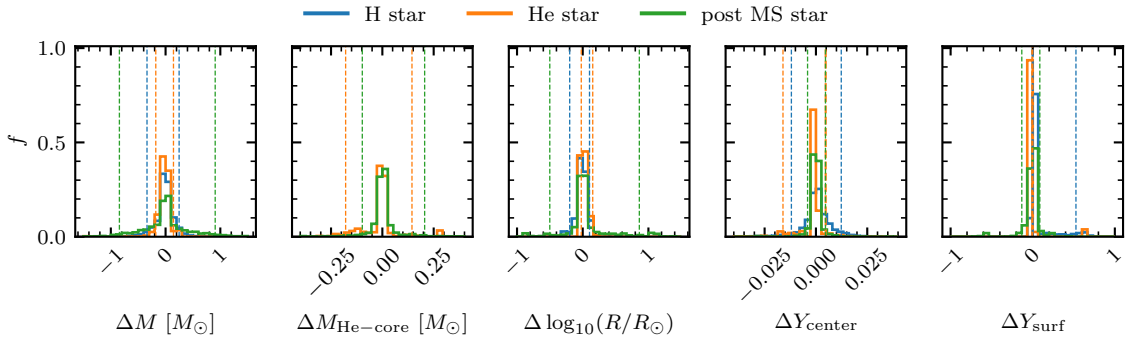

Figure 1.14: Distributions of the differences between the matched values of single-star models at the beginning of the detached step and the values from the previous step. From the left to the right, we show the differences in mass ΔM, helium core mass $\Delta M_{\mathrm{He-core}}$ and logarithm of the radius $\Delta \log_{10}(R/R_\odot)$, as well as the difference in central and surface helium abundances Y_{center} and Y_{surf}. Vertical, dashed lines from left to right indicate the 5-th and 95-th percentiles of the distributions. Credit: Fragos et al. (2023)

First, we match the non-degenerate stars from the binary grids to the closest model within the linearly interpolated single-star time series by minimizing the sum of the squares of several key parameters describing the structure of each star. For H-rich MS stars, post-MS stars, and He-rich stars, different parameters–including stellar mass, radius, central abundances, and surface abundances–are used. Then, the star's evolution follows the matched time series. The quality of the matching can be quantified by calculating the differences between the matched values of various quantities and the corresponding values from the previous step. Figure 1.14 shows the distribution of such differences in the analysis of `POSYDON` v1. It can be seen that the matching is generally good, meaning that a star in the detached phase can be represented by a single-star model in most cases. However, a small fraction of partially stripped stars cannot be well matched to single-star models, and the evolution is slightly different because the rotation of the star is not actually modeled in single star grids. These issues can be addressed in future versions by incorporating single-star models with varying rotation rates and different degrees of stripping for interpolation.

Meanwhile, the orbital separation, eccentricity, and angular velocity of the stars evolve by solving a set of coupled ordinary differential equations that govern their rates of change, taking into account mass loss, tidal effects, magnetic braking, and gravitational radiation. The detached step terminates either when the star fills its Roche lobe or reaches the end of its life in the interpolated time series.

Machine learning algorithms

The binary grids only cover a finite parameter space of binaries. In POSYDON, there are two ways to evolve an arbitrary binary. The first method is the nearest-neighbor scheme, which finds the closest binary evolutionary track within the binary grids for a given binary. The second method is through machine learning algorithms to predict the final outcome of a binary given its initial masses and orbital period. We refer to this as the initial–final interpolation. To achieve this, we train the grids to build a classifier, which predicts the mass-transfer case of a binary and its compact-object type, as well as an interpolator, which predicts the binary's properties.

Binary population synthesis with detailed modeling

As a developer of POSYDON, I contributed to its development in multiple ways. I assembled the first working version of the detached step for two non-degenerate stars, wrote the step for calculating the orbital evolution of double compact objects, and contributed to the construction of the binary grids. During the construction of POSYDON binary grids, I identified two issues within the MESA binary module related to incorrect model of reverse mass transfer and the out-of-sync updates of transfer and accretion rates when using implicit wind scheme. I implemented fixes for both issues, which ensured the robustness and consistency of our binary evolution grids.

POSYDON has three key features that distinguish it from other BPS codes. First, it models stellar rotation and angular momentum transport both within stars and in orbits with spin-orbit coupling, ensuring that the stellar rotational effects are properly incorporated and enabling a comprehensive estimation of BH spins. Second, mass transfer is computed directly using MESA rather than relying on parametric methods. The stellar adjustments such as stellar responses to mass loss or mass gain are treated, providing a more realistic modeling of binary interaction. This ensures a more accurate treatment of mass transfer phases, especially case A mass transfer, than in other codes. Third, POSYDON tracks the evolution of the stellar cores and abundance profiles taking into account binary interactions. Leveraging this access to stellar interior information, critical physical processes such as CE evolution and SN explosions can be treated in a self-consistent manner. By virtue of the powerful capabilities of POSYDON, we aim to bring BPS studies to an unprecedented level of reliability and physical accuracy.

Chapter 2

POPULATION OF WIND-FED BLACK HOLE HIGH-MASS X-RAY BINARIES

Since the first detection of GW merger events, astrophysicists have eagerly sought to learn about binary evolution through GW observations. However, among all massive binaries, only a small fraction ultimately evolves into GW sources. To gain a more complete picture, it is essential to examine all phases of binary evolution–such as the X-ray binary phase–via joint theoretical studies. As shown in Figure 1.11, double compact objects may appear as HMXBs during certain stages of their evolution. In principle, HMXBs are potential progenitors of GW sources. It is worth noting that the HMXBs and GW sources observed today are likely to be different populations of binaries. This is partly because the two distinct observation techniques probe different cosmic environments and spacetime. Moreover, due to selection effects, the observed HMXBs and GW sources could have distinct formation histories. Nonetheless, within the framework of binary evolution, they are expected to fit into a unified picture and offer us valuable insights into various physical processes that govern both single-star and binary evolution.

GW observations of BBHs and NSBHs indicate that most BHs are consistent with low spins, whereas historical spin measurements of BHs in the wind-fed BH-HMXBs generally suggest high spins. Reconciling these apparently conflicting observations remains a longstanding challenge. Although the observed systems may indeed originate from different populations, the theoretical origin of high spins still requires explanation. In this work, we explore the possibility that the BHs acquire substantial spins from super-Eddington accretion. By drawing insights from state-of-the-art super-Eddington accretion disk simulations, we aimed to investigate the role of RLOF in shaping the spin distribution of wind-fed BH-HMXBs.

Hirai et al. (2021) investigated the formation of accretion disks in wind-fed BH-HMXBs and found that such systems appear as bright X-ray sources only if the donor star's Roche-lobe filling factor exceeds approximately $80-90\%$. Building on their conclusions, we adopt this criterion in our population study of observable wind-fed BH-HMXBs. This result implies that most observed wind-fed BH-HMXBs are very close to entering, or have just exited, a RLOF phase. This proximity to RLOF provides a second motivation for examining the specific role that RLOF plays in these systems.

The manuscript presented in the following was published in *Astronomy & Astrophysics*,

referred to as Xing et al. (2025b).

A&A, 693, A27 (2025)
https://doi.org/10.1051/0004-6361/202451275

51
Astronomy & Astrophysics

Formation of wind-fed black hole high-mass X-ray binaries: The role of Roche-lobe-overflow post black hole formation

Zepei Xing[1,2,⋆], Tassos Fragos[1,2], Emmanouil Zapartas[3], Tom M. Kwan[4], Lixin Dai[4], Ilya Mandel[5,6], Matthias U. Kruckow[1,2], Max Briel[1,2], Jeff J. Andrews[7], Simone S. Bavera[1,2], Seth Gossage[8], Konstantinos Kovlakas[11,12], Kyle A. Rocha[8,9], Meng Sun[8], and Philipp M. Srivastava[8,10]

[1] Département d'Astronomie, Université de Genève, Chemin Pegasi 51, CH-1290 Versoix, Switzerland
[2] Gravitational Wave Science Center (GWSC), Université de Genève, CH1211 Geneva, Switzerland
[3] Institute of Astrophysics, FORTH, N. Plastira 100, Heraklion 70013, Greece
[4] Department of Physics, The University of Hong Kong, Pokfulam Road, Hong Kong
[5] School of Physics and Astronomy, Monash University, Clayton, VIC 3800, Australia
[6] OzGrav: The Australian Research Council Centre of Excellence for Gravitational Wave Discovery, Clayton, VIC 3800, Australia
[7] Department of Physics, University of Florida, 2001 Museum Rd, Gainesville, FL 32611, USA
[8] Center for Interdisciplinary Exploration and Research in Astrophysics (CIERA), Northwestern University, 1800 Sherman Ave, Evanston, IL 60201, USA
[9] Department of Physics & Astronomy, Northwestern University, 2145 Sheridan Road, Evanston, IL 60208, USA
[10] Electrical and Computer Engineering, Northwestern University, 2145 Sheridan Road, Evanston, IL 60208, USA
[11] Institute of Space Sciences (ICE, CSIC), Campus UAB, Carrer de Magrans, 08193 Barcelona, Spain
[12] Institut d'Estudis Espacials de Catalunya (IEEC), Carrer Gran Capità, 08034 Barcelona, Spain

Received 27 June 2024 / Accepted 27 October 2024

ABSTRACT

The three dynamically confirmed wind-fed black hole high-mass X-ray binaries (BH-HMXBs) are suggested to all contain a highly spinning black hole (BH). However, based on the theories of efficient angular momentum transport inside the stars, we expect that the first-born BHs in binary systems should have low spins, which is consistent with gravitational-wave observations. As a result, the origin of the high BH spins measured in wind-fed BH-HMXBs remains a mystery. In this paper, we conduct a binary population synthesis study on wind-fed BH-HMXBs at solar metallicity with the use of the newly developed code `POSYDON`, considering three scenarios for BH accretion: Eddington-limited, moderately super-Eddington, and fully conservative accretion. Taking into account the conditions for accretion-disk formation, we find that regardless of the accretion model, these systems are more likely to have already experienced a phase of Roche-lobe overflow after the BH formation. To account for the extreme BH spins, highly conservative accretion onto BHs is required, when assuming the accreted material carries the specific angular momentum at the innermost stable orbit. Besides, in our simulations we found that the systems with donor stars within the mass range of 10−20 $M_\odot$ are prevalent, posing a challenge in explaining simultaneously all observed properties of the BH-HMXB in our Galaxy, Cygnus X-1, and potentially hinting that the accretion efficiency onto non-degenerate stars, before the formation of the BH, is also more conservative than assumed in our simulations.

Key words. stars: black holes – stars: evolution – X-rays: binaries

1. Introduction

Black hole (BH) X-ray binaries contain a BH accreting material from a companion star generating X-ray emission. Depending on the donor star mass and accretion processes, BH X-ray binaries can be classified as low-mass X-ray binaries (BH-LMXBs) and high-mass X-ray binaries (BH-HMXBs). The BH-LMXBs consist of a low-mass donor star (~2 $M_\odot$) that transfers mass through Roche-lobe overflow (RLO) onto the BH. The BH-HMXBs typically involve a massive ($\gtrsim$10 $M_\odot$) OB-type donor star and a BH that accretes a fraction of the companion's stellar wind. Only three wind-fed BH-HMXBs have been dynamically confirmed: Cygnus X-1, LMC X-1, and M33 X-7 (we list their properties in Table 1). All of them have been observed to contain a BH with a high spin and a donor star that is still on its main sequence (MS), almost filling its Roche lobe. Nevertheless, there are several candidate BH-HMXBs, including SS433 (Seifina & Titarchuk 2010), Cygnus X-3 (Zdziarski et al. 2013), HD96670 (Gomez & Grindlay 2021), IC10 X-1 (Prestwich et al. 2007; Laycock et al. 2015), and NGC300 X-1 (Crowther et al. 2010), whose nature remains debated.

To explain why BH-HMXBs are much less numerous than Wolf-Rayet + O star binaries in our Galaxy – the latter being thought to be the progenitor of the former – it has been proposed that the binaries are detectable as BH-HMXBs only when the stellar winds carry sufficient angular momentum (AM) to form an accretion disk (e.g., Illarionov & Sunyaev 1975; Vanbeveren et al. 2020; Sen et al. 2021). More recently, Hirai & Mandel (2021), through semi-analytical modeling of the steady-state equations for asymmetric winds, found that an accretion disk is formed when the MS donor's Roche-lobe filling factor, $f_{\rm RL}$, defined as the ratio between the stellar radius and its Roche lobe radius, is $\gtrsim$0.8−0.9, providing an explanation for the high $f_{\rm RL}$ of all three known systems.

Intriguingly, based on either the disk continuum fitting or the reflection line fitting methods, the BHs in these systems are almost maximally spinning (see, e.g., McClintock et al.

⋆ Corresponding author; Zepei.Xing@unige.ch

2014; Reynolds 2014, 2021, and references therein). However, these methods are subject to potential uncertainties, which we discuss in Sect. 4.1. The binary BH (BBH) population from gravitational-wave observations indicates low aligned spins for BHs (e.g., Abbott et al. 2019, 2023; Miller et al. 2020; Roulet et al. 2021). Arguments have been made that BH-HMXBs and BBHs originate from two distinct binary populations, (Fishbach & Kalogera 2022) and due to selection effects, it is natural that these two populations show different properties (Liotine et al. 2023). Binary population synthesis (BPS) studies have shown that only a small fraction of BH-HMXBs result in BBH mergers (Neijssel et al. 2021; Gallegos-Garcia et al. 2022; Romero-Shaw et al. 2023).

However, the question of where the extreme spins come from has not yet been answered. Prescriptions of efficient AM transport within stellar interiors, such as the Tayler-Spruit (TS) dynamo (Spruit 2002), the revised prescription by Fuller et al. (2019), and the calibrated TS dynamo presented in Eggenberger et al. (2022), can explain the rotation profile of the Sun (Eggenberger et al. 2005) and the core-rotation rate of low-mass red giants and subgiants from asteroseismic measurements (Beck et al. 2012; Mosser et al. 2012; Deheuvels et al. 2014; Gehan et al. 2018). These theories predict low natal BH spins in general (Fuller & Ma 2019) but especially for the first-born BHs in binary systems (Fragos & McClintock 2015). The second-born BHs can obtain spins through tidal interactions between their progenitors and the first-born BHs, which usually occur in tight orbits following common-envelope events. In the framework of efficient AM transport, the effective inspiral spin distribution of BBHs can be reproduced in the isolated binary evolution channel (Qin et al. 2018; Bavera et al. 2020, 2021; Belczynski et al. 2020; Olejak & Belczynski 2021).

Looking at BH-HMXBs, Qin et al. (2019) investigated two possible scenarios that can produce spinning BHs, namely the case A mass transfer (MT) channel and the chemical homogeneous evolution channel, and concluded that only if the internal AM transport is inefficient during the late evolution of the progenitor stars can high-spin BHs be produced. The scenario is not yet supported by any other observational evidence or theoretical arguments. Another way for BHs to acquire significant spins is through super-Eddington accretion (Moreno Méndez 2011). The observed isotropic-equivalent X-ray luminosity of ultraluminous X-ray sources (e.g., Winter et al. 2006; Kovlakas et al. 2020) can exceed the Eddington limit by a few orders of magnitude. However, the possible geometrical beaming of the X-ray emission means that the actual accretion rate onto the BH does not have to be significantly super Eddington (King et al. 2001; Poutanen et al. 2007; Kovlakas et al. 2022). Qin et al. (2022) explored the possibility of highly super-Eddington accretion and its impact on BH spin in the context of BH-HMXBs. This study, however, was limited in that they only considered one specific binary configuration, they did not model the evolution of the binary prior to the BH formation, and they neglected the fact that observed BH-HMXBs, such as Cygnus X-1, are currently detached.

In this work, we use the newly developed BPS code POSYDON (Fragos et al. 2023), which incorporates extensive grids of detailed stellar structure and binary evolution models, to investigate the population of wind-fed BH-HMXBs. Among other advantages, detailed binary evolution simulations can accurately model the case A MT. The case A MT phase after BH formation is of great importance for the formation of wind-fed BH-HMXBs, but it is often treated poorly in rapid BPS codes due to the lack of information about the internal structure of stars (Dorozsmai & Toonen 2024).

The paper is organized as follows. In Sect. 2, we briefly introduce the new binary-star model grids and the details of our BPS study. In Sect. 3, we present the results of our binary models and population properties. We discuss the implications of this work on wind-fed BH-HMXBs in Sect. 4 and summarize the conclusions of this paper in Sect. 5.

2. Method

For all the computations presented in this paper, we used the publicly available BPS code POSYDON[1], which incorporates single- and binary-star model grids at solar metallicity simulated with the stellar evolution code Modules for Experiments in Stellar Astrophysics (MESA, Paxton et al. 2011, 2013, 2015, 2018, 2019; Jermyn et al. 2023). The specific details of the stellar and binary physics employed in the production of pre-calculated grids are outlined in Fragos et al. (2023). Here we highlight the wind prescriptions and the assumptions for mass accretion onto non-degenerate stars adopted in our models. We utilized the Dutch scheme in MESA for stars with an initial mass exceeding 8 $M_\odot$. Specifically, we applied the wind-loss prescription of de Jager et al. (1988) for cool stars with effective temperatures below 10 000 K and the Vink et al. (2001) scheme for hot stars with effective temperatures above 11 000 K. For temperatures between these two thresholds, we implemented a linear interpolation of the wind-loss rates. Additionally, for hot stars with a surface hydrogen fraction below 0.4, we adopted the Wolf-Rayet wind prescription proposed by Nugis & Lamers (2000). For accretion onto a non-degenerate star, we accounted for the rotation of the accretor. The transferred material, carrying AM, spins up the outer layers of the accretor, differentiating between ballistic and Keplerian disk MT scenarios (de Mink et al. 2013). As the accretor's rotational velocity increases, the accretion rate is reduced by the enhancement of the stellar winds (Langer 1998). Crucially, accretion halts when the accretor approaches critical rotation, with its stellar winds intensifying as needed to maintain sub-critical rotation.

By default, in POSYDON, accretion onto BHs is assumed to be Eddington limited. As part of this work, beyond the publicly available grids, we computed two additional binary-star model grids of binaries consisting of a compact object and a hydrogen-rich MS star (CO-HMS grids), where we varied the accretion efficiency onto BHs. The two additional grids share the same initial parameters and input physics with the original grid. In the first new grid, we consider the limiting case of the fully conservative accretion onto the BH, while in the second one, the accretion efficiency η was established based on general relativistic radiation magnetohydrodynamic (GRRMHD) simulations (Kwan et al., in prep.). In that study, the authors carried out a series of simulations of super-Eddington disks in the magnetically arrested disk (MAD) state following the setup in Dai et al. (2018) and Thomsen et al. (2022) but around stellar-mass BHs. They varied the BH mass, spin and accretion rate $\dot{M}_{\rm acc}$ achieved in equilibrium states across different simulations to explore how these parameters affect the energy output and outflow properties. Based on the simulation results, they obtained an averaged fit for the relation between η and the MT rate $\dot{M}_{\rm tr}$ (which is assumed to

[1] We utilized the version of the POSYDON code identified by the commit hash 8602bc3, available at https://github.com/POSYDON-code/POSYDON/, along with the POSYDON v1.0 dataset published at https://zenodo.org/records/14205146 and the dataset assuming super-Eddington accretion published at https://zenodo.org/records/14216817.

Table 1. Properties of wind-fed BH-HMXBs.

BH-HMXB	$M_{\rm BH}$ [$M_\odot$]	$M_{\rm donor}$ [$M_\odot$]	$P_{\rm orb}$ [d]	$\chi_{\rm BH}$	$f_{\rm RL}$	$L_{\rm x}$ [erg s^{-1}]	Z[$Z_\odot$]	Reference
Cygnus X-1	21.2 ± 2.2	$40.6^{+7.6}_{-7.1}$	5.60	$0.95^{+0.04}_{-0.084}$	0.997	2.1×10^{37}	$\gtrsim$1.0	1, 2, 3, 4
LMC X-1	10.91 ± 1.41	31.79 ± 3.48	3.91	$0.897^{+0.077}_{-0.176}$	0.971	2.3×10^{38}	~0.3	4, 5
M33 X-7	$11.4^{+3.3}_{-1.7}$	38^{+22}_{-10}	3.45	0.84 ± 0.05 [(a)]	0.899	$(0.5-2) \times 10^{38}$	0.1–0.5	6, 7, 8, 9

Notes. [(a)]Ramachandran et al. (2022) updated a BH spin of ≈0.6. (1) Orosz et al. (2011); (2) Shimanskii et al. (2012); (3) Miller-Jones et al. (2021); (4) Draghis et al. (2024); (5) Orosz et al. (2009); (6) Pietsch et al. (2006); (7) Orosz et al. (2007); (8) Liu et al. (2008, 2010); (9) Ramachandran et al. (2022).

equal the sum of the mass accretion rate and the outflow rate obtained in the GRRMHD simulation):

$$\eta(\dot{m}) \equiv \frac{\dot{M}_{\rm acc}}{\dot{M}_{\rm tr}} = 0.33\,(\dot{m})^{-0.08}, \tag{1}$$

for $\dot{m} \geq 10$, where $\dot{m}$ is the MT rate in units of the Eddington accretion rate $\dot{M}_{\rm Edd}$. In cases where $0 < \dot{m} < 10$, we adopted an accretion rate of $\min(\dot{M}_{\rm tr}, 10\,\dot{M}_{\rm Edd}\,\eta(10))$. Generally, η ranges within 10% and 30% and is inversely correlated with $\dot{M}_{\rm tr}$.

For our synthetic HMXB population models, we simulated 500 000 binaries for each accretion model, starting from two stars at zero-age MS. The primary star masses range within 10 and 120 $M_\odot$, with the distribution determined by the initial mass function from Kroupa (2001). The secondary masses fall within the interval of 7 and 120 $M_\odot$, following a flat distribution from the minimum to the primary star mass. The initial orbital period distribution follows Sana et al. (2013) from 1 d to 6000 d, with an extension down to 0.75 d, being uniform in logarithmic space. We identified wind-fed BH-HMXBs by searching for detached binaries containing a BH and a companion star with a Roche-lobe filling factor, $f_{\rm RL}$, falling between $0.9 \lesssim f_{\rm RL} < 1$, which is valid across most of the parameter variations explored by Hirai & Mandel (2021). We set a minimal mass of 10 $M_\odot$ for the companion star during the wind-fed phase. In all presented population models, we used the nearest-neighbor scheme for the interpolation between models in a grid (see Sect. 7 in Fragos et al. 2023).

To determine the explodability of the pre-supernova core and the BH mass from the core properties, we adopted the Patton & Sukhbold (2020) prescription and supernova engine from Sukhbold et al. (2016). We assumed the supernova kick velocities of the BHs from core-collapse supernova follow a Maxwellian distribution with a velocity dispersion of $\sigma_{\rm CCSN} = 265\,{\rm km\,s^{-1}}$ (Hobbs et al. 2005), rescaled by a factor of $1.4\,M_\odot/M_{\rm BH}$. The natal spin of a BH is calculated based on the internal rotational profile of the BH progenitor star, right before core collapse (see Sect. 8.3.4 in Fragos et al. 2023). The further evolution of the BH spin parameter $\chi_{\rm BH}$ is calculated by assuming the accreted material carries the specific AM at the innermost stable circular orbit (ISCO). After the accretion of an infinitesimal mass, the dimensionless BH spin parameter $\chi_{\rm BH,f}$ can be calculated as (Bardeen 1970):

$$\chi_{\rm BH,f} = \frac{r_{\rm ISCO,i}^{1/2}}{3}\frac{M_{\rm i}}{M_{\rm f}}\left\{4 - \left[3\,r_{\rm ISCO,i}\left(\frac{M_{\rm i}}{M_{\rm f}}\right)^2 - 2\right]^{1/2}\right\}, \tag{2}$$

where $M_{\rm i}$ and $M_{\rm f}$ are the BH masses before and after accretion, respectively – with $(M_{\rm f} - M_{\rm i}) \ll M_{\rm f}$ – and $r_{\rm ISCO,i}$ is the initial normalized ISCO radius that can be calculated as $r_{\rm ISCO,i} = 3 + Z_2 - [(3-Z_1)(3+Z_1+2Z_2)]^{1/2}$, with $Z_1 = 1 + (1-\chi_{\rm BH,i}^2)^{1/3}[(1+\chi_{\rm BH,i})^{1/3} + (1-\chi_{\rm BH,i})^{1/3}]$ and $Z_2 = (3\chi_{\rm BH,i}^2 + Z_1^2)^{1/2}$. The BH spin is updated at every timestep for the binary-star models in the CO-HMS grid.

To estimate the X-ray luminosity of the wind-fed BH-HMXBs, we calculated the wind mass accretion rate $\dot{M}_{\rm w,acc}$ onto the BHs based on the results of Hirai & Mandel (2021), who integrated the mass flux through the accretion radius in their simulations. The mass accretion fraction, defined as the ratio of the mass accretion rate to the total mass-loss rate from the donor star, exhibits a similar trend as the Bondi–Hoyle accretion (Bondi & Hoyle 1944), although it is subject to large model uncertainties related to wind acceleration parameters and Eddington factors (Hirai & Mandel 2021). As a rough estimate, we adopted the values of the mass accretion fraction at $f_{\rm RL} \to 1$ from Hirai & Mandel (2021) based on their reference parameter configuration, and subsequently interpolated or extrapolated across various mass ratios. Thus, the X-ray luminosity is given as

$$L_{\rm x} = \epsilon \dot{M}_{\rm w,acc} c^2, \tag{3}$$

where $\epsilon = 0.1$ is the radiative efficiency of accretion.

3. Results

3.1. Individual wind-fed BH-HMXBs

We first illustrate a reference binary-star evolutionary model that at some point in its evolution appears as a bright wind-fed BH-HMXB system. The reference binary initially consists of a primary star of 34.9 $M_\odot$ and a secondary star of 28.7 $M_\odot$ with an orbital period of 10.4 d. The binary went through a case A MT phase and subsequently a case B MT phase. The primary star formed a BH of 12.2 $M_\odot$ with an initial spin of 0.047. The secondary lost mass due to stellar winds but gained ≈0.8 $M_\odot$ from accretion. In Figure 1, we show the evolution of the binary from ≈0.3 Myr before it entered the wind-fed HMXB phase until the stage when the donor star undergoes significant contraction during its helium-burning phase. One can see that as the donor star evolves, it keeps expanding until it fills its Roche lobe. It stays at the wind-fed HMXB phase for a short period of ≈0.1 Myr before the RLO phase. After a fast RLO phase, the donor star loses nearly half of the envelope mass, and its surface helium mass fraction increases by approximately a factor of two. This is consistent with the observations of Cygnus X-1, where the donor star's surface helium abundance is enhanced by more than a factor of two (Shimanskii et al. 2012). The donor star's center helium mass fraction increased to 0.9, indicating that the star is approaching the end of its MS. At this stage, the change in the hydrogen and helium abundance profiles of the partially stripped star leads to changes in the mass-radius relation during the MS (see, e.g., Quast et al. 2019; Farrell et al. 2022). The donor star

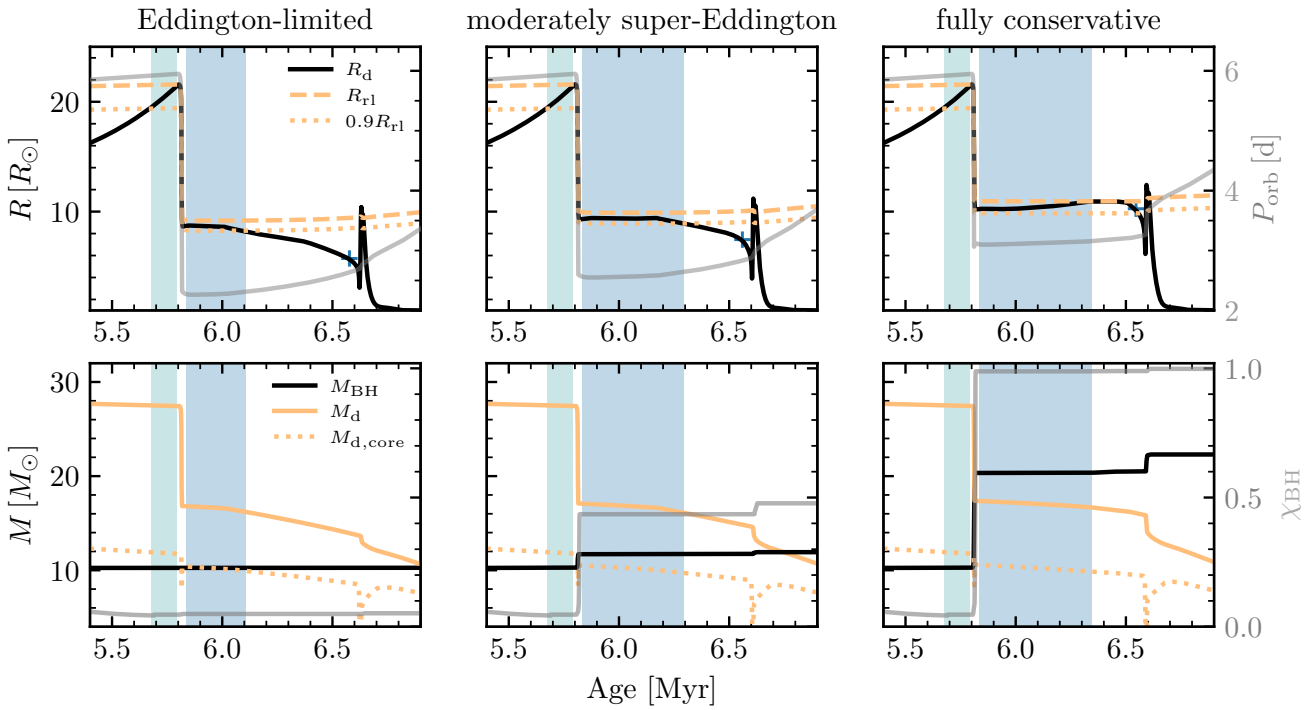

Fig. 1. Evolution of an example binary through the wind-fed HMXB phase under three BH accretion scenarios. The top panels show the evolution of the donor star radius (black solid line), Roche lobe radius (orange dashed line), 0.9 times the Roche lobe radius (orange dotted line), and orbital period (gray solid line). The green and blue areas indicate the duration of the wind-fed BH-HMXB phase before and after MT via RLO, respectively. The plus symbol denotes the end of the MS for the donor star. The bottom panels show the evolution of the BH mass (black solid line), donor star mass (orange solid line), donor star convective core mass (orange dotted line), and BH spin (gray solid line).

contracts due to the mass loss, and the binary becomes detached again. Then, the donor star stays very close to the Roche lobe radius, and the binary appears as a wind-fed HMXB for a longer period of ≈0.3−0.5 Myr. Under the assumption of Eddington-limited accretion, the BH barely accretes any mass during the fast MT phase. Alternatively, the BH accretes ≃2 $M_\odot$ and spins up to $\chi_{BH} \approx 0.45$, assuming the moderately super-Eddington accretion scenario, while it reaches a nearly maximum spin with fully conservative accretion. Because the transferred material that is not accreted by the BH leaves the system and carries away the BH's specific orbital AM, the Eddington-limited accretion leads to the largest binary orbital shrinkage due to MT. Moreover, Eddington-limited accretion results in the most significant stripping of the envelope, which subsequently leads to the quickest introduction of the Wolf-Rayet wind. Consequently, the duration of the second wind-fed phase is the shortest for the Eddington-limited accretion scenario. In the scenario of fully conservative accretion, the donor star experiences the least stripping and continues expanding after the fast RLO. As a result, following a long wind-fed phase, the binary enters a second slow RLO phase during the late MS stage of the donor star. Regardless of the differences, for all three accretion scenarios, the binary spends more time as an observable wind-fed HMXB after the RLO phase, rather than before.

3.2. Population of wind-fed BH-HMXBs

The individual binary models described in Sect. 3.1 provided us with some insights into the formation of wind-fed BH-HMXBs. However, it is a population study that can reveal whether the features identified in the evolution of a few individual binary models are representative of the whole population and would allow us to evaluate their significance. Binaries that remain in a bright wind-fed BH-HMXB phase over a longer period of time are more likely to be detected. Consequently, we present distributions of the population properties for wind-fed BH-HMXBs in our simulations, weighted by the duration of the wind-fed HMXB phase for each binary.

While in Sect. 3.1 we describe the evolutionary history of one reference binary, several variations of evolutionary pathways are present in our BH-HMXB population models. For the moderately super-Eddington accretion model, for example, we found that prior to BH formation, 48.3% of binaries went through both case A and case B MT, 21.6% only experienced case A MT, 11.9% avoided any MT, 11.6% underwent case B MT, and 6.5% entered a contact phase. The contact phase involves two MS stars in a close orbit and remains stable during MT. In `POSYDON`, we treated it using the `contact` MT scheme within `MESA`, following Marchant et al. (2016). The first two channels dominate the population, characterized by similar initial conditions. The binaries that avoided MT contain a relatively massive primary star above ≈60 $M_\odot$ (Bavera et al. 2023). However, due to strong stellar winds, the BHs originating from these massive stars do not exhibit a significantly different mass distribution. Among these channels, the case B MT channel is the only one showing a longer pre-RLO duration. These binaries tend to have wide orbits before RLO and more evolved secondary stars, resulting in a shorter post-RLO wind-fed phase. We display the fractions of the evolutionary pathways for all three accretion scenarios in Table A.1 in Appendix A.

Figure 2 shows the expected distributions of orbital periods, component masses, BH spins, and X-ray luminosity for an observable wind-fed BH-HMXB population under the moderately super-Eddington accretion model. The figure distinguishes

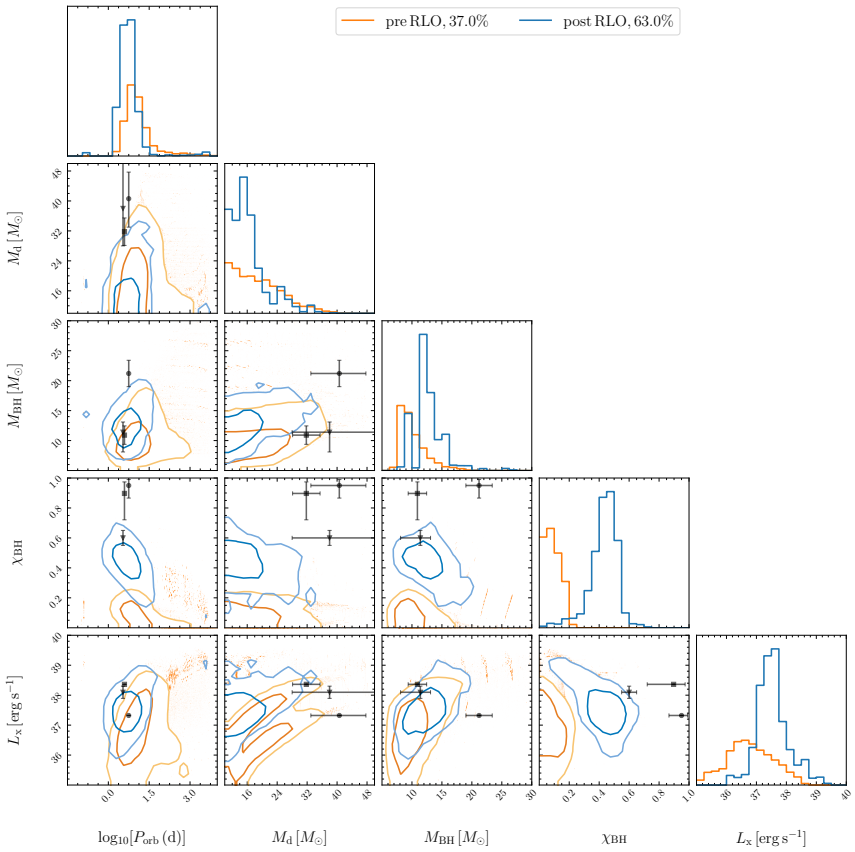

Fig. 2. Corner plot showing the time-weighted distributions of the properties of wind-fed BH-HMXBs from the moderately super-Eddington accretion scenario. The dark and light blue contours represent the 68% and 95% confidence regions, respectively, for the orbital period, donor star mass, BH mass, BH spin, and X-ray luminosity of systems after RLO. Similarly, the dark and light orange contours are for systems before RLO. The black dot, square, and triangle with error bars indicate the positions of Cygnus X-1, LMC X-1, and M33 X-7, respectively.

wind-fed BH-HMXBs that are observable before and after an RLO phase, respectively shown with orange and blue colors. Notably, there is a higher probability of observing a wind-fed BH-HMXB after the occurrence of MT via RLO, constituting 63% of the total duration. Romero-Shaw et al. (2023) also mention that in their BPS models, some binaries engage in a second wind-fed BH-HMXB phase after MT via RLO when the mass ratio is close to unity. Our detailed binary models show that when weighted by duration, the binaries that are in the post-RLO wind-fed BH-HMXB phase are predominant, which are characterized by a broader range of mass ratios. This can be seen in the subplot of M_d versus M_{BH} in Figure 2, where the mass ratio can reach approximately two. Compared to rapid BPS codes, which typically move across single stellar tracks during MT phases, `POSYDON` models the readjustment of mass-losing stars. Consequently, the partially stripped MS donor stars can shrink more substantially than rapid BPS codes generally predict, leading to a higher contribution from the post-RLO wind-fed BH-HMXB phase. The wind-fed BH-HMXB phase following RLO onto the BH constitutes an even higher fraction (almost 80% by duration) of bright BH-HMXBs, with X-ray luminosities above $10^{37}\,\mathrm{erg\,s^{-1}}$ (see Appendix D).

As the MS donor stars should be in close orbits, nearly filling the Roche lobes, the majority of the binaries exhibit orbital periods of ∼1−20 d, which is anticipated. The binaries that are in wide orbits extending to thousands of days in period contain post-MS donor stars. Those supergiant donor stars evolve much faster than MS stars, resulting in small contributions to the whole population. A smaller fraction of stripped stars, fitting in close orbits with orbital periods less than 1 d, meet the requirement after experiencing common envelope evolution. Overall, MS donor stars account for ≈90% of the whole population. However, it is important to note that Hirai & Mandel (2021) focused on line-driven winds from MS stars, and their conclusions about disk formation are only applicable to massive MS stars. Post-MS stars may have less stringent conditions for disk formation. Nevertheless, our population results indicate that post-MS donor stars are unlikely to make significant contributions due to their short evolutionary timescales.

Regarding the donor star masses, there is a clear difference between the observations and the simulation samples. The three observed binaries contain donor stars above $\approx 30\,M_\odot$, while majority of donor stars are below $\approx 20\,M_\odot$ in our simulations. The three observed BH-HMXBs have different metallicities. As a result, direct comparison of donor star masses is not robust, as the simulations were conducted at solar metallicity. The implications of the distribution of the donor star masses are discussed in Sect. 4. The donor stars are mostly close to the terminal-age MS. We have included the distributions of the central and surface helium abundance of the donor stars in Appendix B.

The BH masses in the wind-fed BH-HMXB population are mostly within the range of ∼8−17 $M_\odot$, and moderately super-Eddington accretion has increased the BH masses by a few solar masses compared to their birth values. For the BH spins, a bimodal distribution is evident, with the two peaks corresponding to the population before and after RLO. Finally, we show

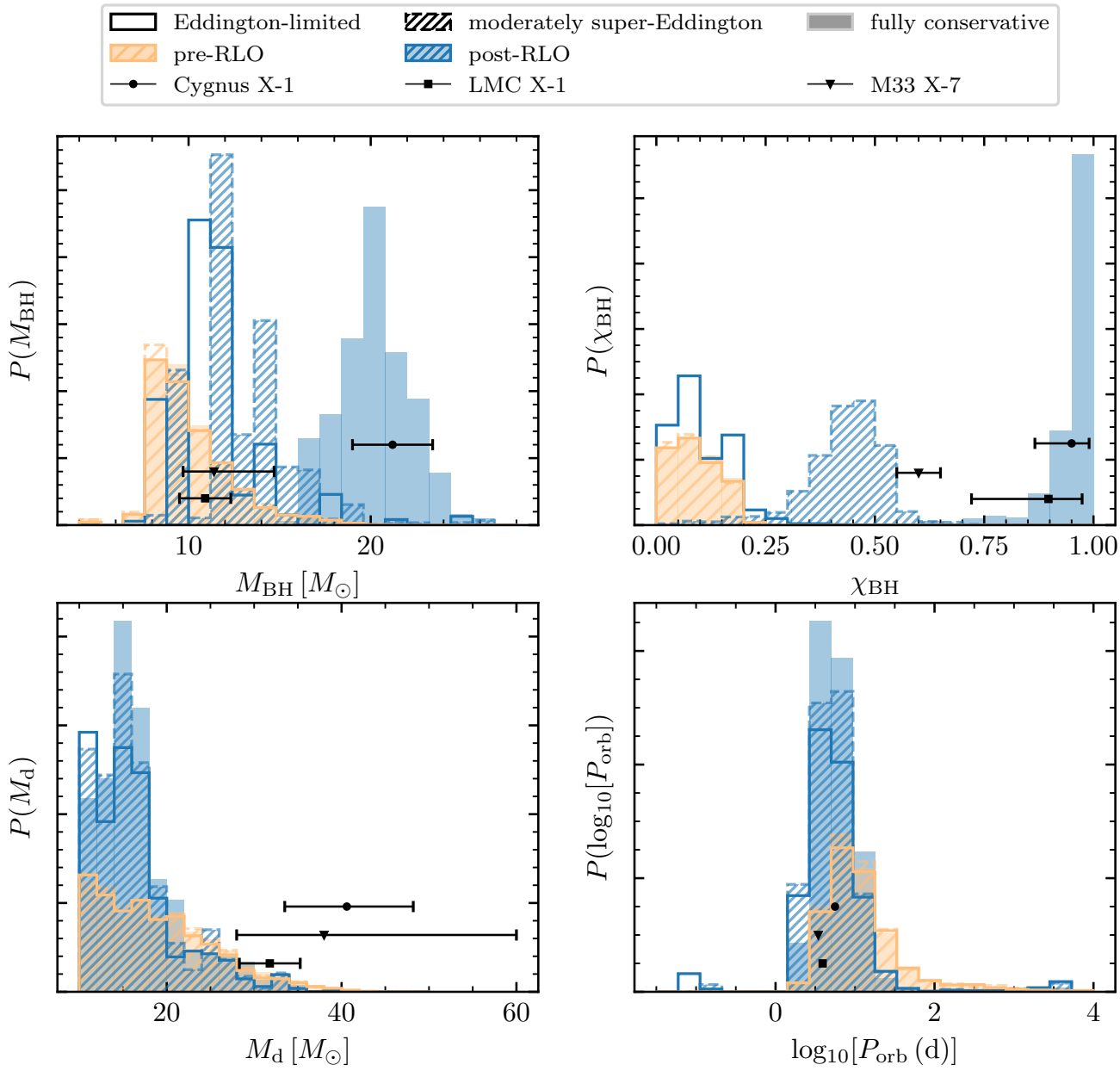

Fig. 3. Time-weighted probability distributions of the BH mass (top left), BH spin (top right), donor star mass (bottom left), and orbital period (bottom right) in wind-fed BH-HMXBs. The blue and orange colors indicate post-RLO and pre-RLO sub-populations, respectively. The unfilled bins, hashed bins, and filled bins represent the Eddington-limited, moderately super-Eddington, and fully conservative accretion scenarios, respectively. The black dot, square, and triangle with error bars, placed at arbitrary probability values, respectively indicate the properties of Cygnus X-1, LMC X-1, and M33 X-7.

a rough estimate of the X-ray luminosity, acknowledging the model uncertainties associated with the accretion fraction calculated in Hirai & Mandel (2021). We find that on average the post-RLO sub-population exhibits higher X-ray luminosities compared with the pre-RLO one. This is a result of the fact that on average the post-RLO sub-population has stronger stellar winds and higher mass ratios ($q = M_{\rm BH}/M_{\rm d}$) compared to the pre-RLO one.

The HMXB population properties resulting from the other two accretion models can be found in Appendix C. The most notable distinctions caused by accretion are evident in BH masses and spins. In Figure 3, the top panels show the time-weighted probability distributions of the BH mass and spin for the three accretion scenarios, distinguishing between the wind-fed phases before and after MT via RLO. In the pre-RLO HMXB sub-populations, the distributions are the same, as expected. Most of the BH masses are below $\approx 15\,M_\odot$, and the spins are below ≈ 0.2. In the case of Eddington-limited accretion, the BH mass and spin ranges remain nearly unchanged after the RLO, but the mean of the BH mass shifts toward higher values. The higher normalization of the distribution denotes that on average the duration of the post-RLO wind-fed HMXB phase is longer, and that the probability of observing a wind-fed BH-HMXB after it has experienced an RLO phase is higher. Moderately super-Eddington accretion slightly increases the BH masses and spins up the BHs to a range of $\chi_{\rm BH} \sim 0.2$–0.6. For fully conservative accretion, a bimodal distribution of BH masses emerges, as the BHs could accrete a substantial amount of mass through

RLO to be in the range of ∼15−25 $M_\odot$. After accretion, BH spins become extremely high, exceeding ≈0.9 for a majority of them. In the bottom panels of Figure 3, we present the probability distributions of the donor star mass and the orbital period in which the three scenarios exhibit no significant differences. The fully conservative scenario leads to more stable MT, resulting in the disappearance of stripped stars coming from common envelope evolution. Regardless of the accretion scenarios, the total duration of the wind-fed BH-HMXB phase following MT via RLO is always longer than that before MT. The fraction of post-RLO duration relative to the total duration is greater than 60% for all three accretion scenarios.

4. Discussion

4.1. Black hole spins

Our study has shown that, assuming efficient AM transport inside stars, the BHs in wind-fed BH-HMXBs are born with spins $\lesssim$0.2. Eddington-limited accretion does not lead to significant changes in the spins. The moderately super-Eddington accretion model can produce BHs with spins of $\chi_{\rm BH} \sim 0.3$–0.6, whereas the fully conservative MT can spin up most of the BHs to extreme spins if the accreted material carries the specific AM at ISCO. It is evident that explaining the observed BH spins in BH-HMXBs poses a challenge in the absence of substantial accretion onto the BHs. Even when considering the impact of supernova processes on the natal BH spins, such as those arising from slow ejecta (Schrøder et al. 2018) or shock instability (Moreno Méndez & Cantiello 2016), the attainment of extreme spins remains elusive. Batta et al. (2017) found that BHs with high spins of ∼0.8 can be produced, but only if the fallback material reaches the position of the companion star and extracts AM from the orbit.

The moderately super-Eddington accretion model is also insufficient to reproduce the extreme BH spins in BH-HMXBs. In the GRRMHD simulations used to estimate the BH accretion efficiency for our moderately super-Eddington model, ordered magnetic fields are shown to thread the super-Eddington disks. These disks eventually enter the MAD state, where the AM carried by the transferred material near the BH is less than the AM at the ISCO (e.g., Lowell et al. 2024). Therefore, the increase in BH spins in our simulations should be considered as an upper limit. Additionally, BHs fed by MADs launch powerful jets that can effectively spin down the BHs when the spin is very large (Tchekhovskoy et al. 2012; Lowell et al. 2024). If the disks around the BHs in HMXBs easily reach the MAD state, it naturally excludes the possibility that the AM of the BH is obtained through gas accretion. However, if the disk does not contain enough magnetic flux to enter a MAD state, the accretion process can spin up the BH to a very high equilibrium spin value (Gammie et al. 2004). Such a disk does not have significant magnetic pressure to power magnetic outflow, and it is expected that BHs accrete a higher fraction of the disk gas from the non-MAD state super-Eddington disks, which leads to higher accretion efficiency and thus higher BH spins. In the fully conservative accretion model, we find that a large fraction of BHs accreted more material than their initial masses, indicating that the accretion is more than adequate to produce extreme spins.

It is essential to note that the two primary methods for measuring BH spins in HMXBs may be susceptible to systematic uncertainties (Taylor & Reynolds 2018; Salvesen & Miller 2021; Falanga et al. 2021) and model dependency (Belczynski et al. 2024; Zdziarski et al. 2024a). For example, Zdziarski et al. (2024b) argue that when considering a warm, optically thick, thermal Comptonizing layer on top of the disk, the spin of Cygnus X-1 is measured to be low, $\chi_{\rm BH} \lesssim 0.3$. Yet, if the extreme measured spins are real, explaining them in the context of super-Eddington accretion requires that mass and AM accretion efficiencies higher than those predicted by GRRMHD simulations of MAD-state super-Eddington disks be considered.

If both the mass accretion and AM transport to BHs are efficient enough to produce highly spinning BHs, the properties of coalescing BBH populations would also likely be influenced. During the evolution of merging BBHs, RLO accretion onto the first-born BH is anticipated. The BHs can undergo spin-up due to efficient accretion. In this case, we would not expect the first-born BHs to exhibit nearly zero spins in BBH mergers. Shao & Li (2022) employed mildly super-Eddington accretion of case A MT onto BHs, highlighting its capability to account for the observed highly spinning BHs in BBH mergers. Bavera et al. (2021) found that highly conservative accretion onto BHs effectively reduces the contribution from the stable MT channel for BBH mergers, as the binaries do not shrink sufficiently during MT to coalesce due to gravitational waves within the Hubble time. However, most rapid BPS codes, such as `COSMIC`, which was utilized by Bavera et al. (2021) to model the MT phase, are recognized for their inadequate treatment of case A MT (Dorozsmai & Toonen 2024). In contrast, BPS codes that utilize detailed binary models and assume fully conservative accretion onto BHs (e.g., Briel et al. 2023) indicate that the stable MT channel remains viable. However, a direct comparison between the models presented in these studies should be done with caution, as they also differ in several other key physics assumptions. The specific properties of BBHs, the distribution of effective inspiral spins, and their formation channels under efficient BH accretion scenarios should be investigated in future studies.

4.2. Donor star masses

The three observed wind-fed BH-HMXBs exhibit donor stars with masses $\gtrsim$30 $M_\odot$. In our population studies, we found that donor stars within ∼10−20 $M_\odot$ are expected to be prevalent in wind-fed BH-HMXBs at solar metallicity. One caveat in comparing our population models to the observed properties of the three known wind-fed BH-HMXBs is that our population models assume solar metallicity, while the observed systems have varied metallicities. Specifically, M33 X-7 has been suggested to have a metallicity between 0.1 $Z_\odot$ (Orosz et al. 2007) and 0.5 $Z_\odot$ (Ramachandran et al. 2022). Similarly, LMC X-1 is expected to have sub-solar metallicity, consistent with the Large Magellanic Cloud metallicity. For these two systems, comparisons with our simulations are not straightforward, as lower metallicities can lead to the formation and survival of more massive stars. For Cygnus X-1, however, a solar or even a supersolar metallicity (Shimanskii et al. 2012) is suggested, making its 40 $M_\odot$ donor star hard to reconcile with our simulations (but see discussion in Neijssel et al. (2021)).

The prevalence of ∼10−20 $M_\odot$ stars in our simulations can be explained as follows. Firstly, the accretion onto non-degenerate stars in `POSYDON` is regulated by stellar rotation, typically leading to low accretion efficiency (Fragos et al. 2023). Consequently, the secondary stars generally do not gain substantial mass before the BH formation. Such inefficient accretion has been suggested to prevent the formation of merging NS–BH with first-born NSs (Xing et al. 2024) and potentially contributes to discrepancies between the predicted and observed Be

X-ray binary donor mass distributions (Vinciguerra et al. 2020; Akira Rocha et al. 2024). In the case of wind-fed BH-HMXBs, if the mass accretion efficiency is higher during earlier evolutionary stages, the donor star could have accreted more mass before BH formation, potentially alleviating the tension between our simulations and the observations. Certainly, increased mass accretion efficiency could also lead to a wider orbit, with less material removing orbital AM, which potentially influences the subsequent evolution of the binary and thus the properties of the HMXB. However, AM loss during MT between non-degenerate stars remains highly uncertain (e.g., MacLeod & Loeb 2020) and different treatments can alter the orbital evolution (e.g., Sen et al. 2022) and MT stability (Willcox et al. 2023). Whether the ejected material forms a circumbinary disk (e.g., Wei et al. 2024; Valli et al. 2024) also affects the orbital evolution. A comprehensive study combining mass accretion and AM loss is needed in order to fully understand the effects of MT on the donor star's mass. Such studies are currently limited with POSYDON, as computing multiple grids of detailed binary evolution models is expensive. Using rapid BPS codes with parametric methods provides a simpler way to explore the trends arising from these variations (Romero-Shaw et al. 2023; Willcox et al. 2023).

Secondly, at solar metallicity, when the primary star becomes a BH, the secondary star should have lost a significant fraction of its mass through stellar winds if it was initially a massive star $\gtrsim 40\,M_\odot$. Moreover, many BH-HMXBs should be in the second wind-fed phase after the donor stars have transferred mass to the BHs through RLO. Romero-Shaw et al. (2023) produced wind-fed BH-HMXBs with donor stars that can reach $\sim 70\,M_\odot$ at solar metallicity. In our simulations, when the BH forms, the massive donor star has lost a substantial amount of mass due to stellar winds and MT, reducing its mass to below $\approx 50\,M_\odot$. A major difference arises from the modeling of stellar winds of massive stars at the MS stage. We found that massive stars $\gtrsim 80\,M_\odot$ at solar metallicity have strong winds that can deplete the hydrogen envelope and induce Wolf–Rayet winds during their MS stage (Bavera et al. 2023). As a result, the maximum donor star mass in our simulations is below $50\,M_\odot$.

Moreover, according to the initial mass function, the number of low-mass stars surpasses the number of high-mass stars. With a flat distribution of the initial mass ratio and without any selection effect on the donor stars, it is natural to expect a prevalence of $\sim 10-20\,M_\odot$ donor stars as they are more common and have longer lifetimes compared with a $\sim 40\,M_\odot$ star.

The differences between modeled and observed donor star masses might indicate that certain physical assumptions or treatments in our stellar and binary evolution are not robust. Wind prescriptions, mass accretion efficiency for non-degenerate stars, and AM loss from non-conservative MT, as suggested in Romero-Shaw et al. (2023), could all impact the population properties. Therefore, it is imperative to investigate them further with the goal of seeking a consistent model that can be applied to diverse binary systems.

Another avenue worth exploring involves investigating the selection effects that favor massive donor stars. Our estimation of X-ray luminosity is too rough to be quantitatively analyzed, as we only adopted one set of parameters to estimate the accretion efficiency for all binaries from Hirai & Mandel (2021) and interpolated or extrapolated among different mass ratios. Moreover, the mass accretion rate obtained in Hirai & Mandel (2021) is an upper limit because not all mass passing through the accretion radius is guaranteed to be accreted. In our simulations, most donor stars with masses within $\sim 10-20\,M_\odot$ can produce an X-ray luminosity over $10^{37}\,\mathrm{erg\,s^{-1}}$. However, if we apply the low-end efficiency in Hirai & Mandel (2021) to all binaries, those with an X-ray luminosity above $10^{37}\,\mathrm{erg\,s^{-1}}$ account for $\approx 21\%$ of the total population, and $\approx 56\%$ of them contain a donor star greater than $20\,M_\odot$. A corner plot showing the property distributions for these X-ray bright binaries can be found in Appendix D.

5. Conclusions

The three observed wind-fed BH-HMXBs demonstrate high BH spins, the origin of which remains an open question. We used the new-generation BPS code POSYDON to investigate the population properties of wind-fed BH-HMXBs, adopting three CO-HMS grids with different assumed accretion efficiencies onto BHs. We summarize the key conclusions as follows:

1. Wind-fed BH-HMXBs at solar metallicity are more likely to have already been though a fast RLO phase after the BH formation. Regardless of the mass-accretion models, in our simulations, the total duration of wind-fed BH-HMXBs in a post-RLO phase is higher than that in a pre-RLO phase. After MT via RLO, the partially stripped donor star contracts due to the changes in its hydrogen and helium abundance profile, remaining close to its Roche lobe. At this stage, the binary stays detached for a long period, appearing as a wind-fed BH-HMXB. We highlight the importance of employing detailed modeling in BPS studies, which includes a self-consistent treatment of MT and subsequent readjustment of stars experiencing mass loss or gain.
2. An accretion efficiency prescription inspired by GRRMHD simulations can produce BHs with moderate spins in the range of $\sim 0.3-0.6$, while fully conservative MT can spin up BHs to near-maximal spins, when assuming that the accreted material carries the specific AM at the ISCO. To explain the high spins observed in the three wind-fed BH-HMXBs by super-Eddington accretion, mass and AM accretion efficiency onto BHs higher than that predicted by GRRMHD simulation of super-Eddington disks in the MAD state is required.
3. In our simulations, MS donor stars with masses in the range of $\sim 10-20\,M_\odot$ dominate the wind-fed BH-HMXB population at solar metallicity. This is in tension with the fact that the only confirmed wind-fed BH-HMXB in our Galaxy, Cygnus X-1, contains a donor star of $\approx 40\,M_\odot$. Assuming the mass measurements are reliable, observational selection effects that favor massive donor stars need to be further explored and an accretion model onto non-degenerate stars that leads to more conservative MT needs to be considered.

We emphasize the critical role of detailed binary modeling, informed by insights from GRRMHD simulations, in advancing our understanding of the formation of wind-fed BH-HMXBs and their observed properties. Future efforts should focus on refining BH accretion models with improved GRRMHD predictions and re-evaluating observations and potential selection effects to reconcile the discrepancies between theoretical predictions and observed systems.

Acknowledgements. The POSYDON project is supported primarily by two sources: the Swiss National Science Foundation (PI Fragos, project numbers PP00P2_211006 and CRSII5_213497) and the Gordon and Betty Moore Foundation (PI Kalogera, grant award GBMF8477). This project has received funding from the European Union's Horizon 2020 research and innovation programme under the Marie Sklodowska-Curie RISE action, grant agreement No 873089 (ASTROSTAT- II). Z.X. acknowledges support from the China Scholarship Council (CSC). E.Z. acknowledges funding support from the Hellenic

Foundation for Research and Innovation (H.F.R.I.) under the "3rd Call for H.F.R.I. Research Projects to support Post-Doctoral Researchers" (Project No: 7933). S.S.B., T.F., and Z.X. were supported by the project number PP00P2_211006. T.K. and L.D. acknowledge the support from the National Natural Science Foundation of China and the Hong Kong Research Grants Council (12122309, N_HKU782/23, 17305523, 17314822). S.S.B. was also supported by the project number CRSII5_213497. M.B. ackowledges support from the Boninchi Foundation. K.A.R. and M.S. are supported by the Gordon and Betty Moore Foundation (PI Kalogera, grant award GBMF8477) K.A.R. is also supported by the Riedel Family Fellowship. K.A.R. also thanks the LSSTC Data Science Fellowship Program, which is funded by LSSTC, NSF Cybertraining Grant No. 1829740, the Brinson Foundation, and the Moore Foundation; their participation in the program has benefited this work. K.K. acknowledges support from the Spanish State Research Agency, through the María de Maeztu Program for Centers and Units of Excellence in R&D, No. CEX2020-001058-M. J.J.A. acknowledges support for Program number (JWST-AR-04369.001-A) provided through a grant from the STScI under NASA contract NAS5-03127. I.M. acknowledges support from the Australian Research Council Centre of Excellence for Gravitational Wave Discovery (OzGrav), through project number CE230100016.

References

Abbott, B. P., Abbott, R., Abbott, T. D., et al. 2019, ApJ, 882, L24
Abbott, R., Abbott, T. D., Acernese, F., et al. 2023, Phys. Rev. X, 13, 011048
Akira Rocha, K., Kalogera, V., Doctor, Z., et al. 2024, arXiv e-prints [arXiv:2403.07172]
Bardeen, J. M. 1970, Nature, 226, 64
Batta, A., Ramirez-Ruiz, E., & Fryer, C. 2017, ApJ, 846, L15
Bavera, S. S., Fragos, T., Qin, Y., et al. 2020, A&A, 635, A97
Bavera, S. S., Fragos, T., Zevin, M., et al. 2021, A&A, 647, A153
Bavera, S. S., Fragos, T., Zapartas, E., et al. 2023, Nat. Astron., 7, 1090
Beck, P. G., Montalban, J., Kallinger, T., et al. 2012, Nature, 481, 55
Belczynski, K., Klencki, J., Fields, C. E., et al. 2020, A&A, 636, A104
Belczynski, K., Done, C., Hagen, S., Lasota, J.-P., & Sen, K. 2024, A&A, 690, A21
Bondi, H., & Hoyle, F. 1944, MNRAS, 104, 273
Briel, M. M., Stevance, H. F., & Eldridge, J. J. 2023, MNRAS, 520, 5724
Crowther, P. A., Barnard, R., Carpano, S., et al. 2010, MNRAS, 403, L41
Dai, L., McKinney, J. C., Roth, N., Ramirez-Ruiz, E., & Miller, M. C. 2018, ApJ, 859, L20
de Jager, C., Nieuwenhuijzen, H., & van der Hucht, K. A. 1988, A&AS, 72, 259
de Mink, S. E., Langer, N., Izzard, R. G., Sana, H., & de Koter, A. 2013, ApJ, 764, 166
Deheuvels, S., Doğan, G., Goupil, M. J., et al. 2014, A&A, 564, A27
Dorozsmai, A., & Toonen, S. 2024, MNRAS [arXiv:2207.08837]
Draghis, P. A., Miller, J. M., Costantini, E., et al. 2024, ApJ, 969, 40
Eggenberger, P., Maeder, A., & Meynet, G. 2005, A&A, 440, L9
Eggenberger, P., Moyano, F. D., & den Hartogh, J. W. 2022, A&A, 664, L16
Falanga, M., Bakala, P., La Placa, R., et al. 2021, MNRAS, 504, 3424
Farrell, E., Groh, J. H., Meynet, G., & Eldridge, J. J. 2022, MNRAS, 512, 4116
Fishbach, M., & Kalogera, V. 2022, ApJ, 929, L26
Fragos, T., & McClintock, J. E. 2015, ApJ, 800, 17
Fragos, T., Andrews, J. J., Bavera, S. S., et al. 2023, ApJS, 264, 45
Fuller, J., & Ma, L. 2019, ApJ, 881, L1
Fuller, J., Piro, A. L., & Jermyn, A. S. 2019, MNRAS, 485, 3661
Gallegos-Garcia, M., Fishbach, M., Kalogera, V., L Berry, C. P., & Doctor, Z. 2022, ApJ, 938, L19
Gammie, C. F., Shapiro, S. L., & McKinney, J. C. 2004, ApJ, 602, 312
Gehan, C., Mosser, B., Michel, E., Samadi, R., & Kallinger, T. 2018, A&A, 616, A24
Gomez, S., & Grindlay, J. E. 2021, ApJ, 913, 48
Hirai, R., & Mandel, I. 2021, PASA, 38, e056a
Hobbs, G., Lorimer, D. R., Lyne, A. G., & Kramer, M. 2005, MNRAS, 360, 974
Illarionov, A. F., & Sunyaev, R. A. 1975, A&A, 39, 185
Jermyn, A. S., Bauer, E. B., Schwab, J., et al. 2023, ApJS, 265, 15
King, A. R., Davies, M. B., Ward, M. J., Fabbiano, G., & Elvis, M. 2001, ApJ, 552, L109
Kovlakas, K., Zezas, A., Andrews, J. J., et al. 2020, MNRAS, 498, 4790
Kovlakas, K., Fragos, T., Schaerer, D., & Mesinger, A. 2022, A&A, 665, A28
Kroupa, P. 2001, MNRAS, 322, 231
Langer, N. 1998, A&A, 329, 551
Laycock, S. G. T., Maccarone, T. J., & Christodoulou, D. M. 2015, MNRAS, 452, L31
Liotine, C., Zevin, M., Berry, C. P. L., Doctor, Z., & Kalogera, V. 2023, ApJ, 946, 4
Liu, J., McClintock, J. E., Narayan, R., Davis, S. W., & Orosz, J. A. 2008, ApJ, 679, L37
Liu, J., McClintock, J. E., Narayan, R., Davis, S. W., & Orosz, J. A. 2010, ApJ, 719, L109
Lowell, B., Jacquemin-Ide, J., Tchekhovskoy, A., & Duncan, A. 2024, ApJ, 960, 82
MacLeod, M., & Loeb, A. 2020, ApJ, 895, 29
Marchant, P., Langer, N., Podsiadlowski, P., Tauris, T. M., & Moriya, T. J. 2016, A&A, 588, A50
McClintock, J. E., Narayan, R., & Steiner, J. F. 2014, Space Sci. Rev., 183, 295
Miller, S., Callister, T. A., & Farr, W. M. 2020, ApJ, 895, 128
Miller-Jones, J. C. A., Bahramian, A., Orosz, J. A., et al. 2021, Science, 371, 1046
Moreno Méndez, E. 2011, MNRAS, 413, 183
Moreno Méndez, E., & Cantiello, M. 2016, New Astron., 44, 58
Mosser, B., Goupil, M. J., Belkacem, K., et al. 2012, A&A, 548, A10
Neijssel, C. J., Vinciguerra, S., Vigna-Gómez, A., et al. 2021, ApJ, 908, 118
Nugis, T., & Lamers, H. J. G. L. M. 2000, A&A, 360, 227
Olejak, A., & Belczynski, K. 2021, ApJ, 921, L2
Orosz, J. A., McClintock, J. E., Narayan, R., et al. 2007, Nature, 449, 872
Orosz, J. A., Steeghs, D., McClintock, J. E., et al. 2009, ApJ, 697, 573
Orosz, J. A., McClintock, J. E., Aufdenberg, J. P., et al. 2011, ApJ, 742, 84
Patton, R. A., & Sukhbold, T. 2020, MNRAS, 499, 2803
Paxton, B., Bildsten, L., Dotter, A., et al. 2011, ApJS, 192, 3
Paxton, B., Cantiello, M., Arras, P., et al. 2013, ApJS, 208, 4
Paxton, B., Marchant, P., Schwab, J., et al. 2015, ApJS, 220, 15
Paxton, B., Schwab, J., Bauer, E. B., et al. 2018, ApJS, 234, 34
Paxton, B., Smolec, R., Schwab, J., et al. 2019, ApJS, 243, 10
Pietsch, W., Haberl, F., Sasaki, M., et al. 2006, ApJ, 646, 420
Poutanen, J., Lipunova, G., Fabrika, S., Butkevich, A. G., & Abolmasov, P. 2007, MNRAS, 377, 1187
Prestwich, A. H., Kilgard, R., Crowther, P. A., et al. 2007, ApJ, 669, L21
Qin, Y., Fragos, T., Meynet, G., et al. 2018, A&A, 616, A28
Qin, Y., Marchant, P., Fragos, T., Meynet, G., & Kalogera, V. 2019, ApJ, 870, L18
Qin, Y., Shu, X., Yi, S., & Wang, Y.-Z. 2022, RAA, 22, 035023
Quast, M., Langer, N., & Tauris, T. M. 2019, A&A, 628, A19
Ramachandran, V., Oskinova, L. M., Hamann, W. R., et al. 2022, A&A, 667, A77
Reynolds, C. S. 2014, Space Sci. Rev., 183, 277
Reynolds, C. S. 2021, ARA&A, 59, 117
Romero-Shaw, I., Hirai, R., Bahramian, A., Willcox, R., & Mandel, I. 2023, MNRAS, 524, 245
Roulet, J., Chia, H. S., Olsen, S., et al. 2021, Phys. Rev. D, 104, 083010
Salvesen, G., & Miller, J. M. 2021, MNRAS, 500, 3640
Sana, H., de Koter, A., de Mink, S. E., et al. 2013, A&A, 550, A107
Schrøder, S. L., Batta, A., & Ramirez-Ruiz, E. 2018, ApJ, 862, L3
Seifina, E., & Titarchuk, L. 2010, ApJ, 722, 586
Sen, K., Xu, X. T., Langer, N., et al. 2021, A&A, 652, A138
Sen, K., Langer, N., Marchant, P., et al. 2022, A&A, 659, A98
Shao, Y., & Li, X.-D. 2022, ApJ, 930, 26
Shimanskii, V. V., Karitskaya, E. A., Bochkarev, N. G., et al. 2012, Astron. Rep., 56, 741
Spruit, H. C. 2002, A&A, 381, 923
Sukhbold, T., Ertl, T., Woosley, S. E., Brown, J. M., & Janka, H. T. 2016, ApJ, 821, 38
Taylor, C., & Reynolds, C. S. 2018, ApJ, 855, 120
Tchekhovskoy, A., McKinney, J. C., & Narayan, R. 2012, J. Phys. Conf. Ser., 372, 012040
Thomsen, L. L., Kwan, T. M., Dai, L., et al. 2022, ApJ, 937, L28
Valli, R., Tiede, C., Vigna-Gómez, A., et al. 2024, A&A, 688, A128
Vanbeveren, D., Mennekens, N., van den Heuvel, E. P. J., & Van Bever, J. 2020, A&A, 636, A99
Vinciguerra, S., Neijssel, C. J., Vigna-Gómez, A., et al. 2020, MNRAS, 498, 4705
Vink, J. S., de Koter, A., & Lamers, H. J. G. L. M. 2001, A&A, 369, 574
Wei, D., Schneider, F. R. N., Podsiadlowski, P., et al. 2024, A&A, 688, A87
Willcox, R., MacLeod, M., Mandel, I., & Hirai, R. 2023, ApJ, 958, 138
Winter, L. M., Mushotzky, R. F., & Reynolds, C. S. 2006, ApJ, 649, 730
Xing, Z., Bavera, S. S., Fragos, T., et al. 2024, A&A, 683, A144
Zdziarski, A. A., Mikolajewska, J., & Belczynski, K. 2013, MNRAS, 429, L104
Zdziarski, A. A., Banerjee, S., Chand, S., et al. 2024a, ApJ, 962, 101
Zdziarski, A. A., Chand, S., Banerjee, S., et al. 2024b, ApJ, 967, L9

Appendix A: Formation channels of wind-fed BH-HMXBs

Here we present the fractions of evolutionary pathways prior to BH formation for wind-fed BH-HMXBs in Table A.1 across the three BH accretion scenarios. All scenarios exhibit similar fractions.

Appendix B: Surface and center helium abundance

In this section, we present the population property distributions, in the form of a corner plot, that includes center helium abundance $Y_{\rm center}$ and surface helium abundance $Y_{\rm surf}$ of the donor star under the moderately super-Eddington accretion scenario. In Figure B.1, we show the time-weighted distribution of orbital period, donor star mass, BH spin, donor star's center helium abundance, and surface helium abundance. For both pre-RLO and post-RLO systems, the majority of the donor stars have $Y_{\rm center}$ above ≈ 0.8, which means that they are approaching the terminal-age MS. As a consequence of RLO, the outer layer of the envelope of the donor stars is stripped, leading to an evident increase in $Y_{\rm surf}$.

Appendix C: Population property distributions for Eddington-limited and fully conservative BH accretion

Here we display population property distributions, in the form of corner plots, for the population properties of wind-fed BH-HMXBs under the model assumptions of Eddington-limited and fully conservative BH accretion. Figure C.1 shows the same distributions as Figure 2 but for the Eddington-limited accretion model. The BH spins are $\lesssim$0.3, with no significant BH spin-up observed to distinguish the populations before and after MT via RLO. Figure C.2 shows the case of fully conservative BH accretion. Bimodal distributions can be seen for BH masses and spins due to accretion. Most of the BHs can be spun up to have spins above 0.8 after MT via RLO and the binaries remain at this stage longer. The distributions of orbital periods and donor star masses appear similar across different BH accretion models.

Appendix D: Population property distributions for X-ray bright sources

When adopting the low-end wind accretion efficiency from Hirai & Mandel (2021), a large fraction of the binaries with donor stars below $20\,M_\odot$ exhibit X-ray luminosities below $10^{37}\,{\rm erg\,s^{-1}}$. To illustrate the characteristics of X-ray bright systems, we display a corner plot of the binaries with X-ray luminosity exceeding $10^{37}\,{\rm erg\,s^{-1}}$ in Figure D.1. About 79% of them are post-RLO systems. The donor stars exhibit a relatively flat distribution from 10 to $30\,M_\odot$, extending up to $\approx 40\,M_\odot$. The X-ray bright systems are characterized by a higher proportion of massive donor stars because of their strong winds. In Figure D.2, we show the distribution of mass ratio $q = M_{\rm d}/M_{\rm BH}$ versus orbital period for wind-fed BH-HMXBs under the moderately super-Eddington accretion model for both the entire population and the X-ray bright systems. For the entire population, the post-RLO systems have mass ratios mostly ranging from approximately 0.8 to 1.6, with a small fraction reaching around 2. For the X-ray bright systems, their mass ratios show a flatter distribution from approximately 0.8 to 2.4.

Table A.1. Fractions of evolutionary pathways of wind-fed BH-HMXBs

BH accretion scenario	case A	case B	case A and case B	no MT	contact
Eddington-limited	20.3%	13.1%	48.9%	12.5%	5.2%
moderately super-Eddington	21.6%	11.6%	48.3%	11.9%	6.5%
fully conservative	22.4%	9.8%	48.5%	12.2%	7.0%

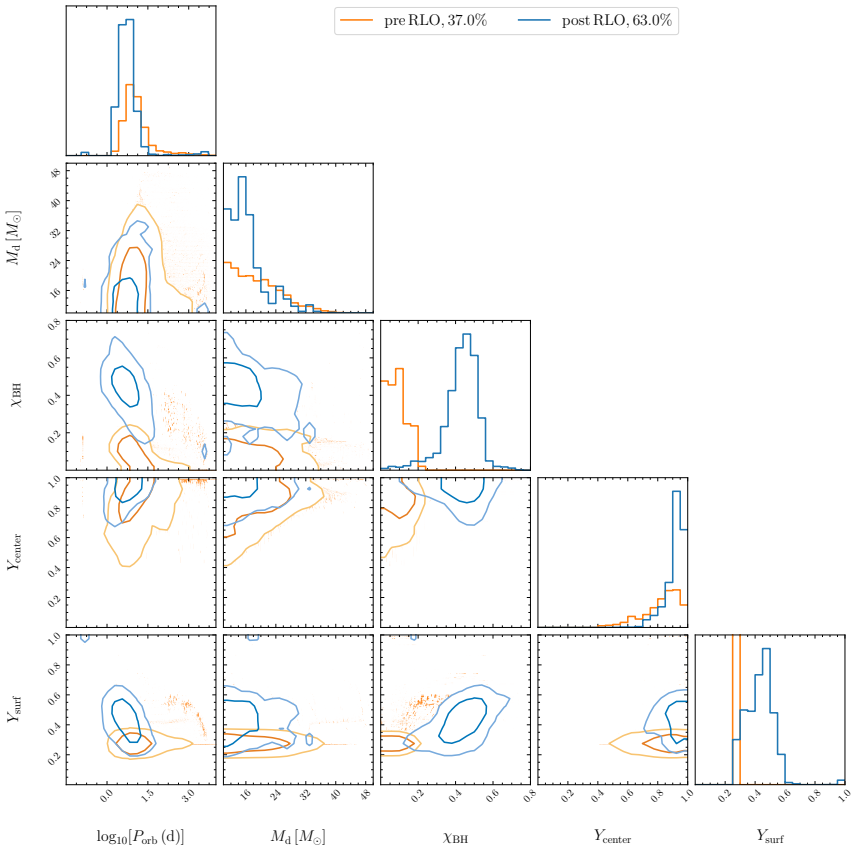

Fig. B.1. Corner plot similar to Figure 2 including the surface and center helium abundance.

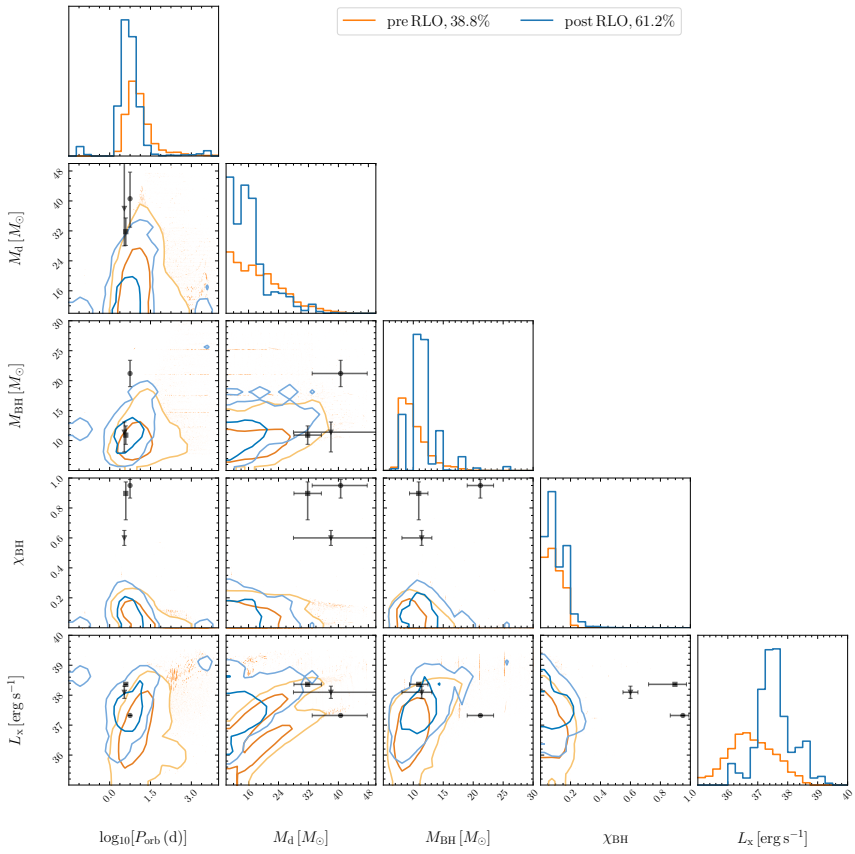

Fig. C.1. Same as Figure 2 but for Eddington-limited BH accretion.

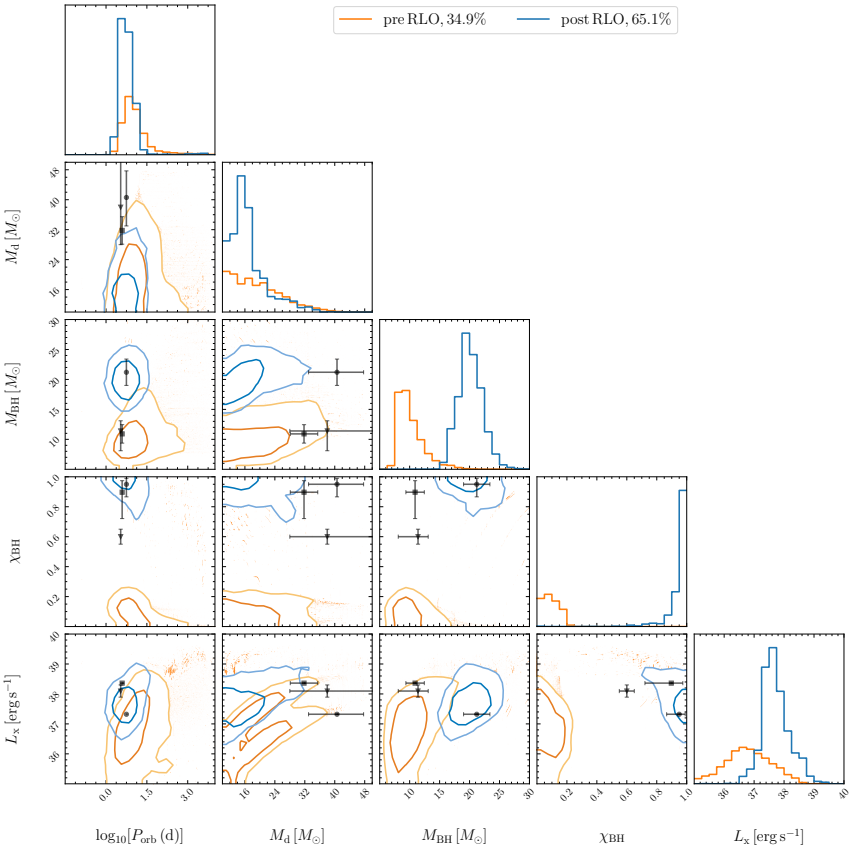

Fig. C.2. Same as Figure 2 but for fully conservative BH accretion.

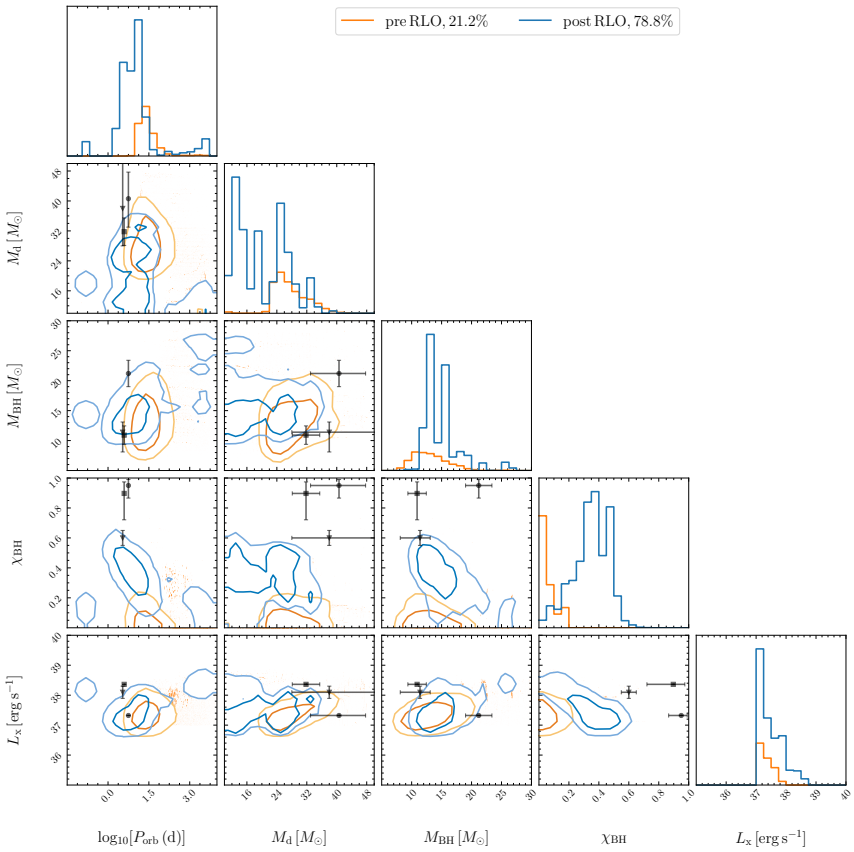

Fig. D.1. Same as Figure 2 but for binaries with X-ray luminosity exceeding 10^{37} erg s^{-1}, following the application of low wind accretion efficiency.

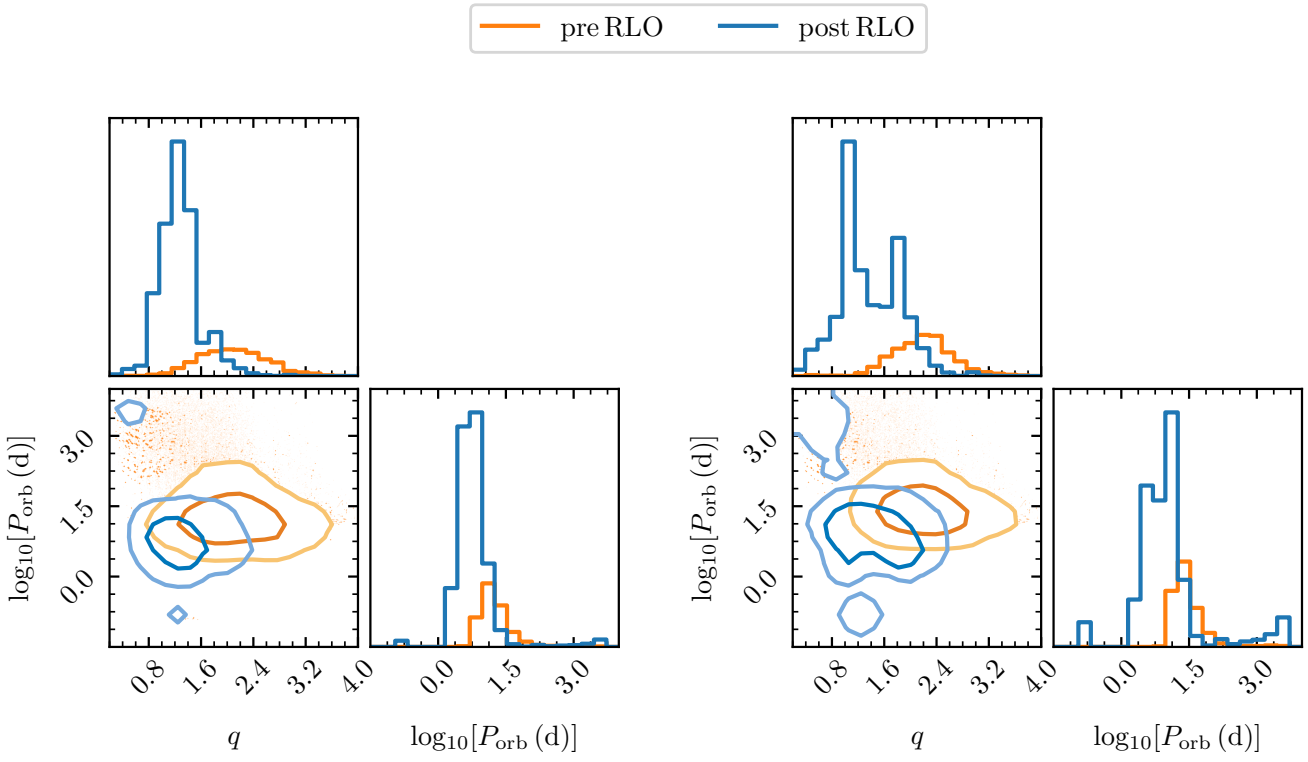

Fig. D.2. Distribution of mass ratio versus orbital period for wind-fed BH-HMXBs. The left panel shows the distribution for the entire population and the right panel shows the distribution for systems with X-ray luminosity exceeding 10^{37} erg s^{-1}, assuming low wind accretion efficiency.

2.8 Supplementary discussion and comments

2.8.1 Super-Eddington disk simulations

Observations suggest that super-Eddington accretion may occur in various astrophysical systems, including ULXs, microquasars such as SS433 (Fabrika, 2004), and tidal disruption events around supermassive BHs (Burrows et al., 2011). Theoretically, BH accretion rate can exceed the Eddington limit when radiation from the disk escapes in directions different from the inflow (Shakura et al., 1973). One of the earliest semi-analytic models for super-Eddington accretion is the slim disk model, which includes photo trapping effects (Abramowicz et al., 1988). In this regime, radiation plays a key role by influencing the geometry and overall properties of the accretion disk. Early numerical investigations by Ohsuga et al. (2005) provided the first 2D global radiation hydrodynamics simulations of BH super-Eddington accretion. Jiang et al. (2014) conducted a radiation magnetohydrodynamics simulation showing that super-Eddington disks can generate strong radiation-driven winds above the Eddington limit. Sądowski et al. (2013) and Sądowski et al. (2014) first incorporated radiation into general relativistic radiation magnetohydrodynamics (GRRMHD) simulations, enabling detailed modeling of wind and jet launching near BHs.

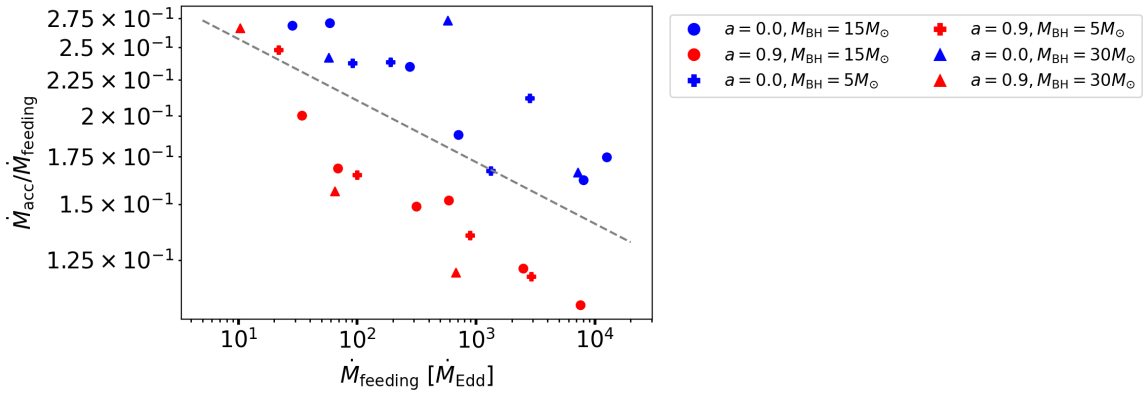

Figure 2.9: The ratio of the BH accretion rate to the mass transfer rate for different BH models, shown as a function of the mass transfer rate in the super-Eddington accretion simulations. Credit: Tom Kwan.

The 3D GRRMHD simulations this work relies on constitute the first systematic study of a highly magnetized, super-Eddington accretion disk around stellar-mass BHs (Kwan et al., in prep.). The study employs the GRRMHD code `HARMRAD` (Sądowski et al., 2013; McKinney et al., 2014) with M1 closure scheme (Levermore et al., 1981). A total of 32 simulations of super-Eddington magnetically arrested disks (MADs, Narayan et al., 2003) are performed, with three BH masses of $5, 15, 30\,M_\odot$, two spin configurations 0.0 and 0.9, and a series of

accretion rates. They calculated the ratio of mass accretion rate $\dot{M}_{\rm acc}$ to the total feeding rate $\dot{M}_{\rm feeding}$, defined as $\dot{M}_{\rm acc} + \dot{M}_{\rm wind}$, for different BH properties. Figure 2.9 shows the ratio as a function of the mass transfer rate. Overall, the accretion efficiency is $\sim 10-30\%$. The simulations suggest that higher BH spins and larger accretion rates both lead to stronger disk winds and hence a reduced fraction of mass that is accreted. Additionally, it appears that the accretion efficiency is less sensitive to the BH masses. Note that the magnetic field configuration can impact the accretion efficiency. In a standard and normal evolution (SANE, Narayan et al., 2012) disk, the accretion efficiency is expected to be larger because the weaker magnetic fields do not drive strong outflows and jets, unlike MADs, where a substantial fraction of the inflowing mass is expelled from the disk.

2.8.2 Spin measurements in high-mass X-ray binaries

Two primary techniques are widely used to measure BH spin in BH-XRBs. The first is the X-ray reflection method, which is based on modeling the broadened iron emission line in the disk reflection spectrum that is distorted by the Doppler effects and the gravitational redshifts in the strong BH potential (Fabian et al., 1989; Laor, 1991). By assuming the X-ray reflection spectrum is truncated at the ISCO, one can obtain the location of the ISCO, thus the BH spin from the reflection spectroscopy. The disk reflection models are characterized by the disk inclination, elemental abundances, the height of the coronal source, and the BH spin. Systematic uncertainties in this method involves the approximation regarding the structure of the accretion disk and the assumption that the observed spectral structure is from the inner disk reflection. The second technique is the continuum-fitting method, which is based on the fact that the disk spectrum, particularly the peak emission and the temperature, is determined by the position of the ISCO. This approach is sensitive to external parameters such as the source distance, disk inclination, and BH mass. Moreover, the measurement relies on the assumption of the Novikov-Thorne disk model (Novikov et al., 1973), which is the relativistic generalization of the thin disk model (Shakura et al., 1973). The systematic uncertainties in this methods involves errors in measuring these external parameters, errors from the disk model and disk atmosphere model, and the assumption of spin-orbit alignment.

These two methods for BH spin measurements generally yield consistent results (Reynolds, 2021). However, a recent analysis of the XRB system LMC X-3 found a spin of $0.928^{+0.058}_{-0.146}$ (Draghis et al., 2024) using the reflection method, which is in strong disagreement with the results of ~ 0.25 using continuum fitting (Orosz et al., 2014; Jana et al., 2021; Majumder et al., 2024; Svoboda et al., 2024). Besides, a different method was used based on X-ray timing in the case of GRO J1655-40. They obtained a spin of ~ 0.29 for the source, which contrasts markedly with the spin of $0.65-0.75$ obtained from continuum fitting (Shafee

et al., 2006) and > 0.9 inferred from the reflection method (Miller et al., 2009).

2.8.3 Origin of black hole spins

There are generally four sources of BH spin in the context of isolated binary evolution (see Mandel et al., 2020a, for more details). The first is the angular momentum retained from the progenitor star. The progenitor stars can be spun up by tides or accretion and may retain significant angular momentum if it is not lost prior to core collapse. The second is spin acquired during the SN explosion. If the BH forms in an asymmetrical explosion, it can be spun up due to asymmetrical accretion during the explosion (Burrows et al., 2023). Based on the 3D SN simulations in (Burrows et al., 2023), the BH natal spin can reach 0.6. However, it requires an energetic SN explosion and high spins are not universal across models due to the stochastic nature of the impact parameters of fallback and infall plumes. Moreover, for massive BHs, they are likely to form through complete fallback. The third source is angular momentum delivered by fallback material. The amount of angular momentum that can be accreted is sensitive to explosion energies and orbital configurations (Batta et al., 2017; Schrøder et al., 2018). The fourth source is spin-up via accretion from the companion stars.

Spin measurements of BH-HMXBs generally indicate high spins, as found by both the reflection and continuum-fitting methods (e.g., Gou et al., 2009; Gou et al., 2014; Parker et al., 2015; Mudambi et al., 2020). In this study, we incorporate insights from GRRMHD simulations of super-Eddington accretion to investigate whether such accretion scenarios can explain the extreme spins in these systems. Although our findings suggest that BH–HMXBs may indeed undergo a RLOF phase that allows spin-up from accretion, it remains challenging to reach the extremely high spins reported by observations using the accretion efficiencies implied by the simulations of MADs. The SANE disk configuration could potentially lead to a higher accretion efficiency, but it would also need to reach the upper end of the efficiency range to account for the formation of extreme BH spins.

It is also possible that the BH is born with a high natal spin. Possible scenarios include inefficient angular momentum transport in progenitor stars during their late evolutionary stages (Qin et al., 2019), as well as spin acquisition from SN. However, the former scenario lacks both theoretical support and observational evidence. Some CCSN simulations can produce BH spins as high as ~ 0.6 under specific conditions (Burrows et al., 2024), but this applies only to certain cases in particular models and is unlikely for massive BHs.

Our population study thus raises the possibility that the observed BH spins in these systems may be systematically overestimated, given the uncertainties and inconsistencies in the spin-measurement methods. The strong model dependence of spin measurements suggested by

Zdziarski et al. (2024a) and Zdziarski et al. (2024b) should be carefully considered as well.

2.8.4 Implications for Cygnus X-1

Cygnus X-1 is one of the brightest X-ray sources in the sky and the first source widely accepted to be a BH. It contains a BH and an O-type donor star in a 5.6-day orbit. It is the only confirmed BH-HMXB in the Milky Way. Early studies estimated a BH mass of $14.8 \pm 1.0\,M\odot$ and $19.16 \pm 1.90\,M\odot$ for the donor star (Orosz et al., 2011). However, the donor star's mass appeared inconsistent with the expected mass-luminosity relation assuming it is a MS star. Lately, Miller-Jones et al. (2021) reported an updated mass of $21.2 \pm 2.2\,M_\odot$ for the BH and $40.6^{+7.7}_{-7.1}\,M_\odot$ for the donor star. It has been pointed out in Miller-Jones et al. (2021) that such a high-mass BH at solar metallicity implies that the mass loss rates during the luminous blue variable or WR stages may be overestimated. In the `POSYDON` simulations, it is possible to form such a massive BHs at solar metallicity without reducing the mass loss rates deliberately. The issue raised in this work is that our BPS study predicts a much higher fraction of lower-mass BHs and donor stars in the wind-fed BH-HMXB population, which makes it puzzling that the only observed BH-HMXBs in our galaxy exhibits such high masses. From a population perspective, potential explanations for this discrepancy include possible selection effects in X-ray observations, uncertainties in wind loss and angular momentum loss, and uncertainties in binary configurations assumed in standard BPS studies.

An early study by Podsiadlowski et al. (2003) proposed the evolutionary path for Cygnus X-1 that involves RLOF and post-RLOF wind accretion. However, their model predicts that the donor star mass should be comparable to, or lower than, the BH mass when the donor star shrinks back and initiates the second wind-fed phase, which is not consistent with the case of Cygnus X-1. Similar results have been discussed in a recent BPS study of wind-fed BH-HMXBs using the rapid BPS code `COMPAS` (Romero-Shaw et al., 2023). They observed a second wind-fed phase for some systems where the donor star loses substantial amount of mass and be close to an equal mass ratio. This work serves as the first BPS study to employ detailed binary evolution models, which handle the mass transfer phase more accurately, for the BH-HMXB population. Our population results further confirm the implication from Podsiadlowski et al. (2003) that the second wind-fed phase after RLOF is longer the first one, based on updated binary models and selection criteria for wind-fed BH–HMXBs. Moreover, in our binary models, we observe that post-RLOF detachment occurs across a broader range of the mass ratio, peaking around $q \sim 1.2$ and reaching up to ~ 2. Particularly, for the brightest systems, the second wind-fed phase can occur with a mass ratio ranging from ~ 0.8 to 2.2.

Chapter 3

COALESCING NEUTRON STAR–BLACK HOLE BINARIES AT SOLAR METALLICITY

NSBH mergers are the most recently confirmed double compact objects to be detected by GW detectors. Compared to BBH mergers, NSBH mergers tend to have a lower contribution from dynamical formation channels, because NSs do not tend to sink to the center of a dense cluster like BHs and are more likely to be ejected during dynamical processes. Moreover, the formation efficiency of NSBH mergers is less dependent on metallicity. These factors motivated us to study merging NSBH systems using the `POSYDON` code, despite that only a handful of NSBH merger events or candidates have been reported. This work is the first BPS study to utilize the full functionalities of `POSYDON` v1, focusing on uncovering different characteristics across formation channels of merging NSBH binaries at solar metallicity in the isolated formation scenario. It showcased the capability of `POSYDON` in modeling binaries in detail from ZAMS stars to compact object mergers on a large scale appropriate for population studies.

The manuscript presented in the following was published in *Astronomy & Astrophysics*, referred as Xing et al. (2024a).

A&A, 683, A144 (2024)
https://doi.org/10.1051/0004-6361/202347971

69
Astronomy & Astrophysics

From ZAMS to merger: Detailed binary evolution models of coalescing neutron star – black hole systems at solar metallicity

Zepei Xing[1,2], Simone S. Bavera[1,2], Tassos Fragos[1,2], Matthias U. Kruckow[1,2], Jaime Román-Garza[1,2], Jeff J. Andrews[3,4], Aaron Dotter[3], Konstantinos Kovlakas[1,5,6], Devina Misra[1,7], Philipp M. Srivastava[3,8], Kyle A. Rocha[3,8], Meng Sun[3], and Emmanouil Zapartas[9,10]

[1] Département d'Astronomie, Université de Genève, Chemin Pegasi 51, CH-1290 Versoix, Switzerland
e-mail: Zepei.Xing@unige.ch
[2] Gravitational Wave Science Center (GWSC), Université de Genève, CH1211 Geneva, Switzerland
[3] Center for Interdisciplinary Exploration and Research in Astrophysics (CIERA), Northwestern University, 1800 Sherman Ave, Evanston, IL 60201, USA
[4] Department of Physics, University of Florida, 2001 Museum Rd, Gainesville, FL 32611, USA
[5] Institute of Space Sciences (ICE, CSIC), Campus UAB, Carrer de Magrans, 08193 Barcelona, Spain
[6] Institut d'Estudis Espacials de Catalunya (IEEC), Carrer Gran Capità, 08034 Barcelona, Spain
[7] Institutt for Fysikk, Norwegian University of Science and Technology, 7491 Trondheim, Norway
[8] Electrical and Computer Engineering, Northwestern University, 2145 Sheridan Road, Evanston, IL 60208, USA
[9] Institute of Astrophysics, FORTH, N. Plastira 100, Heraklion 70013, Greece
[10] IAASARS, National Observatory of Athens, Vas. Pavlou and I. Metaxa, Penteli 15236, Greece

Received 15 September 2023 / Accepted 21 November 2023

ABSTRACT

Neutron star – black hole (NSBH) merger events bring us new opportunities to constrain theories of stellar and binary evolution and understand the nature of compact objects. In this work, we investigated the formation of merging NSBH binaries at solar metallicity by performing a binary population synthesis study of merging NSBH binaries with the newly developed code POSYDON. The latter incorporates extensive grids of detailed single and binary evolution models, covering the entire evolution of a double compact object progenitor. We explored the evolution of NSBHs originating from different formation channels, which in some cases differ from earlier studies performed with rapid binary population synthesis codes. In this paper, we present the population properties of merging NSBH systems and their progenitors such as component masses, orbital features, and BH spins, and we detail our investigation of the model uncertainties in our treatment of common envelope (CE) evolution and the core-collapse process. We find that at solar metallicity, under the default model assumptions, most of the merging NSBHs have BH masses in the range of 3−11 $M_\odot$ and chirp masses within 1.5−4 $M_\odot$. Independently of our model variations, the BH always forms first with dimensionless spin parameter $\lesssim$0.2, which is correlated to the initial binary orbital period. Some BHs can subsequently spin up moderately ($\chi_{\rm BH} \lesssim 0.4$) due to mass transfer, which we assume to be Eddington limited. Binaries that experience CE evolution rarely demonstrate large tilt angles. Conversely, approximately 40% of the binaries that undergo only stable mass transfer without CE evolution contain an anti-aligned BH. Finally, accounting for uncertainties in both the population modeling and the NS equation of state, we find that 0−18.6% of NSBH mergers may be accompanied by an electromagnetic counterpart.

Key words. gravitation – gravitational waves – binaries: close – stars: black holes – stars: neutron

1. Introduction

After the detection of binary black hole (BH) and binary neutron star (NS) mergers (Abbott et al. 2016, 2017a) by the ground-based gravitational-wave (GW) observatories LIGO (LIGO Scientific Collaboration 2015) and Virgo (Acernese et al. 2015), NS – BH (NSBH) systems had remained elusive until the detection of the NSBH merger events GW200115 and GW200105 (Abbott et al. 2021b). For GW200105, with a high-spin prior for the NS, the BH and NS masses are estimated to be $M_{\rm BH} = 8.9^{+1.2}_{-1.5}\,M_\odot$ and $M_{\rm NS} = 1.9^{+0.3}_{-0.2}\,M_\odot$, respectively. The BH spin magnitude is constrained as $\chi_{\rm BH} = 0.08^{+0.22}_{-0.08}$ and its effective inspiral spin parameter $\chi_{\rm eff} = -0.01^{+0.11}_{-0.15}$. For GW200115, the binary mass components are estimated to be $M_{\rm BH} = 5.7^{+1.8}_{-2.1}\,M_\odot$ and $M_{\rm NS} = 1.5^{+0.7}_{-0.3}\,M_\odot$. The primary spin magnitude, $\chi_{\rm BH} = 0.33^{+0.48}_{-0.29}$, is not well constrained, while the effective inspiral spin parameter is found to be $-0.19^{+0.23}_{-0.35}$. The latter indicates a possible misalignment between the BH spin and the orbital angular momentum. The misalignment angle is estimated to be $2.30^{+0.59}_{-1.18}$ rad (Fragione et al. 2021). Mandel & Smith (2021) then reanalyzed the GW200115 signal with their astrophysically motivated priors and suggested a non-spinning BH for GW200115.

With the release of the third Gravitational-Wave Transient Catalog (GWTC-3), in addition to GW200105 and GW200115, NSBH merger candidates include GW190426 (Abbott et al. 2021a), GW190917 (Abbott et al. 2021c), and GW191219 (Abbott et al. 2023). GW190426 and GW190917 are marginal candidates because their probability of astrophysical origin, $p_{\rm astro}$, is below 0.5, and GW191219 exhibits large model-dependent uncertainties in $p_{\rm astro}$. In the GWTC-3 analysis, GW200105 was also listed as a marginal candidate because its $p_{\rm astro}$ is below 0.5. Nevertheless, it is still an interesting

NSBH candidate with a clear outlier from the noise background (Abbott et al. 2023). The properties of these NSBH candidates are listed in Table 1. Apart from these events, GW190814 (Abbott et al. 2020; Huang et al. 2020; Zhou et al. 2021) and GW200210 (Abbott et al. 2023) are suspected to be NSBH mergers. Both systems possess a compact object that is within the mass range of 2−3 $M_\odot$ and close to the boundary between the heaviest NS and the lightest BH. In the near future, more NSBHs are expected to be detected in the fourth (O4) and fifth (O5) observing runs of ground-based GW detectors at improved sensitivities (Abbott et al. 2018), as well as, in the longer term, the next generation of ground-based observatories, such as the *Einstein* Telescope (Punturo et al. 2010; Hild et al. 2011) and the Cosmic Explorer (Abbott et al. 2017b; Reitze et al. 2019) and future space-based observatories, such as the Laser interferometer Space Antenna (LISA; Amaro-Seoane et al. 2017; Thorpe et al. 2019), TianQin (Luo et al. 2016; Mei et al. 2021), and Taiji (Ruan et al. 2020).

Neutron star – black hole inspiral can present different GW signals, depending on whether the NS is tidally disrupted and whether the mass shedding happens before the NS crosses the innermost-stable circular orbit (ISCO; Kyutoku et al. 2010, 2011; Foucart et al. 2013; Tiwari et al. 2021). If the NS is not plunging as a whole into the BH but is tidally disrupted outside ISCO, the NSBH mergers may have potential electromagnetic counterparts (EMCs) such as kilonovae (Li & Paczyński 1998; Kawaguchi et al. 2020; Zhu et al. 2021; Darbha et al. 2021), short gamma-ray burst emission (Nakar 2007; Pannarale & Ohme 2014; Gompertz et al. 2020), long gamma-ray burst emission (Gottlieb et al. 2023), and radio emission (Piran et al. 2013; Hotokezaka et al. 2016). Generally, stiff NS equations of state corresponding to large NS radii, low-mass BHs, and high BH spins, which affect the position of the ISCO, increase the possibility of generating EMCs (Pannarale et al. 2011; Foucart et al. 2018; Bhattacharya et al. 2019; Román-Garza et al. 2021). The recent study of Fragione (2021) showed that only if the BHs are spinning fast and NSs have stiff equations of state would one expect a significant fraction of NSBH mergers to be associated with EMCs. However, in the classic isolated binary formation channel, it is commonly thought that if the BH forms first, it is likely to have a small spin (Fragos & McClintock 2015; Qin et al. 2018; Fuller & Ma 2019; Bavera et al. 2023) because the angular momentum of the core can be efficiently transported to the outer layer, which would be removed by mass transfer or winds. Alternatively, NSBHs where the NS forms first, which allows for a tidally spun-up BH progenitor, become candidates of EMC sources (Román-Garza et al. 2021; Hu et al. 2022). Despite the possibility, this corresponds to a very small portion of the whole NSBH population (Shao & Li 2021; Broekgaarden et al. 2021; Chattopadhyay et al. 2022).

Regarding the formation mechanisms of merging NSBH binaries, multiple channels have been proposed. These channels include the evolution of isolated field binaries; dynamical interactions in global clusters (Clausen et al. 2013; Ye et al. 2020), nuclear star clusters (Petrovich & Antonini 2017; Arca Sedda 2020; Wang et al. 2021), and young star clusters (Ziosi et al. 2014; Fragione & Banerjee 2020; Rastello et al. 2020; Santoliquido et al. 2020; Arca Sedda 2021); evolution from triples (Fragione & Loeb 2019; Trani et al. 2022); and chemical homogeneous evolution (Marchant et al. 2017). The isolated binary evolution channel is widely explored through binary population synthesis (BPS) methods (Tutukov & Yungelson 1993; Fryer et al. 1999; Voss & Tauris 2003; Dominik et al. 2012, 2015; de Mink & Belczynski 2015; Ablimit & Maeda 2018; Giacobbo & Mapelli 2018; Kruckow et al. 2018; Neijssel et al. 2019; Belczynski et al. 2020; Tang et al. 2020; Zevin et al. 2020; Broekgaarden et al. 2021; Shao & Li 2021; Iorio et al. 2023). These methods estimate a merger rate density of NSBHs consistent with the observations, given appropriate physical assumptions. However, relying solely on the merger rate density is not sufficient for constraining model uncertainties. The merger rate density is subject to many uncertainties in binary and stellar evolution such as common envelope (CE) evolution, mass transfer processes, supernova (SN) mechanisms, and natal kicks, as well as the metallicity-specific star formation rate density and its redshift evolution (see, e.g., Broekgaarden et al. 2021, for a review). Varying model assumptions can make the rate predictions plausible, but this alone is not enough to obtain decisive constraints on the uncertain physical processes without detailed modeling and systematic joint investigations of all GW observables. As a result, the relatively well measured GW observables such as chirp masses and effective spins, which include the information of individual compact object masses, BH spins, and spin-orbit tilt angles, provide valuable constraints on the astrophysical models.

In this work, we present detailed binary evolution models that follow the entire evolution of binaries from zero-age main sequence (ZAMS) to the formation of merging NSBHs for the first time. We used the population synthesis framework `POSYDON` (Fragos et al. 2023) to carry out a BPS study of NSBH systems that will merge within a Hubble time. We focused on NSBH populations at solar metallicity and investigated their formation channels in detail. With `POSYDON`, we can evolve binaries using extensive simulation grids of stellar structure and binary evolution simulations computed with the stellar evolution code Modules for Experiments in Stellar Astrophysics (MESA, Paxton et al. 2011, 2013, 2015, 2018, 2019; Jermyn et al. 2023). The detailed simulations allow us to track the changes of the internal structure of the stars, taking into account both single-star evolution and binary interactions, as well as the angular momentum transport in the interior of the stars and between binary components. This enables us to make a self-consistent estimation of mass-transfer rate and thus an accurate appraisal of the mass transfer stability. Furthermore, the feedback of mass changes from stellar winds or mass transfer on the stellar structure is modeled self-consistently (see, e.g., Bavera et al. 2023). Such model advancement allows us to infer the end of the mass-transfer phase more accurately, resolving potentially partially stripped envelopes (Klencki et al. 2022). When the binary ensues into a CE phase, we are able to calculate the binding energy self-consistently from the internal structure of the actual donor star model. Finally, we can estimate the properties of compact objects such as masses and BH spins based on the internal stellar-structure profiles of the immediate progenitor stars.

This paper is organized as follows. In Sect. 2, we briefly introduce `POSYDON` and describe the most important input physics in the code. We present individual examples of binaries leading to the formation of NSBH, as well as the population properties of merging NSBH in Sect. 3, and we show the impact of a set of model uncertainties in CE evolution and core-collapse prescriptions in Sect. 4. Finally, we discuss our findings in Sect. 5 and summarize them in Sect. 6.

2. The binary population synthesis code – `POSYDON`

We used the newly developed BPS code `POSYDON` to study merging NSBHs. In contrast to most rapid BPS codes, `POSYDON`

Table 1. Median and 90% symmetric credible intervals on component masses, chirp masses, and effective inspiral spins for the NSBH merger event candidates.

Event	$M_{\rm BH}\,[M_\odot]$	$M_{\rm NS}\,[M_\odot]$	$M_{\rm chirp}\,[M_\odot]$	$\chi_{\rm eff}$
GW200115 [(1)]	$5.7^{+1.8}_{-2.1}$	$1.5^{+0.7}_{-0.3}$	$2.42^{+0.05}_{-0.07}$	$-0.19^{+0.23}_{-0.35}$
GW200105 [(1)]	$8.9^{+1.2}_{-1.5}$	$1.9^{+0.3}_{-0.2}$	$3.41^{+0.08}_{-0.07}$	$-0.01^{+0.11}_{-0.15}$
GW190426 [(2)]	$5.7^{+3.9}_{-2.3}$	$1.5^{+0.8}_{-0.5}$	$2.41^{+0.08}_{-0.08}$	$-0.03^{+0.32}_{-0.30}$
GW190917 [(3)]	$9.7^{+3.4}_{-3.9}$	$2.1^{+1.1}_{-0.4}$	$3.7^{+0.2}_{-0.2}$	$-0.08^{+0.21}_{-0.43}$
GW191219 [(4)]	$31.1^{+2.2}_{-2.8}$	$1.17^{+0.07}_{-0.06}$	$4.32^{+0.12}_{-0.17}$	$-0.00^{+0.07}_{-0.09}$

References. [(1)]Abbott et al. (2021b). [(2)]Abbott et al. (2021a). [(3)]Abbott et al. (2021c). [(4)]Abbott et al. (2023).

evolves binaries based on detailed stellar and binary models. For a detailed description of the code, we invite the reader to consult Fragos et al. (2023). In what follows, we only summarize some of its key aspects.

POSYDON contains five pre-calculated stellar and binary evolution grids including two single-star grids -a hydrogen (H)-rich star grid and helium (He)-rich star grid- as well as three binary grids in circular orbits with various initial orbital periods, primary masses, and mass ratios; these are the hydrogen ZAMS binary grid; an H-rich star at the onset of Roche-lobe overflow (RLOF) and a compact object grid; and an He-rich ZAMS and a compact object (CO-HeMS) grid. The single-star grids are used to treat the non-interacting binaries in eccentric orbits (see Sect. 8.1 in Fragos et al. 2023). The binary grids were first post-processed so that the data size of the original binary evolution calculations is reduced and additional quantities used in BPS are computed. We then applied classification and interpolation algorithms to the outputs of the three grids, which enabled us to effectively interpolate between the pre-computed binary evolution simulations and estimate the evolution of any arbitrary binary. These algorithms currently allow for the interpolation between the initial and the final state of a binary evolution calculation. As a simpler alternative, we also provide the functionality to evolve individual binaries using nearest-neighbor matching. While the former approach is the default in population synthesis calculations, nearest-neighbor matching can be used in situations where for a specific binary we need to demonstrate its detailed time evolution (see, e.g., Figs. 1 and 2).

2.1. Stellar physics

We summarize the most important stellar physics model assumptions including stellar winds and mixing adopted in our stellar models. Regarding stellar winds, we used the `Dutch` scheme in `MESA` for stars initially more massive than 8 $M_\odot$. Specifically, we adopted the wind prescription of de Jager et al. (1988) for cool stars with effective temperatures below 10 000 K and Vink et al. (2001) for hot stars with effective temperatures above 11 000 K. Between these two temperatures, we linearly interpolated the wind-loss rates. If the surface H fraction of the hot star was below 0.4, we employed the Wolf–Rayet wind mass-loss rates of Nugis & Lamers (2000). For stars initially below 8 $M_\odot$, the `Dutch` scheme was used again when their effective temperature exceeded 12 000 K. On the other hand, for stars cooler than 8000 K, Reimers (1975) wind with a scaling factor $\eta_R = 0.1$ was adopted for those on the red giant branch and the Bloecker (1995) wind with scaling factor $\eta_B = 0.1$ was adopted for those in the thermally pulsating phase. Between 8000 K and 12 000 K, we linearly interpolated the wind-loss rates between the cool and hot winds.

To treat the convective mixing, we adopted the mixing-length theory (MLT, Böhm-Vitense 1958) with a mixing length parameter of $\alpha = 1.93$. For the overshooting mixing, we used the exponential decay formalism (Herwig 2000; Paxton et al. 2011) with the free parameter $f_{\rm ov} = 0.016$ for stars below 4 $M_\odot$ (Choi et al. 2016) and $f_{\rm ov} = 0.0415$ for stars more massive than 8 $M_\odot$. The latter is converted from the result of Brott et al. (2011), that is, $\alpha_{\rm ov} = 0.335$ via the rough ratio ∼10 between the step overshoot formalism parameter $\alpha_{\rm ov}$ and the exponential decay formalism parameter $f_{\rm ov}$ (Claret & Torres 2017). We note that we backed up 0.008 times the scale height from the edge of the convective zone when assigning $f_{\rm ov}$. We made a smooth transition between the two values of $f_{\rm ov}$ for stars within 4−8 $M_\odot$. Additionally, we adopted the Spruit–Tayler dynamo (Spruit 2002) to account for the efficient coupling between the stellar core and envelope. We treated rotation mixing and angular momentum transport following the MIST project (Choi et al. 2016).

2.2. Tidal interactions and binary mass transfer

Tidal interactions in a binary system affect the orbital evolution and the rotational properties of the stars. In a close detached binary, tidal forces efficiently circularize the orbit and lead to the synchronization between the stars' rotation rates and the orbit. We followed Hut (1981) to calculate the evolution of binary separation, eccentricity, and star rotation, considering the difference between convective and radiative envelopes (Hurley et al. 2002; Qin et al. 2018). For the initial state of the binary models, we assumed the spins of two ZAMS stars are synchronized with the orbits.

By virtue of detailed simulations, we were able to model the mass transfer in a self-consistent way, considering the feedback of mass loss or gain along with the angular momentum change for both donors and accretors. For a main-sequence star, we adopted the `contact` scheme in `MESA` to calculate the mass-transfer rate during RLOF. In contrast, for an evolved star, when its center H abundance is below 10^{-6}, we used the `Kolb` scheme (Kolb & Ritter 1990) to allow for a better treatment of the extended envelope. Based on the nature of the accretor, we treated the mass-accretion process differently. In the case of accretion onto a compact object, we limited the accretion at the rate corresponding to the Eddington luminosity, $L_{\rm Edd}$, which can be written as

$$L_{\rm Edd} = \frac{4\pi G M_{\rm acc} c}{\kappa}, \tag{1}$$

where G is the gravitational constant, c is the speed of light, $M_{\rm acc}$ is the mass of the accretor, and κ is the opacity. The excess mass transferred is assumed to be lost as isotropic wind, carrying with it the specific orbital angular momentum of the accretor. In the case of accretion onto a non-degenerate star, we considered a rotation-dependent accretion. The transferred material carrying angular momentum will spin up the outer layer of the accretor, considering both ballistic and Keplerian disk mass transfer (de Mink et al. 2013). The accretor's rotation will reduce the accretion rate by enhancing its stellar wind (Langer 1998). Most importantly, accretion is ceased when the accretor reaches critical rotation, implicitly boosting its winds as much as needed in order to not exceed $\omega/\omega_{\rm crit} \sim 1$.

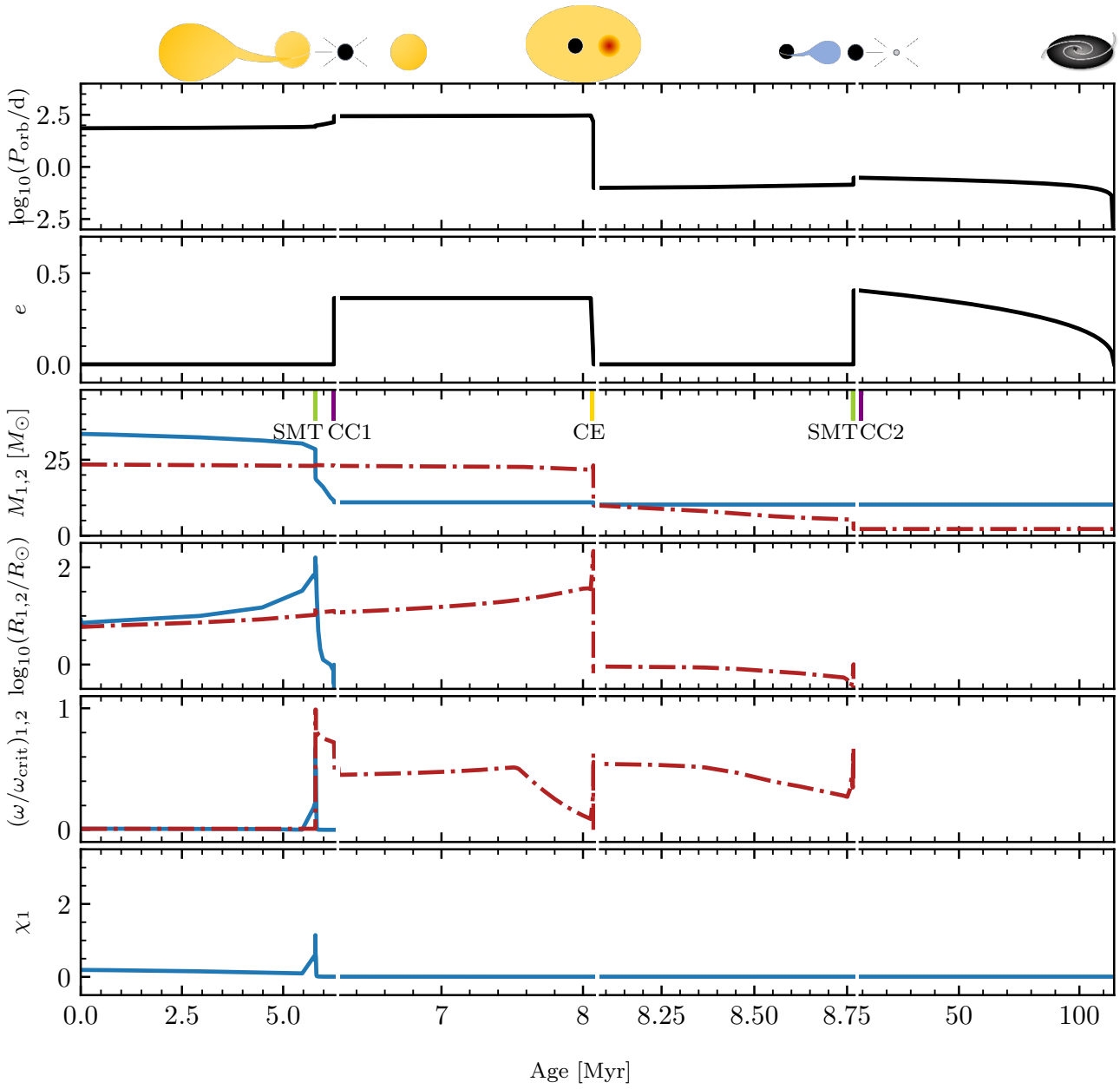

Fig. 1. Evolutionary path, from ZAMS to the merger, of an NSBH binary from channel Ia. From top to bottom, we show the evolution of the orbital period $P_{\rm orb}$, eccentricity e, component masses $M_{1,2}$, star radii $R_{1,2}$, surface angular velocity over the critical value $(\omega/\omega_{\rm crit})_{1,2}$, and the spin of the primary χ_1. The solid blue line represents the star that evolves to form a BH, while the red dashed-dotted line represents the star that becomes an NS. In the panel of stellar mass evolution, we indicate the onset of the stable mass transfer (SMT), the first core collapse (CC1), the common envelope (CE) phase, and the second core collapse (CC2) with the short vertical lines.

2.3. Common-envelope evolution

Common-envelope evolution is crucial for the formation of close double compact objects. If the binary experiences unstable mass transfer and the donor is not a main-sequence star or a stripped He star, the binary will enter a CE phase. Then, the companion transports orbital energy and angular momentum to the CE, causing dramatic orbital shrinkage. If the CE is successfully ejected during this process, the binary will avoid a merger and go into a detached phase with the core of the donor and the companion. In our detailed binary evolution simulations, we considered the following conditions as the criteria for the onset of unstable mass transfer. Firstly, whenever the mass-transfer rate exceeded $0.1\,M_\odot\,{\rm yr}^{-1}$, we assumed it becomes unstable as the mass transfer is only expected to be more rapid after reaching this limit. Secondly, we checked if the star had mass loss from the second Lagrangian point (L2). The mass loss from the L2 point is considered to take away a significant amount of angular momentum from the binary leading to a rapid orbital shrinkage and triggering CE evolution (Tylenda et al. 2011; Nandez et al. 2014). For the case where the donor is a post-main-sequence star, we checked L2 RLOF following the implementation of Misra et al. (2020), while for the case of two main-sequence stars, we calculated the L2 radius using the prescription from Marchant et al. (2016). Thirdly, for a compact object accretor, if its photon trapping radius (Begelman 1979) extended beyond the Roche-lobe

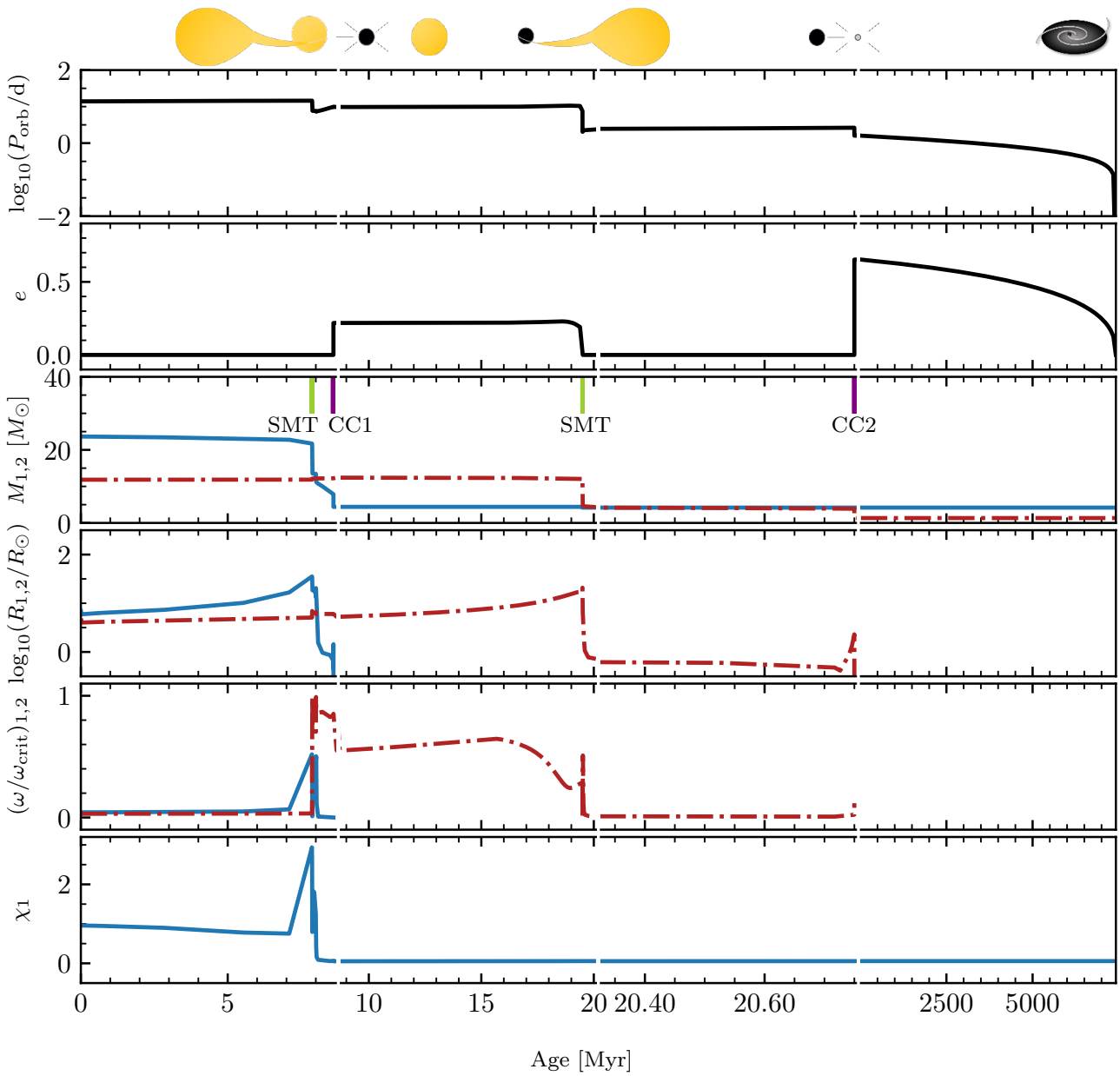

Fig. 2. Same as Fig. 1, but for an NSBH binary formed through channel IIa.

radius, the binary would enter CE evolution. Finally, if both binary components filled their Roche lobe, that is the binary was in a contact phase, and at least one of the stars had evolved beyond its main sequence, we assumed the binary had entered a CE phase.

To treat CE evolution, we used the $\alpha-\lambda$ formalism (Webbink 1984; Livio & Soker 1988). The value of $\lambda_{\rm CE}$ depends on the mass and evolutionary stage of the stars, affected by the internal structure and internal energy of the star (de Kool 1990; Dewi & Tauris 2000). At the onset of the CE phase, we calculated the value of λ self-consistently using the stellar profile. To encompass the model uncertainty on the boundary of the core and the envelope, we implemented three hydrogen abundances for the definitions of the He core-envelope boundary, which are $X_{\rm H} = 0.01, 0.1$ and 0.3. We took the value 0.1 as the default. The $\alpha_{\rm CE}$ parameter determines how efficient the orbital energy can be converted to eject the envelope. The value of $\alpha_{\rm CE}$ is still uncertain and not necessarily constant for stars with different properties. We took $\alpha_{\rm CE} = 1.0$ as the default value. With these two parameters, we can calculate the binding energy of the envelope and the post-CE orbit where the transferred orbital energy is enough to disperse the envelope. If in the post-CE orbit computed by the $\alpha-\lambda$ formalism the core of the donor and the companion were not filling their Roche lobe, we considered the CE phase to be successful.

2.4. Core-collapse physics and compact-object formation

We adopted the Fryer et al. (2012) delayed core-collapse prescription by default to calculate the remnant baryonic mass of core-collapse SN (CCSN). The pre-SN carbon-oxygen core mass $M_{\rm CO,core}$ determines whether the star explodes and the fall-back fraction $f_{\rm fb}$ of the ejected mass. In addition, we explored other core-collapse prescriptions including the Fryer et al. (2012) rapid prescription and the Patton & Sukhbold (2020) prescription. The latter determines the explodability of a

star based on the $M_{\rm CO,core}$ and the carbon mass fraction of the stellar core at the point of carbon ignition. For electron-capture SN (ECSN), we considered stars with the final He core masses in the range of 1.4–2.5 $M_\odot$ (Podsiadlowski et al. 2004) as their progenitors.

To covert the remnant baryonic mass to gravitational mass for the compact objects, we followed the method of Zevin et al. (2020). Furthermore, we assumed the maximum mass for an NS to be 2.5 $M_\odot$ (see discussion in Abbott et al. 2020, and references therein). Finally, we estimate the birth BH spins based on the final stellar profiles in our grids following the method described in Appendix D of Bavera et al. (2021), while we assumed the spins of NSs are zero for simplicity.

A newly born compact object may receive an SN natal kick because of asymmetric mass ejection and neutrino mass loss that can tilt the orbit, alter the orbital separation and eccentricity, or even disrupt the binary. By default, we adopted a natal-kick velocity following a Maxwellian distribution with a velocity dispersion of $\sigma_{\rm CCSN} = 265\,{\rm km\,s^{-1}}$ (Hobbs et al. 2005) for CCSN and $\sigma_{\rm ECSN} = 20\,{\rm km\,s^{-1}}$ for ECSN (Giacobbo & Mapelli 2019). The BH kick velocities follow the CCSN distribution, rescaled by a factor of $1.4\,M_\odot/\,M_{\rm BH}$. We calculated the orbital tilt θ introduced by the natal kick using Eq. (5) from Kalogera (1996), which is defined as the angle between the angular momentum of the post-SN orbit and the spin vector of the compact object.

After the formation of the BH, the secondary star may initiate a mass-transfer phase. In that case, we assumed that the secondary star's spin would always be aligned with the first post-SN orbit. The accretion process onto BHs is expected to affect both the magnitude and the direction of the BH spins (Fragos et al. 2010). In addition, the accretion disk may become a warped disk due to the Lensing–Thirring effect (Scheuer & Feiler 1996), which would accelerate the alignment between the BH spin and the orbit. However, in the case of binaries with stellar-mass BHs, the effect can be very weak (King et al. 2005). We assumed that the transferred material has the specific angular momentum at ISCO. The BH's angular momentum J can be divided into two components, along (J_y) and perpendicular (J_x) to the angular momentum of the orbit. For simplicity, we assumed the BH gains all the mass at once and the transferred angular momentum contributes to changing J_y. After accretion, the total angular momentum of the BH is equal to $\sqrt{J_{y,\rm acc}^2 + J_x^2}$, the tilt angle from the first SN, θ_1, becomes $\arccos(J_{y,\rm acc}/J)$, and the updated BH spin $\chi_{\rm BH}$ is determined by J. The simplified assumption might lead to the underestimation of the change on BH spin and tilt because the specific angular momentum of the ISCO is constantly changing during the accretion phase. However, we find that this has only a marginal impact on the majority of the binaries, as discussed in the next section.

When the second SN happens, the orbit is tilted again. The final tilt angle of the BH can be calculated from the two tilt angles θ_1 and θ_2:

$$\cos\theta = \cos\theta_1\cos\theta_2 \pm \sin\theta_1\sin\theta_2\cos\alpha, \tag{2}$$

where $\alpha \in [0, \pi]$ is the angle of the relative position of two SN in the orbit, which we chose randomly as we attributed random mean anomaly for the two SN kicks. When $\alpha = 0$ or π, the three vectors – the BH spin, the first post-SN orbital plane, and the second post-SN orbital plane – all lie in the same plane. This occurs either when both SNs take place at the same relative position within the orbit or at opposite sides of the orbit. In such cases, the final tilt is the addition or subtraction of the two tilt angles, which is also determined by whether the tilts are in the same or opposite directions.

With the information of component spins and orbital tilt angles, we can calculate the effective inspiral spin defined as

$$\chi_{\rm eff} = \frac{M_{\rm BH}\chi_{\rm BH}\cos\theta_{\rm BH} + M_{\rm NS}\chi_{\rm NS}\cos\theta_{\rm NS}}{M_{\rm BH} + M_{\rm NS}}, \tag{3}$$

where $\theta_{\rm BH}$ and $\theta_{\rm NS}$ are the misalignment angles between spin vectors of compact objects and the vector along the final orbital angular momentum. $\theta_{\rm BH}$ is equal to the final tilt angle θ in Eq. (2). Because we assume $\chi_{\rm NS} = 0$, $\chi_{\rm eff}$ is determined by the component masses, BH spin, and the final tilt angle.

2.5. Initial binary properties

For each of our populations synthesis models, we evolved 10^7 binaries, starting from two H-rich ZAMS stars. We randomly sample the initial masses of the primary stars, $M_{1,i}$ in the range of 7–120 $M_\odot$, following a distribution of the initial mass function from Kroupa (2001). The secondary masses, $M_{2,i}$ are in the range of 0.35–120 $M_\odot$ following a uniform distribution between the minimum and $M_{1,i}$ (Kobulnicky & Fryer 2007). The distribution of the initial orbital separation is logarithmically flat between 1 and $10^5\,R_\odot$, and we assumed zero eccentricity for the primordial binaries. To display the population properties of merging NSBHs, we applied a burst star formation history, which assumes all stars form at the same time.

3. Results

3.1. Formation channels

In our simulation, we found BHs always form first in merging NSBH systems. We identified two main formation channels for the merging NSBH systems. One involves stable mass transfer before the formation of the first-born compact object and CE evolution between a BH and a nondegenerate star (≈70%; the percentage refers to the number of merging NSBH systems per unit of simulated stellar mass) and the other one involves only a stable mass transfer episode(s) during the evolution (≈30%). Each channel can be further divided into two sub-channels based on the details of the mass transfer episodes, as we discuss in the following sections. For each channel, we illustrate the evolutionary path of a typical binary for the dominant sub-channel from a `POSYDON` simulation as an example.

3.1.1. Stable mass transfer and common envelope evolution channel

We refer to the channel involving stable mass transfer between two nondegenerate stars and a CE phase after the BH formation as channel I. The first stable mass-transfer phase occurs when the primary star begins expanding during the H shell-burning stage or the He core-burning stage. After the mass-transfer phase, the primary star loses its H-rich envelope through stellar winds. The stripped star then undergoes CCSN, forming a BH. After the first core collapse, the binary remains detached until the secondary star enters post-main-sequence phase and fills the Roche lobe. The second mass-transfer phase is unstable, leading to a CE phase. If the CE evolution is successful, the secondary star will lose the H-rich envelope with the ejection of the CE, leaving behind an He star. About 94% of the binaries undergo a third mass-transfer episode -a case-BB stable mass-transfer phase- between the BH and the He star, followed by the secondary

star exploding and forming an NS. We refer to this channel as channel Ia. Alternatively, the remaining binaries evolve without undergoing any further mass-transfer episode after the CE phase. This is regarded as channel Ib. An illustration of the evolutionary phases are indicated at the top of Fig. 1, in which we show the evolutionary path of a typical NSBH merger evolving through channel Ia.

The binary in Fig. 1 initially has a primary star of 33.50 $M_\odot$, a secondary star of 23.45 $M_\odot$, and an orbital period of 72.0 d. The primary loses mass through stellar winds down to 28.50 $M_\odot$ before the mass-transfer phase initiates. The stable mass transfer starts at 5.795 Myr after the birth of the binary system, lasting for only ∼15 000 yr. The secondary is spun up quickly due to the accretion, gaining about 0.4 $M_\odot$ in total. The primary experiences CCSN at 6.257 Myr forming a BH of 10.98 $M_\odot$ with a negligible spin of $\chi_{\rm BH} = 0.005$, and the binary goes into the detached phase. As the secondary evolves, the mass transfer from the secondary onto the BH starts, shrinking the orbit. Soon after the onset of the mass transfer, the secondary radius exceeds the L2 Roche lobe radius, leading to a CE phase at 8.073 Myr. When the CE is ejected, the secondary is a stripped He-rich star of 9.97 $M_\odot$, and it expands at the end of the He-burning phase, leading to a case-BB mass-transfer phase. Eventually, the secondary collapses to a 2.20 $M_\odot$ NS at 8.766 Myr, and the binary merges at 552.3 Myr due to energy and angular momentum loss from GW radiation.

3.1.2. Stable mass transfer channel

We refer to the channel that involves only stable mass transfer episode(s) as channel II. About 96.4% of them undergo two stable mass-transfer phases. The binary first undergoes a stable case-A or case-B mass-transfer phase, resulting in the donors being partially stripped at the end of the main sequence. Consequently, the primary stars do not enter a giant phase as in channel I, but gradually shrink after evolving off the main sequence. After the formation of the BH, the binary experiences stable case-A or case-B mass transfer and some of them may experience both case-A and case-B mass transfer at the second mass-transfer phase. Finally, the secondary star explodes forming an NS. We refer to this channel as channel IIa. In cases where the primary stars are more massive than ≈60 $M_\odot$, the binaries may avoid the first mass transfer. This is because at solar metallicity, our POSYDON stellar models predict that the stars above ≈60 $M_\odot$ do not expand to the red supergiant state with radii of ∼1000 $R_\odot$ (Bavera et al. 2023). The mass loss through stellar winds from the stars keeps widening the orbits until the first core collapse. Subsequently, the binaries undergo case-A or case-B stable mass transfer from the secondary onto the BH and the secondary stars become NSs in the end. This sub-channel accounts for about 4.6% of channel II, and we refer to it as channel IIb. Without an efficient orbital shrinkage mechanism, at the time of NS formation, binaries from channel II have relatively wide orbits compared with those of channel I. Consequently, only the NSBHs formed with eccentric orbits (caused by SN natal kicks) result in a delay time shorter than a Hubble time.

Figure 2 shows a a typical binary evolving through the channel IIa, which initially has a 23.66 $M_\odot$ primary, an 11.83 $M_\odot$ secondary, and an orbital period of 13.90 d. The first stable mass-transfer phase starts at 7.867 Myr and ends at 7.882 Myr when the primary is still a main-sequence star. The secondary star reaches near-critical rotation during the mass-transfer phase, with the rate as high as $\approx 10^{-2.5}\,M_\odot\,{\rm yr}^{-1}$. After a short time of being detached from the secondary, the primary evolves off the main sequence, and the mass transfer starts again at 8.003 Myr and ends at 8.012 Myr with a peak of $\approx 10^{-3.3}\,M_\odot\,{\rm yr}^{-1}$. During the mass-transfer phase, the secondary star accretes about 0.4 $M_\odot$ in total. In the meantime, the primary loses its envelope through mass transfer and winds. At 8.600 Myr, the primary explodes to form a BH of 4.40 $M_\odot$ with a dimensionless spin parameter of $\chi_{\rm BH} = 0.05$. Then, a stable mass-transfer phase ensues from the secondary onto the BH. The secondary later explodes to form an NS of 1.28 $M_\odot$ at 21.73 Myr. Finally, the binary merges at 6116 Myr.

Our results regarding formation channels demonstrate disparities with previous population studies. In the investigations by Dominik et al. (2012) and Broekgaarden et al. (2021), which utilized rapid BPS codes based on the SSE fitting formulae (Hurley et al. 2000), the NSBH formation is heavily dominated by channel I (≳90%) at solar metallicity. Iorio et al. (2023), employing updated single stellar tracks in their simulations, predicted a reduced fraction of about 50% for channel I at solar metallicity. However, their fraction of channel II becomes marginal at high metallicities. These discrepancies stem from differences in stellar models implemented in BPS codes and the approach to treating mass transfer stability.

3.2. Population properties of merging NSBHs

In this section, we present the population properties of merging NSBHs and their progenitors, including component masses, orbital properties, BH spins, final tilt angles, and effective spins. We selected all the NSBH systems that merge within a Hubble time and distinguish them by the formation channels[1].

3.2.1. Progenitors of merging NSBHs

In the left panel of Fig. 3, we show the initial orbital periods $P_{{\rm orb},i}$ versus the initial primary masses $M_{1,i}$ of merging NSBHs. The majority of the binaries from channel I have $P_{{\rm orb},i}$ above ≈50 d, and most of the binaries evolving through channel II have closer orbits with $P_{{\rm orb},i}$ in the range from a few days to a few tens of days. Binaries with initial primary masses high enough to produce a BH and initial periods ≲50 d are more likely to result in post-BH-formation orbits that subsequently lead to stable case-A or case-B mass transfer, from the secondary star onto the BH this time. Even if the mass ratio is such that the mass transfer is unstable, the CE evolution will result in a merger, as the donor star is still very compact. For binaries with initial periods ≳50 d, even when they result in post-BH formation binaries that undergo stable mass transfer, the final orbital periods at the formation of NSBH that are too wide to lead to a merger within a Hubble time. In contrast, the progenitor binaries from channel I, must have initial periods ≳50 d, such that the post-BH formation orbital periods are wide enough to not only lead to unstable mass transfer, but they also have the secondary star sufficiently evolved at the onset of the unstable mass transfer so that CE evolution can lead to the successful ejection of the envelope. The interplay of all these processes determines the relatively sharp

[1] For ≲2% of the total number of simulated NSBH binaries, specifically those originating from areas where the parameter space is close to the boundary between stable and unstable mass transfer, our classifiers fail to classify the type of the resulting compact object. While we are still able to correctly infer the masses and orbital properties for these binary compact objects, we cannot properly estimate the BH spins. Given the small number of systems that encounter this issue, we decided to exclude them from our analysis. This known technical issue of POSYDON v1 will be addressed in future releases.

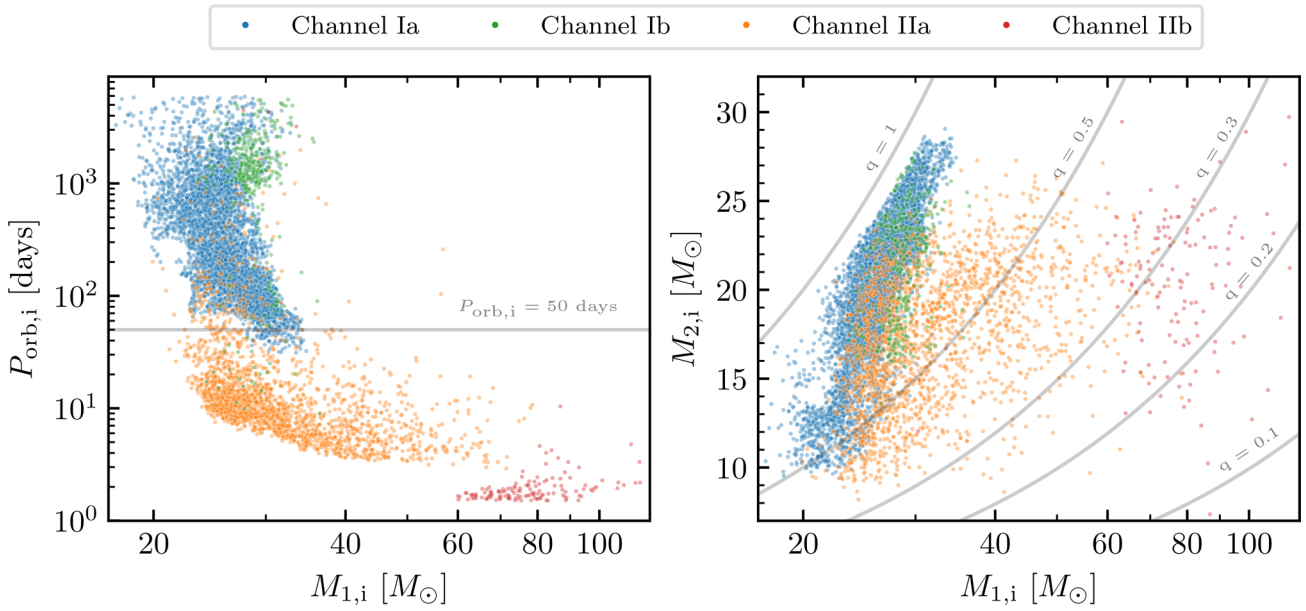

Fig. 3. Initial properties of progenitors of merging NSBHs. The blue, green, orange, and red dots represent binaries from channels Ia, Ib, IIa, and IIb, respectively. The left panel shows the primary masses versus initial binary orbital periods. The gray line indicates a 50 day orbital period for reference. The right panel displays the component masses with the gray lines indicating different mass ratios q, defined as $M_{2,i}/M_{1,i}$.

boundary in initial orbital periods that separate channel I and channel II.

In channel II, the binaries with the most massive primary stars have the shortest initial orbital periods of a few days. The strong winds of the massive stars will keep widening the orbit during the early evolution, resulting in orbital periods of ≈10 d in the end. These binaries experience no RLOF mass transfer before the BH formation because the massive primary stars do not expand to become supergiant stars.

The ZAMS masses of the progenitor stars of merging NSBHs are shown in the right panel of Fig. 3. The primary stars that evolve into BHs have initial masses $M_{1,i}$ varying from ≈17 to ≈120 $M_\odot$, with the majority of them in the range of ≈20 to ≈40 $M_\odot$. The secondary stars that form NSs have initial masses $M_{i,2}$ lying within the range of ≈8 to ≈30 $M_\odot$. Most of the binaries evolving through channel I exhibit initial mass ratios $q = M_{i,2}/M_{i,1}$ greater than 0.5, while binaries originating from channel II display a broader range of mass ratios. Notably, binaries from channel II have small mass ratios and can reach below 0.2. The right panel of Fig. 3 also shows the scarcity of massive (≳40 $M_\odot$) primary stars in channel I. Given the adopted stellar physics parameters in `POSYDON`, a 40 $M_\odot$ can lead to the formation of BH as massive as 18 $M_\odot$. Such massive BHs, when paired with secondary stars that are potential NS progenitors (≲28 $M_\odot$), they experience stable mass transfer independently of the post-BH formation orbital periods and thus cannot be progenitors of merging NSBHs from channel I.

3.2.2. Compact objects in merging NSBHs

The left panel of Fig. 4 shows the orbital periods and eccentricities of the merging NSBHs at the time of double compact object formation. Channel I is capable of forming merging NSBH systems in close obits ≲0.1 d due to CE evolution, whereas channel II can only form them in orbits ≳1 d. A large number of the NSBH systems forming without undergoing a CE phase have too long delay times to merge within a Hubble time, except for those that obtain a high eccentricity from natal kick at the second SN. The merging NSBHs from channel II have eccentricities ≳0.5.

In Fig. 4 on the right, we show the BH and NS masses of merging NSBHs as well as the 90% confidence intervals of NSBH merger candidates GW200115, GW200105, GW190917, and GW190426. GW191219 is not included because its BH mass is much larger than the maximal values in our population. The median of the component masses of the four candidates are within the mass range of merging NSBHs from our model. However, we cannot rule out the possibility that they were formed in a lower metallicity environment. Overall, the NS masses cover a mass range from ≈1.26 to ≈2.4 $M_\odot$, and the BH masses are from ≈2.5 to ≈20 $M_\odot$. Channel I forms BHs less massive than ≈12 $M_\odot$, while channel II is able to produce more massive BHs, but only a small fraction of them are above 15 $M_\odot$. The Fryer et al. (2012) delayed mechanism we adopted to calculate the compact object mass from CCSN does not produce a BH mass gap from 2.5−5 $M_\odot$. The BHs in the mass gap account for 16.2% of the total NSBH population. In the Fryer et al. (2012) delayed prescription, the discontinuity of calculating proto-compact object mass at $M_{\rm CO,core}$ of 3.5 $M_\odot$ introduces an NS mass gap of ≈0.1 $M_\odot$ around 1.7 $M_\odot$. However, the existence of this gap is not observed in practice. In our simulation, the interpolation applied to obtain the NS masses smooths out the discontinuity. In the Fryer et al. (2012) delayed prescription, if the final $M_{\rm CO,core}$ of the compact object progenitor is less massive than 2.5 $M_\odot$, a constant NS mass of ≈1.27 $M_\odot$ is predicted. Accordingly, we can see the concentration at that mass especially for channel II. In channel I, the NS progenitors are more likely to have lower $M_{\rm He,core}$ in the range of 1.4−2.5 $M_\odot$, leading to ECSN and the formation of NSs at ≈1.26 $M_\odot$.

We calculated the BH spins using the stellar profiles of the BH progenitors at the onset of the SN event (see Sect. 8.3.4 in Fragos et al. 2023). The BH spins versus initial orbital periods is shown in Fig. 5, where the left panel shows the BH spins at birth and the right panel shows the final BH spins after accretion. From the left panel, we can see a significant correlation between

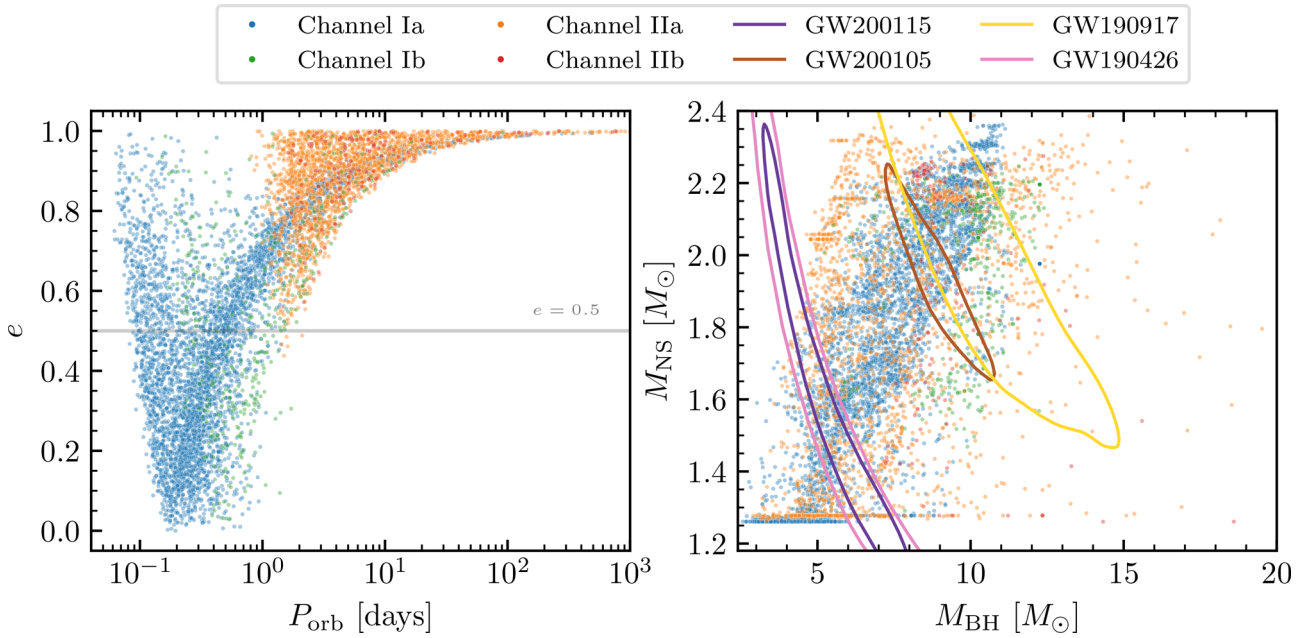

Fig. 4. Properties of merging NSBHs during formation of double compact object system. The left panel shows the orbital periods and eccentricities. The right panel shows the BH and NS masses and the 90% confidence intervals of GW200115, GW200105, GW190917, and GW190426.

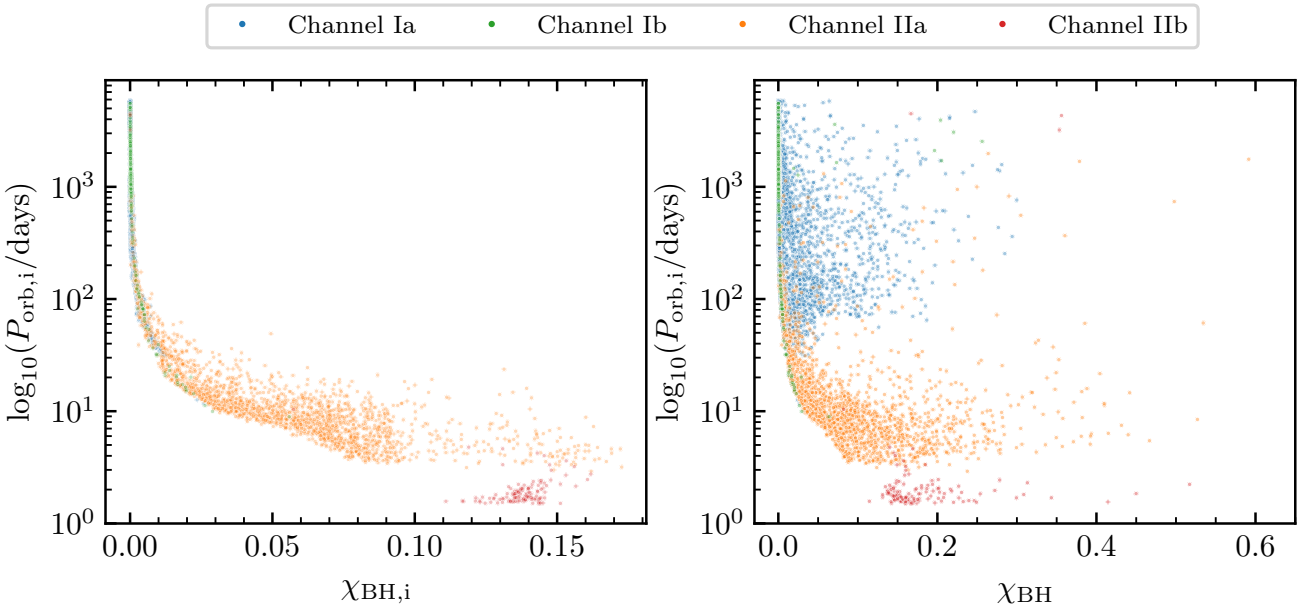

Fig. 5. BH spins versus initial orbital periods of merging NSBHs at BH birth (left) and after NS formation (right).

the BH spins and the initial orbital periods where shorter orbital periods correspond to higher BH spins. The prevalence of short initial orbital periods among the binaries in channel II results in a substantial number of BHs with non-negligible spins. In our models, the BHs always form from the primary stars. As we assume efficient angular momentum transport inside stars in our models, the primary stars are expected to lose most of their angular momentum through mass transfer and winds, forming BHs with negligible spins. However, the orbits of the initially close binaries can remain tight before the first core collapse, and tides could help spin up the progenitor stars. In this case, although the stars lose the envelope with nearly all the stellar angular momentum, the stripped primary stars preserve a portion of angular momentum contributing to the BH spins. Nevertheless, neither channel produces BHs with spins larger than ≈0.2 at BH birth, consistent with (Qin et al. 2018; Fuller & Ma 2019; Belczynski et al. 2020).

From the right panel, we can see that BHs can be moderately spun up by accretion. For channel I, the BHs gain spins less than ≈0.3 through case-BB stable mass transfer. For channel II, the BH spins increase mainly due to case-A stable mass transfer. Most of the BH spins still stay below 0.2, 8.4% of them are within the 0.2−0.4 range and only 0.7% of them exceed 0.4. In channel II, the inclination angle between the BH spin and the orbit is typically small because the pre-SN orbit is tightly bound and hard to tilt significantly with natal kicks. In channel I, some binaries possess large tilt angles or are even anti-aligned after the BH formation. However, the BH spins are close to zero. As

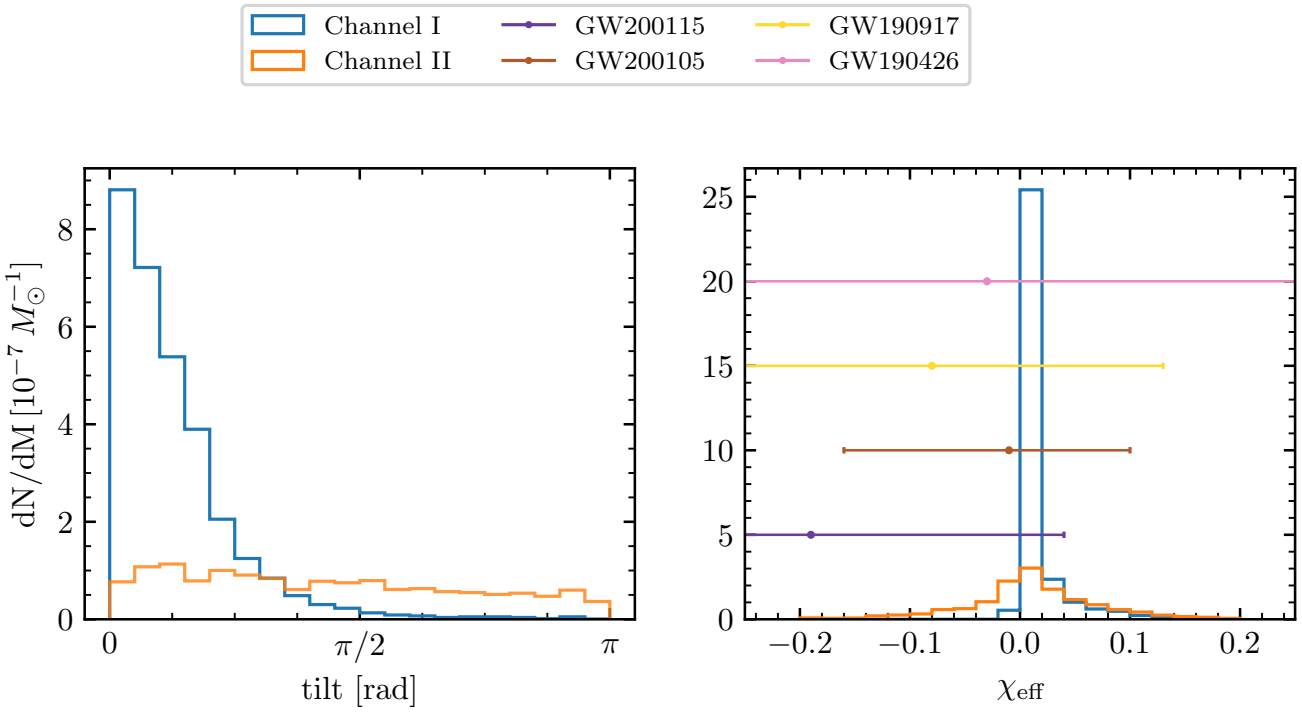

Fig. 6. Distribution of final tilt angles and effective inspiral spins for channel I (blue) and II (orange). The colored circles and corresponding error bars in the right panel show the median and 90% credible intervals of effective inspiral spins for the NSBH merger event candidates. For some of the observed systems, the error bars extend outside the range of the figure (see also Table 1).

a result, the impact of the simplified assumption on the spin evolution due to accretion is negligible for most of the binaries.

3.2.3. Spin-orbit tilt and effective inspiral spin

In Fig. 6, we show the distribution of the tilt angles between the BH spin and the orbital angular momentum, and the effective inspiral spins for the two channels. The numbers shown in the figure are normalized with the total underlying simulated mass of the population in units of $10^{-7}\,M_\odot^{-1}$. A large fraction of binaries from channel I have small tilt angles, and only about 2% of them end up with anti-alignment between the BH spin vector and orbital angular momentum vector. In contrast, for channel II, about 40% of the binaries have final tilt angles $>\pi/2$ rad.

The difference for the two channels is attributed to the different orbital velocity at the time of the second SN. In channel II, binaries experience a natal kick with a velocity comparable to the orbital velocity to provide high eccentricity to the orbit. Hence, the kick can tilt the orbit easily. In channel I, most binaries are in tightly bound orbits with high orbital velocities; thus, natal kicks in excess of $\gtrsim$1000 km s^{-1} would be required to tilt the orbit significantly. With the final tilt angles and BH spins, we calculated the effective spins of NSBH systems. The right panel of Fig. 6 shows the distribution of the effective inspiral spins for the two channels as well as the median and cut-off 90% credible intervals of effective inspiral spins for the NSBH merger event candidates. Most of the binaries from channel I possess BHs with nearly zero spins and small tilt angles, so the distribution of the effective spins peaks sharply at zero. A small fraction of BHs that have spun up due to accretion, contribute to the presence of systems with positive $\chi_{\rm eff} \gtrsim 0.02$. Channel II produces a larger fraction of spinning BHs and anti-aligned systems compared with channel I, leading to a flatter distribution of effective spins in the range of ≈ -0.2 to ≈ 0.2. The number of the binaries exhibiting non-negligible positive $\chi_{\rm eff}$, for example, $\chi_{\rm eff} \gtrsim 0.05$, is comparable between the two channels. In contrast, it is only channel II that can produce NSBH mergers with $\chi_{\rm eff} \lesssim -0.02$. Binaries with $\chi_{\rm eff}$ below -0.1 and above 0.1 account for only $\approx$2% for channel I and $\approx$14% for channel II.

3.2.4. Associated electromagnetic counterparts

Observations of EMCs associated with NSBH mergers can provide unique insights into the GW physics and put constraints on the NS equation of state. To date, no EMC has been associated with identified NSBH merger candidates. To predict the fractions of NSBH mergers associated with an EMC in our simulations, we follow the method presented in Foucart et al. (2018), which involves calculating the remnant mass outside the ISCO. We considered three scenarios for the NS radii of 11 km, 12 km, and 13 km. In the calculations, we also took into account the misaligned angles between the BH spins and the orbits using the component of the BH spin that is aligned with the orbital angular momentum.

The first line of Table 2 shows the fractions of NSBH mergers that are associated with an EMC under the different assumptions of NS radii. When assuming an NS radius of $R_{\rm NS} = 11$ km, the fraction of NSBH systems associated with an EMC for channel I is 1.69% and only 0.62% for channel II. In total, the fraction is 1.35%. These NSBHs feature light NSs $<1.29\,M_\odot$ and light BHs $<3.54\,M_\odot$. Even when assuming an NS radius of $R_{\rm NS} = 12$ km, the BH masses in these NSBHs remain below $4.77\,M_\odot$. This suggests that the NSBH mergers associated with EMCs involve a BH that falls within the mass gap of $2.5-5\,M_\odot$. The largest NS radius assumption of $R_{\rm NS} = 13$ km predicts a larger fraction of 15.80%, 9.83%, and 13.92% for channel I, channel II, and the total, respectively. The maximal BH masses of the binaries with EMCs reach up to $5.87\,M_\odot$, and the NS

Table 2. EMC fractions for different model assumptions of NS radii and model variations.

Models	Channel I			Channel II			Total		
	R_{NS} = 13 km	R_{NS} = 12 km	R_{NS} = 11 km	R_{NS} = 13 km	R_{NS} = 12 km	R_{NS} = 11 km	R_{NS} = 13 km	R_{NS} = 12 km	R_{NS} = 11 km
default	15.80%	8.71%	1.69%	9.83%	3.31%	0.62%	13.92%	7.01%	1.35%
α_{CE} = 0.5	3.71%	0.60%	0	10.84%	3.95%	0.55%	8.97%	3.07%	0.41%
$\lambda_{CE}^{X_H=0.3}$	8.43%	5.17%	1.94%	11.15%	3.72%	0.22%	9.46%	4.62%	1.29%
$\lambda_{CE}^{X_H=0.01}$	9.18%	1.24%	0.19%	10.66%	3.31%	0.39%	9.96%	2.32%	0.30%
σ_{CCSN} = 150 km s^{-1}	19.52%	10.92%	3.08%	15.36%	7.64%	1.21%	18.64%	10.23%	2.68%
σ_{CCSN} = 450 km s^{-1}	14.50%	8.37%	1.84%	5.98%	1.75%	0	11.79%	6.26%	1.25%
Fryer-rapid	0.015%	0	0	5.08%	0	0	1.47%	0	0
Patton&Sukhbold	0.025%	0.013%	0	0.29%	0.084%	0.042%	0.087%	0.029%	0.0097%

masses extend to 1.59 $M_\odot$. In this scenario, approximately 88%, 75%, and 85% of BHs in NSBH mergers associated with EMCs are within the mass gap for channel I, channel II, and the total, respectively.

Previous studies (Román-Garza et al. 2021; Hu et al. 2022) showed that if the NS forms first in an NSBH system, the BH progenitor can be spun up efficiently through tidal interactions with the NS, which results in a BH with high birth spin. The latter increases the possibility of having EMC. However, in our simulation, NSBHs with NS forming first account for a negligible fraction (<0.01%). This is different from the results in Román-Garza et al. (2021), where the fraction of NSBHs with NS formed first can be higher than 10%. We attribute the difference to the modeling of accretion onto nondegenerate stars. While in Román-Garza et al. (2021) the rapid BPS code `COSMIC` (Breivik et al. 2020) was used to simulate the binaries from two ZAMS stars until the formation of compact object–stripped He star binaries, in this study, we used the detailed simulations throughout the evolution of the binaries. The mass accretion model adopted for nondegenerate accretors in Breivik et al. (2020), which only limits the accretion when it exceeds ten times the thermal-timescale mass-transfer rate of the accretor, is significantly more efficient compared with the rotation-dependent model (de Mink et al. 2013) adopted in `POSYDON`'s detailed binary evolution calculations. In this model, the accreted material carries with it the specific angular momentum of a Keplerian accretion disk whose inner edge is at the surface of the accreting star. As a star is accreting mass, it is being spun up due to the high specific angular momentum of the accreted material, and it typically reaches critical rotation after accreting only a fraction of a solar mass. After the accreting star reaches critical rotation at its surface, we assume that further accretion of material ceases. Overall, this process results in very inefficient mass transfer ($\lesssim$10%), except in case-A mass transfer, where tidal spin down from the companion star counteracts the spin up due to accretion and accretion efficiencies of ≈30% can be reached (see also Langer et al. 2020).

The amount of mass that can be accreted onto the secondary, during the initial mass-transfer phase between two nondegenerate stars, plays a crucial role in determining whether the formation of the NS can precede the formation of the BH (Sipior et al. 2004; Broekgaarden et al. 2021). The accretion model adopted in `POSYDON`'s detailed binary evolution calculations results in low accretion efficiency and thus does not lead to enough mass accreted by the secondary stars to form BHs, while the primary stripped star forms an NS first. Shao & Li (2021) also predicted a very low fraction of NSBHs where the NS formed first, when using a similar rotation-dependent model. An additional factor that may lead to an increased fraction of first-born NSs in NSBH populations modeled by rapid codes is that case-A mass transfer, which is most often involved in the formation of NSBH binaries with first-born NSs, is not accurately modeled in rapid BPS codes (especially those using Hurley's fitting formulae; Hurley et al. 2000). The primary reason for this is that the formulae do not track the mass of the developing He core of the main-sequence star and the radius evolution of the star used to infer the end of the mass transfer does not take into account altered structure of the stripped donor star. Both these factors can lead to more extended case-A mass-transfer cases, where a larger fraction of the donor star is transferred onto the accretor (see Dorozsmai & Toonen 2022, for an extended discussion).

In our detailed binary evolution calculations, the accretion efficiency in case-A mass-transfer phases between two nondegenerate stars can reach up to ≈30%, which is in principle sufficient to result in a first-born NS and a second-born BH. However, the orbits of those binaries after the formation of the NS are still compact, and the subsequent mass transfer from the secondary star onto the NS, which is unstable due to the high mass ratio, leads to a merger during the CE evolution.

4. Model variations

Binary evolution modeling is subject to various uncertainties that can affect the BPS results significantly. Thus, it is always instructive to investigate the effects of model variations. Because `POSYDON` allows on-the-fly calculations at the stage of core collapse and CE evolution, we are able to apply different models for core collapse and CE evolution, showing their impact on the population properties of merging NSBHs. In contrast, changing physical assumptions such as the accretion efficiency, as discussed in the previous section (see also Sect. 5.1), would require us to rerun the entire library of pre-calculated binary evolution models, and thus it is outside the scope of this work.

4.1. Variations in common envelope prescriptions

In CE evolution, we considered the variations of the core-envelope boundary and α_{CE} parameters. We explored two more values of the H abundance, which are 0.01 and 0.3 (the default value is 0.1), to define the core-envelope boundary. Different core-envelope boundaries will directly affect the binding energy of the envelope. With lower H abundance for core-envelope definition, the boundary will be deeper inwards the star and the binding energy of the envelope that needed to be overcome will increase, leading to a smaller λ_{CE}. In addition, as the default

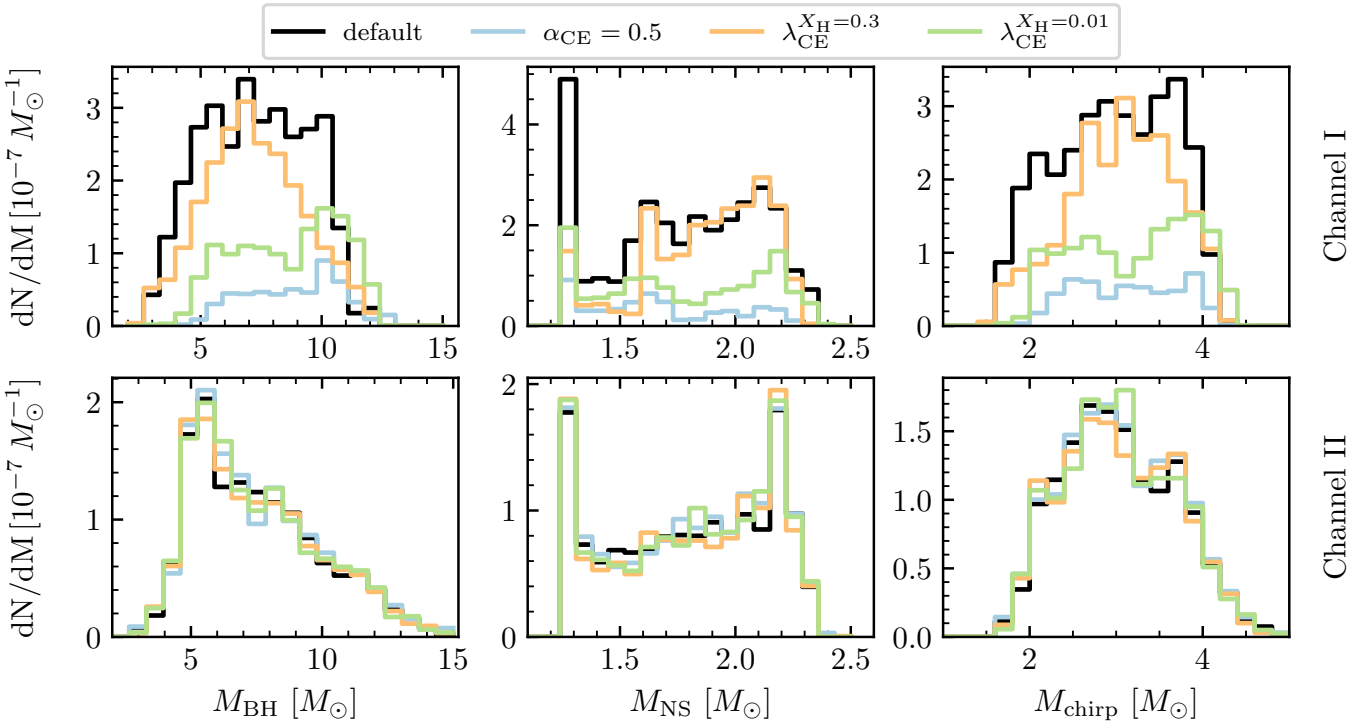

Fig. 7. Distributions of BH masses, NS masses, and chirp masses of merging NSBHs, scaled by the stellar mass of the parent population, for different parameters associated with CE evolution. The top and bottom correspond to channels I and II, respectively. The default model corresponds to $\alpha_{\rm CE} = 1.0$ and adopts $\lambda_{\rm CE}^{X_{\rm H}=0.1}$.

$\alpha_{\rm CE} = 1.0$, we apply a smaller $\alpha_{\rm CE}$ parameter of 0.5 as a model variation for comparison.

In Fig. 7, we show the distributions of NS masses, BH masses, and chirp masses for merging NSBHs under different parameters associated with CE evolution. The variations in CE evolution do not affect the stable mass transfer process and thus overall distributions have no differences for channel II. We can see that the $\lambda_{\rm CE}^{X_{\rm H}=0.3}$ model produces BHs peaking at around 7 $M_\odot$, while the other two variations have a larger fraction of BHs around 10 $M_\odot$. The $\lambda_{\rm CE}^{X_{\rm H}=0.01}$ model leads to a smaller core of the donor star and larger binding energy of the envelope, which makes the envelope harder to expel. A smaller value of $\alpha_{\rm CE}$ increases the energy needed to expel the donor's envelope. Consequently, a reduced $\alpha_{\rm CE}$ effectively decreases the overall number of binaries from channel I. For these two models, a heavy BH is favored because it reserves more orbital energy in the same orbit. The $\lambda_{\rm CE}^{X_{\rm H}=0.3}$ model results in wider post-CE orbits, which increases the probability of having merger delay times longer than the Hubble time. In addition, the $\lambda_{\rm CE}^{X_{\rm H}=0.3}$ model produces high-mass progenitor stars for the NSs, which are reflected by the relatively small number of light NSs. Perhaps most notably, for the two model variations with less efficient CE evolution (models $\alpha_{\rm CE} = 0.5$ and $\lambda_{\rm CE}^{X_{\rm H}=0.01}$), it is channel II that becomes the dominant one, with the fraction of merging NSBH binaries coming from channel I becoming 26.2% and 47.6%, respectively. Notably, as the model variations in CE do not impact channel II, the variability observed in each bin across the four models in channel II indicates the statistical uncertainties in our population. To assess this, we generated four random subsets for each model, estimating the statistical uncertainties to be consistent with assuming Poisson statistics errors. More importantly, we find that the characteristic features of the distributions are robust against statistical uncertainties.

In Fig. 8, we show the distributions of the final orbit tilt angle, effective spin, and delay time for different parameters associated with CE evolution. The variations in CE evolution have limited impact on the distribution of tilt angles and effective spins, other than the overall change in the normalization of the distribution. The merger delay time distribution, on the other hand, is sensitive to the $\alpha_{\rm CE}$ parameter and core-envelope definition. A smaller $\alpha_{\rm CE}$ or a smaller $\lambda_{\rm CE}$ means more orbital energy is needed to eject the envelope, suggesting a closer post-CE orbit, thus a shorter delay time. Under these two models, most binaries have delay time below $\approx 10^{8.5}$ yr. On the contrary, we can see that the $\lambda_{\rm CE}^{X_{\rm H}=0.3}$ model predicts more merging NSBHs with long delay times $\gtrsim 10^{9.5}$ yr because the core-envelope boundary moves outward, the envelope's binding energy decreases and CE evolution leads to less dramatic orbital shrinkage.

We notice that with the $\lambda_{\rm CE}^{X_{\rm H}=0.3}$ model, merging NSBHs can also form through double CE evolution. These binaries have initial mass ratios close to unity and orbital periods of several tens of days. They will enter a contact phase after both stars have evolved off the main sequence, which we assume leads to a double CE phase. When the CE is ejected successfully, two stripped He cores will find themselves to be left in an orbit of a few days. Afterward, the two stars will remain detached till the formation of NSBHs. However, the number of the merging NSBHs originating from this channel is extremely limited; these only account for 0.1% of the total. We thus do not discuss this channel any further.

4.2. Variations in core-collapse prescriptions

The properties of the compact object formed from a star naturally depend on adopted prescription for core-collapse process. These prescriptions map the properties of the structure of

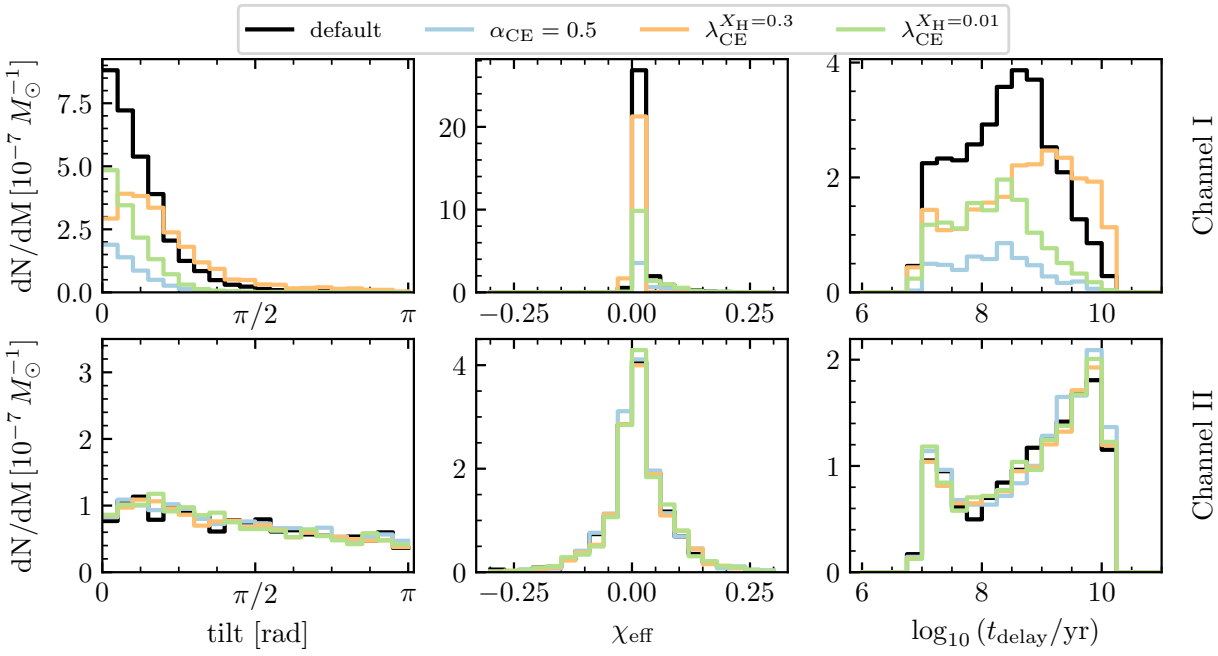

Fig. 8. Orbital tilt, effective spin, and delay time distributions for variations in CE evolution in channel I (top) and channel II (bottom).

the star right before the core collapse to the properties of the formed compact object, with different prescriptions predicting not only different compact object properties, but even different compact object types, for the same progenitor star structure. In this study, beside the default Fryer et al. (2012) delayed prescription, we considered two varying core-collapse prescriptions: the Fryer et al. (2012) rapid prescription and the Patton & Sukhbold (2020) prescription.

Similarly to in Fig. 7, we show the mass distributions for the two variation models compared with the default model in Fig. 9. The Fryer et al. (2012) rapid prescription produces a mass gap of 2.5−5 $M_\odot$ between NSs and BHs. It generates BHs within a mass range of ∼6−12 $M_\odot$ in channel I and an abundance of BHs with masses of ∼6−7 $M_\odot$ in channel II. The Patton & Sukhbold (2020) prescription predicts a BH mass range of ∼8−15 $M_\odot$ in both channels. Few NSs from the Fryer et al. (2012) rapid model exceed 2 $M_\odot$. For the Patton & Sukhbold (2020) prescription, the NS masses accumulate within 1.1−1.5 $M_\odot$. As for the chirp mass, the Fryer et al. (2012) delayed prescription predicts a distribution between 1.5−4 $M_\odot$. The Fryer et al. (2012) rapid prescription provides a narrower range between 2.5−4 $M_\odot$ because of the deficiency of the BHs in the mass gap and heavy NSs above 2 $M_\odot$. The Patton & Sukhbold (2020) prescription predicts a chirp mass range of 2.5−3.5 $M_\odot$ and a peak at ≈3 $M_\odot$.

Apart from the core-collapse prescription, a potential natal kick imparted onto the newly formed compact object also plays an important role in the formation of double compact objects. We considered two different values for the dispersion of the assumed Maxwellian kick velocity distribution for CCSN, $\sigma_{\rm CCSN} = 150\,{\rm km\,s^{-1}}$ and $\sigma_{\rm CCSN} = 450\,{\rm km\,s^{-1}}$ (the default value is $\sigma_{\rm CCSN} = 265\,{\rm km\,s^{-1}}$). Figure 10 shows the tilt, effective spin, and delay time for the three different dispersion values of the CCSN natal-kick velocity distribution. Natal kicks significantly affect both the orbital properties of the NSBH systems and the overall merger rate. Smaller kicks decrease the possibility of binary disruptions or excessive delay times caused by SNs, thus enhancing the formation rate of merging NSBHs. Furthermore, small kicks produce a large number of merging NSBHs with small tilt angles. In channel II, compared with the default model, the model of $\sigma_{\rm CCSN} = 150\,{\rm km\,s^{-1}}$ predicts more systems with aligned BHs, but almost the same number of anti-aligned systems. Larger kicks generate a flatter distribution of tilt angles, but the small total number limits the number of anti-aligned systems. The peak below 10^8 yr in the delay time distribution corresponds to highly eccentric binaries. In contrast, we can see that in channel I, there is no significant secondary peak below short delay times (10^8 yr). The binaries in these channels tend to have short orbits and high orbital velocities right before the formation of the second compact object. Hence, is it is very unlikely to form NSBH binaries with extreme eccentricities, which are required to achieve merger delay times of the order of 10^7 yr. Kicks in excess of $\gtrsim 1000\,{\rm km\,s^{-1}}$ would be necessary for this scenario, which is why we only see a mild excess of very short merger delay times for the highest dispersion value of our assumed kick distribution.

4.3. Fraction of associated electromagnetic counterparts

Table 2 lists the predicted fractions of NSBH mergers that could potentially produce EMCs under different models and for three assumed NS radii. We estimate the fractions in the range of 0−18.64%. The $\alpha_{\rm CE} = 0.5$ model and the $\lambda_{\rm CE}^{X_{\rm H}=0.01}$ model yield lower fractions compared with the default model because in channel I, these two models predict a limited population of low-mass BHs ($\lesssim 6\,M_\odot$). The $\lambda_{\rm CE}^{X_{\rm H}=0.01}$ model also gives a smaller fraction, which can be attributed to a reduced proportion of low-mass NSs ($\lesssim 1.5\,M_\odot$) in the model. The model of $\sigma_{\rm CCSN} = 150\,{\rm km\,s^{-1}}$ predicts the highest fraction of NSBH mergers that are accompanied by an EMC. The variations of core-collapse prescriptions exert the most substantial impact, as they yield different mass distributions for the compact objects. The Fryer et al. (2012) rapid model does not produce BHs within the mass gap of 2.5−5 $M_\odot$. In the absence of low-mass BHs, the EMC fraction experiences a significant decline. Only when assuming the largest NS radius does the fraction in channel II become not marginal (5.08%). The BH masses are below 7.07 $M_\odot$ and their

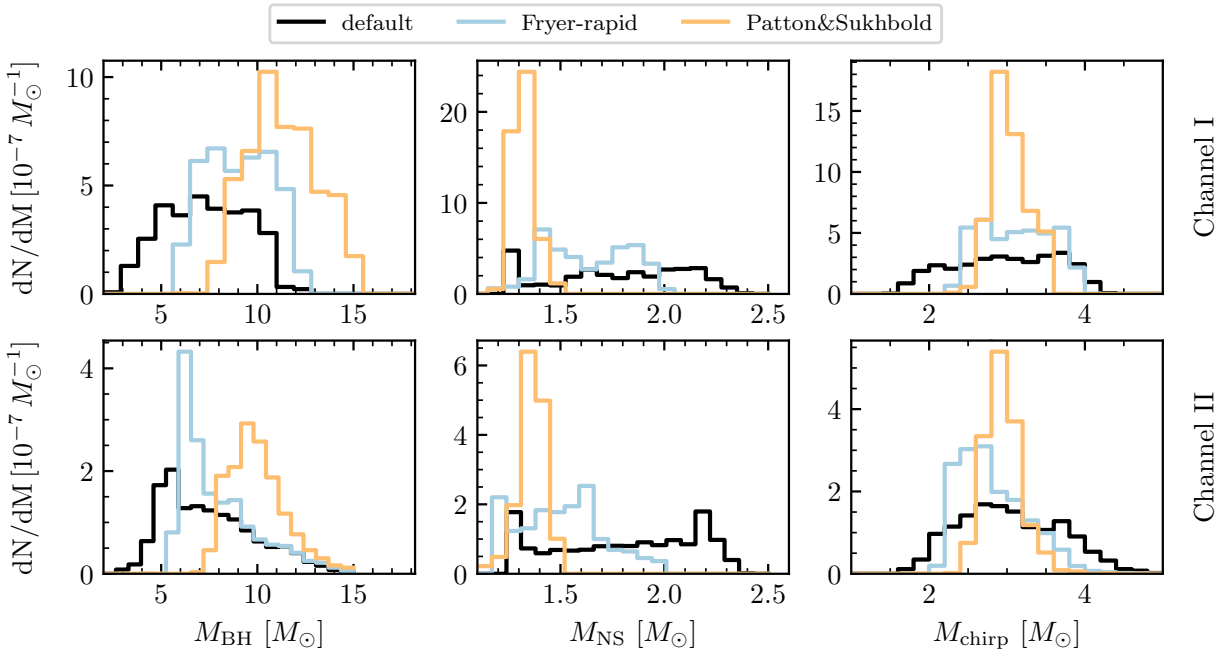

Fig. 9. Same as Fig. 7, but with different core-collapse mechanisms. The default model corresponds to Fryer-delayed prescription.

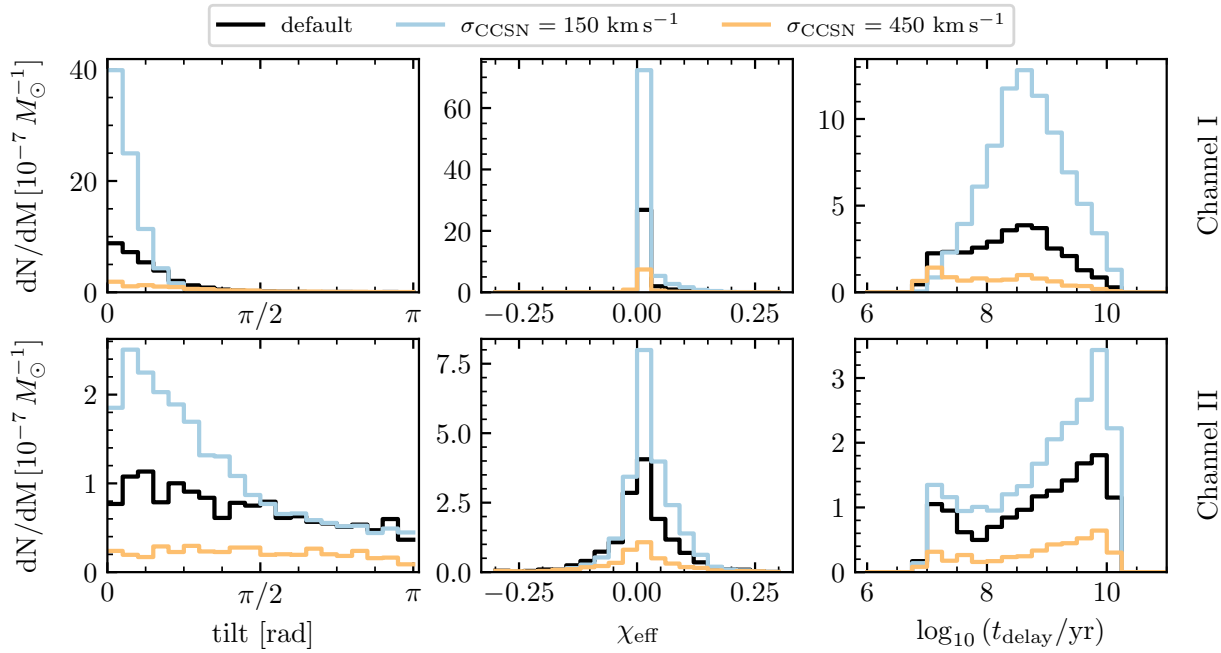

Fig. 10. Same as Fig. 8, but with different natal kick velocity distributions for CCSN. The default model corresponds to $\sigma_{\rm CCSN} = 265\,{\rm km\,s^{-1}}$.

spins are in the range of 0.02−0.13. The inclination toward channel II is attributed to the low-mass BHs within this channel possessing slightly higher spins. The Patton & Sukhbold (2020) prescription predicts BH masses above $\approx 8\,M_\odot$, leading to negligible EMC fractions.

5. Discussion

5.1. Uncertainties in stellar and binary physics

Apart from the model variations in how we treat the core collapse and the CE phases discussed in the last section, other not fully understood stellar and binary evolution physics can also affect the BPS results in a significant way. The accretion efficiency onto a nondegenerate star is such an example for the formation of merging NSBH binaries. In our pre-computed grids of detailed binary evolution models, we adopted a rotation-dependent accretion model (de Mink et al. 2013), which assumes the accretion would be suppressed if the accretor reaches critical rotation. While this is a physically self-consistent way to treat the accretion of matter and angular momentum onto a star, some authors (Paczynski 1991; Popham & Narayan 1991) suggest that a critically rotating star can still accrete mass because the viscous coupling between the star and the accretion disk can regulate the angular momentum transport without affecting the mass accretion. In this case, the mass transfer efficiency can be much higher

than our model. However, it is not clear whether the accretion would still be limited by other factors, such as the inflation of the accreting star due to high mass-transfer rate. Detailed binary evolution models that connect the accretion efficiency onto a star with such accretion disk models are not yet available.

The treatment of accretion onto a BH may also affect the properties of the NSBH population, especially the spin of the BH, which in turn determines whether the merger of the NSBH binary will be accompanied by an EMC. Radiation, general-relativistic, and magneto-hydrodynamics simulation of a super-critical accretion disk around BHs (e.g., Sądowski & Narayan 2016) suggest that the accretion rate may significantly exceed the Eddington limit. This possibility has been explored in the context of BH high-mass X-ray binaries (Moreno Méndez et al. 2008; Qin et al. 2022) and coalescing binary BH populations (e.g., Bavera et al. 2021; Briel et al. 2023). However, the effect of super-Eddington accretion on the formation and the properties of merging NSBH, and especially the probability of being accompanied by EMCs, is less well studied. We leave the exploration of different assumption regarding the accretion physics onto both nondegenerate stars and compact objects for a future study.

5.2. An additional formation channel

We found that in some binaries with an initial binary mass ratio close to unity, after a stable mass transfer from the primary to the secondary, the secondary evolves off the main sequence before the primary explodes and starts a reverse mass-transfer phase[2]. At the beginning of the reverse mass-transfer phase, the accretor has been almost or totally stripped. It accretes hydrogen from the secondary, quickly creating a thin layer of hydrogen at the surface. The accretion tends to make the star spin up and expand. However, the accretor will reach critical rotation and cease further accretion before it has a chance to expand significantly. The remainder of the mass-transfer phase will proceed effectively as fully nonconservative mass transfer.

The behavior we described above depends completely on our assumption of mass-transfer efficiency on a nondegenerate star (see discussion in Sect. 5.1). If we consider instead the possibility that the accretion continues onto critically rotating stars, we would expect that the stripped He stars, after accreting a small amount of hydrogen, will swell up substantially and fill the Roche lobe. This would result in a CE evolution quickly after the onset of reverse mass transfer. Under the assumption that the reverse mass transfer would become unstable and initiate CE evolution immediately, we evolve these binaries further with `POSYDON`. It turned out that this evolutionary path can be important for the formation of merging NSBHs. The interesting part is that after the CE phase, two He stars will be left in a close orbit, and the two stars can be effectively spun up by tidal interactions. The BHs formed through this channel can have high spins at birth. Therefore, a thorough study on the accretion physics is needed in order to obtain the full picture of binary evolution and the formation of double compact objects.

[2] In the revision of `MESA` used for the calculation of `POSYDON`'s grids of binary evolution models (`MESA` revision 11701), as well as the current revision at the time of writing this paper (r23.05.1), the modeling of reverse mass transfer in the `Kolb` scheme is not supported. To implement the proper modeling of reverse mass transfer within the `Kolb` scheme, we had to make small modifications in the `MESA` code base. These modifications are documented here, https://github.com/MESAHub/mesa/issues/545, and they will be included in future revisions of `MESA`.

5.3. Local merger rate density

In this study, we focused on models at solar metallicity. Thus, we did not calculate the merger rate density that can be directly compared with the estimate from GW detection. However, multiple works have shown that in contrast to BBH, the NSBH formation rate has limited connection with metallicity (Neijssel et al. 2019; Román-Garza et al. 2021; Broekgaarden et al. 2022; Iorio et al. 2023). In order to obtain a general idea on the local merger rate density from our simulation, we made the estimation by only integrating the star formation rate around solar metallicity. To do that, we followed the procedure described in Bavera et al. (2023) integrating the star formation rate in a metallicity range of $[0.5\,Z_\odot, 2\,Z_\odot]$. In this way, we underestimated the contribution of NSBH mergers at high redshifts where star formation at low metallicity is significant. Under these assumptions, our default model predicts a local merger rate density of $60.11\,\mathrm{Gpc^{-3}\,yr^{-1}}$, while the model variations we considered generate local merger rate densities in the range of $17.00\,\mathrm{Gpc^{-3}\,yr^{-1}}$ to $155.64\,\mathrm{Gpc^{-3}\,yr^{-1}}$.

5.4. Observation of NSBH populations with electromagnetic waves

Before merging, the NS may appear as a radio pulsar, making the system a pulsar-BH binary. Detection of pulsar-BH binaries can give us valuable insights on the formation and evolution of NSBH binaries, extending our objects to different populations of NSBH binaries. BPS studies have estimated up to thousands of pulsar-BH binaries in the Milky Way (Chattopadhyay et al. 2021; Shao & Li 2021; Pol et al. 2021). They could be observed by the radio telescopes such as the Square Kilometre Array (SKA; Kramer et al. 2004), MeerKAT (Booth et al. 2009), the Five-Hundred Metre Aperture Spherical Radio Telescope (FAST; Nan et al. 2011), and the Arecibo radio telescope (Cordes et al. 2006). Pulsar-BH binaries with orbital periods shorter than a day may be observed by both radio telescopes and GW detector LISA (Chattopadhyay et al. 2021). These joint observations could be further used to constrain model uncertainties in the formation of NSBH systems.

6. Summary

In this study, we investigated the formation channels and population properties of merging NSBH systems formed from isolated binary evolution at solar metallicity using the newly developed BPS code `POSYDON`. `POSYDON` incorporates detailed stellar and binary models calculated based on the binary-star evolution code `MESA`. The main findings of our work are:

- We identify two main formation channels of NSBH mergers. In channel I (≈70%), the binaries undergo a stable mass transfer prior to the formation of the BH, a CE phase after the formation of the BH, and a subsequent case-BB stable mass-transfer phase (channel Ia, ≈94%) or no case-BB mass transfer (channel Ib, ≈6%). In channel II (≈30%), the binaries go through only stable mass transfer. Most binaries within channel II experience two stable mass-transfer phases, one prior to and another after the BH formation (channel IIa, ≈95.4%). In addition, a small portion of the binaries, which contain massive primary stars above $\approx 60\,M_\odot$, are stripped because of strong stellar winds and avoid mass transfer before the BH formation (channel IIb, ≈4.6%).
- Independently of the formation channels and the explored model uncertainties, our models suggest that the BHs always

form first in merging NSBH systems. The primary reason for this difference compared with other NSBH BPS studies in the literature is our adopted model of rotation-dependent accretion efficiency onto nondegenerate stars, which generally results in highly nonconservative mass transfer.

– Most binaries in channel I have initial orbital periods $\gtrsim$50 d and mass ratios $\gtrsim$0.5. Given the initially large orbital separation of these binaries, the majority of the BHs form with near-zero spins, assuming efficient angular momentum transport within the stars. After their formation, BHs can still be spun up due to mass accretion during the case-BB mass-transfer phase. However, since we assume that the accretion onto a compact object is Eddington limited, this effect is not significant.
– Compared with channel I, most of the binaries formed through channel II have initial orbital periods $\lesssim$50 d and a wider spread of initial mass ratios. Those binaries end up in relatively wide orbits before the second core collapse, as the second stable mass-transfer phase does not shrink the orbit as efficiently as the CE. Natal kicks during the second SN can significantly alter those orbits and in some cases result in highly eccentric NSBH binaries. It is the high eccentricity (>0.5) of the orbits after the NS formation that causes the binary to merge within a Hubble time. Furthermore, binaries in channel II, due to tides in their close initial orbits and the further possible shrinking of the orbit during the first mass-transfer episode, have primary stars that can retain some angular momentum until the end of their lives. The angular momentum preserved in the core contributes to nonzero small spins ($\lesssim$0.2) for the BHs. The BHs can be further spun up moderately because of the mass-transfer phase following the BH formation.
– Binaries from channel I mostly have small orbital tilt angles, while for channel II, binaries with large tilt angles ($>\pi/2$ rad) account for a significant fraction. The reason for the latter is that the NSBH binaries that experienced a sufficiently high kick to become highly eccentric manage to merge within a Hubble time in channel II, and the kick can easily tilt the orbit in such wide systems. This feature also contributes to the distinctive distributions of effective spin for the two channels. For channel I, the negligible BH spins and the small tilt angles make the distribution of effective spin peak at zero, with an excess at positive values. In contrast, for channel II, the effective spins extend to ≈ -0.2 and $\approx$0.2.
– With the information of compact object masses, BH spins, and orbital tilt angles, we estimate the fraction of merging NSBHs that we expect to be accompanied by an EMC. We find that when assuming a stiff equation of state for the NSs ($R_{\rm NS}$ = 13 km), the EMC fraction is about 13.92%, while for a soft equation of state ($R_{\rm NS}$ = 11 km) it is about 1.35%. The binaries that have potential EMC favor light BHs and NSs. Approximately 85% of BHs are within the mass gap of 2.5−5 $M_\odot$ when assuming $R_{\rm NS}$ = 13 km, and in the other two cases all BHs are expected to fall within the mass gap. Incorporating uncertainties in both the population modeling and the neutron-star equation of state, we estimate that between 0 and 18.6% of NSBH mergers could potentially exhibit an EMC.
– In addition to our default BPS model, we investigated a range of model uncertainties, including different prescriptions and model parameters for the CE and core-collapse phase. Different parameters for CE evolution affect channel I in terms of the absolute number of merging NSBHs and the compact object masses. The $X_{\rm H}$ = 0.01 core-envelope boundary definition results in a smaller core and thus higher binding energy of the envelope compared with the default 0.1 $X_{\rm H}$, while a smaller $\alpha_{\rm CE}$ means more orbital energy is needed to overcome the binding energy. These two variations predict fewer merging NSBHs and a preference for massive BHs $\approx$10 $M_\odot$. The $\lambda_{\rm CE}^{X_{\rm H}=0.3}$ model leads to a larger post-CE orbital separation. The formation rate of merging NSBHs is lower because of excessive delay time for binaries going through CE evolution. Variations in the core-collapse prescriptions affect both channels concerning the formation efficiency of merging NSBHs, as well as their mass distributions and orbital properties. With our default Fryer et al. (2012) delayed model, most merging NSBHs have BHs less massive than $\approx$11 $M_\odot$, chirp masses in a range of 1.5−4 $M_\odot$, and NS masses within 1.26−2.4 $M_\odot$. The Fryer et al. (2012) rapid core-collapse prescription produces the mass gap between NSs and BHs and NSs less massive than $\approx$2 $M_\odot$. The Patton & Sukhbold (2020) prescription produces a narrow NS mass range of 1.1−1.5 $M_\odot$. Assuming a Maxwellian distribution of natal-kick velocities with a smaller dispersion (150 km s^{-1} versus the 265 km s^{-1} of our default model) predicts more merging NSBHs with a larger proportion of them exhibiting small tilt angles. Besides, a smaller kick velocity dispersion produces more merging NSBHs with long delay times, as it is less efficient in forming very eccentric NSBH binaries.

The utilization of detailed stellar and binary models in BPS studies enables enhanced modeling accuracy and self-consistent treatment of stellar evolution and binary interactions, providing us with more accurate and informative results. As we expect a growing number of GW events to be detected in the future, it becomes imperative to employ increasingly accurate BPS models; this is a crucial component in the unraveling of the origin and formation mechanisms of observed double compact objects and in refining our understanding of underlying stellar and binary physics.

Acknowledgements. We thank Christopher Berry for helpful comments. The POSYDON project is supported primarily by two sources: the Swiss National Science Foundation (PI Fragos, project numbers PP00P2_211006 and CRSII5_213497) and the Gordon and Betty Moore Foundation (PI Kalogera, grant award GBMF8477). Z.X. acknowledges support from the Chinese Scholarship Council (CSC). S.S.B., T.F., M.K., and Z.X. were supported by the project number PP00P2_211006. S.S.B. was also supported by the project number CRSII5_213497. A.D., K.A.R., P.M.S. and M.S. were supported by the project number GBMF8477. K.K. acknowledges support from the Spanish State Research Agency, through the María de Maeztu Program for Centers and Units of Excellence in R&D, No. CEX2020-001058-M. E.Z. acknowledges funding support from the European Research Council (ERC) under the European Union's Horizon 2020 research and innovation programme (Grant agreement No. 772086). The computations were performed at Northwestern University on the Trident computer cluster (funded by the GBMF8477 award) and at the University of Geneva on the Yggdrasil computer cluster. This research was partly supported by the computational resources and staff contributions provided5for the Quest high-performance computing facility at Northwestern University, jointly supported by the Office of the Provost, the Office for Research and Northwestern University Information Technology.

References

Abbott, B. P., Abbott, R., Abbott, T. D., et al. 2016, Phys. Rev. Lett., 116, 061102
Abbott, B. P., Abbott, R., Abbott, T. D., et al. 2017a, Phys. Rev. Lett., 119
Abbott, B. P., Abbott, R., Abbott, T. D., et al. 2017b, Class. Quant. Grav., 34, 044001
Abbott, B. P., Abbott, R., Abbott, T. D., et al. 2018, Liv. Rev. Relat., 21, 3
Abbott, R., Abbott, T. D., Abraham, S., et al. 2020, ApJ, 896, L44
Abbott, R., Abbott, T. D., Abraham, S., et al. 2021a, Phys. Rev. X, 11
Abbott, R., Abbott, T. D., Abraham, S., et al. 2021b, ApJ, 915, L5

Abbott, R., Abbott, T. D., Acernese, F., et al. 2021c, ArXiv e-prints [arXiv:2108.01045]
Abbott, R., Abbott, T. D., Acernese, F., et al. 2023, Phys. Rev. X, 13, 041039
Ablimit, I., & Maeda, K. 2018, ApJ, 866, 151
Acernese, F., Agathos, M., Agatsuma, K., et al. 2015, Class. Quant. Grav., 32, 024001
Amaro-Seoane, P., Audley, H., Babak, S., et al. 2017, ArXiv e-prints [arXiv:1702.00786]
Arca Sedda, M. 2020, Commun. Phys., 3, 43
Arca Sedda, M. 2021, ApJ, 908, L38
Bavera, S. S., Fragos, T., Zevin, M., et al. 2021, A&A, 647, A153
Bavera, S. S., Fragos, T., Zapartas, E., et al. 2023, Nat. Astron., 7, 1090
Begelman, M. C. 1979, MNRAS, 187, 237
Belczynski, K., Klencki, J., Fields, C. E., et al. 2020, A&A, 636, A104
Bhattacharya, M., Kumar, P., & Smoot, G. 2019, MNRAS, 486, 5289
Bloecker, T. 1995, A&A, 297, 727
Böhm-Vitense, E. 1958, Z. Astrophys., 46, 108
Booth, R. S., de Blok, W. J. G., Jonas, J. L., & Fanaroff, B. 2009, ArXiv e-prints [arXiv:0910.2935]
Breivik, K., Coughlin, S., Zevin, M., et al. 2020, ApJ, 898, 71
Briel, M. M., Stevance, H. F., & Eldridge, J. J. 2023, MNRAS, 520, 5724
Broekgaarden, F. S., Berger, E., Neijssel, C. J., et al. 2021, MNRAS, 508, 5028
Broekgaarden, F. S., Berger, E., Stevenson, S., et al. 2022, MNRAS, 516, 5737
Brott, I., de Mink, S. E., Cantiello, M., et al. 2011, A&A, 530, A115
Chattopadhyay, D., Stevenson, S., Hurley, J. R., Bailes, M., & Broekgaarden, F. 2021, MNRAS, 504, 3682
Chattopadhyay, D., Stevenson, S., Broekgaarden, F., Antonini, F., & Belczynski, K. 2022, MNRAS, 513, 5780
Choi, J., Dotter, A., Conroy, C., et al. 2016, ApJ, 823, 102
Claret, A., & Torres, G. 2017, ApJ, 849, 18
Clausen, D., Sigurdsson, S., & Chernoff, D. F. 2013, MNRAS, 428, 3618
Cordes, J. M., Freire, P. C. C., Lorimer, D. R., et al. 2006, ApJ, 637, 446
Darbha, S., Kasen, D., Foucart, F., & Price, D. J. 2021, ApJ, 915, 69
de Jager, C., Nieuwenhuijzen, H., & van der Hucht, K. A. 1988, A&AS, 72, 259
de Kool, M. 1990, ApJ, 358, 189
de Mink, S. E., & Belczynski, K. 2015, ApJ, 814, 58
de Mink, S. E., Langer, N., Izzard, R. G., Sana, H., & de Koter, A. 2013, ApJ, 764, 166
Dewi, J. D. M., & Tauris, T. M. 2000, A&A, 360, 1043
Dominik, M., Belczynski, K., Fryer, C., et al. 2012, ApJ, 759, 52
Dominik, M., Berti, E., O'Shaughnessy, R., et al. 2015, ApJ, 806, 263
Dorozsmai, A., & Toonen, S. 2022, MNRAS, accepted [arXiv:2207.08837]
Foucart, F., Deaton, M. B., Duez, M. D., et al. 2013, Phys. Rev. D, 87, 084006
Foucart, F., Hinderer, T., & Nissanke, S. 2018, Phys. Rev. D, 98, 081501
Fragione, G. 2021, ApJ, 923, L2
Fragione, G., & Banerjee, S. 2020, ApJ, 901, L16
Fragione, G., & Loeb, A. 2019, MNRAS, 490, 4991
Fragione, G., Loeb, A., & Rasio, F. A. 2021, ApJ, 918, L38
Fragos, T., & McClintock, J. E. 2015, ApJ, 800, 17
Fragos, T., Tremmel, M., Rantsiou, E., & Belczynski, K. 2010, ApJ, 719, L79
Fragos, T., Andrews, J. J., Bavera, S. S., et al. 2023, ApJS, 264, 45
Fryer, C. L., Woosley, S. E., & Hartmann, D. H. 1999, ApJ, 526, 152
Fryer, C. L., Belczynski, K., Wiktorowicz, G., et al. 2012, ApJ, 749, 91
Fuller, J., & Ma, L. 2019, ApJ, 881, L1
Giacobbo, N., & Mapelli, M. 2018, MNRAS, 480, 2011
Giacobbo, N., & Mapelli, M. 2019, MNRAS, 482, 2234
Gompertz, B. P., Levan, A. J., & Tanvir, N. R. 2020, ApJ, 895, 58
Gottlieb, O., Metzger, B. D., Quataert, E., et al. 2023, ApJ, 958, L33
Herwig, F. 2000, A&A, 360, 952
Hild, S., Abernathy, M., Acernese, F., et al. 2011, Class. Quant. Grav., 28, 094013
Hobbs, G., Lorimer, D. R., Lyne, A. G., & Kramer, M. 2005, MNRAS, 360, 974
Hotokezaka, K., Nissanke, S., Hallinan, G., et al. 2016, ApJ, 831, 190
Hu, R.-C., Zhu, J.-P., Qin, Y., et al. 2022, ApJ, 928, 163
Huang, K., Hu, J., Zhang, Y., & Shen, H. 2020, ApJ, 904, 39
Hurley, J. R., Pols, O. R., & Tout, C. A. 2000, MNRAS, 315, 543
Hurley, J. R., Tout, C. A., & Pols, O. R. 2002, MNRAS, 329, 897
Hut, P. 1981, A&A, 99, 126
Iorio, G., Mapelli, M., Costa, G., et al. 2023, MNRAS, 524, 426
Jermyn, A. S., Bauer, E. B., Schwab, J., et al. 2023, ApJS, 265, 15
Kalogera, V. 1996, ApJ, 471, 352
Kawaguchi, K., Shibata, M., & Tanaka, M. 2020, ApJ, 893, 153
King, A. R., Lubow, S. H., Ogilvie, G. I., & Pringle, J. E. 2005, MNRAS, 363, 49
Klencki, J., Istrate, A., Nelemans, G., & Pols, O. 2022, A&A, 662, A56
Kobulnicky, H. A., & Fryer, C. L. 2007, ApJ, 670, 747
Kolb, U., & Ritter, H. 1990, A&A, 236, 385
Kramer, M., Backer, D. C., Cordes, J. M., et al. 2004, New Astron. Rev., 48, 993
Kroupa, P. 2001, MNRAS, 322, 231
Kruckow, M. U., Tauris, T. M., Langer, N., Kramer, M., & Izzard, R. G. 2018, MNRAS, 481, 1908
Kyutoku, K., Shibata, M., & Taniguchi, K. 2010, Phys. Rev. D, 82, 044049
Kyutoku, K., Okawa, H., Shibata, M., & Taniguchi, K. 2011, Phys. Rev. D, 84, 064018
Langer, N. 1998, A&A, 329, 551
Langer, N., Schürmann, C., Stoll, K., et al. 2020, A&A, 638, A39
Li, L.-X., & Paczyński, B. 1998, ApJ, 507, L59
LIGO Scientific Collaboration (Aasi, J., et al.) 2015, Class. Quant. Grav., 32, 074001
Livio, M., & Soker, N. 1988, ApJ, 329, 764
Luo, J., Chen, L.-S., Duan, H.-Z., et al. 2016, Class. Quant. Grav., 33, 035010
Mandel, I., & Smith, R. J. E. 2021, ApJ, 922, L14
Marchant, P., Langer, N., Podsiadlowski, P., Tauris, T. M., & Moriya, T. J. 2016, A&A, 588, A50
Marchant, P., Langer, N., Podsiadlowski, P., et al. 2017, A&A, 604, A55
Mei, J., Bai, Y. Z., Bao, J., et al. 2021, Prog. Theor. Exp. Phys., 2021, 05A107
Misra, D., Fragos, T., Tauris, T. M., Zapartas, E., & Aguilera-Dena, D. R. 2020, A&A, 642, A174
Moreno Méndez, E., Brown, G. E., Lee, C.-H., & Park, I. H. 2008, ApJ, 689, L9
Nakar, E. 2007, Phys. Rep., 442, 166
Nan, R., Li, D., Jin, C., et al. 2011, Int. J. Mod. Phys. D, 20, 989
Nandez, J. L. A., Ivanova, N., & Lombardi, J. C., Jr. 2014, ApJ, 786, 39
Neijssel, C. J., Vigna-Gómez, A., Stevenson, S., et al. 2019, MNRAS, 490, 3740
Nugis, T., & Lamers, H. J. G. L. M. 2000, A&A, 360, 227
Paczynski, B. 1991, ApJ, 370, 597
Pannarale, F., & Ohme, F. 2014, ApJ, 791, L7
Pannarale, F., Tonita, A., & Rezzolla, L. 2011, ApJ, 727, 95
Patton, R. A., & Sukhbold, T. 2020, MNRAS, 499, 2803
Paxton, B., Bildsten, L., Dotter, A., et al. 2011, ApJS, 192, 3
Paxton, B., Cantiello, M., Arras, P., et al. 2013, ApJS, 208, 4
Paxton, B., Marchant, P., Schwab, J., et al. 2015, ApJS, 220, 15
Paxton, B., Schwab, J., Bauer, E. B., et al. 2018, ApJS, 234, 34
Paxton, B., Smolec, R., Schwab, J., et al. 2019, ApJS, 243, 10
Petrovich, C., & Antonini, F. 2017, ApJ, 846, 146
Piran, T., Nakar, E., & Rosswog, S. 2013, MNRAS, 430, 2121
Podsiadlowski, P., Langer, N., Poelarends, A. J. T., et al. 2004, ApJ, 612, 1044
Pol, N., McLaughlin, M., & Lorimer, D. 2021, ApJ, submitted [arXiv:2109.04512]
Popham, R., & Narayan, R. 1991, ApJ, 370, 604
Punturo, M., Abernathy, M., Acernese, F., et al. 2010, Class. Quant. Grav., 27, 194002
Qin, Y., Fragos, T., Meynet, G., et al. 2018, A&A, 616, A28
Qin, Y., Shu, X., Yi, S., & Wang, Y.-Z. 2022, Res. Astron. Astrophys., 22, 035023
Rastello, S., Mapelli, M., Di Carlo, U. N., et al. 2020, MNRAS, 497, 1563
Reimers, D. 1975, Problems in Stellar Atmospheres and Envelopes (New York: Springer-Verlag New York, Inc.), 229
Reitze, D., Adhikari, R. X., Ballmer, S., et al. 2019, BAAS, 51, 35
Román-Garza, J., Bavera, S. S., Fragos, T., et al. 2021, ApJ, 912, L23
Ruan, W.-H., Guo, Z.-K., Cai, R.-G., & Zhang, Y.-Z. 2020, Int. J. Mod. Phys. A, 35, 2050075
Sądowski, A., & Narayan, R. 2016, MNRAS, 456, 3929
Santoliquido, F., Mapelli, M., Bouffanais, Y., et al. 2020, ApJ, 898, 152
Scheuer, P. A. G., & Feiler, R. 1996, MNRAS, 282, 291
Shao, Y., & Li, X.-D. 2021, ApJ, 920, 81
Sipior, M. S., Portegies Zwart, S., & Nelemans, G. 2004, MNRAS, 354, L49
Spruit, H. C. 2002, A&A, 381, 923
Tang, P. N., Eldridge, J. J., Stanway, E. R., & Bray, J. C. 2020, MNRAS, 493, L6
Thorpe, J. I., Ziemer, J., Thorpe, I., et al. 2019, BAAS, 51, 77
Tiwari, S., Ebersold, M., & Hamilton, E. Z. 2021, Phys. Rev. D, 104, 123024
Trani, A. A., Rastello, S., Di Carlo, U. N., et al. 2022, MNRAS, 511, 1362
Tutukov, A. V., & Yungelson, L. R. 1993, MNRAS, 260, 675
Tylenda, R., Hajduk, M., Kamiński, T., et al. 2011, A&A, 528, A114
Vink, J. S., de Koter, A., & Lamers, H. J. G. L. M. 2001, A&A, 369, 574
Voss, R., & Tauris, T. M. 2003, MNRAS, 342, 1169
Wang, H., Stephan, A. P., Naoz, S., Hoang, B.-M., & Breivik, K. 2021, ApJ, 917, 76
Webbink, R. F. 1984, ApJ, 277, 355
Ye, C. S., Fong, W.-F., Kremer, K., et al. 2020, ApJ, 888, L10
Zevin, M., Spera, M., Berry, C. P. L., & Kalogera, V. 2020, ApJ, 899, L1
Zhou, X., Li, A., & Li, B.-A. 2021, ApJ, 910, 62
Zhu, J.-P., Wu, S., Yang, Y.-P., et al. 2021, ApJ, 917, 24
Ziosi, B. M., Mapelli, M., Branchesi, M., & Tormen, G. 2014, MNRAS, 441, 3703

3.8 Supplementary discussion and comments

3.8.1 Differences from previous studies using rapid codes

Dominik et al. (2012) employed the rapid BPS code `StarTrack` to study the formation channels of double compact objects. They investigated the key physical processes involved in binary evolution, including CE binding energy parameter $\lambda_{\rm CE}$, SN mechanisms, the maximum NS mass and stellar wind-loss rates. Their study focused on how these factors influence the formation channels and rates of DNSs, NSBHs and BBHs.

They introduced two approaches for CE evolution when a donor star is on the HG: the pessimistic and optimistic approach. The arguments are as follows. For MS stars, a clear core-envelope boundary does not exist, as the helium core is still developing. Similarly, HG stars lack a clear entropy jump related with the core-envelope structure (Ivanova et al., 2004) and when the core-envelope division appears remains unclear. Because of this uncertainty, these two approaches have been proposed. The pessimistic approach assumes that CE evolution always leads to a merger if the donor star is on the HG, whereas the optimistic approach does not have this limitation. This empirical criterion for CE phases was adopted to constrain the high efficiency of the CE channels predicted by many rapid BPS codes. In `POSYDON`, we set the optimistic approach as the default because the pessimistic approach has not been supported or validated by more refined simulations.

In their population study, 95.4% of NSBHs are formed through the classic channel without case BB mass transfer–corresponding to channel Ib in our study–at solar metallicity under the optimistic approach. The stable mass transfer channel (channel IIa) in their simulations is trivial. In contrast, our results indicate that the stable mass transfer channel contributes about 30% to the entire NSBH merger population at solar metallicity, and the channel involving case BB mass transfer plays a more significant role. The fractions of each formation channel at solar metallicity can be found in Table 4 of Dominik et al. (2012).

Similar results regarding the formation channels of NSBHs at solar metallicity have been found in Broekgaarden et al. (2021), which used the rapid BPS code `COMPAS`. They found that the classic channel accounts for 86% and the stable mass transfer channel accounts for 4% of the detectable NSBH population, respectively. Note that these fractions represent the population for all metallicities and include the selection effects. The specific contributions of each formation channel at solar metallicity can be found in Figure 5 of Broekgaarden et al. (2021) and the contribution of the classic channel increases at solar metallicity. Our finding that only the classic formation channel and the stable mass transfer channel are significant at solar metallicity is consistent with their results. However, they found that the classic

channel is predominant at solar metallicity, despite adopting the pessimistic approach for CE evolution.

Both codes `StarTrack` and `COMPAS` are `BSE`-like codes that based on the stellar tracks `SSE`. It is therefore not surprising that they yield similar results regarding the formation channels of merging NSBH systems at solar metallicity. However, different treatments in their modeling, such as the choice of the pessimistic or optimistic approach, winds prescriptions, and mass transfer efficiency, lead to discrepancies in the predicted formation channels at sub-solar metallicities.

Another noteworthy comparison is with Iorio et al. (2023), which employed the BPS code `SEVN`. Specifically, `SEVN` allows using different single-star evolutionary tracks than `SSE`, while still following the `BSE` framework for binary evolution. They attributed the discrepancies in the formation channels of DNSs between their results and those obtained from `SSE`-based codes (`StarTrack` and `COMPAS`) to differences in the radial evolution of single stars, which alters the phases of binary interactions. Regarding the NSBH population, they found that across all metallicities, the classic channel contributes a lower fraction of 51%, while the stable mass transfer channel is more significant with a fraction of 25%, compared to the results of Dominik et al. (2012) and Broekgaarden et al. (2021). They suggested that the differences are driven by the different stellar evolution models. However, at solar metallicity, their simulations predict a nearly zero contribution from the stable mass transfer channel, which is still inconsistent with our results. The relative contributions of different formation channels of NSBH mergers can be found in Figure 14 of Iorio et al. (2023). The abrupt drop in the relative fraction of the stable mass transfer channel at high metallicity in their study comes from a fundamental limitation in how mass transfer stability is determined in `BSE`-like codes. Under the `BSE` classification scheme for stellar types, mass transfer at high metallicity occurs most likely when the donor star is in the red-giant phase. In the meantime, for red-giant donor stars, the critical mass ratio, which is used to determine mass transfer stability, is low. This treatment results in an overwhelmingly high fraction of systems undergoing CE evolution.

Our study has illustrated that detailed modeling of mass transfer and refined approaches for determining mass transfer stability can significantly alter these outcomes. By using self-consistent treatments of mass transfer, including the calculation of mass transfer rate via RLOF, the stellar response to mass transfer, and the varied prescriptions for mass transfer stability, our detailed binary evolution models in `POSYDON` predict a higher fraction of binaries undergoing stable mass transfer at solar metallicity. Furthermore, if we adopt the pessimistic approach for CE evolution used in their study, the stable mass transfer channel

would be even more significant. These comparisons lead to a common conclusion that all of these key factors, such as the treatment of critical processes, stellar evolution models, and binary interactions, can introduce substantial variations in BPS predictions. In this regard, POSYDON has the potential to drive BPS studies to a more accurate and physically consistent stage by incorporating detailed binary simulations.

3.8.2 Effect of metallicity on the formation of neutron star–black hole mergers

As POSYDON v1 is limited to solar-metallicity grids, one of our motivations for investigating NSBHs is that their formation efficiency is less sensitive to metallicity compared to BBH mergers, where formation of BBHs is inefficient at high metallicities. This trend, showing that the number of NSBH mergers as a function of metallicity, has been demonstrated in multiple studies.

Giacobbo et al. (2018a) studied the impact of metallicity on double compact object formation using the BPS code MOBSE. In Figure 14 of their study, they present the number of merging double compact objects as a function of metallicity, showing that only when adopting very low SN natal kicks does the formation efficiency of merging NSBHs decline significantly at solar metallicity. In Figure 1 of Neijssel et al. (2019), they displays the number of double compact object mergers per unit star-forming mass from COMPAS as a function of metallicity. Instead of a steep decline in BBHs at high metallicity, the formation efficiency of NSBHs remains nearly flat at sub-solar metallicities, with a slight decrease at solar metallicity and approaching zero at higher metallicities.

However, in Giacobbo et al. (2020), in which MOBSE was used, the formation efficiency of merging NSBHs suffers a sudden decline at solar metallicity by several orders of magnitude. Similarly, Broekgaarden et al. (2022), using COMPOS, found that most of there models predict a flat NSBH formation efficiency distribution up to solar metallicity, followed by a steep decline at higher metallicities. In Klencki et al. (2018), StarTrack simulations also show a more than one order of magnitude decline in NSBH merger formation efficiency at solar metallicity. They attributed this to the stellar evolution models in BSE, where systems at solar metallicity are more likely to initiate a RLOF during the HG phase and lead to unsuccessfully CE under the pessimistic approach.

A comparison was made in Iorio et al. (2023), whose Figure 20 presents different formation efficiency curves from various studies. With SEVN, their results suggested that this trend is less significant, with only a one-order-of-magnitude drop at solar metallicity and no sudden decline at higher metallicities. They suggested that this difference also arises from the substantially different single-star models at very high metallicities.

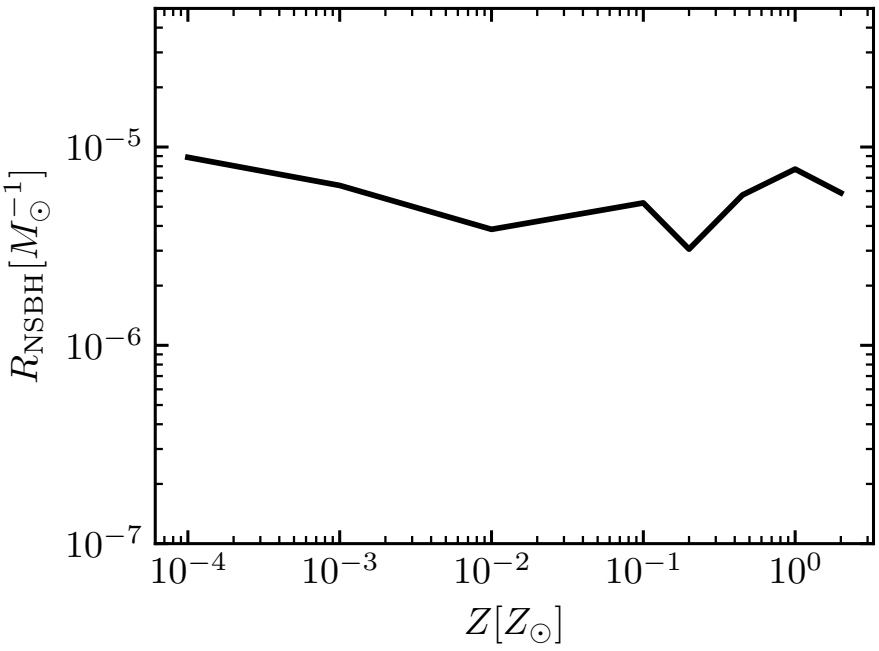

Figure 3.11: Formation efficiency of NSBH mergers as a function of metallicity from POSYDON v2.

As multi-metallicity grids are available in POSYDON v2, we can directly compute the formation efficiency of NSBH mergers as a function of metallicity using our code. Here, I present the metallicity-dependent formation efficiency of NSBH mergers from POSYDON v2. In general, the formation efficiency does not exhibit strong sensitivity to metallicity. The formation efficiency does not decline at solar and super-solar metallicity but instead increases at solar metallicity. Firstly, in POSYDON, we rely on not only state-of-the-art single star tracks but also detailed binary models. The treatment of mass transfer is based on 1D simulations, and mass transfer stability is determined based on multiple criteria. Our simulations indicate that at high metallicities, the stable mass transfer channel can contribute to NSBH mergers. Secondly, we do not adopt the ac-hoc pessimistic approach for CE evolution. Because of this, the overall formation rate of the CE channel is higher than in the other studies using rapid codes, where the pessimistic approach is always assumed.

3.8.3 Distinguishing formation channels

This study is the first BPS study that follows the full evolution of stellar rotation and BH spin, which is one of the key features in POSYDON that makes it outstanding. This allows us to self-consistently obtain the channel-wise distribution of effective spins of merging NSBHs. Previously, studies using rapid BPS codes could only assume zero spins or assign arbitrary

spins to BHs in order to conduct parameter studies, explore effective spin distributions, and estimate the EMC fractions of the merging NSBH population. Although this study focuses only on solar metallicity and other formation channels are expected to contribute at low metallicities, the physics governing BH spins and orbital tilts is universal and robust in our analysis.

Firstly, the initially close binaries that are more likely to undergo the stable mass transfer channel can acquire slightly higher natal BH spins due to tidal effects. Secondly, when the second SN occurs to form the NSs, binaries from the classic channels are more difficult to become anti-aligned as a result of the SN kicks because they are more tightly bound in close orbits due to prior CE evolution. These two factors lead to a distinct distribution of effective spins, which may serve as an observational signature for probing the formation history of merging NSBHs.

Chapter 4

MASS-GAP NEUTRON STAR–BLACK HOLE MERGERS

On April 5 2024, the LVK collaboration announced the detection of GW230529, which is most likely an NSBH merger, with the BH mass highly likely falling within the lower mass gap between NSs and BHs. This mass gap was initially inferred from the BH mass distribution in LMXBs (see subsection 1.1.2.2 for more details). In the early 2000s, Fryer et al. (2001) proposed that introducing a step function for the dependence of explosion energy on progenitor mass could produce a mass gap of $2-5\,M_{\odot}$ in remnant masses. Later, Fryer et al. (2012) introduced the Fryer-delayed and Fryer-rapid prescriptions, providing a possible physical interpretation for the step function, with the Fryer-rapid prescription specifically leading to the formation of the gap. However, the existence of the mass gap cannot be theoretically constrained. From 3D SN simulations, the presence of the mass gap depends on specific physical assumptions. For example, mass-gap BHs can form under scenarios involving fallback onto proto-NSs, where the BH masses are related to the explosion energy.

At the time of the release of GW230529, multi-metallicity single-star and binary evolution models, along with the `POSYDON` v2 code, were available for conducting comprehensive BPS studies. The BPS results from `POSYDON` v2 can be directly compared with the LVK observations by integrating the redshift- and metallicity-dependent star formation history (SFH). Thus, this study presents an exciting opportunity to explore mass-gap BHs and other characteristics of NSBH mergers. This study is the first BPS study to utilize `POSYDON` v2 and the multi-metallicity data.

The arXiv open-access version of the manuscript, referred as Xing et al. (2024b), is presented as follows.

Astronomy & Astrophysics manuscript no. NSBH
October 29, 2024

Mass-gap Black Holes in Coalescing Neutron Star Black Hole Binaries

Zepei Xing[1,2,4,⋆], Vicky Kalogera[3,4], Tassos Fragos[1,2], Jeff J. Andrews[5], Simone S. Bavera[1,2], Max Briel[1,2], Seth Gossage[4], Konstantinos Kovlakas[6,7], Matthias U. Kruckow[1,2], Kyle A. Rocha[3,4], Meng Sun[4], Philipp M. Srivastava[3,8], Emmanouil Zapartas[9]

[1] Département d'Astronomie, Université de Genève, Chemin Pegasi 51, CH-1290 Versoix, Switzerland
[2] Gravitational Wave Science Center (GWSC), Université de Genève, CH1211 Geneva, Switzerland
[3] Department of Physics & Astronomy, Northwestern University, 2145 Sheridan Road, Evanston, IL 60208, US
[4] Center for Interdisciplinary Exploration and Research in Astrophysics (CIERA), 1800 Sherman, Evanston, IL 60201, USA
[5] Department of Physics, University of Florida, 2001 Museum Rd, Gainesville, FL 32611, USA
[6] Institute of Space Sciences (ICE, CSIC), Campus UAB, Carrer de Magrans, 08193 Barcelona, Spain
[7] Institut d'Estudis Espacials de Catalunya (IEEC), Carrer Gran Capità, 08034 Barcelona, Spain
[8] Electrical and Computer Engineering, Northwestern University, 2145 Sheridan Road, Evanston, IL 60208, USA
[9] Institute of Astrophysics, FORTH, N. Plastira 100, Heraklion, 70013, Greece

Received XXYYZZ; Accepted XXYYZZ

ABSTRACT

The existence of a mass gap of $3-5\,M_\odot$ between the heaviest neutron stars (NSs) and the lightest black holes (BHs), inferred from the BH mass distribution in low mass X-ray binaries (LMXBs), has been suggested for decades. The recently reported gravitational-wave source GW230529 has been confidently identified as a neutron star–black hole (NSBH) merger, with the BH mass falling within this lower mass gap. This detection provides strong evidence against the existence of the latter and introduces new implications for the coalescing NSBH population, including a revised BH mass distribution and an updated local merger rate. In this study, we employ `POSYDON`, a binary population synthesis code that integrates detailed single- and binary-star models, to investigate coalescing NSBH binaries formed through isolated binary evolution. In particular, we focus on the BH mass distribution of the intrinsic NSBH merger population. We find that, with a high common-envelope efficiency of $\alpha_{\rm CE} = 2$, the BH masses in NSBH mergers concentrate in the lower mass gap, aligning more closely with observations. However, after accounting for the constraints of the selection bias against mass-gap BHs in LMXBs, which suggests that the maximum NS birth mass is below $\simeq 2\,M_\odot$, we find that introducing a high $\alpha_{\rm CE}$ is not required to match observations. Additionally, we explore the impact of core-collapse supernova kicks on the BH mass distribution and the local merger rate density of NSBH mergers. Finally, we present the property distributions of observable NSBH mergers from our simulation and find that they match well with the observations. With a self-consistent estimate of BH spins, we find that the fraction of electromagnetic counterparts in observable populations is $\approx 4-30\%$, depending on different NS equations of state. Future detections of coalescing NSBH binaries would provide invaluable insights into SN mechanisms, common envelope evolution, and NS physics.

Key words. Gravitational waves – Stars: neutron – Stars: black holes – binaries: close

1. Introduction

The first observation consistent with masses for neutron star–black hole (NSBH) merger events was announced by Abbott et al. (2021a) in 2021. The event, GW200105, has component masses $M_{\rm BH} = 8.9^{+1.2}_{-1.5}\,M_\odot$ and $M_{\rm NS} = 1.9^{+0.3}_{-0.2}\,M_\odot$, and effective inspiral spin parameter $\chi_{\rm eff} = -0.01^{+0.11}_{-0.15}$, strongly peaking around zero. The other event, GW200115, has component masses $M_{\rm BH} = 5.7^{+1.8}_{-2.1}\,M_\odot$ and $M_{\rm NS} = 1.5^{+0.7}_{-0.3}\,M_\odot$, and effective inspiral spin parameter $\chi_{\rm eff} = -0.19^{+0.23}_{-0.35}$. The possible negative $\chi_{\rm eff}$ suggests the BH spin is antialigned with the orbit. However, Mandel & Smith (2021) later argued that a nonspinning BH is more consistent with astrophysical understanding. From these two events, Abbott et al. (2021a) inferred a local merger rate density of $\mathcal{R}_{\rm NSBH} = 45^{+75}_{-33}\,{\rm Gpc^{-3}yr^{-1}}$.

In April 2024, Abac et al. (2024) reported a detection of a NSBH merger event, GW230529, during the forth observing run of LIGO, Virgo, and KAGRA (LVK) network. The primary mass of GW230519 is estimated to be $3.6^{+0.8}_{-1.2}\,M_\odot$ and the secondary mass is $1.4^{+0.6}_{-0.2}\,M_\odot$. The effective inspiral-spin $\chi_{\rm eff}$ is measured to be $-0.10^{+0.12}_{-0.17}$, which suggests either an anti-aligned spin component or negligible spins. The $\chi_{\rm eff}$ is correlated with the mass ratio $q = M_{\rm NS}/M_{\rm BH}$, with more negative $\chi_{\rm eff}$ corresponding to a more comparable mass ratio. Including the new event GW230529, Abac et al. (2024) updated the inferred local merger rate density to $\mathcal{R}_{\rm NSBH} = 85^{+116}_{-57}\,{\rm Gpc^{-3}yr^{-1}}$.

Prior to gravitational wave (GW) observations, the BH mass distribution inferred from the X-ray binary populations indicated a low-mass boundary of $\simeq 5\,M_\odot$ (Bailyn et al. 1998; Özel et al. 2010; Farr et al. 2011). In the meantime, the maximum NS mass has been suggested to be below $\simeq 2.4\,M_\odot$ based on X-ray and radio observations (Linares et al. 2018; Kandel & Romani 2020; Romani et al. 2022), below $\simeq 2.52\,M_\odot$ from GW observations (Abbott et al. 2020a), and below $\simeq 3\,M_\odot$ based on theoretical constraints (Rhoades & Ruffini 1974; Kalogera & Baym 1996;

⋆ e-mail: Zepei.Xing@unige.ch

Godzieba et al. 2021). The lightest BH and the heaviest NS lead to a mass gap of $\sim 3-5\,M_\odot$. Several candidate systems have been suggested to contain a BH in the mass gap from electromagnetic observations (Zdziarski et al. 2013; Heida et al. 2017; Thompson et al. 2019; Casares et al. 2022) and from GW detections (Abbott et al. 2020c, 2021b, 2023, 2024), but none have been confirmed with high confidence. Fryer et al. (2012) built two analytical supernova (SN) prescriptions based on different assumptions of the instability growth timescale to map the carbon-oxygen core mass to compact object remnant mass. With the rapid prescription, the mass gap can be generated, while the delayed prescription predicts a continuous remnant mass distribution. No theoretical constraints are able to determine which one is more representative.

GW230529 is the first detection of a compact binary whose primary component is highly likely to fall within the mass gap, potentially resolving the longstanding debate on the existence of the mass gap. Assuming that the range of $3-5\,M_\odot$ represents the mass gap, Abac et al. (2024) provided a merger rate for binaries with components within the gap of $\mathcal{R}_{\rm gap} = 24^{+28}_{-16}\,{\rm Gpc^{-3}yr^{-1}}$ or $\mathcal{R}_{\rm gap} = 33^{+89}_{-29}\,{\rm Gpc^{-3}yr^{-1}}$ based on two different population models. A key question is why the mass-gap BHs are hidden in the low mass X-ray binary (LMXB) population. Siegel et al. (2023) investigated selection biases against mass-gap BHs, taking into account that a dynamical BH mass measurement requires the existence of transient behaviors of the corresponding LMXBs. They found that with rapid population synthesis simulations, all model combinations predict detection of LMXBs containing mass-gap BHs. However, using detailed binary stellar-evolution models, they found that observational biases against mass-gap BHs appear when the maximum NS birth mass is less than $\simeq 2\,M_\odot$. If the maximum NS birth mass is greater, the mass gap would be filled by BHs formed through accretion induced collapse in LMXBs and we should have observed plenty of them.

In this study, we use the binary population synthesis code POSYDON (Fragos et al. 2023), which incorporates extensive grids of detailed stellar binary-evolution models, to study the formation of coalescing NSBH systems across the Universe. Particularly, we focus on the BH mass distributions of coalescing NSBHs and the effects of model variations of common envelope (CE) evolution and SN kicks. With POSYDON, we are able to self-consistently estimate the BH spins and, thus, more accurately infer the fraction of associated electromagnetic counterparts.

2. Methods

To simulate populations of binaries, we employ an updated version (v2.0) of the publicly available code POSYDON[1] (Andrews et al. in prep.), which integrates detailed single- and binary-star model grids, simulated using the stellar evolution code Modules for Experiments in Stellar Astrophysics (MESA, Paxton et al. 2011, 2013, 2015, 2018, 2019; Jermyn et al. 2023). Compared to POSYDON v1.0 (Fragos et al. 2023), POSYDON v2.0 extends to include grids with eight metallicities $Z = 0.0001, 0.001, 0.01, 0.1, 0.2, 0.45, 1, 2\,Z_\odot$.

We evolve a population of 10^6 binaries for each metallicity, starting from two zero-age main-sequence stars. We sample the primary mass following the initial mass function from Kroupa (2001), within the range of $7 - 120\,M_\odot$. The secondary mass, ranging from $0.5\,M_\odot$ to $120\,M_\odot$, adheres to a flat distribution from the minimal ratio to 1 with respect to the primary mass. The initial orbital periods follow the distribution of Sana et al. (2013) from 1 days to 6000 days. We extend it to 0.35 days with a logarithmic uniform distribution. We assume the initial orbits are circular and the two stars are tidally synchronized. For all the population models presented in this study, we employed the nearest-neighbor interpolation scheme to interpolate between models in the binary grids (see Section 7 in Fragos et al. 2023).

To calculate the compact object masses through core-collapse supernova (CCSN), we adopted the Fryer et al. (2012) delayed prescription, which allows the formation of mass-gap BHs. Regarding the CCSN natal kick velocity for NSs, we adopt a Maxwellian distribution with a velocity dispersion of $\sigma_{\rm CCSN} = 265\,{\rm km\,s^{-1}}$ (Hobbs et al. 2005). Some studies have implied that the NS kick should be weaker. For example, O'Doherty et al. (2023) obtained an velocity dispersion of $\sigma_{\rm CCSN} = 61.6\,{\rm km\,s^{-1}}$ from the populations of NS binaries. It should be considered as the lower limit because their sample excludes the disrupted systems where the NSs received large kicks. As a result, we also consider $\sigma_{\rm CCSN} = 61.6\,{\rm km\,s^{-1}}$ and a moderate value of $\sigma_{\rm CCSN} = 150\,{\rm km\,s^{-1}}$ for the purpose of parameter study. BH kicks follow the same distribution but rescaled by a factor of $1.4\,M_\odot/M_{\rm BH}$.

In POSYDON, the maximum NS mass is, by default, set to be $2.5\,M_\odot$. To account for selection biases against mass-gap BHs in LMXBs, we also consider a maximum NS birth mass of $M_{\rm NS,birth-max} = 2\,M_\odot$ (Siegel et al. 2023). To achieve this, we assume that all compact objects born with masses above $2\,M_\odot$ as predicted by the delayed prescription, are light BHs instead of NSs. This assumption excludes these binaries from the NSBH populations. We acknowledge that we do not include a self-consistent SN prescription for classifying remnant type and predicting the masses of these specific compact objects. A small population of double NSs with one of the NS heavier than $2\,M_\odot$ at birth would turn to NSBHs based on this assumption about the NS maximum birth mass. In our populations, the contribution of these systems is insignificant.

Utilizing the stellar profiles of the BH progenitors at carbon depletion, we calculate the BH spins by following the method described in the Appendix D of Bavera et al. (2021). We assume that the BH spin vector is the same as that of its progenitor, and that the progenitor is always aligned with the orbit. We ignore any change in the BH spin direction due to mass transfer. The final orbital tilt is the combination of two tilts originating from two SN kicks (Xing et al. 2024). We take into account the change of BH spin magnitude due to accretion. However, it has limited effects because we applied Eddington-limited accretion.

For the CE evolution, we employ the $\alpha-\lambda$ prescription (Webbink 1984; de Kool et al. 1987; Livio & Soker 1988). The CE efficiency parameter $\alpha_{\rm CE}$ determines how efficient the energy can be utilized to expel the envelope. By default, we set $\alpha_{\rm CE} = 1$. The parameter $\lambda_{\rm CE}$ depends on the mass and the internal structure and energy profile of the stars at the onset of CE evolution (Dewi & Tauris 2000). Unlike most rapid BPS codes, which use pre-tabulated $\lambda_{\rm CE}$ values obtained from studies on single stars, POSYDON allows for on-the-fly calculations of $\lambda_{\rm CE}$ based on the profiles of the stars. To determine the boundary of the helium core and the envelope, we select the layer where the hydrogen mass fraction $X_{\rm H} = 0.1$ by default (see Section 8.2 in Fragos et al. 2023).

From the simulated binaries, we select those binaries forming a NS and a BH that would merge within a Hubble time to comprise our synthetic population. Then, we distribute the syn-

[1] We utilized the version of the POSYDON code identified by the commit hash 5acad13, available at https://github.com/POSYDON-code/POSYDON/, along with the POSYDON v2.0 dataset will be published here: https://zenodo.org/communities/posydon.

thetic population across the cosmic history of the Universe at every Δt_i (100 Myr by default) cosmic time interval centered on the redshift z_i (see Appendix D in Bavera et al. 2022). To account for the metallicity- and redshift-dependent star formation history (SFH), for each coalescing NSBH system, we calculate its cosmological weight based on the star formation rate density and metallicity distribution from the TNG100 Illustris large-scale cosmological simulation (Nelson et al. 2019). Then, the weighted population represents the intrinsic population. Finally, we calculate the detection probability $p_{\rm det}$ for each binary assuming a network of LIGO-Hanford, LIGO-Livingston, and Virgo at `design` sensitivity (see Abbott et al. 2020b) to generate the observable populations.

3. Results

3.1. The Role of Common Envelope Efficiency

In Figure 1, we show the distribution of BH and NS masses for the intrinsic populations in our simulations, with $\alpha_{\rm CE} = 1$ on the left and $\alpha_{\rm CE} = 2$ on the right. Additionally, we present the 1D BH mass distributions and compare them with the distribution inferred from the three events GW230529, GW200105, and GW200115 (Abac et al. 2024). We also show the contributions from two main formation channels that we defined: channel CE, for which the binary experiences CE evolution either before or after the BH formation, and channel SMT, where the binary undergoes at least one stable mass transfer phase without any CE evolution. In channel CE, the classical pathway dominates, where the two non-degenerate stars undergo stable mass transfer, and after the primary star forms a BH, the secondary star and the BH initiate a CE phase. More frequently, the binary experiences a subsequent case BB mass transfer, where the secondary helium star expands to fill the Roche lobe due to shell helium burning. In channel SMT, most binaries undergo two stable mass transfer phases, one before and one after the BH formation. Some binaries avoid mass transfer before BH formation and experience stable mass transfer afterward.

Utilizing our default parameter settings, with $\alpha_{\rm CE} = 1$, we can see two prominent peaks: one around $M_{\rm BH} \simeq 4 - 5\,M_\odot$ and $M_{\rm NS} \simeq 1.3\,M_\odot$, and another at $M_{\rm BH} \simeq 7 - 8\,M_\odot$ and $M_{\rm NS} \simeq 2.1 - 2.2\,M_\odot$. The paucity of NSs around $\sim 1.7\,M_\odot$ is caused by the discontinuity of $0.1\,M_\odot$ in the proto-compact object mass equation at carbon-oxygen core masses of $3.5\,M_\odot$ in the Fryer et al. (2012) delayed prescription, which was also discussed in Broekgaarden et al. (2021). The compact object mass depends on not only the initial progenitor mass, but also mass transfer process during the evolution, which affects the final core mass of the progenitor at core-collapse. Especially for NSs, case BB mass transfer plays a crucial role, as the amount of mass remaining after this mass transfer phase directly determines the NS mass. Massive NSs typically originate from helium stars that do not lose much mass through case BB mass transfer or avoid it. If the NS progenitor loses mass to end up with a final helium core in the mass range of $1.4 - 2.5\,M_\odot$ (Podsiadlowski et al. 2004), it will form a NS of $\simeq 1.26\,M_\odot$ through electron-capture SN. If the NS progenitor has a final carbon-oxygen core mass below $2.5\,M_\odot$, based on the Fryer et al. (2012) delayed prescription, it will eventually become a NS of $\simeq 1.27\,M_\odot$. We can see from Figure 1 that these light NSs have a significant contribution in mass-gap NSBHs.

Notably, for the default model, the BH mass distribution shows the highest probability at $\simeq 7\,M_\odot$, not in agreement with the observation. In contrast, when adopting a larger $\alpha_{\rm CE}$ of 2, the BH mass distribution shifts towards lower masses, concentrating around $\simeq 4\,M_\odot$, with a deficiency at $7 - 10\,M_\odot$. The result is consistent with the findings of Zhu et al. (2024), who found a low-mass peak of $3.4\,M_\odot$ within the mass gap when adopting $\alpha_{\rm CE} = 2$. We find that a larger $\alpha_{\rm CE}$ does not increase the merger rate of NSBHs with heavy BHs ($\gtrsim 6\,M_\odot$) but significantly facilitates the formation of NSBHs with light BHs. The reason is that, in the underlying populations, plenty of binaries with light BHs initiated a CE phase and subsequently merged in CE evolution. Compared to binaries containing heavy BHs, they are greater in number but tend to have lower orbital energy, making it harder to eject the envelope of the companion star. Hence, a more efficient energy conversion in CE evolution would substantially increase the number of systems succeeding in CE evolution with light BHs in particular. Additionally, some binaries with heavy BHs would result in wider orbits due to a larger $\alpha_{\rm CE}$, and would no longer merge within a Hubble time. The fraction of channel CE increase from $\approx 70\%$ for $\alpha_{\rm CE} = 1$ to $\approx 86\%$ for $\alpha_{\rm CE} = 2$. The mass-gap NSBHs are largely from channel CE.

Although a larger $\alpha_{\rm CE}$ provides a better match to the observation by producing the peak within the mass gap, we see a mild deficiency in BHs with masses $\gtrsim 7\,M_\odot$. In `POSYDON`, when calculating the parameter $\lambda_{\rm CE}$, we integrate both the gravitational energy and internal energy of the envelope, subtracting the recombination energy. As a result, we are inclined to adopt $\alpha_{\rm CE}$ values not greater than 1, as no other energy source is evident to justify a large $\alpha_{\rm CE}$ of 2.

3.2. Supernova Natal Kicks

In this section, we investigate the impact of SN kicks on the BH mass distributions of coalescing NSBH binaries. In Figure 2 we show the distribution of BH and NS masses in coalescing NSBH populations for another two different SN kick velocities of $\sigma_{\rm CCSN} = 150\,{\rm km\,s^{-1}}$ and $\sigma_{\rm CCSN} = 61.6\,{\rm km\,s^{-1}}$. The populations are generated using $\alpha_{\rm CE} = 1$. We can see that a lower kick velocity of $\sigma_{\rm CCSN} = 150\,{\rm km\,s^{-1}}$ does not significantly alter the BH mass distribution but only slightly increase the fraction of lower mass-gap BHs compared to the default $\sigma_{\rm CCSN} = 265\,{\rm km\,s^{-1}}$ shown in Figure 1. In the case of $\sigma_{\rm CCSN} = 61.6\,{\rm km\,s^{-1}}$, the peak shifts toward lower BH masses and the channel CE becomes completely dominant. This occurs because the underlying population favors light BHs going through CE evolution, and weak kicks prevent these binaries from being disrupted. Moreover, binaries going through SMT typically require high eccentricities induced by strong kicks to merge within a Hubble time. As a result, weak kicks reinforce the dominance of channel CE. The fraction of channel CE is 75% and 97% for $\sigma_{\rm CCSN} = 150\,{\rm km\,s^{-1}}$ and $\sigma_{\rm CCSN} = 61.6\,{\rm km\,s^{-1}}$, respectively.

Although lower kick velocities slightly raise the percentage of lower mass-gap BHs, the overall distribution does not align well with the observation. For $\sigma_{\rm CCSN} = 61.6\,{\rm km\,s^{-1}}$, the fraction of NSBH mergers with BH masses above $\simeq 11\,M_\odot$ becomes marginal. Furthermore, this low kick velocity increases the local merger rate density of NSBHs to an excessively high value. We estimate the local merger rate density of NSBH mergers for varied kick velocities at redshift zero. The three kick velocities $\sigma_{\rm CCSN} = 265\,{\rm km\,s^{-1}}$, $\sigma_{\rm CCSN} = 150\,{\rm km\,s^{-1}}$, and $\sigma_{\rm CCSN} = 61.6\,{\rm km\,s^{-1}}$ correspond to local merger rate densities of $72\,{\rm Gpc^{-3}\,yr^{-1}}$, $193\,{\rm Gpc^{-3}\,yr^{-1}}$, and $408\,{\rm Gpc^{-3}\,yr^{-1}}$, respectively. The rate for the lowest kick velocity, $\sigma_{\rm CCSN} = 61.6\,{\rm km\,s^{-1}}$, is significantly higher than the upper limit of the NSBH local merger rate estimated from LVK analysis.

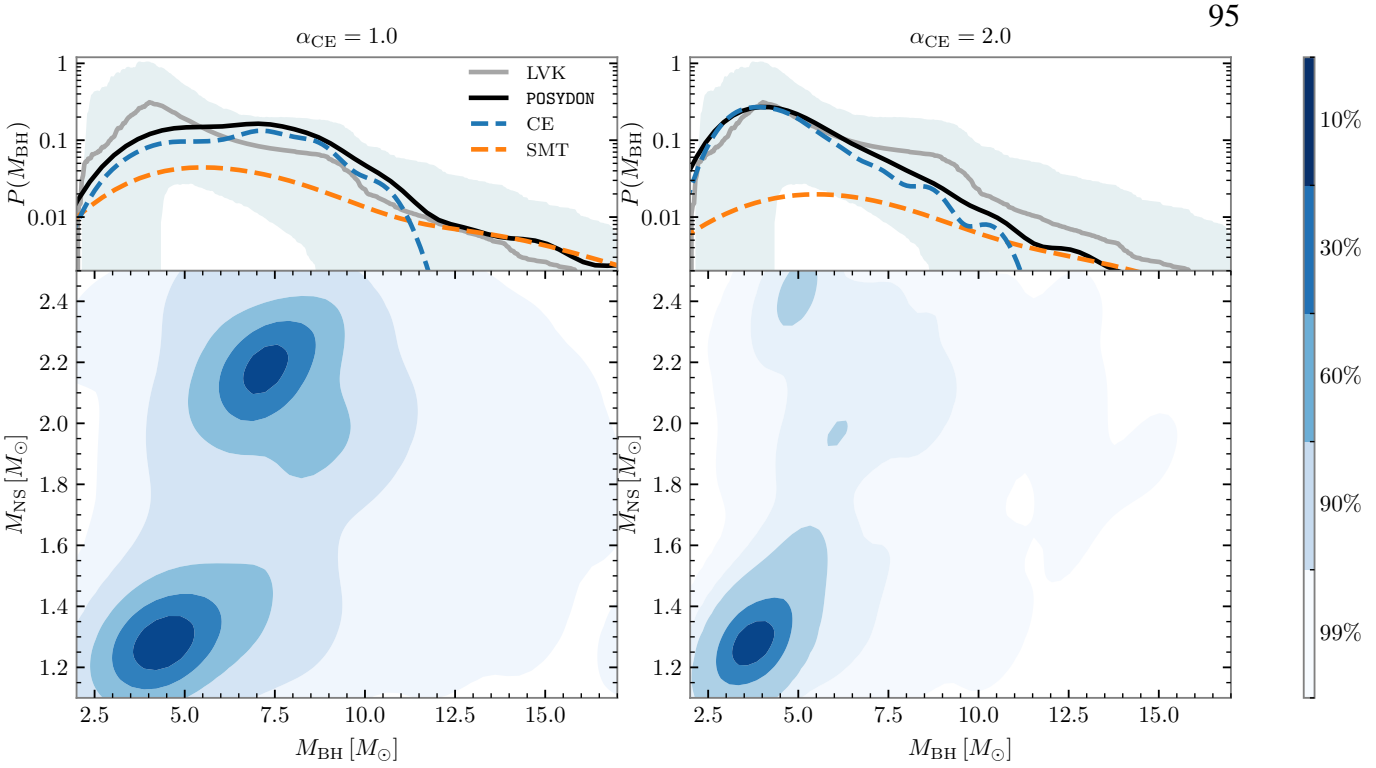

Fig. 1. NS and BH mass distributions of our intrinsic coalescing NSBH populations. Left and right panels correspond to the populations generated with CE parameter $\alpha_{\rm CE} = 1$ and 2, respectively. The top panels show the BH mass distributions inferred from the three detected events in grey line with 90% credible interval in teal shaded region and from our population model in black line. The contributions from channel CE and channel SMT are in blue dashed line and orange dashed line, respectively. The bottom panels show the kernel density estimate plot of component masses ranging from 1% to 90% credible interval region.

3.3. Account for the Mass-Gap Black Holes in Low Mass X-ray Binaries

In this section, we consider the constraints on the maximum NS birth mass. Following the investigation of selection bias against mass-gap BHs in the LMXB population (Siegel et al. 2023), we exclude binaries with NS birth masses exceeding the maximum value of $2\,M_\odot$ from our intrinsic population. Figure 3 shows the distributions of NS and BH masses from the same populations presented in Figure 1 and Figure 2, but with the maximum NS birth mass set to $2\,M_\odot$. With this restriction, we can see that the default setting with $\alpha_{\rm CE} = 1$ and $\sigma_{\rm CCSN} = 265\,{\rm km\,s^{-1}}$ also predicts a prominence of BH masses around the high-end edge of the lower mass gap. The number of high-mass BHs around $7\,M_\odot$ is reduced, as most of them are paired with high-mass NSs above $2\,M_\odot$, which are removed from the population. Now, a higher $\alpha_{\rm CE} = 2$ predicts an overabundance of mass-gap BHs, particularly BHs lighter than $\simeq 4\,M_\odot$, and a paucity of BHs with mass above $\simeq 7\,M_\odot$. Less than $\approx 10\%$ of coalescing NSBH systems contain BHs outside the mass gap. In this case, the coalescing NSBHs containing BHs more massive than $\simeq 7.5\,M_\odot$ are formed through channel SMT. Both models with lower kick velocities predict a BH mass peak within $4-5\,M_\odot$. The moderate kick velocity $\sigma_{\rm CCSN} = 150\,{\rm km\,s^{-1}}$ exhibits the best match to the BH mass distribution inferred from the observation regarding the peak and the tail for massive BHs.

The local merger rate densities of NSBHs and mass-gap NSBHs for all the model variations are summarized in Table 1. With the restriction on NS birth mass, $\mathcal{R}_{\rm gap}$ barely changes, as mass-gap BHs are accompanied by low-mass NSs. With $M_{\rm NS,birth-max} = 2\,M_\odot$, the three kick velocities $\sigma_{\rm CCSN} = 265\,{\rm km\,s^{-1}}$, $\sigma_{\rm CCSN} = 150\,{\rm km\,s^{-1}}$, and $\sigma_{\rm CCSN} = 61.6\,{\rm km\,s^{-1}}$ correspond to local merger rate densities of $40\,{\rm Gpc^{-3}\,yr^{-1}}$, $119\,{\rm Gpc^{-3}\,yr^{-1}}$, and $274\,{\rm Gpc^{-3}\,yr^{-1}}$, respectively. The lowest kick velocity $\sigma_{\rm CCSN} = 61.6\,{\rm km\,s^{-1}}$ still predicts a merger rate density exceeding the upper limit of the updated rate inferred from the three events. This is reasonable as the velocity should be considered as a lower limit (O'Doherty et al. 2023). In the other two cases, the predicted merger rates are consistent with the inferred merger rates.

3.4. Observable Population

In the previous sections, we presented BH and NS mass distributions of the intrinsic coalescing NSBH populations in our simulations, which are not directly comparable to observed events. In Figure 4, we display the properties of the observable population for the model of $\alpha_{\rm CE} = 1$, $M_{\rm NS,birth-max} = 2\,M_\odot$, and $\sigma_{\rm CCSN} = 150\,{\rm km\,s^{-1}}$, including the distributions of the BH mass, NS mass, mass ratio, and the BH spin at the direction of the orbit $\chi_{\rm BH,z}$. We also display the properties of the three observed events in the figure. We can see that our simulation can match the properties of the three events well. A higher detection probability for BHs around $\simeq 7\,M_\odot$ and NSs around $\simeq 1.9\,M_\odot$ appears, which is consistent with the event GW200105, with respect to the intrinsic population. The mass ratio distribution centers at $\simeq 0.2$ and can barely reach 0.5. The $\chi_{\rm BH,z}$ is centered at zero, with a spread to $\simeq 0.1$ and a small bump at $\simeq 0.25$. Most BHs have negligible natal spins because BH progenitors lose most of their angular momentum through mass transfer and winds. The small bump at $\simeq 0.25$ corresponds to initially close binaries where tides can

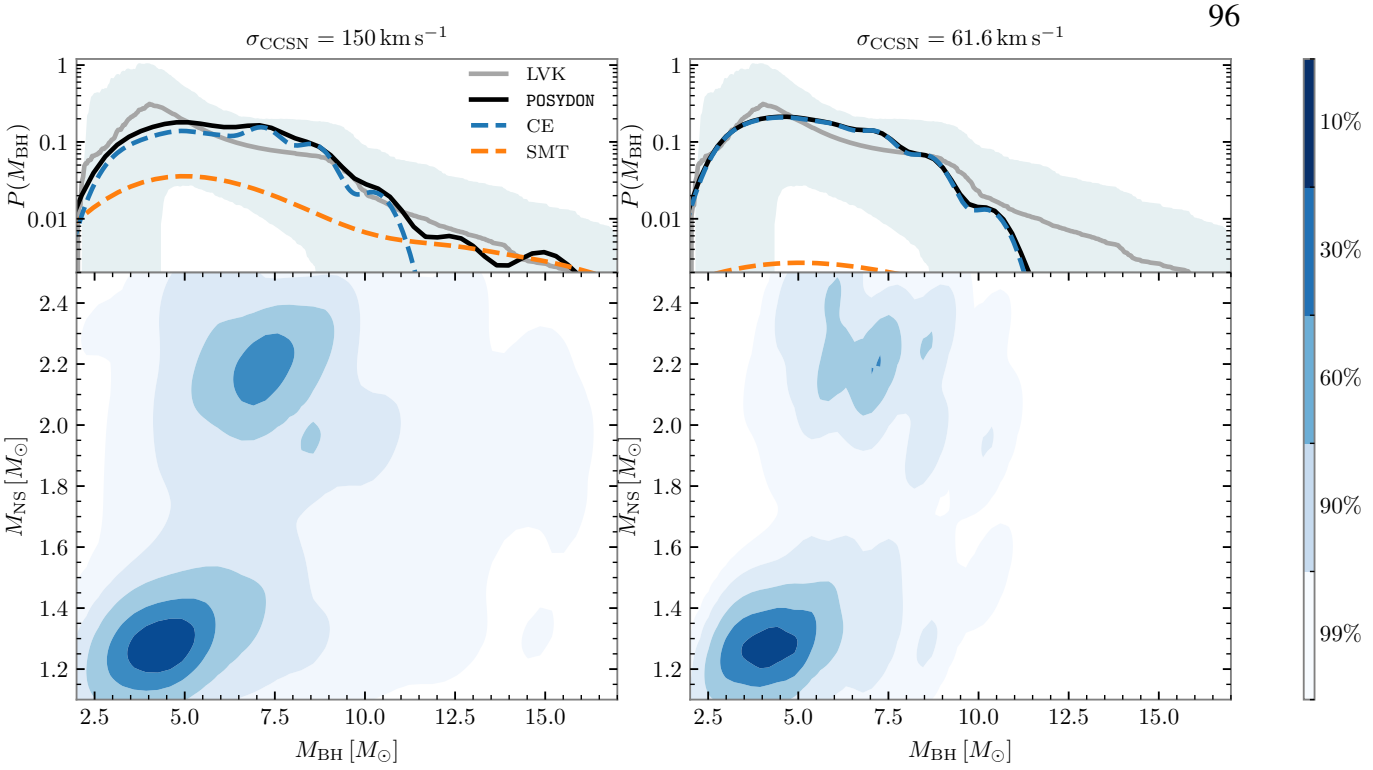

Fig. 2. Same as Figure 1 with $\alpha_{\rm CE}$=1, but with different kick velocities of $\sigma_{\rm CCSN}$ = 150 and 61.6 km s^{-1}.

Table 1. Local Merger Rate Density of NSBH Mergers for Different Models

Model	$\mathcal{R}_{\rm NSBH}$[Gpc^{-3}yr^{-1}]	$\mathcal{R}_{\rm gap}$[Gpc^{-3}yr^{-1}]
POSYDON default	72	11
$\alpha_{\rm CE}$ = 2	162	57
$\sigma_{\rm CCSN}$ = 150 km s^{-1}	193	41
$\sigma_{\rm CCSN}$ = 61.6 km s^{-1}	408	105
$M_{\rm NS,birth-max}$ = 2 $M_\odot$	40	10
$\alpha_{\rm CE}$ = 2, $M_{\rm NS,birth-max}$ = 2 $M_\odot$	110	55
$\sigma_{\rm CCSN}$ = 150 km s^{-1}, $M_{\rm NS,birth-max}$ = 2 $M_\odot$	119	40
$\sigma_{\rm CCSN}$ = 61.6 km s^{-1}, $M_{\rm NS,birth-max}$ = 2 $M_\odot$	274	103

Notes. Inferred rates from LVK: $\mathcal{R}_{\rm NSBH} = 85^{+116}_{-57}$ Gpc^{-3}yr^{-1} and $\mathcal{R}_{\rm gap} = 24^{+28}_{-16}$ Gpc^{-3}yr^{-1} or 33^{+89}_{-29} Gpc^{-3}yr^{-1} (Abac et al. 2024).
POSYDON default: $\alpha_{\rm CE}$ = 1, $M_{\rm NS,birth-max}$ = 2.5 $M_\odot$, $\sigma_{\rm CCSN}$ = 265 km s^{-1}

spin up the BH progenitors. Because we assume that BH accretion is Eddington-limited, the accretion spin-up is not significant. The BHs can be spun up by case BB mass transfer but the increase is typically below 0.1. BH spins as high as $\simeq$ 0.5 are attributed to stable case A mass transfer, but the fraction of such cases is negligible. The three events are consistent with nearly zero $\chi_{\rm BH,z}$. For GW230529, if its primary compact object is a massive NS, as the mass ratio is anti-correlated with the primary mass, the secondary NS is expected to be massive at birth, even exceeding the threshold of 2 $M_\odot$. If its primary is a BH, it is more likely that the BH mass is at the higher end.

3.5. Electromagnetic Counterparts

To estimate the fraction of potential associated electromagnetic counterparts (EMCs) in NSBH mergers, we utilize the empirical formula provided by Foucart et al. (2018) to calculate the remnant mass outside the innermost stable circular orbit (ISCO) of the BH resulting from the tidal disruption of the NS. The systems having non-zero remnant mass outside ISCO are considered to produce EMCs such as short gamma-ray bursts and kilonovae. We assume three NS radii $R_{\rm NS}$ = 11 km, 12 km, and 13 km, encompassing a range of NS equations of state from soft to stiff. For the default model with $\alpha_{\rm CE}$ = 1 and $\sigma_{\rm CCSN}$ = 265 km s^{-1}, we obtain EMC fractions for the intrinsic population of 3%, 16%, and 26% for $R_{\rm NS}$ = 11 km, 12 km, and 13 km, respectively. In our preferred model, with $\alpha_{\rm CE}$ = 1, $\sigma_{\rm CCSN}$ = 150 km s^{-1}, and

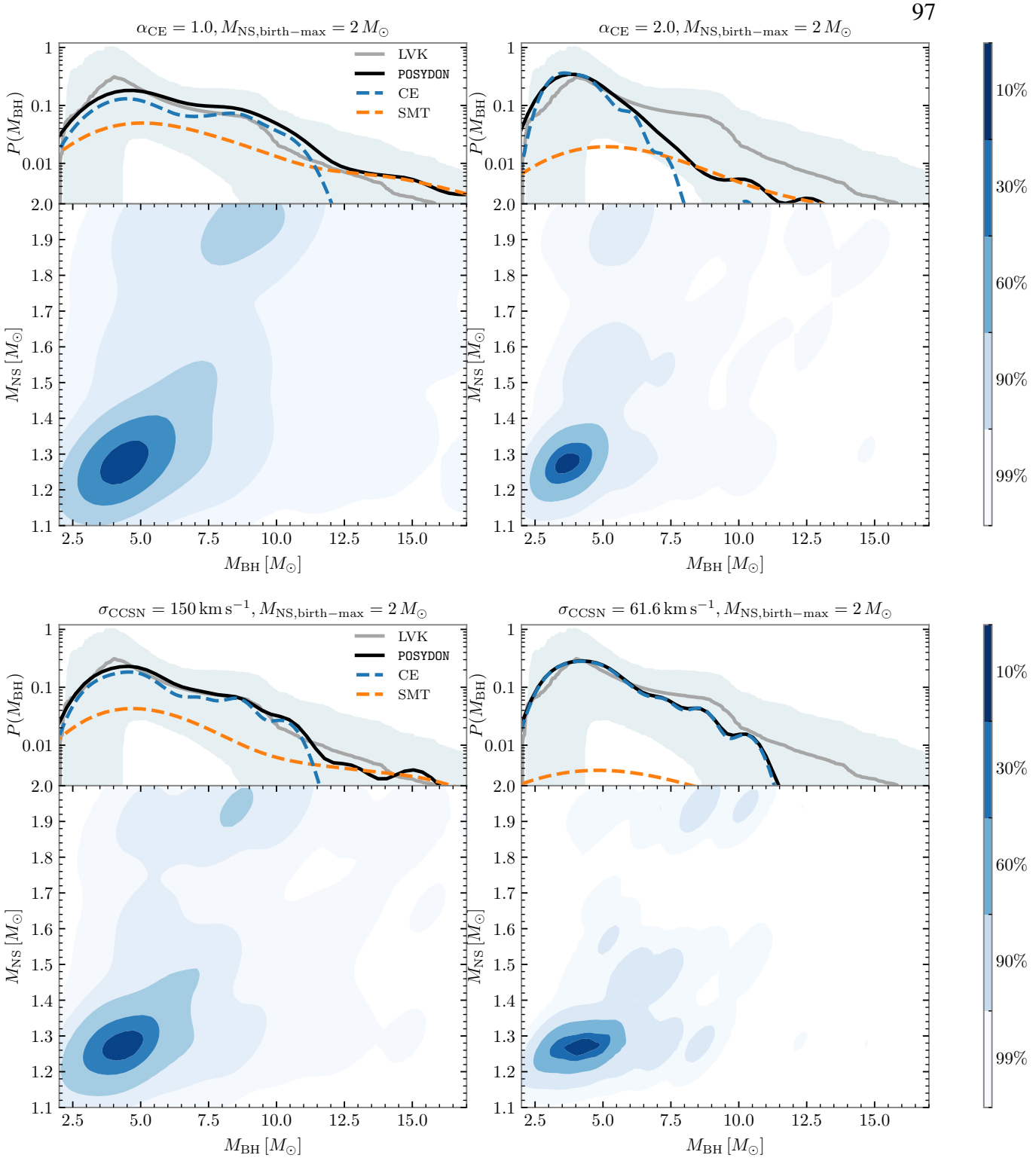

Fig. 3. NS and BH mass distributions of our intrinsic coalescing NSBH population, assuming the maximum NS birth mass is $2\,M_\odot$.

$M_{\rm NS,birth-max} = 2\,M_\odot$, the fractions increase to 11%, 36%, and 57%. The EMC fractions increase substantially because the preferred model predicts a larger fraction of systems with light BHs and light NSs, which increase the chance of tidal disruption for the NSs outside the ISCO.

Shifting from the intrinsic to the observable populations, we estimate the EMC fractions for observable systems. The default model yields EMC fractions of 1%, 6%, and 10% for $R_{\rm NS} = 11$ km, 12 km, and 13 km, respectively. Under our preferred model, we find EMC fractions of 4%, 20%, and 31%. The detection of GW230529 shifts the BH mass distributions toward lower masses in NSBH merger populations, leading to an increased chance of observing associated EMCs, especially if the NS equation of state is stiff.

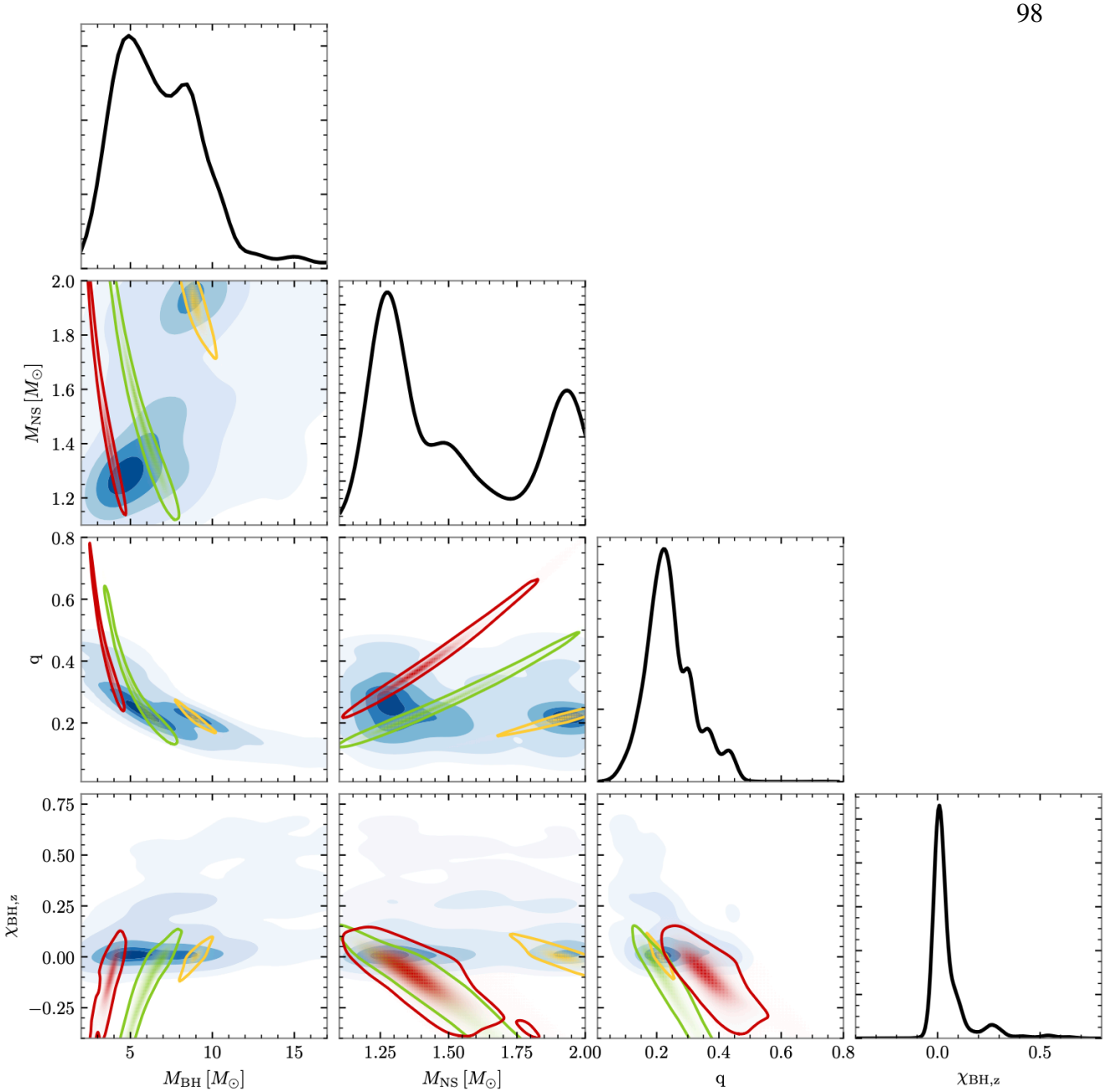

Fig. 4. Corner plot of the observable population of coalescing NSHBs in our simulation, generated with $\alpha_{\rm CE} = 1$, $\sigma_{\rm CCSN} = 150\,{\rm km\,s^{-1}}$ and $M_{\rm NS,birth-max} = 2\,M_\odot$. We show the BH mass, NS mass, mass ratio, and BH spin component parallel to the direction of the orbital plane. The red, green, and yellow contours indicate the 90% confidence interval of GW230529, GW200115, and GW200105, respectively.

4. Discussion

4.1. Uncertainties

One of the primary uncertainties in our BPS study is the SN prescription, specifically the association between pre-SN progenitor core masses and the compact object masses. The Fryer et al. (2012) delayed prescription allows for mapping compact objects within the lower-mass gap. However, the discontinuity in NS mass around $1.7\,M_\odot$ is neither supported by the observations nor motivated by SN physics. Furthermore, the restriction on the maximum NS birth mass cannot be reconciled self-consistently with the Fryer et al. (2012) delayed prescription, suggesting a potential need for a different relationship between heavy helium or carbon-oxygen core masses and compact object masses. Prescriptions that link the progenitor's helium or carbon-oxygen core properties to the outcome compact object remnant properties play a key role in modeling BH and NS mass distributions in population studies and determining the fraction of associated EMCs. Future observations of double compact object mergers will put further constraints on SN prescriptions and advance our understanding of SN physics.

The models of metallicity- and redshift-dependent SFH and the assumptions made in distributing our populations across cosmic time can affect primarily the rates but also the shapes of NSBH property distributions (Broekgaarden et al. 2021). We leave the exploration of these factors to future studies when the data sample grows large enough for aiding to allow for a proper statistical comparison. Furthermore, investigating varia-

tions in stellar physics like the wind prescriptions and overshooting parameters, and in binary physics like the mass transfer efficiency is beyond the scope of this study, as changing these model assumptions would require constructing new binary simulation grids. However, the POSYDON framework allows for potential future investigations into these key physics self-consistently and precisely by integrating new grids of detailed binary models.

4.2. Maximum Neutron Star Birth Mass

Several massive NSs has been found with mass exceeding $2\,M_\odot$, for example PSR J2215+5135 with $M_{\rm NS} = 2.27^{+0.17}_{-0.15}\,M_\odot$ (Linares et al. 2018), PSR J0740+6620 with $M_{\rm NS} = 2.08 \pm 0.07\,M_\odot$ (Fonseca et al. 2021), J1810+1744 with $M_{\rm NS} = 2.13 \pm 0.04\,M_\odot$ (Romani et al. 2021), and PSR J0952-0607 with $M_{\rm NS} = 2.35 \pm 0.17\,M_\odot$ (Romani et al. 2022). All of these NSs are millisecond pulsars with a low-mass main-sequence or a white dwarf companion. They are expected to have accreted mass from their companion and been recycled. As a result, their birth masses remain unknown and could be less than $2\,M_\odot$. In contrast, for double NSs detected in our Galaxy, the second-born NSs are typically low-mass, which can be directly interpreted as their birth mass. In the population of eclipsing NS high-mass X-ray binaries, the NSs are very young and are not expected to have accreted a significant amount of mass. In the study by Falanga et al. (2015), most NSs in high-mass X-ray binaries are measured to be below $\sim 2\,M_\odot$, with one possible exception of Vela X-1, which contains a NS with mass $M_{\rm NS} = 2.12 \pm 0.16\,M_\odot$. Nevertheless, with the uncertainty in the measurement, one cannot rule out the possibility that the maximum NS birth mass is restricted around $2\,M_\odot$.

4.3. Could NS Form First?

Xing et al. (2024) found that the BH always forms first in the population of coalescing NSBHs at solar metallicity from POSYDON simulations. This is because the rotation-dependent accretion model for non-degenerate stars in POSYDON suggests a low accretion efficiency for case B mass transfer in general, which limits the probability of mass reversal. Similar trends that low accretion efficiency for non-degenerate accretors predicting low fraction of first-born NSs in NSBH populations are also found in other population studies (Kruckow et al. 2018; Shao & Li 2021; Broekgaarden et al. 2021). Liotine et al. (in prep.) also find that POSYDON predicts low formation rate of millisecond pulsar BH binaries, where the NSs form prior to the BHs to be recycled by the BH progenitors. In some close binaries, where tides can spin down the accretor and enhance the mass accretion, rejuvenation could occur. However, the first born NSs are highly likely to enter a CE phase with massive BH progenitors and subsequently merge due to their low orbital energy (see a detailed discussion in Xing et al. 2024). In this study, we find that this conclusion also holds true for varied metallicities.

We posit that if the accretion efficiency is actually high enough to lead to mass reversal for binaries in wide orbits, the NS could form first in coalescing NSBHs. Román-Garza et al. (2021) predicted that the fraction of NSBH mergers with NS form first can reach about 10% when assuming accretion onto non-degenerate stars is limited only by the thermal timescale of the accetor, which makes the accretion efficiency much higher than the rotation-dependent accretion model. In this case, the NSs have chance to accrete mass from the BH progenitors. However, in mass transfer phases when the BH progenitors are still hydrogen-rich stars, the large mass ratios would lead to unstable mass transfer quickly before the NS can accrete a significant amount of mass. Furthermore, if the binaries survive CE, the helium stars that are massive enough to form BHs would not experience rapid expansion, suggesting that the NSs might not have the chance to gain mass through case BB mass transfer as in LMXBs. Liotine et al. (in prep.) found that a small group of NSBHs with first-born NSs form through double CE process between two non-degenerate stars. Similarly, the NSs cannot accrete much mass from the BH progenitors. In conclusion, we expect that even if the NS forms first in coalescing NSBHs, the NS is likely to be close to its birth mass.

5. Conclusion

The detection of the new event GW230529, which very likely contains a compact object with mass in the lower mass gap, has refreshed our understanding of the coalescing NSBH populations. The inclusion of GW230529 in population inference analysis yields a new BH mass distribution for coalescing NSBHs and an updated merger rate. Most importantly, it provides strong evidence that the lower mass gap does not exist. We conduct a population synthesis study on coalescing NSBHs to investigate how the CE process and SN kick velocity affect their properties, and to reconcile the detection of mass-gap BHs from GWs with their absence in LMXBs.

We find that, using the POSYDON default model with $\alpha_{\rm CE} = 1$, $\sigma_{\rm CCSN} = 265\,{\rm km\,s^{-1}}$, and $M_{\rm NS,birth-max} = 2.5\,M_\odot$, the BH masses are not centered within the lower mass gap as implied by observations. Increasing the CE efficiency to $\alpha_{\rm CE} = 2$ can facilitate the formation of NSBH mergers with mass-gap BHs efficiently. These light BHs going through CE are greater in number in the underlying population, although hard in surviving CE due to low orbital energy. A higher CE efficiency would increase the success rate of CE for these light BHs, and thus lead to a surge of coalescing NSBH with mass-gap BHs. Furthermore, we find that lower kick velocities can increase the contribution of mass-gap BHs that go through CE in coalescing NSBHs. However, varying kick velocities alone is insufficient to match the BH mass distribution inferred from observations.

To explain the selection bias against mass-gap BHs in LMXBs, Siegel et al. (2023) found that a maximum NS birth mass of $\simeq 2\,M_\odot$ should be considered. With the restriction of NS birth mass in the Fryer et al. (2012) delayed prescription, we find that a large $\alpha_{\rm CE}$ is not necessary for explaining the updated BH mass distribution from the analysis including GW230529. In this case, a kick velocity of $\sigma_{\rm CCSN} = 150\,{\rm km\,s^{-1}}$ can better match the BH mass distribution compared with $\sigma_{\rm CCSN} = 265\,{\rm km\,s^{-1}}$ and predicts a reasonable local merger rate density for coalescing NSBHs and mass-gap NSBHs. A lower kick of $\sigma_{\rm CCSN} = 61.6\,{\rm km\,s^{-1}}$, obtained from NS binary systems without accounting for disrupted NSs, lead to an overly high merger rate.

We also show that the properties of the three NSBH merger events are consistent with our observable population. The isolated binary evolution channel predicts low BH spins in general. As a result, assuming it formed through the isolated binary evolution channel, the primary star mass of GW230529 can be well constrained to be located within the lower mass gap at the higher end. Moreover, the detection of GW230529 leads to an increase in the EMC fraction of coalescing NSBHs predicted by population models, as light BHs and NSs are easier to result in tidal disruption.

Our study has illustrated that coalescing NSBH population is valuable for understanding SN mechanisms, CE evolution, and

NS physics. Future detections of NSBH merger events could reveal weather the NS birth mass is limited, provide insights into SN remnant mass prescriptions, and further put constraints on CE efficiency and NS equations of state.

Acknowledgements. This work was supported by the Swiss National Science Foundation (project number PP00P2_211006). The POSYDON project is supported primarily by two sources: the Swiss National Science Foundation (PI Fragos, project numbers PP00P2_211006 and CRSII5_213497) and the Gordon and Betty Moore Foundation (PI Kalogera, grant award GBMF8477). Z.X. acknowledges support from the China Scholarship Council (CSC). E.Z. acknowledges funding support from the Hellenic Foundation for Research and Innovation (H.F.R.I.) under the "3rd Call for H.F.R.I. Research Projects to support Post-Doctoral Researchers" (Project No: 7933). M.B. acknowledges support from the Boninchi Foundation. K.A.R. is also supported by the Riedel Family Fellowship and thanks the LSSTC Data Science Fellowship Program, which is funded by LSSTC, NSF Cybertraining Grant No. 1829740, the Brinson Foundation, and the Moore Foundation; their participation in the program has benefited this work. K.K. acknowledges support from the Spanish State Research Agency, through the María de Maeztu Program for Centers and Units of Excellence in R&D, No. CEX2020-001058-M. J.J.A. acknowledges support for Program number (JWST-AR-04369.001-A) provided through a grant from the STScI under NASA contract NAS5-03127.

References

Abac, A. G., Abbott, R., Abouelfettouh, I., et al. 2024, ApJ, 970, L34
Abbott, B. P., Abbott, R., Abbott, T. D., et al. 2020a, ApJ, 892, L3
Abbott, B. P., Abbott, R., Abbott, T. D., et al. 2020b, Living Reviews in Relativity, 23, 3
Abbott, R., Abbott, T. D., Abraham, S., et al. 2021a, ApJ, 915, L5
Abbott, R., Abbott, T. D., Abraham, S., et al. 2021b, ApJ, 923, 14
Abbott, R., Abbott, T. D., Abraham, S., et al. 2020c, ApJ, 896, L44
Abbott, R., Abbott, T. D., Acernese, F., et al. 2023, Physical Review X, 13, 041039
Abbott, R., Abbott, T. D., Acernese, F., et al. 2024, Phys. Rev. D, 109, 022001
Andrews, J., Bavera, S., Briel, M., et al. in prep.
Bailyn, C. D., Jain, R. K., Coppi, P., & Orosz, J. A. 1998, ApJ, 499, 367
Bavera, S. S., Fragos, T., Zapartas, E., et al. 2022, A&A, 657, L8
Bavera, S. S., Fragos, T., Zevin, M., et al. 2021, A&A, 647, A153
Broekgaarden, F. S., Berger, E., Neijssel, C. J., et al. 2021, MNRAS, 508, 5028
Casares, J., Muñoz-Darias, T., Torres, M. A. P., et al. 2022, MNRAS, 516, 2023
de Kool, M., van den Heuvel, E. P. J., & Pylyser, E. 1987, A&A, 183, 47
Dewi, J. D. M. & Tauris, T. M. 2000, A&A, 360, 1043
Falanga, M., Bozzo, E., Lutovinov, A., et al. 2015, A&A, 577, A130
Farr, W. M., Sravan, N., Cantrell, A., et al. 2011, ApJ, 741, 103
Fonseca, E., Cromartie, H. T., Pennucci, T. T., et al. 2021, ApJ, 915, L12
Foucart, F., Hinderer, T., & Nissanke, S. 2018, Phys. Rev. D, 98, 081501
Fragos, T., Andrews, J. J., Bavera, S. S., et al. 2023, ApJS, 264, 45
Fryer, C. L., Belczynski, K., Wiktorowicz, G., et al. 2012, ApJ, 749, 91
Godzieba, D. A., Radice, D., & Bernuzzi, S. 2021, ApJ, 908, 122
Heida, M., Jonker, P. G., Torres, M. A. P., & Chiavassa, A. 2017, ApJ, 846, 132
Hobbs, G., Lorimer, D. R., Lyne, A. G., & Kramer, M. 2005, MNRAS, 360, 974
Jermyn, A. S., Bauer, E. B., Schwab, J., et al. 2023, ApJS, 265, 15
Kalogera, V. & Baym, G. 1996, ApJ, 470, L61
Kandel, D. & Romani, R. W. 2020, ApJ, 892, 101
Kroupa, P. 2001, MNRAS, 322, 231
Kruckow, M. U., Tauris, T. M., Langer, N., Kramer, M., & Izzard, R. G. 2018, MNRAS, 481, 1908
Linares, M., Shahbaz, T., & Casares, J. 2018, ApJ, 859, 54
Liotine, C., Kalogera, V., Briel, M., et al. in prep.
Livio, M. & Soker, N. 1988, ApJ, 329, 764
Mandel, I. & Smith, R. J. E. 2021, ApJ, 922, L14
Nelson, D., Springel, V., Pillepich, A., et al. 2019, Computational Astrophysics and Cosmology, 6, 2
O'Doherty, T. N., Bahramian, A., Miller-Jones, J. C. A., et al. 2023, MNRAS, 521, 2504
Özel, F., Psaltis, D., Narayan, R., & McClintock, J. E. 2010, ApJ, 725, 1918
Paxton, B., Bildsten, L., Dotter, A., et al. 2011, ApJS, 192, 3
Paxton, B., Cantiello, M., Arras, P., et al. 2013, ApJS, 208, 4
Paxton, B., Marchant, P., Schwab, J., et al. 2015, ApJS, 220, 15
Paxton, B., Schwab, J., Bauer, E. B., et al. 2018, ApJS, 234, 34
Paxton, B., Smolec, R., Schwab, J., et al. 2019, ApJS, 243, 10
Podsiadlowski, P., Langer, N., Poelarends, A. J. T., et al. 2004, ApJ, 612, 1044
Rhoades, C. E. & Ruffini, R. 1974, Phys. Rev. Lett., 32, 324
Román-Garza, J., Bavera, S. S., Fragos, T., et al. 2021, ApJ, 912, L23
Romani, R. W., Kandel, D., Filippenko, A. V., Brink, T. G., & Zheng, W. 2021, ApJ, 908, L46
Romani, R. W., Kandel, D., Filippenko, A. V., Brink, T. G., & Zheng, W. 2022, ApJ, 934, L17
Sana, H., de Koter, A., de Mink, S. E., et al. 2013, A&A, 550, A107
Shao, Y. & Li, X.-D. 2021, ApJ, 920, 81
Siegel, J. C., Kiato, I., Kalogera, V., et al. 2023, ApJ, 954, 212
Thompson, T. A., Kochanek, C. S., Stanek, K. Z., et al. 2019, Science, 366, 637
Webbink, R. F. 1984, ApJ, 277, 355
Xing, Z., Bavera, S. S., Fragos, T., et al. 2024, A&A, 683, A144
Zdziarski, A. A., Mikolajewska, J., & Belczynski, K. 2013, MNRAS, 429, L104
Zhu, J.-P., Hu, R.-C., Kang, Y., et al. 2024, arXiv e-prints, arXiv:2404.10596

4.7 Supplementary discussion and comments

4.7.1 Neutron star–black hole merger rate density as a function of redshift

The evolution of the Universe encodes the history of star formation and chemical enrichment. To simulate GW sources from the isolated binary scenario, it is critical to realistically describe the cosmic evolution of stellar populations, specifically the redshift- and metallicity-dependent SFH. This can be decoupled as the star formation rate density (SFR) over cosmic time and the metallicity distribution at each redshift. In `POSYDON` v2, the IllustrisTNG large-scale cosmological simulation is used as the default framework, with several empirical models as alternatives for describing SFH. The models of SFR as a function of redshift and metallicity distributions are shown in Figure 4.5. For empirical models, the distribution of metallicity is typically assumed to be log-normally distributed around the mean metallicity at a given redshift. In contrast, IllustrisTNG is a state-of-the-art cosmological simulation that provides the simulation-based metallicity distributions.

By incorporating the redshift- and metallicity-dependent SFH in the BPS study of merging NSBH systems, we can obtain the merger rate density as a function of redshift. In Figure 4.6, we show the merger rate density $\mathcal{R}_{\rm NSBH}$ over redshifts and contributions from the most prominent formation channels for the model with $\alpha_{\rm CE} = 1$, $\sigma_{\rm CCSN} = 265\,{\rm km\,s^{-1}}$, and $M_{\rm NS,birth-max} = 2\,M_\odot$ from Xing et al. (2024b) on the left and for $\sigma_{\rm CCSN} = 150\,{\rm km\,s^{-1}}$ on the right. These two models provide the best fits to the BH mass spectrum inferred from LVK observations, which is shown in Xing et al. (2024b).

The channels contributing to the local merger rate in descending order are the classic channel, the stable mass transfer channel, the no mass transfer channel, and the double CE channel. For the high-kick model, at very high redshifts, the classic channel and the stable mass transfer channel have comparable contributions. For the low-kick model, the merger rate increases for all channels and the contribution from the classic channel becomes more significant. All channels follow the trend of star formation history, shown in Figure 4.5, but peak at lower redshifts due to merger delay times. The stable mass transfer channel is flatter compared to other channels, as they have the broadest range of delay times.

4.7.2 Spins in merging neutron star–black hole systems

In this section, I present the BH spin and effective inspiral spin distributions in our merging NSBH population. In Figure 4.7, the left panel displays the BH natal spins in the merging NSBH population for the model with $\alpha_{\rm CE} = 1$, $\sigma_{\rm CCSN} = 150\,{\rm km\,s^{-1}}$, and $M_{\rm NS,birth-max} = 2\,M_\odot$, with contributions from the four main formation channels shown separately. In

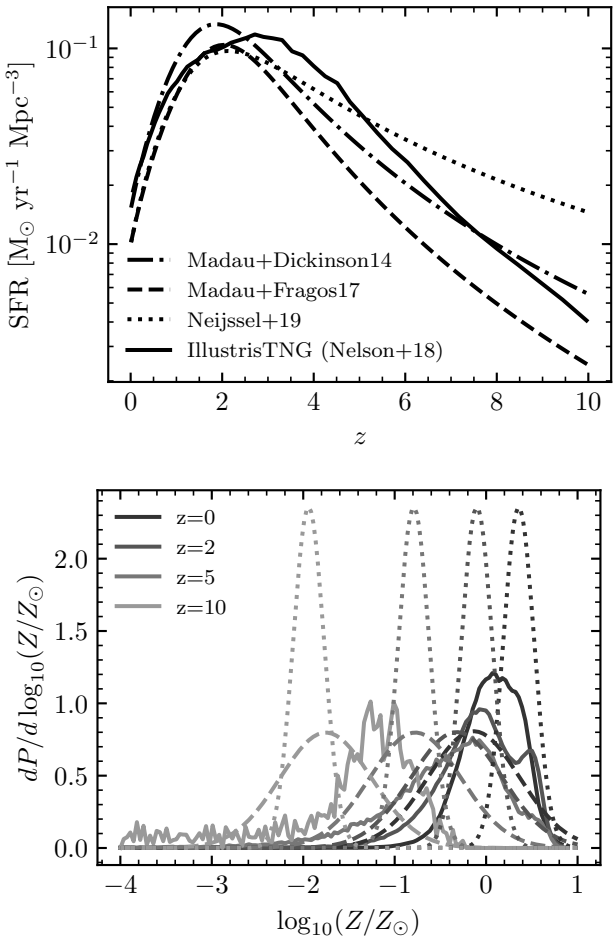

Figure 4.5: The SFR density as a function of redshift for four different models (top panel) incorporated in POSYDON v2, and the metallicity distribution of star formation at four separate redshifts for three of the star-formation models (bottom panel). Credit: Andrews et al. (2024).

POSYDON simulations, BHs always form first, this statement remains valid in the case of multiple metallicities. Thus, the BH natal spin distributions for the classic channel and the stable mass transfer channel follow the expectations discussed in Chapter 3. Binaries in the classic channel tend to have wider initial orbits than those in the stable mass transfer channel. As a result, tidal effects are more significant in the stable mass transfer channel, leading to higher BH natal spins. Conversely, BH natal spins in the classic channel are concentrated around zero. For the no mass transfer channel, these binaries have tight orbits as well, as discussed in Xing et al. (2024a), resulting in BH natal spins similar to those in the stable mass transfer channel. Regarding the double CE channel, since the BH progenitor undergoes CE evolution that shrinks the orbit significantly, tidal interactions can spin up the

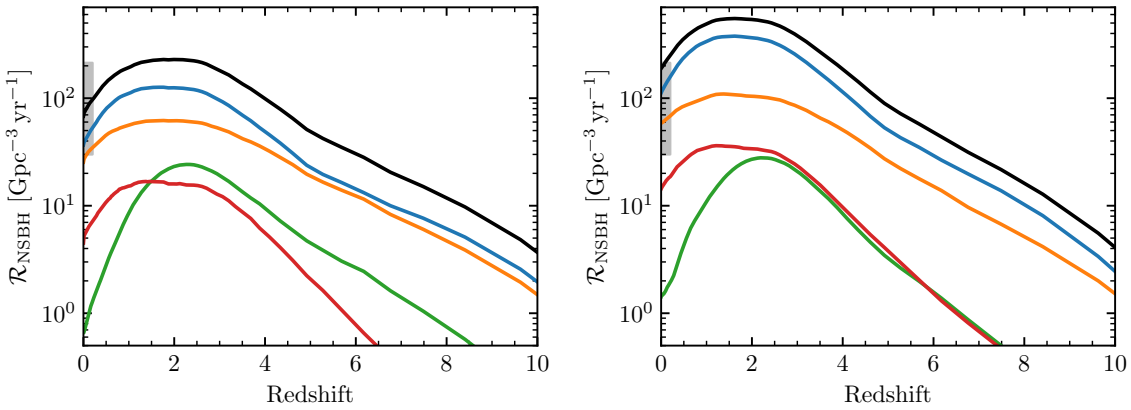

Figure 4.6: NSBH merger rate as a function of redshift from POSYDON simulations. The left panel shows the model with $\alpha_{\rm CE} = 1$, $\sigma_{\rm CCSN} = 265\,{\rm km\,s^{-1}}$, and $M_{\rm NS,birth-max} = 2\,M_\odot$; and the right panel with $\sigma_{\rm CCSN} = 150\,{\rm km\,s^{-1}}$. The gray bar shows the merger rate density inferred from Abac et al. (2024).

progenitor before core collapse. As a result, all BHs in this channel have natal spins around 0.15 – 0.2.

The right panels in Figure 4.7 shows the BH spins at merger. A subset of BHs from the classic channel can acquire spins up to 0.2, primarily through case BB mass transfer. A small fraction of BHs from the stable mass transfer channel can be spun up by accretion up to 0.6. These results are consistent with findings at solar metallicity (Xing et al., 2024a).

Figure 4.8 shows the distribution of inspiral effective spins $\chi_{\rm eff}$. The distribution is centered around zero, with the classic channel being dominate. Only a small fraction of them reach negative values of $\chi_{\rm eff} \sim -0.1$. For the double CE channel and no mass transfer channel, their generally tight orbits make it difficult for SN kicks to significantly tilt the orbits, preventing highly negative $\chi_{\rm eff}$. As expected, the stable mass transfer channel exhibits the broadest $\chi_{\rm eff}$ distribution, as they have the highest BH spins and the widest orbits, which can be more easily tilted.

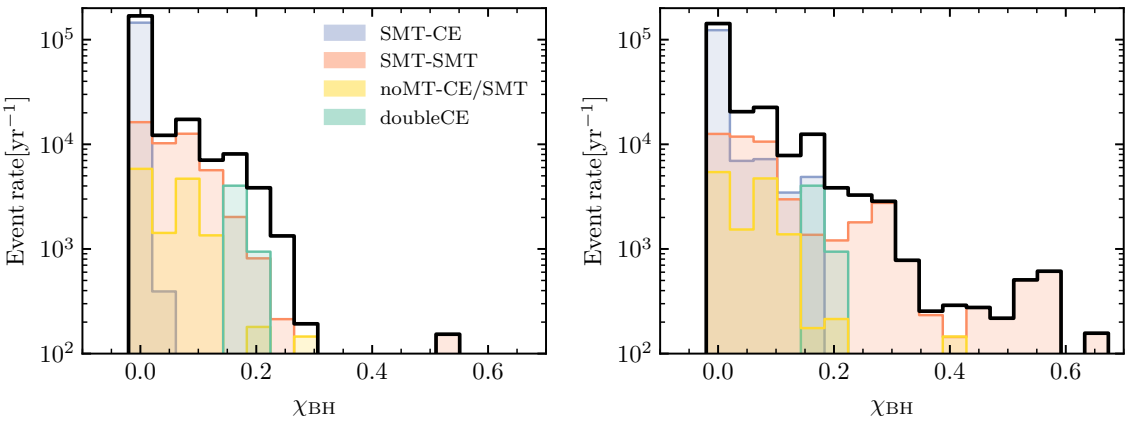

Figure 4.7: Distributions of BH natal spins (left) and spins at merger (right) in merging NSBHs from our simulation.

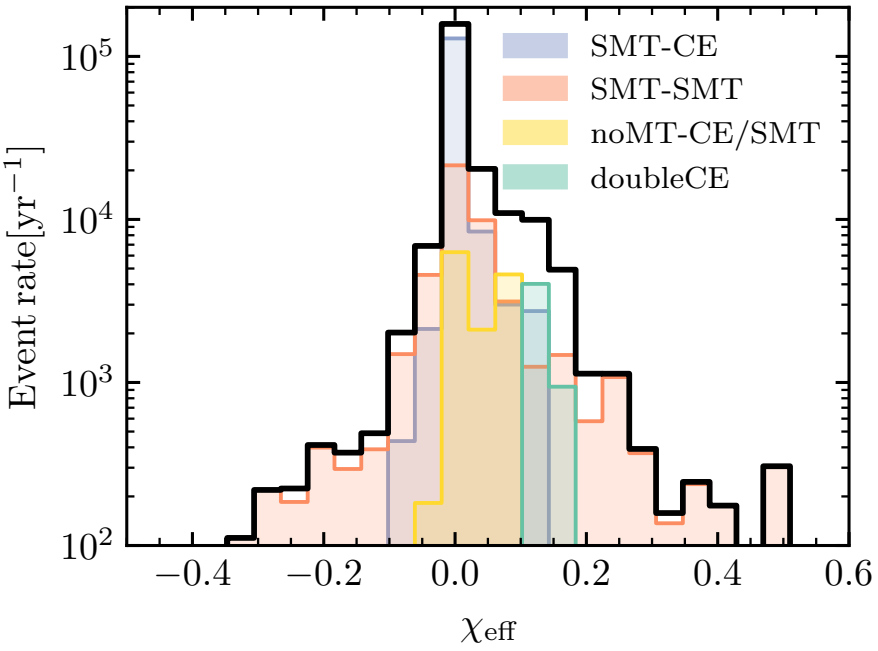

Figure 4.8: Distribution of effective inspiral spins in merging NSBHs from our simulation.

Chapter 5

CONCLUSIONS AND OUTLOOK

In this thesis, I present population synthesis studies of compact object binaries that contain BHs and NSs, conducted with the next-generation BPS code `POSYDON`. Specifically, this thesis focuses on the population of wind-fed BH-HMXBs and merging NSBH systems. The long-standing open questions surrounding these binary systems, including the origin of BH spins in these systems, their formation history and channel tracing, the existence of mass-gap BHs and potential associated EMCs, make them particularly intriguing. Joint observations from electromagnetic and GW detections offer valuable insights that can help further improve our understanding of the physics related to BHs and NSs, stellar evolution, and binary interactions. As a result, it has become imperative to employ more advanced and physically motivated approaches to interpret these observational data and address key questions in this field.

The novel BPS code `POSYDON` that we have been developing is making a difference and helping us to investigate these interesting systems and address the most important and essential questions involved. As one of the core developers of the novel BPS code `POSYDON`, I contributed to the construction of detailed binary evolution grids calculated with the stellar-evolution code `MESA` and to the development of the `POSYDON` framework, which integrates full stellar structure and binary evolution modeling into BPS studies. `POSYDON` stands apart from other codes in three key aspects: (i) it accounts for stellar rotation and spin-orbit coupling, enabling accurate BH spin estimates; (ii) mass transfer is directly computed with `MESA`, capturing stellar responses to mass change for improved modeling of binary interactions; (iii) `POSYDON` tracks stellar core evolution and abundance profiles self-consistently, allowing for a more physically realistic treatment of CE evolution and SN explosions. With the remarkable power and potential of `POSYDON`, we aim to elevate BPS studies to an unprecedented level of reliability and physical accuracy.

In Chapter 2, I present the BPS study on wind-fed BH-HMXBs using `POSYDON`, focusing on the role of RLOF after BH formation on the observed properties, particularly BH spins. We identified wind-fed BH-HMXBs in our simulations by adopting the disk formation criteria from Hirai et al. (2021), which require the donor star to have a RL filling factor above ~ 0.9. To investigate possible BH spin-up through accretion, we constructed two additional CO-HMS grids that allow super-Eddington accretion onto BHs. One grid assumes fully

conservative mass transfer, while in the other, we adopt an accretion efficiency based on GRRMHD simulations of super-Eddington MADs around stellar-mass BHs. We have shown that after transferring mass onto BHs via RLOF, the donor stars can shrink back and initiate a second wind-fed HMXB phase, which lasts longer than the first one that appears before RLOF. Based on the BPS results, we found that the observed wind-fed HMXBs are more likely to have already been through a RLOF phase. This was not observed in previous BPS studies because rapid BPS codes poorly handle mass transfer phases and stellar response to mass transfer. Our calculations revealed that a full explanation of the extreme spins observed in BH-HMXBs through accretion requires a mass accretion efficiency that exceeds the predictions of GRRMHD simulations for super-Eddington MADs.

Chapter 3 introduces the BPS study using `POSYDON` on merging NSBH systems at solar metallicity. This study represents the first BPS study that utilized the full functionalities of `POSYDON` v1, focusing on identifying different characteristics across formation channels of merging NSBHs. We found that a significantly larger fraction of merging NSBHs underwent only stable mass transfer during their formation, compared to other studies using rapid BPS codes. This discrepancy arises from our more realistic treatment of binary mass transfer and the use of multiple mass transfer stability criteria, as opposed to parametric and empirical methods. With access to stellar rotation profiles in `POSYDON`, we estimated BH spins self-consistently. We demonstrated that merging NSBHs exhibit different distributions of BH spins and orbital tilts depending on whether the binaries undergo unstable mass transfer or only stable mass transfer. These differences lead to distinct distributions of effective inspiral spins for the two main channels, providing a potential signature to probe the formation history of merging NSBHs.

In Chapter 4, I present the study of merging NSBH systems conducted with `POSYDON` v2. The newly detected event GW230529 is most likely an NSBH merger, with the BH mass falling within the lower mass gap between NSs and BHs, which was inferred from BH mass distributions in LMXBs. Siegel et al. (2023) investigated possible selection biases against mass-gap BHs, considering that BH mass measurement requires transient behaviors of LMXBs, and observed that selection biases are present if NS birth mass is below $\sim 2\,M_\odot$. Inspired by the new BH mass distribution inferred from GW observations and the studies on the formation of mass-gap BHs, we investigated the effect of multiple physical processes on BH mass distribution in merging NSBHs, including CE efficiency, SN natal kicks, and NS birth masses. We showed that increasing the energy conversion efficiency $\alpha_{\rm CE}$ during CE evolution can efficiently facilitate the formation of mass-gap NSBHs. However, when taking into account that the maximum NS birth mass is $\sim 2\,M_\odot$, the BH mass distribution aligns

with the distribution inferred from GW observations, without requiring a high CE efficiency parameter. Additionally, we found that different natal kick velocities do not significantly alter the shape of BH mass distribution but do impact the local merger rate.

Over the past two decades, many BPS codes have been developed. Among them, the most extensively used ones are `BSE`-like codes, which have been frequently employed to explore the population properties of all kinds of binary systems from various perspectives. However, BPS studies are facing a difficult situation in several aspects. First, different studies imply inconsistent conclusions on binary evolution theories or predict distinct population properties for the same type of binary system. The discrepancies could result from differences in the treatments of some critical processes across different codes or arise from divergences in the underlying physical assumptions. Second, different binary populations require different parameters or physical models to explain the observations. `POSYDON` has the potential to make BPS studies–currently complex and lacking widespread consensus–more reliable and cohesive, and advance the field to a new level by bridging sophisticated 3D simulations and physically driven models with detailed 1D binary modeling for BPS studies.

The formation and evolution channels of compact object binaries are still subject to uncertainties in single-star physics and critical processes in binary evolution, including mass transfer, CE evolution, and SN kicks. For example, mass transfer efficiency between non-degenerate stars is a crucial factor that can significantly influence the evolutionary pathways of binary systems. However, different binary systems suggest varying efficiencies, and no theoretical models can explain all cases within a unified framework. Thus, to ensure consistency, accurate modeling based on sophisticated simulations or semi-analytical studies of mass transfer should be incorporated into BPS studies. Otherwise, it is hard to evaluate the predictions based on model-dependent assumptions.

Current and upcoming electromagnetic and GW observations of stellar objects and binary systems will continue to refine our understanding of the critical physics in stellar and binary evolution by constraining theoretical models and introducing new challenges to the classic framework. For instance, ground-based facilities such as the Very Large Telescope Interferometer (GRAVITY Collaboration et al., 2017; Lopez et al., 2022) and space telescopes including the Hubble Space Telescope (Roman-Duval et al., 2020; Sana et al., 2024) and Gaia (Gaia Collaboration et al., 2023) have been and will continue to provide valuable data on various types of stars and binary systems. For GW observations, next-generation ground-based detectors such as the Einstein Telescope (Hild et al., 2011) and Cosmic Explorer (Reitze et al., 2019), along with space-based observatories like LISA (Amaro-Seoane et al., 2017) and TianQi (Luo et al., 2016), will extend GW detections to much higher red-

shifts. The rich information provided by these observations, combined with comprehensive and self-consistent BPS studies, will illuminate some of the most uncertain processes in stellar and binary evolution, ultimately refining and completing the theoretical framework.

Appendix A

CIRCUMBINARY PLANET

During my Ph.D., I completed a project that aimed to combine detailed binary evolution and N-body dynamical evolution to investigate the dynamics of circumbinary planets around interacting binaries. To achieve this, I created the tool `NBSE` to couple binary evolution data from `MESA` and the N-body simulation code `REBOUND`. In this work, we used the binary configuration in `POSYDON` for the modeling of a mass-transferring binary that eventually forms a stripped star with a MS star companion. Furthermore, to consider the tidal effects on the orbital evolution of the planets between the stars and the circumbinary planets, we followed the method in `POSYDON` for distinguishing equilibrium tides from dynamical tides. This interdisciplinary study demonstrated that the concept of detailed binary modeling within `POSYDON` can foster a broad impact across various fields of astrophysics connected with stellar and binary systems.

The manuscript presented in the following was published in *Monthly Notices of the Royal Astronomical Society*, referred as Xing et al. (2025a).

Monthly Notices of the ROYAL ASTRONOMICAL SOCIETY
MNRAS **537,** 285–292 (2025)
Advance Access publication 2025 January 20

https://doi.org/10.1093/mnras/stae2820

Combining REBOUND and MESA: dynamical evolution of planets orbiting interacting binaries

Zepei Xing [1,2★] Santiago Torres,[3] Ylva Götberg,[3] Alessandro A. Trani [4] Valeriya Korol [5] and Jorge Cuadra[6]

[1]*Departement d' Astronomie, Université de Genève, Chemin Pegasi 51, CH-1290 Versoix, Switzerland*
[2]*Gravitational Wave Science Center (GWSC), Université de Genève, CH-1211 Geneva, Switzerland*
[3]*Institute of Science and Technology Austria (ISTA), Am Campus 1, A-3400 Klosterneuburg, Austria*
[4]*Niels Bohr International Academy, Niels Bohr Institute, Blegdamsvej 17, DK-2100 Copenhagen, Denmark*
[5]*Max Planck Institute for Astrophysics, D-85741 Garching, Germany*
[6]*Departamento de Ciencias, Facultad de Artes Liberales, Universidad Adolfo Ibáñez, Av. Padre Hurtado 750, 2562340 Viña del Mar, Chile*

Accepted 2024 December 20. Received 2024 December 18; in original form 2024 October 26

ABSTRACT

Although planets have been found orbiting binary systems, whether they can survive binary interactions is debated. While the tightest-orbit binaries should host the most dynamically stable and long-lived circumbinary planetary systems, they are also the systems that are expected to experience mass transfer, common envelope evolution, or stellar mergers. In this study, we explore the effect of stable non-conservative mass transfer on the dynamical evolution of circumbinary planets. We present a new script that seamlessly integrates binary evolution data from the 1D binary stellar evolution code MESA into the *N*-body simulation code REBOUND. This integration framework enables a comprehensive examination of the dynamical evolution of circumbinary planets orbiting mass-transferring binaries, while simultaneously accounting for the detailed stellar structure evolution. In addition, we introduce a recalibration method to mitigate numerical errors from updates of binary properties during the system's dynamical evolution. We construct a reference binary model in which a 2.21 $M_\odot$ star loses its hydrogen-rich envelope through non-conservative mass transfer to the 1.76 $M_\odot$ companion star, creating a 0.38 $M_\odot$ subdwarf. We find the tightest stable semimajor axis for circumbinary planets to be $\simeq 2.5$ times the binary separation after mass transfer. Accounting for tides by using the interior stellar structure, we find that tidal effects become apparent after the rapid mass transfer phase and start to fade away during the latter stage of the slow mass transfer phase. Our research provides a new framework for exploring circumbinary planet dynamics in interacting binary systems.

Key words: planets and satellites: dynamical evolution and stability – planet–star interactions – binaries: close – subdwarfs.

1 INTRODUCTION

The existence of circumbinary planets (CBPs, also known as P-type systems; Dvorak 1984) offers valuable insights into the underlying physics involved in planet formation and the dynamical evolution of planetary systems. After the discovery of the first CBP Kepler-16 b (Doyle et al. 2011), a series of CBPs have been reported from the Kepler (Borucki et al. 2010) and TESS missions (Ricker et al. 2015). Currently, around 28 binary systems have been confirmed to host circumbinary planets, according to the Extrasolar Planets Encyclopaedia[1] and NASA Exoplanet Archive.[2] About 10 of them are orbiting binary systems that contain an evolved star, such as a white dwarf (WD) or a subdwarf. The recently suggested existence of a possible hot Jupiter around the subdwarf and M-dwarf binary Kepler 451 (Esmer et al. 2022) challenges further our understanding of planet formation and dynamics in the context of binary interactions. These binaries are suggested to be post-common envelope binaries (PCEBs; Zorotovic & Schreiber 2013) and are implied to have experienced a dramatic mass transfer episode and a subsequent unstable mass transfer triggering a common envelope (CE) phase. During CE evolution, binaries undergo a rapid and significant orbital shrinkage (Ivanova et al. 2013), ultimately leading to either a merger or the ejection of the CE. It remains unclear whether circumbinary planets form before or after the CE phase. Some studies suggest that these circumbinary planets around PCEBs are the second-generation planets formed from the ejecta of CE (Zorotovic & Schreiber 2013; Schleicher & Dreizler 2014). However, Bear & Soker (2014) argued that, in certain populations, the circumbinary planets are more likely to be the first-generation planets formed prior to CE evolution.

Subdwarfs are low-mass (∼0.35–1 $M_\odot$) exposed helium cores (see e.g. Heber 2016, for a review) that result from envelope-stripping through CE ejections (e.g. Schaffenroth et al. 2022), or stable mass transfer (Han et al. 2002, 2003; Vos et al. 2017). Thousands of subdwarfs are known (Geier 2020), and more and more of their

★ E-mail: Zepei.Xing@unige.ch
[1]https://exoplanetarchive.ipac.caltech.edu
[2]https://exoplanet.eu/planets_binary_circum/

binary companions are being discovered and characterized. The binary companions include low-mass main-sequence stars, WDs, and even more massive Be stars (e.g. Kupfer et al. 2015; Wang et al. 2021; Schaffenroth et al. 2022; Klement et al. 2024). The significant orbital evolution and potentially substantial mass loss that are associated with the formation of a subdwarf challenges the existence of circumbinary planets, but could also provide opportunities for new planetary system architectures to develop. Given the confirmed existence of planets orbiting a tight binary containing a WD (e.g. Rattanamala et al. 2023), it is clear that binary interactions, although violent and dynamic, do not prohibit the presence of planetary systems. Therefore, understanding the impact of subdwarf formation on surrounding planetary systems constitutes one of the most promising avenues for revealing how binary evolution affects planetary systems in general.

Apart from CE evolution, stable mass transfer is also an essential process for the formation of helium WDs (e.g. Sun & Arras 2018; Brown et al. 2020) and subdwarfs (Götberg et al. 2018) in binary systems. The stable mass transfer process can be modelled using 1D stellar evolution codes (Eldridge, Izzard & Tout 2008; Paxton et al. 2015), bolstered by a more comprehensive understanding compared to the CE process. Since our understanding of envelope-stripping through CE ejection is still associated with major uncertainties, the impact the planetary system suffers as a result of the ejection is hard to determine. Because of these large uncertainties, earlier studies on the dynamical response of circumbinary planets in CE evolution have adopted simplified approximations, including assuming a constant mass loss rate for the binary system during the CE phase and ignoring the mechanical impact of the ejecta (Portegies Zwart 2013; Kostov et al. 2016). However, planetary systems orbiting mass-transferring binaries can be treated with a more detailed and accurate approach, because the envelope-stripping mechanism is better understood and takes substantially longer than the CEevolution. In light of this, we investigate the dynamical stability of planetary systems around binaries that undergo stable mass transfer, integrating detailed 1D stellar evolution simulations.

Given the advancements in ongoing and forthcoming surveys (e.g. Roman; Spergel et al. 2015; Penny et al. 2019; Johnson et al. 2020 and TESS; Ricker et al. 2016) that seek planetary systems across diverse host systems, we expect to discover an escalating number of CBPs around various binary systems. These discoveries and insights into expected system architectures and planetary conditions, including stability and habitability (Shevchenko et al. 2019), represent an exciting new direction for planetary science. To prepare for these anticipated findings, further theoretical and numerical explorations of planetary dynamics in conjunction with interacting binaries will be essential.

In this work, we combine *N*-body simulations with detailed stellar and binary evolution models to explore the dynamical evolution of circumbinary planets around binaries through a stable mass transfer phase that leads to the production of a subdwarf B (sdB) binary. In Section 2, we introduce the *N*-Body Binary Stellar Evolution (NBSE) tool, which bridges the stellar evolution code Modules for Experiments in Stellar Astrophysics (MESA; Paxton et al. 2011, 2013, 2015, 2018, 2019; Jermyn et al. 2023) and the *N*-body code REBOUND (Rein & Liu 2012; Rein & Tamayo 2018; Tamayo et al. 2020; Baronett et al. 2022). In Section 3, we demonstrate the application of NBSE to the dynamical evolution of a single circumbinary planet around an interacting binary star. The impact and the implementation of tidal effects due to the interaction of the binary system and CBPs are discussed in Section 4. Finally, we summarize in Section 5.

2 *N*-BODY BINARY STELLAR EVOLUTION (NBSE)

The dynamical evolution of planets around single-evolved stars has been widely studied (e.g. Rasio et al. 1996; Villaver & Livio 2007, 2009; Mustill & Villaver 2012; Veras et al. 2013, 2016; Mustill, Veras & Villaver 2014; Veras 2016; Rao et al. 2018; Ronco et al. 2020; Mustill 2024). These studies include simple stellar evolution models, mainly using the stellar tracks in the single stellar population synthesis codeSSE (Hurley, Pols & Tout 2000). For multiple stellar systems, Hamers et al. (2021) presented the population synthesis code Multiple Stellar Evolution that includes planets, with binary evolution primarily modelled in a simplified way following the binary population synthesis code BSE (Hurley, Tout & Pols 2002).

Recently, Baronett et al. (2022) introduced a machine-independent implementation of parameter interpolation and a constant time-lag model for tides without evolving spins in REBOUNDX (Tamayo et al. 2020). This approach allows results from other integration codes to be used as input parameters for REBOUND. As an example of their technique, they integrated stellar evolution data for single stars from MESA into REBOUND, using their interpolation scheme to update stellar parameters such as mass and radius as a function of time. They demonstrated this by simulating the Sun's post-main-sequence influence on the outer giant planets.

In this work, we focus on accurately simulating the binary evolution, particularly the mass transfer phase, together with a circumbinary planetary system. Similar to Baronett et al. (2022), we use the state-of-the-art, open-source stellar evolution code MESA together with the high-performance *N*-body simulation code REBOUND to study the dynamical evolution of CBPs. Compared to BSE-like codes, where the mass transfer rate is obtained based on parametric methods, MESA enables us to calculate mass transfer rates self-consistently considering the rotation of the stars and account for mass and angular momentum loss both through stellar winds and non-conservative mass transfer and tidal effects all along the binary evolution. In this study, we built NBSE,[3] an integrated tool coupling MESA and REBOUND, serving for the study of the dynamical evolution of CBPs involving not only the accurate calculation of single stars but also the binary evolution.

2.1 MESA binary model

First, we construct a binary model that undergoes stable mass transfer, leading to envelope stripping and the formation of an sdB star binary. The reference binary model we compute at solar metallicity consists a primary star with $M_1 = 2.21\,\mathrm{M}_\odot$, a secondary star with $M_2 = 1.76\,\mathrm{M}_\odot$, and an initial orbital period of 6 d in a circular orbit. It represents one of the sdB-forming binaries at the low-mass end of the stripped star binary grids in Götberg et al. (2018). These initial parameters of the binary are chosen to ensure that planets have enough time to form around the central binary. Consequently, we focus on lower initial masses.

To construct the binary evolution model, we adopt the MESA set-up for constructing binary grids within the POSYDON binary population synthesis code (Fragos et al. 2023). In this configuration, the MESADutch scheme is used for the stellar wind prescription with modifications related to stellar state and surface temperature (see section 3.2.2 of Fragos et al. 2023). The tidal effect between the two stars in the binary is treated following the linear approach by

[3] https://github.com/ZepeiX/NBSE

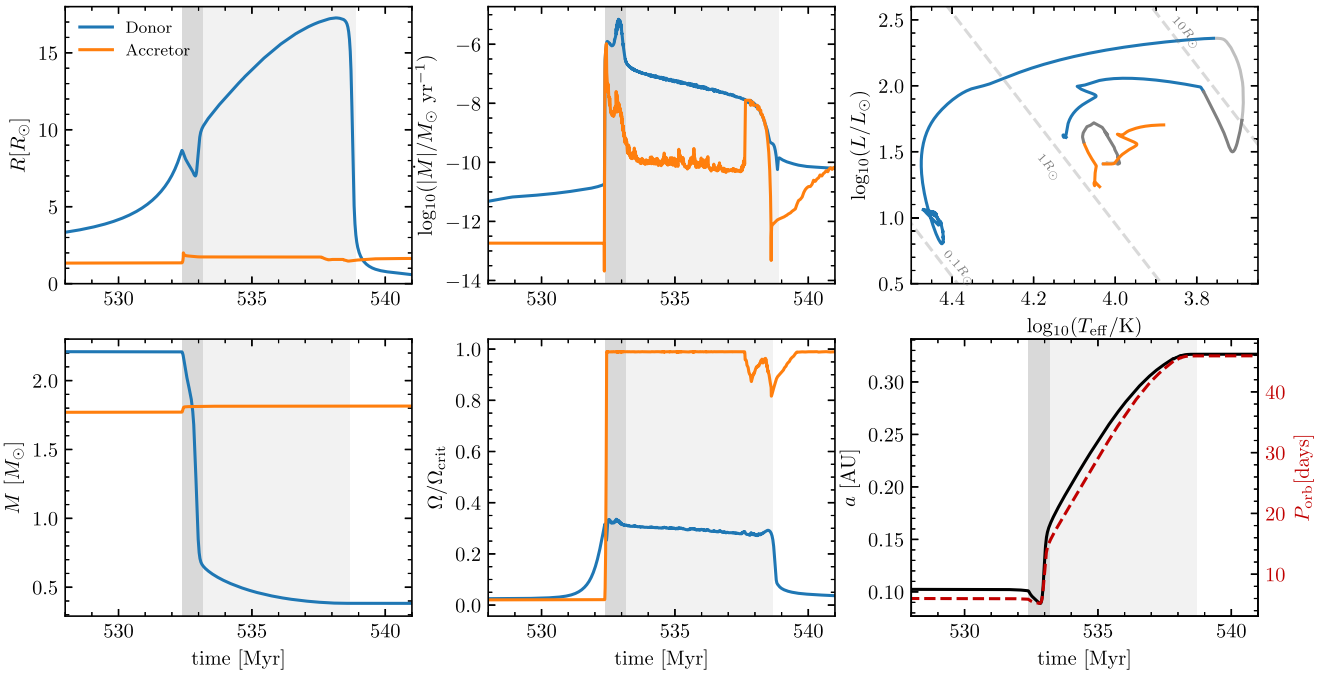

Figure 1. Evolution of the binary system properties during the mass transfer phase. The different panels show the binary stars' radii (top left), the absolute values of mass change rates (top middle), the Hertzsprung–Russell (HR) diagram for both stars (top right), the binary stars' masses (bottom left), the surface rotation velocities over their critical values (bottom middle), and the orbital separation and period (bottom right) as a function of time. The HR diagram shows the fast and slow mass transfer phases with dark grey and light grey lines, respectively. The other plots are marked with dark grey and light grey shaded areas.

calculating the synchronization time-scale, distinguishing radiative and convective layers (Hut 1981; Hurley et al. 2002; Qin et al. 2018).

To calculate the mass transfer rate from Roche lobe overflow, the `Kolb` scheme (Kolb & Ritter 1990) within MESA is used when the donor star has left the main sequence. In the binary models, mass transfer is generally highly non-conservative due to stellar rotation, meaning that most of the transferred mass is lost from the system. The specific angular momentum of the transferred material follows the implementation of de Mink et al. (2013). During mass transfer, the accretor stars are expected to easily spin-up to critical rotation due to accretion (Packet 1981), capping further accretion. The material leaves the system as boosted fast winds, taking away the angular momentum of the accretor star and the orbit. The model is a physically motivated implementation in MESA. However, different binary systems imply varying mass accretion efficiencies. For example sdB and main-sequence binaries do not show evidence of substantial mass accretion (e.g. Vos et al. 2017) but some subdwarf and Be star binaries indicate a high accretion efficiency (e.g. Klement et al. 2024). Further theoretical and observational research is needed to better understand how and under what conditions mass transfer can be efficient.

Fig.1 top panels show the evolution of the radii, of the absolute values of mass change rates, and of the position in the Hertzsprung–Russell (HR) diagram for both stars in our reference binary model. Fig. 1 bottom panels show the evolution of the component masses, of the surface angular velocities over their critical values, and of the orbital separation a and period $P_{\rm orb}$. After leaving the main sequence, the donor star ignites hydrogen in a shell around the helium core. It expands rapidly, filling the Roche lobe at around 532.3 Myr, initiating a fast mass transfer phase for about 0.8 Myr. The mass transfer rate reaches the maximum of $\sim 10^{-5}$ $\mathrm{M}_\odot\ \mathrm{yr}^{-1}$ at about 532.9 Myr. The donor star loses about 1.5 $\mathrm{M}_\odot$ during the fast mass transfer phase. Then, the binary enters a slow mass transfer phase with a mass transfer rate of $\sim 10^{-8}$–$10-7$ $\mathrm{M}_\odot\ \mathrm{yr}^{-1}$, lasting about 6 Myr. At the beginning of the mass transfer phase, the accretor accepts all the material from the donor. In a short period of time the accretor is spun-up, then the accretion rate drops quickly. After the mass transfer process, the donor's hydrogen-rich envelope is stripped, and it shrinks significantly, becoming a subdwarf. Although it is known that subdwarfs are substantially affected by atomic diffusion and gravitational settling, which causes them to show almost a hydrogen-pure atmosphere quickly (Drilling et al. 2013), we do not account for that detail here since we focus on the mass transfer phase. The mass of the donor star decreases from 2.21 to $\simeq 0.38$ $\mathrm{M}_\odot$ and the accretor accretes ≈ 0.04 $\mathrm{M}_\odot$. Because angular momentum is lost from the system during mass transfer, the binary orbit widens from 0.10 to 0.33 au, meaning the orbital period increases from 6 to 46 d.

2.2 Coupling of `MESA` and `REBOUND`

To build-up circumbinary planet systems in REBOUND, we first add two stars with properties matching those of the MESA binary at the starting point of tracing the planet's dynamical evolution. Then, we add a planet in the simulation that can be described by its mass, radius, and orbital elements. We use the `WHFast` integrator, which is a second-order symplectic Wisdom Holman integrator (Rein & Tamayo 2015), with a fixed time-step of 10^{-3} yr to calculate the dynamical evolution of the planet.

Throughout the calculation process, we treat the evolution of the central binary as an isolated binary, which is pre-calculated with MESA. As a result, it is important to refresh and synchronize the binary parameters within REBOUND properly. We linearly interpolate all the binary properties as a function of time to generate a new set of MESA binary output, similar to what was achieved by Baronett

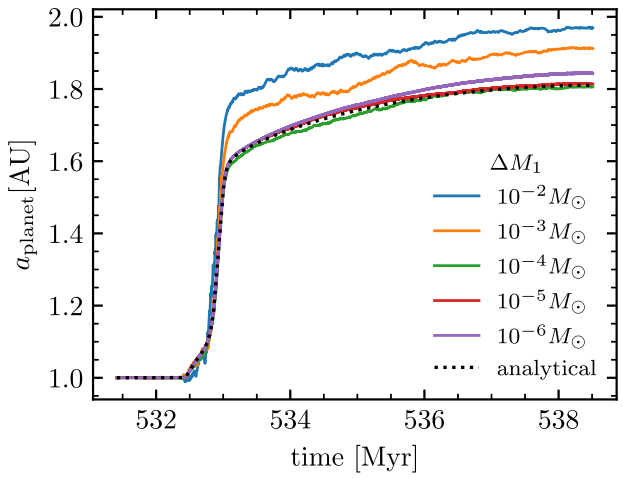

Figure 2. Evolution of the semimajor axis of the planet with different thresholds for the donor star mass change (ΔM_1) within a single customized time-step. The dotted line indicates the analytical orbital evolution due to mass loss from the central object.

et al. (2022). However, updating the binary properties during binary evolution requires more thorough scrutiny. In cases where the binary exists in a stable state, for example the long-lasting main-sequence evolution, it is feasible to update the binary properties at a low frequency.

In contrast, when the binary is experiencing dramatic changes, such as during a rapid mass transfer phase, a reduction in the time interval for the updates becomes essential. In MESA, adaptive time-steps are controlled by various factors, generally decreasing when the system undergoes significant changes. Therefore, it is natural to use the time series from MESA's output as the time points to update the binary properties. However, this approach is insufficient because the minimum time-step required for the binary evolution is longer than that for the planet's dynamical evolution. This discrepancy would introduce systematic errors in the cases where the binary state changes substantially within a single MESA time-step.

Thus, we introduce an input parameter defined as the change of a quantity within one MESA time-step to further adjust the time-steps for the updates. During mass transfer, one of the most rapidly changing parameter is the donor star mass. As a result, we monitor the change of the donor star mass $\Delta M_1 = M_{1,k+1} - M_{1,k}$ for the mass transfer phase, where k denotes the step for MESA output. If ΔM_1 is larger than a specific threshold, we split this particular step evenly into a greater number of smaller intervals to ensure that ΔM_1 for a single new time-step is below the threshold. In this way, we generate a revised sequence of binary properties, pre-determined by the interpolated MESA binary output, along with re-calibrated time intervals, in preparation for the subsequent computation of planetary dynamics.

In order to obtain an appropriate threshold for ΔM_1, a convergence test is conducted by exploring different limits of ΔM_1. We consider a simplified model where the only circumbinary planet is a test particle with an initial semimajor axis of 1 au from the centre of the mass in a circular orbit. We adopt five thresholds for ΔM_1, ranging from 10^{-2} to $10^{-6}\,\mathrm{M}_\odot$, spaced apart by one order of magnitude. We calculate the orbital evolution of the planet from about 2 Myr prior to the mass transfer phase until the end of the mass transfer phase. Fig. 2 shows the evolution of the semi-major axis of the testing planet $a_{\rm planet}$ under different thresholds for ΔM_1 through the binary mass transfer phase. Above $10^{-3}\,\mathrm{M}_\odot$, we find unexpected fluctuations and large deviations from other tracks, indicating large errors. The values of 10^{-4} and $10^{-5}\,\mathrm{M}_\odot$ lead to similar final $a_{\rm planet}$. However, with a further reduction to $10^{-6}\,\mathrm{M}_\odot$, the evolutionary track diverges, deviating from convergence.

To verify our calculation and to find out a suitable threshold for ΔM_1, we do an analytical calculation for the planet's orbit. In our testing case, the distance between the planet and the binary exceeds the binary separation by a considerable degree (initially $a_{\rm planet}/a \sim 10$), which enables us to treat the binary as a single object. Consequently, the mass loss resulting from the binary mass transfer process can be seen as mass loss from a single system. Then, assuming no change in the planet's mass, the change in the semimajor axis of the planet is

$$a_f = a_i \frac{M_{1,i} + M_{2,i}}{M_{1,f} + M_{2,f}}, \tag{1}$$

where a_i and a_f represent the semimajor axis of the planet before and after mass transfer, respectively, while $M_{1,f}$ and $M_{2,f}$ denote the masses of the stars after mass transfer.

To do the comparison, we calculate analytically the expected evolution of the semimajor axis of the planet by inputting the binary masses in equation (1) at each time-step to update binary properties. The black dotted line in Fig. 2 shows how the semimajor axis of the planet evolves because of mass loss from the central object. The analytical calculation aligns most closely with the case of $10^{-5}\,\mathrm{M}_\odot$, resulting in a comparable final $a_{\rm planet}$. In the case of $10^{-6}\,\mathrm{M}_\odot$, the newly determined time intervals for MESA seem too small to allow the integrator to stabilize the planet's orbit. The errors accumulate through the too-frequent updates of the binary properties, leading to an excess of $a_{\rm planet}$. As a result, we adopt $10^{-5}\,\mathrm{M}_\odot$ as the threshold for ΔM_1 through the mass transfer phase in our calculation.

3 EVOLUTION OF A SINGLE CIRCUMBINARY PLANET

With the binary evolution integrated in REBOUND, we demonstrate its use by modelling the dynamical evolution of a single circumbinary planet through the mass transfer phase.

We consider a Jupiter-like planet (1 $M_{\rm Jup}$ and 1 $R_{\rm Jup}$) in a circular orbit starting from 1 Myr prior to the onset of mass transfer and progressing through the mass transfer phase. The initial semimajor axis for the planet and the centre of mass ranges from 0.2 to 0.5 au, spacing apart by 0.05 au, and from 0.5 to 1.0 au with a step size of 0.1 au. Fig. 3 shows the evolution of $a_{\rm planet}$ for Jupiter-like planets with different initial semimajor axes. The black dashed line indicates the separation of the central binary star. We can see that the planets with initial $a_{\rm planet}$ below about 0.3 au are quickly driven to an unstable interaction with the binary by the gravitational forces of the central binary. In the case of 0.35 au, the planet exhibits instability and migrates inward during the onset of the mass transfer phase. As the system enters the fast mass transfer phase, the planet's orbit rapidly expands. During the subsequent slow mass transfer phase, the orbit of the planet displays intensified oscillations as the binary separation gradually increases. Eventually, in the midst of the slow mass transfer phase, the planet's orbit becomes highly unstable, which likely leads to engulfment by the binary or ejection from the system. The planet with an initial semimajor axis of 0.4 au also survives the fast mass transfer phase and enters the chaotic region in-between the stars in the subsequent slow mass transfer phase due to an escalation in orbital instability. The planets initially separated above 0.4 au survive the whole mass transfer process. They all experience

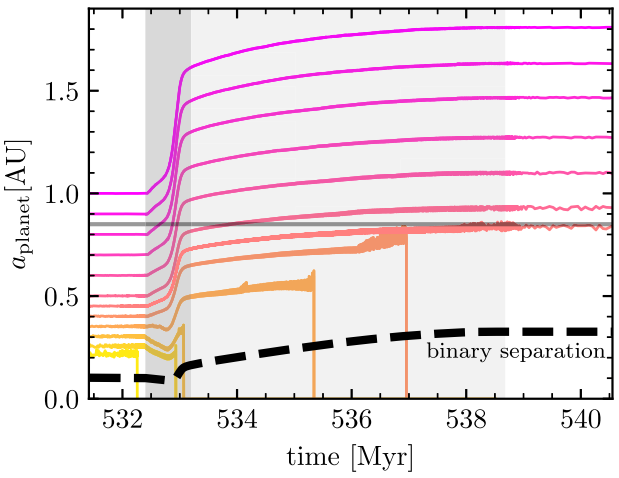

Figure 3. Evolution of the semimajor axis for Jupiter-like planets with different initial semimajor axes. The black dashed line represents the binary separation. The horizontal grey line indicates the closest stable orbit for the circumbinary planet after mass transfer. The fast and slow mass transfer phases are marked with dark grey and light grey shaded areas, respectively.

a rapidly accelerating orbital expansion as the mass transfer rate attains its maximum, followed by a decelerated expansion during the subsequent slow mass transfer phase. The closest stable orbit after mass transfer is located at ≈ 0.85 au, which is ≈ 2.5 times the binary separation after that phase. As the planets are farther away from the central binary, the oscillations of the orbit gradually diminish in intensity in the late slow mass transfer phase. Interestingly, for circumbinary planets around main-sequence binaries, it has been found that the closest stable orbit is located at approximately 2 to 2.5 times the binary separation for low eccentricity binaries (e.g. Dvorak 1986; Dvorak, Froeschle & Froeschle 1989; Wiegert & Holman 1997; Holman & Wiegert 1999; Pilat-Lohinger & Dvorak 2002).

4 NBSE TIDES

Tidal forces grow stronger as the distance between the star and the planet decreases. In the region where the planet's semimajor axis is not significantly larger than the binary separation, it is essential to consider tidal effects on the planet, which can alter the orbital evolution. We apply the prescription in Lu et al. (2023), where they implement self-consistent spin, tidal, and dynamical equations of motion in the REBOUNDX framework. The tidal prescription is based on the approach in Eggleton, Kiseleva & Hut (1998), considering the acceleration from the quadrupolar distortion:

$$\boldsymbol{f}_{\rm QD,1} = r_1^5 k_{\rm L,1}\left(1+\frac{m_2}{m_1}\right)\left[\frac{5(\boldsymbol{\Omega}_1\cdot\boldsymbol{d})^2\boldsymbol{d}}{2d^7}-\frac{\Omega_1^2\boldsymbol{d}}{2d^5} -\frac{(\boldsymbol{\Omega}_1\cdot\boldsymbol{d})\boldsymbol{\Omega}_1}{d^5}-\frac{6Gm_2\boldsymbol{d}}{d^8}\right], \quad (2)$$

and the acceleration from tidal damping:

$$\boldsymbol{f}_{\rm TF,1} = -\frac{9\sigma_1 k_{\rm L,1}^2 r_1^{10}}{2d^{10}}\left(m_2+\frac{m_2^2}{m_1}\right)\cdot [3\boldsymbol{d}(\boldsymbol{d}\cdot\dot{\boldsymbol{d}})+(\boldsymbol{d}\times\dot{\boldsymbol{d}}-\boldsymbol{\Omega}_1 d^2)\times\boldsymbol{d}], \quad (3)$$

where r_1 is the radius of object 1, $k_{\rm L,1}$ denotes the Love number of object 1, while m_1 and m_2 are the masses of object 1 and object 2, respectively. Ω_1 represents the angular velocity of object 1, assuming uniform rotation, and σ_1 is the dissipation constant of object 1. The parameter d denotes the distance between the two objects, and G is the gravitational constant.

In the case of the binary stars experiencing a mass transfer process, the properties of the stars change significantly, especially for the donor star. As a result, it is imperative to obtain accurate parameters for the equation above at different stages. For the stars, we have the stellar profiles provided by MESA, allowing us to calculate all the parameters self-consistently. The Love number is two times the apsidal motion constant k, which can be calculated with the relation (Sterne 1939):

$$k = \frac{3-\eta_2}{4+2\eta_2}. \quad (4)$$

η_2 is a function of the radius r that can be obtained from the equation (Sterne 1939):

$$r\frac{{\rm d}\eta_2}{{\rm d}r}+\eta_2(1-\eta_2)+6\frac{\rho}{\overline{\rho}}(\eta_2+1)-6=0, \quad (5)$$

where ρ is the density at r and $\overline{\rho}$ is the mean density interior to r. We save the density profiles of the stars every 10 steps in MESA to calculate η_2 and then the Love numbers. Afterward, we perform linear interpolation over the time series to determine the evolution of the Love number for both stars. As for the dissipation constant, it is connected with the Love number and the lag time τ (Lu et al. 2023):

$$\sigma_1 = \frac{3r_1^5 k_{L,1}}{4G\tau_1}. \quad (6)$$

The lag time is related to the typical tidal time-scale T, defined in Hut (1981):

$$T_1 = \frac{r_1^3}{Gm_1\tau_1}. \quad (7)$$

Then, we follow the same method in POSYDON configuration to calculate the quantity k/T (see section 4.1 in Fragos et al. 2023) to get access to all the parameters involved in the calculation of tides for the stars. For the Jupiter-like planet, we adopt a typical k_L of 0.565. As for the dissipation constant σ, we use the simplified assumption $Q^{-1}\sim 2n\tau$ (Lu et al. 2023) and set $Q=10^4$ to calculate τ and hence σ, where Q is the specific dissipation function (Goldreich 1963) and n is the orbital mean motion.

The tidal forces between the planet and two stars are performed separately. We update the stellar properties involved in calculating tidal effects with the newly generated MESA time series. We ignore the tidal influence of the planet on the stars' spins as the effects between the stars themselves are pre-dominant, which are accounted for in the MESA simulation. In Fig. 4, we show the evolution of the semimajor axis of a Jupiter-like planet with an initial $a_{\rm planet}$ of 0.5 au, both with and without accounting for tides during the mass transfer phase. At the beginning of the simulation, although the planet is close to the stars, the Love number, dissipation constant, and radius of the stars are at a low level, leading to a negligible impact on the planet's orbit. Then, the donor star keeps expanding, and the Love number increases to a high level. During the fast mass transfer phase, the mass loss from the binary system dominates the dynamical evolution of the planet. After entering the slow mass transfer phase, despite the Love number initiating a decline, the donor star continues to expand, amplifying the significance of tidal effects within the system. Then, as the donor gets stripped and the separation increases, the tidal effect becomes less pronounced. After the mass transfer phase, tidal effect becomes negligible again because the donor star is fully stripped. Our results highlight that continuously tracking the

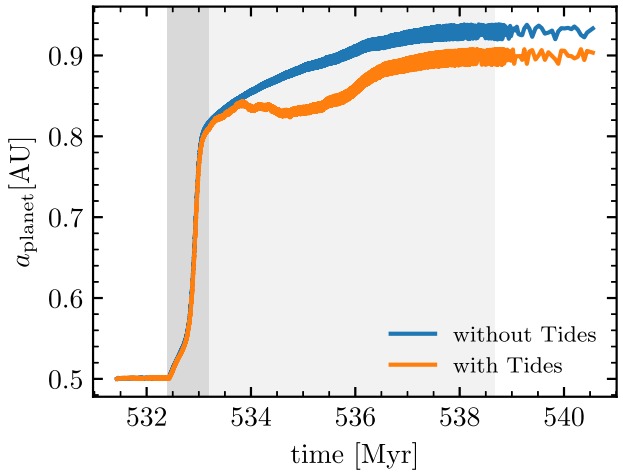

Figure 4. Evolution of the semimajor axis for a Jupiter-like planet, initially situated at a semimajor axis of 0.5 au, both with and without the inclusion of tidal effects. The fast and slow mass transfer phases are marked with dark grey and light grey shaded areas, respectively.

stellar properties for adjusting the parameters used in calculating tidal effects is indispensable when stars undergo rapid changes, such as during mass transfer.

5 DISCUSSION AND SUMMARY

In this work, we developed NBSE, a framework designed to incorporate binary evolution data from the stellar evolution code MESA into the *N*-body simulation code REBOUND. It thus enables studies of the dynamical evolution of circumbinary planets, even throughout phases of binary interaction. To demonstrate how NBSE can be used, we constructed a reference binary model with initial masses of 2.21 and 1.76 $M_\odot$ (corresponding to an initial mass ratio of 0.8) and an orbital period of 6 d, corresponding to an initial orbital separation of 0.1 au. The more massive star initiates stable mass transfer during the hydrogen-shell burning stage prior to the red giant branch (the Hertzsprung gap), which results in complete envelope loss and the formation of a 0.38 $M_\odot$ subdwarf in a wide orbit with a period of 46 d, corresponding to a binary separation of 0.33 au. In post-processing, we then adopt the orbital separation, stellar masses, and radii from the binary evolutionary model, and input these properties into an *N*-body simulation, where we represent both stars as spherical bodies with changing orbital phase, and we also integrate the orbit of a surrounding, coplanar, $1 M_{\rm Jup}$ circumbinary planet.

To mitigate the systematic errors originating from altering binary parameters during the computation of planetary dynamical evolution, we introduce a method for re-calibrating the time sequence for updating MESA binary properties in REBOUND (see Section 2.2). We consider a single Jupiter-like planet around the binary and calculate its dynamical evolution through the mass transfer phase. In our reference model, we find that the nearest stable orbital separation of the circumbinary planet is ≈ 2.5 times the binary separation after the mass transfer phase, which corresponds to ≈ 4.5 times the initial separation before mass transfer. The mass accretion efficiency within the central binary system can influence the closest stable orbit. If the mass transfer is more conservative, less mass is lost from the binary, and the expansion of the planet's orbit should be less significant. In this case, the stabilizing zone for the circumbinary planet can be smaller. Similarly, if the mass ratio of the initial binary were more extreme, the system may tighten, leaving even shorter orbital separations for the planet dynamically stable.

To include tidal forces acting on the planet, we apply the implementation of Lu et al. (2023) in the extended library REBOUNDX, adopting adaptive parameters for tidal effects based on the structure of the stars. We found that the mass loss during the rapid mass transfer phase dominates the planet's dynamical evolution, making the effect of tides negligible. After the rapid mass transfer phase, the significance of tidal effects highly depends on the stellar structure, which undergoes substantial changes during the mass transfer phase. In the case of our simulation, tides become evident at the beginning of the slow mass transfer phase and fade away as the donor star gets stripped and the separation increases.

Our reference binary forms a sdB and A-type star binary with an orbital separation of ∼0.33 au. If a planet survives the mass transfer phase, we expect to find it in an orbit wider than ∼0.85 au around such a binary after the envelope-stripping is complete. Although orbital oscillations are present in the planetary orbit after the host binary has interacted, we expect that the configuration reaches dynamical stability in our model since tides are weak and the gravitational perturbation remains constant. This means that the circumbinary planet likely remains on a similar orbit until it is perturbed again (for example by passing stars or the stellar evolution of the central binary). The long-term dynamical evolution of the circumbinary planet can be further explored with NBSE, including additional physics such as tidal decay (Shevchenko 2018).

We expect a similar formation path to produce binaries with sdB orbiting companion stars down to K-type stars ($\sim 0.7\,M_\odot$), with the companion mass range determined by varied binary physics, such as how stable mass transfer is, the mass transfer efficiency and angular momentum loss (Soberman, Phinney & van den Heuvel 1997). Similarly, it could be that subdwarfs orbiting WDs potentially retain circumbinary planets. As more and more subdwarfs in binary systems are discovered, it is intriguing to search for circumbinary planets around them. Furthermore, subdwarfs are very hot ($\sim 25,000$K) and ~ 10 times more luminous than the Sun. It is, therefore, possible that the effects of radiation on the planets are important. The real survival region and habitable zone for these planets are subject to these effects.

In our reference model, the highest mass transfer rate is $\sim 10^{-5}\,M_\odot\,{\rm yr}^{-1}$. With the threshold $\Delta M_1 = 10^{-5}\,M_\odot$, the minimal time-step for MESA is about 1 yr, which is still much longer than the time-step of the integrator for the dynamical evolution. As a result, the updates of binary data would not lead to a loss of accuracy as long as the changes are adiabatic. If the change is very rapid, like CE evolution, a finer time resolution or a more suitable integrator is required. For a different binary model, a new convergence test must be conducted to determine the threshold of the changing parameter.

Furthermore, we have ignored the interaction between the planet and the material that is lost from the binary. For high mass-loss rates, the gas density of the lost material is likely also higher, suggesting that the influence could be the strongest during the rapid phase at the beginning of mass transfer (see the second panel of Fig. 1). While estimating the impact of the ejected material on the planet would be interesting for an isotropic outflow, it is possible that the ejecta is not isotropic. If, for example the material is ejected through jets, its influence on a circumbinary planet would be negligible. It is also worth noting that subdwarfs stripped through successful CE ejection would produce an ejecta that is more dangerous to circumbinary planets since it is denser. To carefully account for the influence of the ejecta is an interesting next step in our investigation, but beyond the scope of this study.

Our model is a first step towards understanding the dynamical effect on planets that orbit interacting binaries and is therefore approximate. However, we can already note an interesting consequence that binary interaction has on planetary stability: in our example system, a planet is allowed to orbit at about 1 au from the central host star when the system evolves beyond the main-sequence evolution. This would not have been possible if the host star were single since it then would have engulfed the planet, swallowing it whole at red giant branch or asymptotic giant branch (Villaver & Livio 2007; Schröder & Smith 2008). In this regard, the binary interaction preserves tight-orbit planets.

We created NBSE as a starting point for investigating in greater detail the planetary architecture and the conditions of disruption, pollution, and engulfment for planets around single stars and, in particular, interacting binaries. Further development and extension of NBSE could potentially enable us to explore the dynamical evolution of planets with high precision and accuracy around binary systems undergoing more dramatic processes, such as CE evolution and stellar mergers.

ACKNOWLEDGEMENTS

We thank the participants of the 2023 Kavli Summer Program in Astrophysics, hosted by the Max Planck Institute for Astrophysics and funded by the Kavli Foundation. In particular, Holly Preece, Selma de Mink, and Stephen Justham for their feedback and comments on our work. ZX acknowledges support from the China Scholarship Council (CSC). ST acknowledges the funding from the European Union's Horizon 2020 research and innovation programme under the Marie Skłodowska-Curie grant agreement No. 101034413. AAT acknowledges support from the Horizon Europe research and innovation programmes under the Marie Skłodowska-Curie grant agreement no. 101103134.

DATA AVAILABILITY

NBSE is available at https://github.com/ZepeiX/NBSE.

REFERENCES

Baronett S. A., Ferich N., Tamayo D., Steffen J. H., 2022, MNRAS, 510, 6001
Bear E., Soker N., 2014, MNRAS, 444, 1698
Borucki W. J. et al., 2010, Science, 327, 977
Brown W. R. et al., 2020, ApJ, 889, 49
de Mink S. E., Langer N., Izzard R. G., Sana H., de Koter A., 2013, ApJ, 764, 166
Doyle L. R. et al., 2011, Science, 333, 1602
Drilling J. S., Jeffery C. S., Heber U., Moehler S., Napiwotzki R., 2013, A&A, 551, A31
Dvorak R., 1984, Celest. Mech., 34, 369
Dvorak R., 1986, A&A, 167, 379
Dvorak R., Froeschle C., Froeschle C., 1989, A&A, 226, 335
Eggleton P. P., Kiseleva L. G., Hut P., 1998, ApJ, 499, 853
Eldridge J. J., Izzard R. G., Tout C. A., 2008, MNRAS, 384, 1109
Esmer E. M., Baştürk Ö., Selam S. O., Aliş S., 2022, MNRAS, 511, 5207
Fragos T. et al., 2023, ApJS, 264, 45
Geier S., 2020, A&A, 635, A193
Goldreich P., 1963, MNRAS, 126, 257
Götberg Y., de Mink S. E., Groh J. H., Kupfer T., Crowther P. A., Zapartas E., Renzo M., 2018, A&A, 615, A78
Hamers A. S., Rantala A., Neunteufel P., Preece H., Vynatheya P., 2021, MNRAS, 502, 4479
Han Z., Podsiadlowski P., Maxted P. F. L., Marsh T. R., Ivanova N., 2002, MNRAS, 336, 449
Han Z., Podsiadlowski P., Maxted P. F. L., Marsh T. R., 2003, MNRAS, 341, 669
Heber U., 2016, PASP, 128, 082001
Holman M. J., Wiegert P. A., 1999, AJ, 117, 621
Hurley J. R., Pols O. R., Tout C. A., 2000, MNRAS, 315, 543
Hurley J. R., Tout C. A., Pols O. R., 2002, MNRAS, 329, 897
Hut P., 1981, A&A, 99, 126
Ivanova N. et al., 2013, A&AR, 21, 59
Jermyn A. S. et al., 2023, ApJS, 265, 15
Johnson S. A., Penny M., Gaudi B. S., Kerins E., Rattenbury N. J., Robin A. C., Calchi Novati S., Henderson C. B., 2020, AJ, 160, 123
Klement R. et al., 2024, ApJ, 962, 70
Kolb U., Ritter H., 1990, A&A, 236, 385
Kostov V. B., Moore K., Tamayo D., Jayawardhana R., Rinehart S. A., 2016, ApJ, 832, 183
Kupfer T. et al., 2015, A&A, 576, A44
Lu T., Rein H., Tamayo D., Hadden S., Mardling R., Millholland S. C., Laughlin G., 2023, ApJ, 948, 41
Mustill A., 2024, preprint (arXiv:2405.09399)
Mustill A. J., Villaver E., 2012, ApJ, 761, 121
Mustill A. J., Veras D., Villaver E., 2014, MNRAS, 437, 1404
Packet W., 1981, A&A, 102, 17
Paxton B., Bildsten L., Dotter A., Herwig F., Lesaffre P., Timmes F., 2011, ApJS, 192, 3
Paxton B. et al., 2013, ApJS, 208, 4
Paxton B. et al., 2015, ApJS, 220, 15
Paxton B. et al., 2018, ApJS, 234, 34
Paxton B. et al., 2019, ApJS, 243, 10
Penny M. T., Gaudi B. S., Kerins E., Rattenbury N. J., Mao S., Robin A. C., Calchi Novati S., 2019, ApJS, 241, 3
Pilat-Lohinger E., Dvorak R., 2002, Celest. Mech. Dyn. Astron., 82, 143
Portegies Zwart S., 2013, MNRAS, 429, L45
Qin Y., Fragos T., Meynet G., Andrews J., Sørensen M., Song H. F., 2018, A&A, 616, A28
Rao S., Meynet G., Eggenberger P., Haemmerlé L., Privitera G., Georgy C., Ekström S., Mordasini C., 2018, A&A, 618, A18
Rasio F. A., Tout C. A., Lubow S. H., Livio M., 1996, ApJ, 470, 1187
Rattanamala R. et al., 2023, MNRAS, 523, 5086
Rein H., Liu S. F., 2012, A&A, 537, A128
Rein H., Tamayo D., 2015, MNRAS, 452, 376
Rein H., Tamayo D., 2018, MNRAS, 473, 3351
Ricker G. R. et al., 2015, J. Astron. Telesc. Instrum. Syst., 1, 014003
Ricker G. R. et al., 2016, in MacEwen H. A., Fazio G. G., Lystrup M., Batalha N., Siegler N., Tong E. C., eds, Proc. SPIE Conf. Ser. Vol. 9904, Space Telescopes and Instrumentation 2016: Optical, Infrared, and Millimeter Wave. SPIE, Bellingham, p. 99042B
Ronco M. P., Schreiber M. R., Giuppone C. A., Veras D., Cuadra J., Guilera O. M., 2020, ApJ, 898, L23
Schaffenroth V., Pelisoli I., Barlow B. N., Geier S., Kupfer T., 2022, A&A, 666, A182
Schleicher D. R. G., Dreizler S., 2014, A&A, 563, A61
Schröder K. P., Smith R. C., 2008, MNRAS, 386, 155
Shevchenko I. I., 2018, AJ, 156, 52
Shevchenko I. I., Melnikov A. V., Popova E. A., Bobylev V. V., Karelin G. M., 2019, Astron. Lett., 45, 620
Soberman G. E., Phinney E. S., van den Heuvel E. P. J., 1997, A&A, 327, 620
Spergel D. et al., 2015, preprint (arXiv:1503.03757)
Sterne T. E., 1939, MNRAS, 99, 451
Sun M., Arras P., 2018, ApJ, 858, 14
Tamayo D., Rein H., Shi P., Hernandez D. M., 2020, MNRAS, 491, 2885
Veras D., 2016, R. Soc. Open Sci., 3, 150571
Veras D., Mustill A. J., Bonsor A., Wyatt M. C., 2013, MNRAS, 431, 1686

Veras D., Mustill A. J., Gänsicke B. T., Redfield S., Georgakarakos N., Bowler A. B., Lloyd M. J. S., 2016, MNRAS, 458, 3942
Villaver E., Livio M., 2007, ApJ, 661, 1192
Villaver E., Livio M., 2009, ApJ, 705, L81
Vos J., Østensen R. H., Vučković M., Van Winckel H., 2017, A&A, 605, A109
Wang L., Gies D. R., Peters G. J., Götberg Y., Chojnowski S. D., Lester K. V., Howell S. B., 2021, AJ, 161, 248
Wiegert P. A., Holman M. J., 1997, AJ, 113, 1445
Zorotovic M., Schreiber M. R., 2013, A&A, 549, A95

This paper has been typeset from a TEX/LATEX file prepared by the author.

Appendix B

CO-AUTHORED PAPERS USING POSYDON

POSYDON is a powerful BPS tool that can be used in investigating a wide range of astrophysical problems involving critical questions in both single star and binary evolution theories. With POSYDON, we have applied it to study multiple aspects of BH and NS physics and demonstrated its impact in advancing our understanding of these compact objects. This chapter presents a summary of the findings in my co-authored papers that utilized POSYDON.

B.1 Supernova explosion and formation of black holes

In POSYDON, we developed our own single stellar evolutionary models. Bavera et al. (2023) found that our models along with several state-of-the-art single-star models, including GENEVA (Meynet et al., 2003; Ekström et al., 2012) computed with GENEC and MIST (Choi et al., 2016) from MESA, massive stars at solar metallicity exhibit significant differences from the SSE stellar tracks, which form the basis of BSE-like codes. Specifically, SSE predicts significant radial expansion for stars above $\sim 50\,M_{\odot}$, whereas recent detailed simulations suggest that these stars do not expand to red supergiants. The discrepancy arises because these massive star tracks in SSE are from extrapolation, and the radial response to the wind loss is not properly accounted for. The consequence for this is that these stars in SSE lose more mass due to luminous blue variable winds and the final BH masses are reduced. In Figure B.1, Bavera et al. (2023) showed that, using our new stellar models, BHs as massive as $\sim 30\,M_{\odot}$ can be produced at solar metallicity, a result that was not expected from BSE-like codes. These massive BHs at solar metallicity has multiple observational implications for binary systems in the context of GW detections, XRBs, and astrometric binaries.

Based on the single star models in POSYDON, Zapartas et al. (2021) investigated the explodability of stripped-envelope SNe (SESNe) progenitors originating from single stars, considering different SN prescriptions and stellar input physics such as overshooting parameter, stellar rotation, and wind mass loss. These progenitors had either fully stripped their hydrogen envelopes or retained only a thin outer layer before explosion. Zapartas et al. (2021) showed that, unless stronger winds are invoked, most stripped single stars that could produce SESNe collapse into BHs directly without a bright transient, for all but one of the SN prescriptions they adopted. This result suggests that binary progenitors may play a dominant role in producing in producing SESNe.

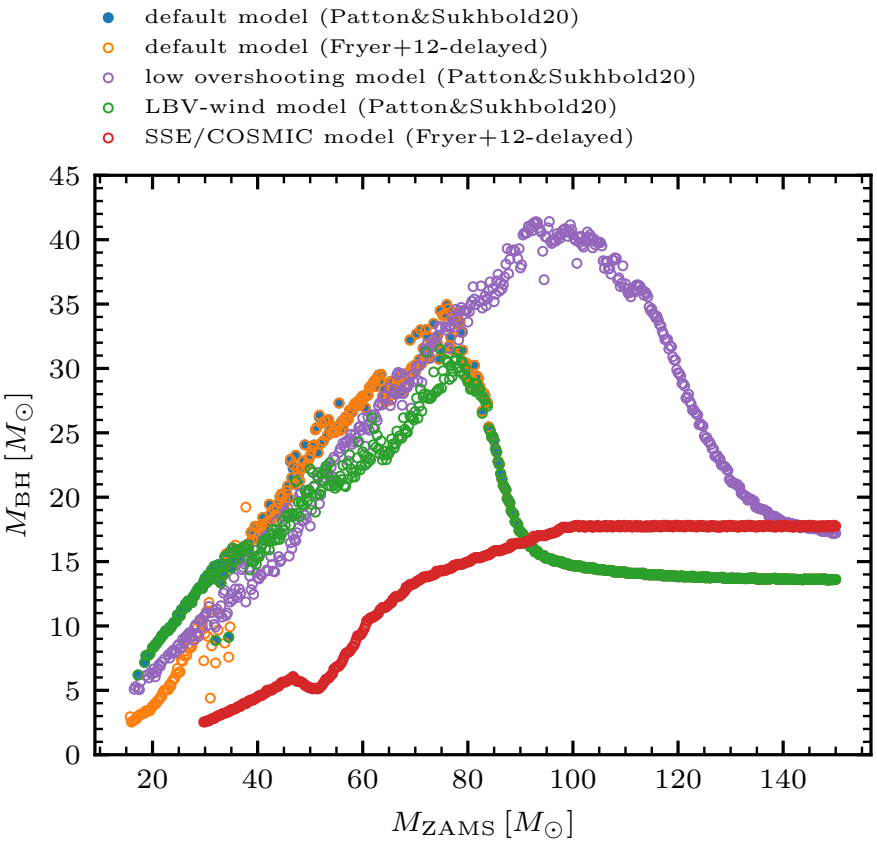

Figure B.1: Black hole mass from single-star evolution as a function of ZAMS mass at solar metallicity. `POSYDON` default model is shown in blue; a model with an alternative SN prescription are shown in orange; the model variation including LBV-like winds is shown in green; and the low-overshooting model is shown in purple. The BH masses from the `SSE` stellar models as implemented in `COSMIC` are show in red. Credit: Bavera et al. (2023).

B.2 X-ray binaries

Be X-ray binaries

Rocha et al. (2024) investigated the formation and characteristics of Galactic Be-XRBs at solar metallicity, taking the advantage of the functionality of `POSYDON` to track the stellar spin evolution. We found that using a rapid rotation threshold of $W \gtrsim 50\%$ as a selection criterion naturally reproduces many features of the observed Galactic Be-XRB population in a self-consistent manner. The fiducial models in `POSYDON` can reproduce their orbital properties. The rotation distribution of Be stars predicted by `POSYDON` produced a peak at $\simeq 65\%$, which results from the tidal spin-down of the Be stars and aligns well with the observations (Zorec et al., 2016; Cochetti et al., 2019; Balona et al., 2021). However, a

secondary peak at $W \gtrsim 99\%$ also appears in the simulations. Additionally, the simulated Be star masses are still systematically lower than the observed distributions, which might indicate that the mass transfer efficiency onto non-degenerate stars is too low in our binary models.

Ultraluminous X-ray binaries

Misra et al. (2024) explored the effect of stellar age on the population of ULXs using `POSYDON`. The population results showed that ULX numbers decline with age, with HMXBs dominating at early ages (< 10Myr), IMXBs becoming more prominent at around < 40Myr, and LMXBs dominating between 100 – 300Myr. The ratio of BH to NS accretors also decreases over time, and the dominant donor star types change with age. Additionally, NS ULXs exhibit stronger geometrical beaming than BH ULXs, resulting in a lower prevalence of NS accretors in observed populations. Combined with the finding that X-ray pulses are suppressed in at least 60% of NS ULXs, this suggests that the fraction of ULXs with detectable X-ray pulses is small, consistent with observational data. This study confirms that ULX properties evolve with stellar age and are closely linked to binary evolution physics.

X-ray luminosity function

One of the most effective tools for studying XRB populations is the X-ray luminosity function (XLF), which represents the number density distribution of XRBs as a function of their X-ray luminosity. Misra et al. (2023) studied the effects of various binary physics on the XLF of HMXBs. The HMXBs are categorized into sub-populations, including Be-XRBs, RLOF HMXBs, and wind-fed HMXBs, further distinguishing NS and BH accretors as well as H-rich and He-rich donor stars. The model variations explored included different SN prescriptions, BH natal kick normalization, the treatment of orbital circularization at the onset of RLOF, CE parameters and disk formation criteria around BHs. Figure B.2 compares the XLF from the simulation with the observational XLF from Lehmer et al. (2019). We can see that there is an excess of XRBs at intermediate luminosities ($10^{38} - 10^{39}$ erg s^{-1}), forming an XLF bump. In the low-luminosity regime, Be-XRBs account for a significant fraction. However, the estimated luminosities of Be-XRBs are based on empirical peak values and require further refinement. The distribution of Be-XRBs in the XLF needs more detailed studies. The overabundance of RLOF BH-HMXBs with H-rich donor stars contributes to the formation of the XLF bump. Stronger BH natal kicks can disrupt wide systems and reduce the number of RLOF BH-HMXBs. However, for close binaries, strong natal kicks can lead to higher-eccentricity systems that evolve into bright RLOF BH-HMXBs. This outcome is influenced by the treatment of binary orbits at the onset of RLOF. By default,

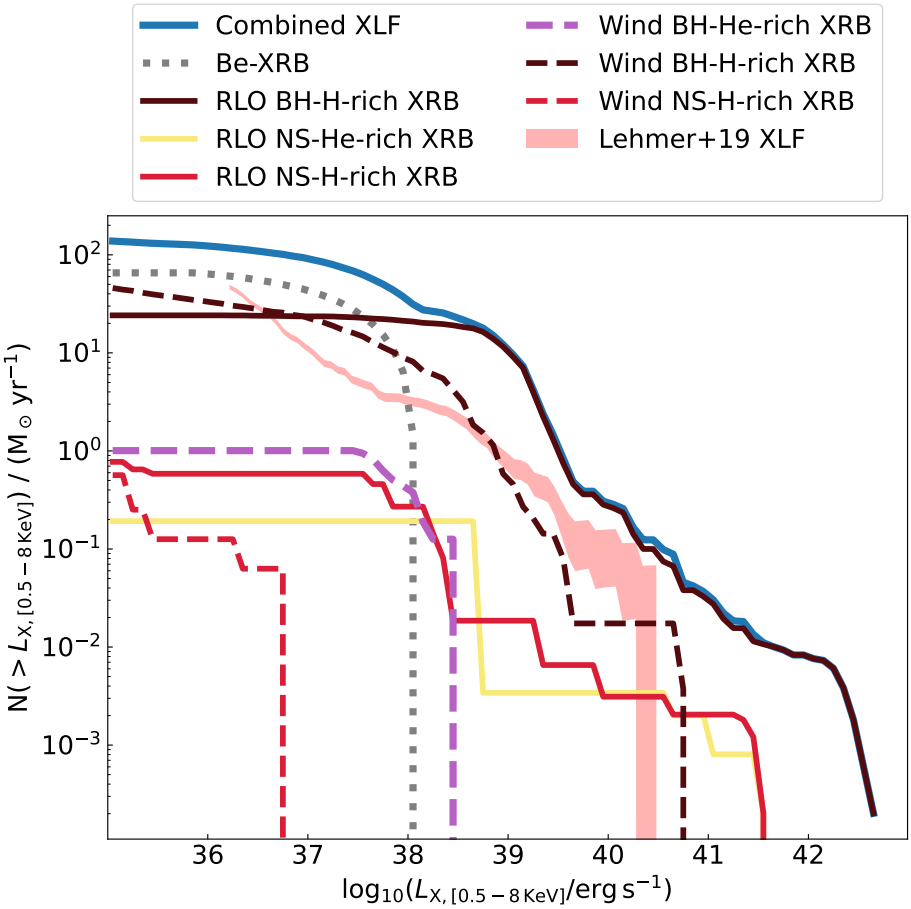

Figure B.2: XLF of the POSYDON synthetic population compared to the observed XLF from Lehmer et al. (2019). The contributions of sub-populations are shown. Credit: Misra et al. (2023).

POSYDON assumes that binary orbits undergo instantaneous circularization at periastron when RLOF occurs in eccentric binaries. However, this assumption may not be accurate for binaries with high eccentricities at the time of mass transfer. Such eccentric sources could appear as transient HMXBs and should be considered when modeling XLFs.

Black hole low-mass X-ray binaries

The BH mass distribution in observed LMXBs indicates a mass gap between BHs and NSs. Siegel et al. (2023) investigated possible selection biases against mass-gap BHs in LMXBs, considering that BH mass measurement requires transient behaviors of LMXBs. With the use of the rapid BPS code COSMIC (Breivik et al., 2020), no significant selection biases were found. However, when using detailed binary modeling with POSYDON, we observed that selection biases are present if NS birth mass is below $\sim 2\,M_\odot$; otherwise, the mass gap

will be filled with BHs from accretion-induced collapse of NSs. These differences originate from how mass transfer is treated in COSMIC versus POSYDON. For BH-LMXBs, POSYDON generally predicts more rapid mass transfer, causing BHs to either leave the gap quickly or undergo only a short transient phase. Conversely, binaries in COSMIC remain in the mass transfer phase for much longer, increasing the likelihood of being transient with a mass-gap BH. This study further highlights the importance of a detailed and physically consistent treatment of mass transfer in binary evolution simulations.

For the specific BH-LMXB MAXI J1305-704, it has been reported to have a space velocity of $\simeq 200\,\mathrm{km\,s^{-1}}$. Kimball et al. (2023) studied this LMXB to gain insights into possible BH natal kick of this system. Through POSYDON binary models and further analysis, Kimball et al. (2023) found that if MAXI J1305-704 formed through isolated binary evolution in the thick Galactic disk, then the SN that produced the BH must have imparted a natal kick of at least $70, \mathrm{km}, \mathrm{s}^{-1}$. This analysis reinforces the idea that at least some BHs receive natal kicks at birth.

B.3 Detached black hole binaries

The discovery of Gaia BHs in wide binaries with low-mass companions challenges traditional isolated binary evolution models. Kruckow et al. (2024) explored an alternative non-interacting formation channel with POSYDON to explain their formation at solar metallicity. In the POSYDON models, strong stellar winds during earlier evolutionary phases prevent the most massive stars from expanding, thereby avoiding RLOF and making a non-interacting formation channel viable. Kruckow et al. (2024) found that stellar winds, particularly WR winds, play a crucial role in limiting BH mass growth for very massive stars, creating a plateau around $13\,M_\odot$ in the BH mass distribution. As a result, wide BH binaries with low-mass companions like Gaia BH1 and Gaia BH2 can form at high metallicity without interactions.

PUBLICATION LIST

First-author journal articles

Z. Xing, V. Kalogera, T. Fragos, J. J. Andrews, S. S. Bavera, M. Briel et al., Mass-gap Black Holes in Coalescing Neutron Star Black Hole Binaries, Under review (2025)

Z. Xing, S. Torres, Y. Götberg, A. A. Trani, V. Korol and J. Cuadra, Combining rebound and mesa: dynamical evolution of planets orbiting interacting binaries, MNRAS 537 (2025) 285

Z. Xing, T. Fragos, E. Zapartas, T. M. Kwan, L. Dai, I. Mandel et al., Formation of wind-fed black hole high-mass X-ray binaries: The role of Roche-lobe-overflow post black hole formation, A&A 693 (2025) A27

Z. Xing, S. S. Bavera, T. Fragos, M. U. Kruckow, J. Román-Garza, J. J. Andrews et al., From ZAMS to merger: Detailed binary evolution models of coalescing neutron star - black hole systems at solar metallicity, A&A 683 (2024) A144

Z. Xing and X.-D. Li, Population Synthesis of Neutron Star X-Ray Binaries Associated with Supernova Remnants, ApJ 920 (2021) 67

Z. Xing and X.-D. Li, On the Rapid Orbital Expansion in the Compact Low-mass X-Ray Binary 2A 1822-371, ApJ 887 (2019) 201

Co-authored journal articles

M. Briel, T. Fragos, O. S. Salafia, G. Ghirlanda, E. Zapartas, **et al.**, A new long gamma-ray burst formation pathway at solar metallicity, Under review (2025)

J. J. Andrews, S. S. Bavera, M. Briel, A. Chattaraj, A. Dotter, T. Fragos **et al.**, POSYDON Version 2: Population Synthesis with Detailed Binary-Evolution Simulations across a Cosmological Range of Metallicities, Under review (2025)

E. Zapartas, S. de Wit, K. Antoniadis, G. Muñoz-Sanchez, D. Souropanis, A. Z. Bo-nanos **et al.**, The effect of mass loss in models of red supergiants in the Small Magellanic Cloud, Under review (2025)

E. Teng, U. Demir, Z. Doctor, P. M. Srivastava, S. Lalvani, V. Kalogera **et al.**, Emulators for stellar profiles in binary population modeling, Under review (2025)

M. U. Kruckow, J. J. Andrews, T. Fragos, B. Holl, S. S. Bavera, M. Briel **et al.**, The Formation of Black Holes in Non-interacting, Isolated Binaries. Gaia Black Holes as Calibrators of Stellar Winds From Massive Stars, A&A 692 (2025) A141

K. A. Rocha, V. Kalogera, Z. Doctor, J. J. Andrews, M. Sun, S. Gossage **et al.**, To Be or Not To Be: The Role of Rotation in Modeling Galactic Be X-Ray Binaries, ApJ 971 (2024) 133

D. Misra, K. Kovlakas, T. Fragos, J. J. Andrews, S. S. Bavera, E. Zapartas **et al.**, Exploring the nature of ultra-luminous X-ray sources across stellar population ages using detailed binary evolution calculations, A&A 682 (2024) A69

T. Fragos, J. J. Andrews, S. S. Bavera, C. P. L. Berry, S. Coughlin, A. Dotter **et al.**, POSYDON: A General-purpose Population Synthesis Code with Detailed Binary-evolution Simulations, ApJS 264 (2023) 45

S. S. Bavera, T. Fragos, E. Zapartas, J. J. Andrews, V. Kalogera, C. P. L. Berry **et al.**, The formation of merging black holes with masses beyond $30M_{\odot}$ at solar metallicity, Nature Astronomy 7 (2023) 1090

J. C. Siegel, I. Kiato, V. Kalogera, C. P. L. Berry, T. J. Maccarone, K. Breivik **et al.**, Investigating the Lower Mass Gap with Low-mass X-Ray Binary Population Synthesis, ApJ 954 (2023) 212

C. Kimball, S. Imperato, V. Kalogera, K. A. Rocha, Z. Doctor, J. J. Andrews **et al.**, A Black Hole Kicked at Birth: MAXI J1305-704, ApJL 952 (2023) 34

D. Misra, K. Kovlakas, T. Fragos, M. Lazzarini, S. S. Bavera, B. D. Lehmer **et al.**, X-ray luminosity function of high-mass X-ray binaries: Studying the signatures of different physical processes using detailed binary evolution calculations, A&A 672 (2023) 99

K. A. Rocha, J. J. Andrews, C. P. L. Berry, Z. Doctor, A. K. Katsaggelos, J. G. Serra Pérez **et al.**, Active Learning for Computationally Efficient Distribution of Binary Evolution Simulations, ApJ 938 (2022) 64

S. S. Bavera, T. Fragos, E. Zapartas, E. Ramirez-Ruiz, P. Marchant, L. Z. Kelley **et al.**, Probing the progenitors of spinning binary black-hole mergers with long gamma-ray bursts, A&A 657 (2022) 8

E. Zapartas, M. Renzo, T. Fragos, A. Dotter, J. J. Andrews, S. S. Bavera **et al.**, Revisiting the explodability of single massive star progenitors of stripped-envelope supernovae, A&A 656 (2021) 19

ACKNOWLEDGEMENTS

First and foremost, I would like to express my sincere gratitude to my supervisor, Prof.Tassos Fragos, who has been giving me the best example of being an exceptional scientist, mentor, and friend. His expertise and guidance formed the foundation of my scientific exploration, while his encouragement and kindness drove me forward throughout my Ph.D. journey. I will never forget the traits I learned from him, being diligent, integrate, curious, and ambitious. Thank you to Tassos for teaching me everything I need to become an astrophysicist.

I am also sincerely grateful to my colleagues and collaborators. At the beginning of my Ph.D., working with Simone Bavera, Devina Misra, Jaime Román-Garza, Konstantinos Kovlakas, and Emmanouil Zapartas has been an invaluable experience. Together we witnessed the first binary simulation from POSYDON. Special thanks to Matthias Kruckow and Max Briel for countless meaningful discussions and particularly for their invaluable assistance in improving this thesis. I want to thank all the wonderful people at CIERA for their warm welcome and the excellent experience during my visiting. I am especially thankful to prof.Vicky Kalogera for providing this incredible opportunity and for her insightful guidance throughout our project. All the memorable interactions and enriching discussions with Kyle Rocha, Monica Gallegos-Garcia, Seth Gossage, Camille Liotine, Elizabeth Teng, Meng Sun, Philipp Srivastava, Chase Kimball, Ilia Kiato, Zoheyr Doctor, Michael Zevin, and Sylvia Biscoveanu are wonderful.

To the entire POSYDON collaborations, I appreciate everyone's hard work for enhancing the code. Special appreciation goes to Jeff Andrews, Abhishek Chattaraj, Eirini Kasdagli, and Dimitris Souropanis. Additionally, I am grateful to all my paper co-authors, Lixin Dai, Tom Kwan, Ilya Mandel, Santiago Torres, Ylva Götberg, Alessandro Trani, Valeriya Korol and Jorge Cuadra. A special thank to Ilya for his kind support in providing a reference letter for my postdoc applications.

Last but not least, I extend my heartfelt thanks to my parents, whose unwavering support in every aspect has been essential throughout my Ph.D. journey. My deepest gratitude and love go to my wife Yuping Wang, my steadfast pillar of strength. You have nurtured a home whose warmth empowers me every day, and–even across a seven-hour time zone–your unwavering encouragement and boundless love continue to shape the person I am.

BIBLIOGRAPHY

Abac et al. (Aug. 2024). "Observation of Gravitational Waves from the Coalescence of a 2.5–4.5 $M_\odot$ Compact Object and a Neutron Star". In: 970.2, L34, p. L34. DOI: 10.3847/2041-8213/ad5beb. arXiv: 2404.04248 [astro-ph.HE].

Abbott et al. (June 2016). "Properties of the Binary Black Hole Merger GW150914". In: 116.24, 241102, p. 241102. DOI: 10.1103/PhysRevLett.116.241102. arXiv: 1602.03840 [gr-qc].

Abbott et al. (Oct. 2017a). "Gravitational Waves and Gamma-Rays from a Binary Neutron Star Merger: GW170817 and GRB 170817A". In: 848.2, L13, p. L13. DOI: 10.3847/2041-8213/aa920c. arXiv: 1710.05834 [astro-ph.HE].

Abbott et al. (Oct. 2017b). "GW170817: Observation of Gravitational Waves from a Binary Neutron Star Inspiral". In: *Phys. Rev. Lett.* 119 (16), p. 161101. DOI: 10.1103/PhysRevLett.119.161101. URL: https://link.aps.org/doi/10.1103/PhysRevLett.119.161101.

Abbott et al. (Oct. 2017c). "Multi-messenger Observations of a Binary Neutron Star Merger". In: 848.2, L12, p. L12. DOI: 10.3847/2041-8213/aa91c9. arXiv: 1710.05833 [astro-ph.HE].

Abbott et al. (Sept. 2019). "GWTC-1: A Gravitational-Wave Transient Catalog of Compact Binary Mergers Observed by LIGO and Virgo during the First and Second Observing Runs". In: *Phys. Rev. X* 9 (3), p. 031040. DOI: 10.1103/PhysRevX.9.031040. URL: https://link.aps.org/doi/10.1103/PhysRevX.9.031040.

Abbott et al. (Mar. 2020a). "GW190425: Observation of a Compact Binary Coalescence with Total Mass $\sim 3.4\ M_\odot$". In: 892.1, L3, p. L3. DOI: 10.3847/2041-8213/ab75f5. arXiv: 2001.01761 [astro-ph.HE].

Abbott et al. (June 2020b). "GW190814: Gravitational Waves from the Coalescence of a 23 Solar Mass Black Hole with a 2.6 Solar Mass Compact Object". In: 896.2, L44, p. L44. DOI: 10.3847/2041-8213/ab960f. arXiv: 2006.12611 [astro-ph.HE].

Abbott et al. (June 2021a). "GWTC-2: Compact Binary Coalescences Observed by LIGO and Virgo during the First Half of the Third Observing Run". In: *Phys. Rev. X* 11 (2), p. 021053. DOI: 10.1103/PhysRevX.11.021053. URL: https://link.aps.org/doi/10.1103/PhysRevX.11.021053.

Abbott et al. (July 2021b). "Observation of Gravitational Waves from Two Neutron Star-Black Hole Coalescences". In: 915.1, L5, p. L5. DOI: 10.3847/2041-8213/ac082e. arXiv: 2106.15163 [astro-ph.HE].

Abbott et al. (Dec. 2023a). "GWTC-3: Compact Binary Coalescences Observed by LIGO and Virgo during the Second Part of the Third Observing Run". In: *Phys. Rev. X* 13 (4), p. 041039. DOI: 10.1103/PhysRevX.13.041039. URL: https://link.aps.org/doi/10.1103/PhysRevX.13.041039.

Abbott et al. (Mar. 2023b). "Population of Merging Compact Binaries Inferred Using Gravitational Waves through GWTC-3". In: *Phys. Rev. X* 13 (1), p. 011048. DOI: 10.1103/PhysRevX.13.011048. URL: https://link.aps.org/doi/10.1103/PhysRevX.13.011048.

Abbott et al. (Jan. 2024). "GWTC-2.1: Deep extended catalog of compact binary coalescences observed by LIGO and Virgo during the first half of the third observing run". In: 109.2, 022001, p. 022001. DOI: 10.1103/PhysRevD.109.022001. arXiv: 2108.01045 [gr-qc].

Ablimit, Iminhaji (Feb. 2023). "A promising formation channel for symbiotic X-ray binaries: cases of IGR J17329-2731 and 4U 1700+24". In: 519.1, pp. 1327–1335. DOI: 10.1093/mnras/stac3551. arXiv: 2212.00997 [astro-ph.HE].

Abramowicz, M. A. et al. (Sept. 1988). "Slim Accretion Disks". In: 332, p. 646. DOI: 10.1086/166683.

Abt, H. A. (Jan. 1983). "Normal and abnormal binary frequencies." In: 21, pp. 343–372. DOI: 10.1146/annurev.aa.21.090183.002015.

Acernese, F. et al. (Jan. 2015). "Advanced Virgo: a second-generation interferometric gravitational wave detector". In: *Classical and Quantum Gravity* 32.2, 024001, p. 024001. DOI: 10.1088/0264-9381/32/2/024001. arXiv: 1408.3978 [gr-qc].

Amaro-Seoane, Pau et al. (Feb. 2017). "Laser Interferometer Space Antenna". In: *arXiv e-prints*, arXiv:1702.00786, arXiv:1702.00786. DOI: 10.48550/arXiv.1702.00786. arXiv: 1702.00786 [astro-ph.IM].

Andrews, Jeff J. and Vicky Kalogera (May 2022). "Constraining Black Hole Natal Kicks with Astrometric Microlensing". In: 930.2, 159, p. 159. DOI: 10.3847/1538-4357/ac66d6. arXiv: 2203.15156 [astro-ph.HE].

Andrews, Jeff J. et al. (Nov. 2024). "POSYDON Version 2: Population Synthesis with Detailed Binary-Evolution Simulations across a Cosmological Range of Metallicities". In: *arXiv e-prints*, arXiv:2411.02376, arXiv:2411.02376. DOI: 10.48550/arXiv.2411.02376. arXiv: 2411.02376 [astro-ph.GA].

Antoniou, V. and A. Zezas (June 2016). "Star formation history and X-ray binary populations: the case of the Large Magellanic Cloud". In: 459.1, pp. 528–553. DOI: 10.1093/mnras/stw167. arXiv: 1603.08011 [astro-ph.HE].

Archibald, Anne M. et al. (June 2009). "A Radio Pulsar/X-ray Binary Link". In: *Science* 324.5933, p. 1411. DOI: 10.1126/science.1172740. arXiv: 0905.3397 [astro-ph.HE].

Armas Padilla, M. et al. (Sept. 2023). "UltraCompCAT: A comprehensive catalogue of ultra-compact and short orbital period X-ray binaries". In: 677, A186, A186. DOI: 10.1051/0004-6361/202346797. arXiv: 2305.07691 [astro-ph.HE].

Arzoumanian, Zaven et al. (Apr. 2018). "The NANOGrav 11-year Data Set: High-precision Timing of 45 Millisecond Pulsars". In: 235.2, 37, p. 37. DOI: 10.3847/1538-4365/aab5b0. arXiv: 1801.01837 [astro-ph.HE].

Aso, Yoichi et al. (Aug. 2013). "Interferometer design of the KAGRA gravitational wave detector". In: 88.4, 043007, p. 043007. DOI: 10.1103/PhysRevD.88.043007. arXiv: 1306.6747 [gr-qc].

Atri, P. et al. (Nov. 2019). "Potential kick velocity distribution of black hole X-ray binaries and implications for natal kicks". In: 489.3, pp. 3116–3134. DOI: 10.1093/mnras/stz2335. arXiv: 1908.07199 [astro-ph.HE].

Avakyan, A. et al. (July 2023). "XRBcats: Galactic low-mass X-ray binary catalogue". In: 675, A199, A199. DOI: 10.1051/0004-6361/202346522. arXiv: 2303.16168 [astro-ph.HE].

Bachetti, M. et al. (Oct. 2014). "An ultraluminous X-ray source powered by an accreting neutron star". In: 514.7521, pp. 202–204. DOI: 10.1038/nature13791. arXiv: 1410.3590 [astro-ph.HE].

El-Badry, Kareem et al. (May 2023a). "A red giant orbiting a black hole". In: 521.3, pp. 4323–4348. DOI: 10.1093/mnras/stad799. arXiv: 2302.07880 [astro-ph.SR].

El-Badry, Kareem et al. (Jan. 2023b). "A Sun-like star orbiting a black hole". In: 518.1, pp. 1057–1085. DOI: 10.1093/mnras/stac3140. arXiv: 2209.06833 [astro-ph.SR].

El-Badry, Kareem et al. (Apr. 2024a). "A 1.9 solar-mass neutron star candidate in a 2-year orbit". In: *The Open Journal of Astrophysics* 7, 27, p. 27. DOI: 10.33232/001c.116675. arXiv: 2402.06722 [astro-ph.SR].

El-Badry, Kareem et al. (July 2024b). "A population of neutron star candidates in wide orbits from Gaia astrometry". In: *The Open Journal of Astrophysics* 7, 58, p. 58. DOI: 10.33232/001c.121261. arXiv: 2405.00089 [astro-ph.SR].

Bahramian, Arash and Nathalie Degenaar (2023). "Low-Mass X-ray Binaries". In: *Handbook of X-ray and Gamma-ray Astrophysics*, 120, p. 120. DOI: 10.1007/978-981-16-4544-0_94-1.

Bailyn, Charles D. et al. (May 1998). "The Mass Distribution of Stellar Black Holes". In: 499.1, pp. 367–374. DOI: 10.1086/305614. arXiv: astro-ph/9708032 [astro-ph].

Balbinot, E. et al. (July 2024). "The 33 $M_\odot$ black hole Gaia BH3 is part of the disrupted ED-2 star cluster". In: 687, L3, p. L3. DOI: 10.1051/0004-6361/202450425. arXiv: 2404.11604 [astro-ph.GA].

Balona, Luis A. and Dogus Ozuyar (Nov. 2021). "TESS Observations of Be Stars: General Characteristics and the Impulsive Magnetic Rotator Model". In: 921.1, 5, p. 5. DOI: 10.3847/1538-4357/ac1a77. arXiv: 2008.06288 [astro-ph.SR].

Batta, Aldo, Enrico Ramirez-Ruiz, and Chris Fryer (Sept. 2017). "The Formation of Rapidly Rotating Black Holes in High-mass X-Ray Binaries". In: 846.2, L15, p. L15. DOI: 10.3847/2041-8213/aa8506. arXiv: 1708.00570 [astro-ph.HE].

Bavera, Simone S. et al. (Sept. 2023). "The formation of merging black holes with masses beyond 30 $M_\odot$ at solar metallicity". In: *Nature Astronomy* 7, pp. 1090–1097. DOI: 10.1038/s41550-023-02018-5. arXiv: 2212.10924 [astro-ph.HE].

Baym, Gordon et al. (Nov. 2019). "New Neutron Star Equation of State with Quark-Hadron Crossover". In: 885.1, 42, p. 42. DOI: 10.3847/1538-4357/ab441e. arXiv: 1903.08963 [astro-ph.HE].

Begelman, M. C. (Apr. 1979). "Can a spherically accreting black hole radiate very near the Eddington limit?" In: 187, pp. 237–251. DOI: 10.1093/mnras/187.2.237.

Belczynski, Krzysztof, Vassiliki Kalogera, and Tomasz Bulik (June 2002). "A Comprehensive Study of Binary Compact Objects as Gravitational Wave Sources: Evolutionary Channels, Rates, and Physical Properties". In: 572.1, pp. 407–431. DOI: 10.1086/340304. arXiv: astro-ph/0111452 [astro-ph].

Belczynski, Krzysztof et al. (Jan. 2008). "Compact Object Modeling with the StarTrack Population Synthesis Code". In: 174.1, pp. 223–260. DOI: 10.1086/521026. arXiv: astro-ph/0511811 [astro-ph].

Bethe, H. A. and J. R. Wilson (Aug. 1985). "Revival of a stalled supernova shock by neutrino heating". In: 295, pp. 14–23. DOI: 10.1086/163343.

Bisnovatyi-Kogan, G. S. (Jan. 1993). "Asymmetric neutrino emission and formation of rapidly moving pulsars". In: *Astronomical and Astrophysical Transactions* 3.4, pp. 287–294. DOI: 10.1080/10556799308230566. arXiv: astro-ph/9707120 [astro-ph].

Biswas, Bhaskar and Stephan Rosswog (Aug. 2024). "Simultaneously Constraining the Neutron Star Equation of State and Mass Distribution through Multimessenger Observations and Nuclear Benchmarks". In: *arXiv e-prints*, arXiv:2408.15192, arXiv:2408.15192. DOI: 10.48550/arXiv.2408.15192. arXiv: 2408.15192 [astro-ph.HE].

Bondi, H. and F. Hoyle (Jan. 1944). "On the mechanism of accretion by stars". In: 104, p. 273. DOI: 10.1093/mnras/104.5.273.

Bozzo, E. et al. (May 2016). "Clumpy wind accretion in supergiant neutron star high mass X-ray binaries". In: 589, A102, A102. DOI: 10.1051/0004-6361/201628341. arXiv: 1603.05187 [astro-ph.HE].

Breivik, Katelyn, Sourav Chatterjee, and Shane L. Larson (Nov. 2017). "Revealing Black Holes with Gaia". In: 850.1, L13, p. L13. DOI: 10.3847/2041-8213/aa97d5. arXiv: 1710.04657 [astro-ph.SR].

Breivik, Katelyn et al. (July 2020). "COSMIC Variance in Binary Population Synthesis". In: 898.1, 71, p. 71. DOI: 10.3847/1538-4357/ab9d85. arXiv: 1911.00903 [astro-ph.HE].

Bressan, Alessandro et al. (Nov. 2012). "PARSEC: stellar tracks and isochrones with the PAdova and TRieste Stellar Evolution Code". In: 427.1, pp. 127–145. DOI: 10.1111/j.1365-2966.2012.21948.x. arXiv: 1208.4498 [astro-ph.SR].

Broekgaarden, Floor S. et al. (Dec. 2021). "Impact of massive binary star and cosmic evolution on gravitational wave observations I: black hole-neutron star mergers". In: 508.4, pp. 5028–5063. DOI: 10.1093/mnras/stab2716. arXiv: 2103.02608 [astro-ph.HE].

Broekgaarden, Floor S. et al. (Nov. 2022). "Impact of massive binary star and cosmic evolution on gravitational wave observations - II. Double compact object rates and properties". In: 516.4, pp. 5737–5761. DOI: 10.1093/mnras/stac1677. arXiv: 2112.05763 [astro-ph.HE].

Brown, G. E. (Feb. 1995). "Neutron Star Accretion and Binary Pulsar Formation". In: 440, p. 270. DOI: 10.1086/175268.

Burdge, Kevin B. et al. (Nov. 2024). "The black hole low-mass X-ray binary V404 Cygni is part of a wide triple". In: 635.8038, pp. 316–320. DOI: 10.1038/s41586-024-08120-6. arXiv: 2404.03719 [astro-ph.HE].

Burrows and John Goshy (Oct. 1993). "A Theory of Supernova Explosions". In: 416, p. L75. DOI: 10.1086/187074.

Burrows and John Hayes (Jan. 1996). "Pulsar Recoil and Gravitational Radiation Due to Asymmetrical Stellar Collapse and Explosion". In: 76.3, pp. 352–355. DOI: 10.1103/PhysRevLett.76.352. arXiv: astro-ph/9511106 [astro-ph].

Burrows, Tianshu Wang, and David Vartanyan (Dec. 2024). "Channels of Stellar-mass Black Hole Formation". In: *arXiv e-prints*, arXiv:2412.07831, arXiv:2412.07831. DOI: 10.48550/arXiv.2412.07831. arXiv: 2412.07831 [astro-ph.SR].

Burrows et al. (Aug. 2011). "Relativistic jet activity from the tidal disruption of a star by a massive black hole". In: 476.7361, pp. 421–424. DOI: 10.1038/nature10374. arXiv: 1104.4787 [astro-ph.HE].

Burrows et al. (Nov. 2023). "A Theory for Neutron Star and Black Hole Kicks and Induced Spins". In: *arXiv e-prints*, arXiv:2311.12109, arXiv:2311.12109. DOI: 10.48550/arXiv.2311.12109. arXiv: 2311.12109 [astro-ph.HE].

Callister, T. A. (Oct. 2024). "Observed Gravitational-Wave Populations". In: *arXiv e-prints*, arXiv:2410.19145, arXiv:2410.19145. DOI: 10.48550/arXiv.2410.19145. arXiv: 2410.19145 [astro-ph.HE].

Canal, Ramon, Jordi Isern, and Javier Labay (Jan. 1990). "The origin of neutron stars in binary systems." In: 28, pp. 183–214. DOI: 10.1146/annurev.astro.28.1.183.

Chakrabarti, Sukanya et al. (July 2023). "A Noninteracting Galactic Black Hole Candidate in a Binary System with a Main-sequence Star". In: 166.1, 6, p. 6. DOI: 10.3847/1538-3881/accf21. arXiv: 2210.05003 [astro-ph.GA].

Chan, Conrad, Bernhard Müller, and Alexander Heger (July 2020). "The impact of fallback on the compact remnants and chemical yields of core-collapse supernovae". In: 495.4, pp. 3751–3762. DOI: 10.1093/mnras/staa1431. arXiv: 2003.04320 [astro-ph.SR].

Choi, Jieun et al. (June 2016). "Mesa Isochrones and Stellar Tracks (MIST). I. Solar-scaled Models". In: 823.2, 102, p. 102. DOI: 10.3847/0004-637X/823/2/102. arXiv: 1604.08592 [astro-ph.SR].

Cochetti, Y. R. et al. (Jan. 2019). "Spectro-interferometric observations of a sample of Be stars. Setting limits to the geometry and kinematics of stable Be disks". In: 621, A123, A123. DOI: 10.1051/0004-6361/201833551. arXiv: 1811.11055 [astro-ph.SR].

Colbert, Edward J. M. and Richard F. Mushotzky (July 1999). "The Nature of Accreting Black Holes in Nearby Galaxy Nuclei". In: 519.1, pp. 89–107. DOI: 10.1086/307356. arXiv: astro-ph/9901023 [astro-ph].

Colgate, Stirling A. and Richard H. White (Mar. 1966). "The Hydrodynamic Behavior of Supernovae Explosions". In: 143, p. 626. DOI: 10.1086/148549.

Corral-Santana, J. M. et al. (Mar. 2016). "BlackCAT: A catalogue of stellar-mass black holes in X-ray transients". In: 587, A61, A61. DOI: 10.1051/0004-6361/201527130. arXiv: 1510.08869 [astro-ph.HE].

Cromartie, H. T. et al. (Jan. 2020). "Relativistic Shapiro delay measurements of an extremely massive millisecond pulsar". In: *Nature Astronomy* 4, pp. 72–76. DOI: 10.1038/s41550-019-0880-2. arXiv: 1904.06759 [astro-ph.HE].

Dashwood Brown, Cordelia, Poshak Gandhi, and Yue Zhao (Jan. 2024). "On the natal kick of the black hole X-ray binary H 1705-250". In: 527.1, pp. L82–L87. DOI: 10.1093/mnrasl/slad151. arXiv: 2310.11492 [astro-ph.HE].

de Kool, M., E. P. J. van den Heuvel, and E. Pylyser (Sept. 1987). "An evolutionary scenario for the black hole binary A0620-00." In: 183, pp. 47–52.

De Luca, A. (Dec. 2017). "Central compact objects in supernova remnants". In: *Journal of Physics Conference Series*. Vol. 932. Journal of Physics Conference Series. IOP, 012006, p. 012006. DOI: 10.1088/1742-6596/932/1/012006. arXiv: 1711.07210 [astro-ph.HE].

de Mink, S. E. and I. Mandel (Aug. 2016). "The chemically homogeneous evolutionary channel for binary black hole mergers: rates and properties of gravitational-wave events detectable by advanced LIGO". In: 460.4, pp. 3545–3553. DOI: 10.1093/mnras/stw1219. arXiv: 1603.02291 [astro-ph.HE].

de Mink, S. E. et al. (Feb. 2013). "The Rotation Rates of Massive Stars: The Role of Binary Interaction through Tides, Mass Transfer, and Mergers". In: 764.2, 166, p. 166. DOI: 10.1088/0004-637X/764/2/166. arXiv: 1211.3742 [astro-ph.SR].

Demorest, P. B. et al. (Oct. 2010). "A two-solar-mass neutron star measured using Shapiro delay". In: 467.7319, pp. 1081–1083. DOI: 10.1038/nature09466. arXiv: 1010.5788 [astro-ph.HE].

Dewi, J. D. M., Ph. Podsiadlowski, and A. Sena (June 2006). "Double-core evolution and the formation of neutron star binaries with compact companions". In: 368.4, pp. 1742–1748. DOI: 10.1111/j.1365-2966.2006.10233.x. arXiv: astro-ph/0602510 [astro-ph].

Dominik, Michal et al. (Nov. 2012). "Double Compact Objects. I. The Significance of the Common Envelope on Merger Rates". In: 759.1, 52, p. 52. DOI: 10.1088/0004-637X/759/1/52. arXiv: 1202.4901 [astro-ph.HE].

Draghis, Paul A. et al. (July 2024). "Systematically Revisiting All NuSTAR Spins of Black Holes in X-Ray Binaries". In: 969.1, 40, p. 40. DOI: 10.3847/1538-4357/ad43ea. arXiv: 2311.16225 [astro-ph.HE].

Duchêne, Gaspard and Adam Kraus (Aug. 2013). "Stellar Multiplicity". In: 51.1, pp. 269–310. DOI: 10.1146/annurev-astro-081710-102602. arXiv: 1303.3028 [astro-ph.SR].

Eggenberger, P., A. Maeder, and G. Meynet (Sept. 2005). "Stellar evolution with rotation and magnetic fields. IV. The solar rotation profile". In: 440.1, pp. L9–L12. DOI: 10.1051/0004-6361:200500156. arXiv: astro-ph/0508455 [astro-ph].

Eggenberger, P., F. D. Moyano, and J. W. den Hartogh (Aug. 2022). "Rotation in stellar interiors: General formulation and an asteroseismic-calibrated transport by the Tayler instability". In: 664, L16, p. L16. DOI: 10.1051/0004-6361/202243781. arXiv: 2309.17396 [astro-ph.SR].

Eggenberger, P. et al. (Aug. 2008). "The Geneva stellar evolution code". In: 316.1-4, pp. 43–54. DOI: 10.1007/s10509-007-9511-y.

Eggleton (Jan. 1971). "The evolution of low mass stars". In: 151, p. 351. DOI: 10.1093/mnras/151.3.351.

– (Jan. 1972). "Composition changes during stellar evolution". In: 156, p. 361. DOI: 10.1093/mnras/156.3.361.

– (May 1983). "Aproximations to the radii of Roche lobes." In: 268, pp. 368–369. DOI: 10.1086/160960.

Eggleton and Ludmila Kiseleva-Eggleton (Aug. 2002). "The Evolution of Cool Algols". In: 575.1, pp. 461–473. DOI: 10.1086/341215. arXiv: astro-ph/0209201 [astro-ph].

Eichler, David et al. (July 1989). "Nucleosynthesis, neutrino bursts and γ-rays from coalescing neutron stars". In: 340.6229, pp. 126–128. DOI: 10.1038/340126a0.

Ekström, S. et al. (Jan. 2012). "Grids of stellar models with rotation. I. Models from 0.8 to 120 $M_{\odot}$ at solar metallicity (Z = 0.014)". In: 537, A146, A146. DOI: 10.1051/0004-6361/201117751. arXiv: 1110.5049 [astro-ph.SR].

Eldridge, J. J. and C. A. Tout (Sept. 2004). "The progenitors of core-collapse supernovae". In: 353.1, pp. 87–97. DOI: 10.1111/j.1365-2966.2004.08041.x. arXiv: astro-ph/0405408 [astro-ph].

Eldridge, J. J. et al. (Nov. 2017). "Binary Population and Spectral Synthesis Version 2.1: Construction, Observational Verification, and New Results". In: 34, e058, e058. DOI: 10.1017/pasa.2017.51. arXiv: 1710.02154 [astro-ph.SR].

Esposito, P. et al. (Sept. 2015). "Periodic signals from the Circinus region: two new cataclysmic variables and the ultraluminous X-ray source candidate GC X-1". In: 452.2, pp. 1112–1127. DOI: 10.1093/mnras/stv1379. arXiv: 1506.05808 [astro-ph.HE].

Fabian, A. C. et al. (May 1989). "X-ray fluorescence from the inner disc in Cygnus X-1." In: 238, pp. 729–736. DOI: 10.1093/mnras/238.3.729.

Fabrika, S. (Jan. 2004). "The jets and supercritical accretion disk in SS433". In: 12, pp. 1–152. DOI: 10.48550/arXiv.astro-ph/0603390. arXiv: astro-ph/0603390 [astro-ph].

Fan, Yi-Zhong et al. (Feb. 2024). "Maximum gravitational mass M_{TOV}=2.2 $5_{-0.07}{}^{+0.08}M_{\odot}$ inferred at about 3% precision with multimessenger data of neutron stars". In: 109.4, 043052, p. 043052. DOI: 10.1103/PhysRevD.109.043052. arXiv: 2309.12644 [astro-ph.HE].

Farah, Amanda M., Maya Fishbach, and Daniel E. Holz (Feb. 2024). "Two of a Kind: Comparing Big and Small Black Holes in Binaries with Gravitational Waves". In: 962.1, 69, p. 69. DOI: 10.3847/1538-4357/ad0558. arXiv: 2308.05102 [astro-ph.HE].

Farmer, R. et al. (Dec. 2019). "Mind the Gap: The Location of the Lower Edge of the Pair-instability Supernova Black Hole Mass Gap". In: 887.1, 53, p. 53. DOI: 10.3847/1538-4357/ab518b. arXiv: 1910.12874 [astro-ph.SR].

Farr, Will M. et al. (Nov. 2011). "The Mass Distribution of Stellar-mass Black Holes". In: 741.2, 103, p. 103. DOI: 10.1088/0004-637X/741/2/103. arXiv: 1011.1459 [astro-ph.GA].

Faucher-Giguère, Claude-André and Victoria M. Kaspi (May 2006). "Birth and Evolution of Isolated Radio Pulsars". In: 643.1, pp. 332–355. DOI: 10.1086/501516. arXiv: astro-ph/0512585 [astro-ph].

Fishbach, Maya, Daniel E. Holz, and Will M. Farr (Aug. 2018). "Does the Black Hole Merger Rate Evolve with Redshift?" In: 863.2, L41, p. L41. DOI: 10.3847/2041-8213/aad800. arXiv: 1805.10270 [astro-ph.HE].

Fonseca et al. (Dec. 2016). "The NANOGrav Nine-year Data Set: Mass and Geometric Measurements of Binary Millisecond Pulsars". In: 832.2, 167, p. 167. DOI: 10.3847/0004-637X/832/2/167. arXiv: 1603.00545 [astro-ph.HE].

Fonseca et al. (July 2021). "Refined Mass and Geometric Measurements of the High-mass PSR J0740+6620". In: 915.1, L12, p. L12. DOI: 10.3847/2041-8213/ac03b8. arXiv: 2104.00880 [astro-ph.HE].

Fortin, F. et al. (Mar. 2023). "A catalogue of high-mass X-ray binaries in the Galaxy: from the INTEGRAL to the Gaia era". In: 671, A149, A149. DOI: 10.1051/0004-6361/202245236. arXiv: 2302.02656 [astro-ph.HE].

Fortin, F. et al. (Apr. 2024). "A catalogue of low-mass X-ray binaries in the Galaxy: From the INTEGRAL to the Gaia era". In: 684, A124, A124. DOI: 10.1051/0004-6361/202347908. arXiv: 2401.11931 [astro-ph.HE].

Fowler, William A. and F. Hoyle (Dec. 1964). "Neutrino Processes and Pair Formation in Massive Stars and Supernovae." In: 9, p. 201. DOI: 10.1086/190103.

Fragos et al. (June 2009). "Understanding Compact Object Formation and Natal Kicks. II. The Case of XTE J1118 + 480". In: 697.2, pp. 1057–1070. DOI: 10.1088/0004-637X/697/2/1057. arXiv: 0809.1588 [astro-ph].

Fragos et al. (Feb. 2023). "POSYDON: A General-purpose Population Synthesis Code with Detailed Binary-evolution Simulations". In: 264.2, 45, p. 45. DOI: 10.3847/1538-4365/ac90c1. arXiv: 2202.05892 [astro-ph.SR].

Freytag, B. et al. (Feb. 2012). "Simulations of stellar convection with CO5BOLD". In: *Journal of Computational Physics* 231.3, pp. 919–959. DOI: 10.1016/j.jcp.2011.09.026. arXiv: 1110.6844 [astro-ph.SR].

Fryer, Chris L. and Vassiliki Kalogera (June 2001). "Theoretical Black Hole Mass Distributions". In: 554.1, pp. 548–560. DOI: 10.1086/321359. arXiv: astro-ph/9911312 [astro-ph].

Fryer, Chris L. et al. (Apr. 2012). "Compact Remnant Mass Function: Dependence on the Explosion Mechanism and Metallicity". In: 749.1, 91, p. 91. DOI: 10.1088/0004-637X/749/1/91. arXiv: 1110.1726 [astro-ph.SR].

Fryxell, B. et al. (Nov. 2000). "FLASH: An Adaptive Mesh Hydrodynamics Code for Modeling Astrophysical Thermonuclear Flashes". In: 131.1, pp. 273–334. DOI: 10.1086/317361.

Fuller, Jim, Anthony L. Piro, and Adam S. Jermyn (May 2019). "Slowing the spins of stellar cores". In: 485.3, pp. 3661–3680. DOI: 10.1093/mnras/stz514. arXiv: 1902.08227 [astro-ph.SR].

Gaia Collaboration et al. (June 2023). "Gaia Data Release 3. Summary of the content and survey properties". In: 674, A1, A1. DOI: 10.1051/0004-6361/202243940. arXiv: 2208.00211 [astro-ph.GA].

Gaia Collaboration et al. (June 2024). "Discovery of a dormant 33 solar-mass black hole in pre-release Gaia astrometry". In: 686, L2, p. L2. DOI: 10.1051/0004-6361/202449763. arXiv: 2404.10486 [astro-ph.GA].

Georgy, C. et al. (Oct. 2013a). "Grids of stellar models with rotation. III. Models from 0.8 to 120 $M_{\odot}$ at a metallicity Z = 0.002". In: 558, A103, A103. DOI: 10.1051/0004-6361/201322178. arXiv: 1308.2914 [astro-ph.SR].

Georgy, C. et al. (May 2013b). "Populations of rotating stars. I. Models from 1.7 to 15 $M_{\odot}$ at Z = 0.014, 0.006, and 0.002 with Ω/Ω_{crit} between 0 and 1". In: 553, A24, A24. DOI: 10.1051/0004-6361/201220558. arXiv: 1303.2321 [astro-ph.SR].

Giacconi, R. et al. (July 1971). “Discovery of Periodic X-Ray Pulsations in Centaurus X-3 from UHURU”. In: 167, p. L67. DOI: 10.1086/180762.

Giacobbo, Nicola and Michela Mapelli (Oct. 2018a). “The progenitors of compact-object binaries: impact of metallicity, common envelope and natal kicks”. In: 480.2, pp. 2011–2030. DOI: 10.1093/mnras/sty1999. arXiv: 1806.00001 [astro-ph.HE].

– (Jan. 2019). “The impact of electron-capture supernovae on merging double neutron stars”. In: 482.2, pp. 2234–2243. DOI: 10.1093/mnras/sty2848. arXiv: 1805.11100 [astro-ph.SR].

– (Mar. 2020). “Revising Natal Kick Prescriptions in Population Synthesis Simulations”. In: 891.2, 141, p. 141. DOI: 10.3847/1538-4357/ab7335. arXiv: 1909.06385 [astro-ph.HE].

Giacobbo, Nicola, Michela Mapelli, and Mario Spera (Mar. 2018b). “Merging black hole binaries: the effects of progenitor’s metallicity, mass-loss rate and Eddington factor”. In: 474.3, pp. 2959–2974. DOI: 10.1093/mnras/stx2933. arXiv: 1711.03556 [astro-ph.SR].

Golomb, Jacob et al. (Jan. 2025). “Interplay of astrophysics and nuclear physics in determining the properties of neutron stars”. In: 111.2, 023029, p. 023029. DOI: 10.1103/PhysRevD.111.023029. arXiv: 2410.14597 [astro-ph.HE].

Gou, Lijun et al. (Aug. 2009). “A Determination of the Spin of the Black Hole Primary in LMC X-1”. In: 701.2, pp. 1076–1090. DOI: 10.1088/0004-637X/701/2/1076. arXiv: 0901.0920 [astro-ph.HE].

Gou, Lijun et al. (July 2014). “Confirmation via the Continuum-fitting Method that the Spin of the Black Hole in Cygnus X-1 Is Extreme”. In: 790.1, 29, p. 29. DOI: 10.1088/0004-637X/790/1/29. arXiv: 1308.4760 [astro-ph.HE].

GRAVITY Collaboration et al. (June 2017). “First light for GRAVITY: Phase referencing optical interferometry for the Very Large Telescope Interferometer”. In: 602, A94, A94. DOI: 10.1051/0004-6361/201730838. arXiv: 1705.02345 [astro-ph.IM].

Haberl, F. (Apr. 2007). “The magnificent seven: magnetic fields and surface temperature distributions”. In: 308.1-4, pp. 181–190. DOI: 10.1007/s10509-007-9342-x. arXiv: astro-ph/0609066 [astro-ph].

Haberl, F. and R. Sturm (Feb. 2016). “High-mass X-ray binaries in the Small Magellanic Cloud”. In: 586, A81, A81. DOI: 10.1051/0004-6361/201527326. arXiv: 1511.00445 [astro-ph.GA].

Heger, A. and N. Langer (Dec. 2000a). “Presupernova Evolution of Rotating Massive Stars. II. Evolution of the Surface Properties”. In: 544.2, pp. 1016–1035. DOI: 10.1086/317239. arXiv: astro-ph/0005110 [astro-ph].

Heger, A., N. Langer, and S. E. Woosley (Jan. 2000b). “Presupernova Evolution of Rotating Massive Stars. I. Numerical Method and Evolution of the Internal Stellar Structure”. In: 528.1, pp. 368–396. DOI: 10.1086/308158. arXiv: astro-ph/9904132 [astro-ph].

Heger, A. and S. E. Woosley (Mar. 2002). "The Nucleosynthetic Signature of Population III". In: 567.1, pp. 532–543. DOI: 10.1086/338487. arXiv: astro-ph/0107037 [astro-ph].

Hild, S. et al. (May 2011). "Sensitivity studies for third-generation gravitational wave observatories". In: *Classical and Quantum Gravity* 28.9, 094013, p. 094013. DOI: 10.1088/0264-9381/28/9/094013. arXiv: 1012.0908 [gr-qc].

Hirai, Ryosuke and Ilya Mandel (Nov. 2021). "Conditions for accretion disc formation and observability of wind-accreting X-ray binaries". In: 38, e056, e056. DOI: 10.1017/pasa.2021.53. arXiv: 2108.03774 [astro-ph.HE].

Hobbs, G. et al. (July 2005). "A statistical study of 233 pulsar proper motions". In: 360.3, pp. 974–992. DOI: 10.1111/j.1365-2966.2005.09087.x. arXiv: astro-ph/0504584 [astro-ph].

Hoyle, F. and R. A. Lyttleton (Jan. 1939). "The effect of interstellar matter on climatic variation". In: *Proceedings of the Cambridge Philosophical Society* 35.3, p. 405. DOI: 10.1017/S0305004100021150.

Hurley, Jarrod R., Onno R. Pols, and Christopher A. Tout (July 2000). "Comprehensive analytic formulae for stellar evolution as a function of mass and metallicity". In: 315.3, pp. 543–569. DOI: 10.1046/j.1365-8711.2000.03426.x. arXiv: astro-ph/0001295 [astro-ph].

Hurley, Jarrod R., Christopher A. Tout, and Onno R. Pols (Feb. 2002). "Evolution of binary stars and the effect of tides on binary populations". In: 329.4, pp. 897–928. DOI: 10.1046/j.1365-8711.2002.05038.x. arXiv: astro-ph/0201220 [astro-ph].

Igoshev, Andrei P. (May 2020). "The observed velocity distribution of young pulsars - II. Analysis of complete PSRπ". In: 494.3, pp. 3663–3674. DOI: 10.1093/mnras/staa958. arXiv: 2002.01367 [astro-ph.HE].

Igoshev, Andrei P. et al. (Dec. 2021). "Combined analysis of neutron star natal kicks using proper motions and parallax measurements for radio pulsars and Be X-ray binaries". In: 508.3, pp. 3345–3364. DOI: 10.1093/mnras/stab2734. arXiv: 2109.10362 [astro-ph.HE].

Iorio, Giuliano et al. (Sept. 2023). "Compact object mergers: exploring uncertainties from stellar and binary evolution with SEVN". In: 524.1, pp. 426–470. DOI: 10.1093/mnras/stad1630. arXiv: 2211.11774 [astro-ph.HE].

Ivanova, Natalia and Ronald E. Taam (Feb. 2004). "Thermal Timescale Mass Transfer and the Evolution of White Dwarf Binaries". In: 601.2, pp. 1058–1066. DOI: 10.1086/380561. arXiv: astro-ph/0310126 [astro-ph].

Izzard et al. (May 2004). "A new synthetic model for asymptotic giant branch stars". In: 350.2, pp. 407–426. DOI: 10.1111/j.1365-2966.2004.07446.x. arXiv: astro-ph/0402403 [astro-ph].

Izzard et al. (Dec. 2006). “Population nucleosynthesis in single and binary stars. I. Model”. In: 460.2, pp. 565–572. DOI: 10.1051/0004-6361:20066129.

Izzard et al. (Dec. 2009). “Population synthesis of binary carbon-enhanced metal-poor stars”. In: 508.3, pp. 1359–1374. DOI: 10.1051/0004-6361/200912827. arXiv: 0910.2158 [astro-ph.SR].

Jana, Arghajit et al. (Nov. 2021). “NuSTAR and Swift observations of the extragalactic black hole X-ray binaries”. In: 507.4, pp. 4779–4787. DOI: 10.1093/mnras/stab2448. arXiv: 2108.10546 [astro-ph.HE].

Janka, Hans-Thomas (Mar. 2017). “Neutron Star Kicks by the Gravitational Tug-boat Mechanism in Asymmetric Supernova Explosions: Progenitor and Explosion Dependence”. In: 837.1, 84, p. 84. DOI: 10.3847/1538-4357/aa618e. arXiv: 1611.07562 [astro-ph.HE].

Jermyn, Adam S. et al. (Mar. 2023). “Modules for Experiments in Stellar Astrophysics (MESA): Time-dependent Convection, Energy Conservation, Automatic Differentiation, and Infrastructure”. In: 265.1, 15, p. 15. DOI: 10.3847/1538-4365/acae8d. arXiv: 2208.03651 [astro-ph.SR].

Jiang, Yan-Fei, James M. Stone, and Shane W. Davis (Dec. 2014). “A Global Three-dimensional Radiation Magneto-hydrodynamic Simulation of Super-Eddington Accretion Disks”. In: 796.2, 106, p. 106. DOI: 10.1088/0004-637X/796/2/106. arXiv: 1410.0678 [astro-ph.HE].

Kalogera, Vassiliki and Gordon Baym (Oct. 1996). “The Maximum Mass of a Neutron Star”. In: 470, p. L61. DOI: 10.1086/310296. arXiv: astro-ph/9608059 [astro-ph].

Khokhlov, S. A. et al. (Apr. 2018). “Toward Understanding the B[e] Phenomenon. VII. AS 386, a Single-lined Binary with a Candidate Black Hole Component”. In: 856.2, 158, p. 158. DOI: 10.3847/1538-4357/aab49d. arXiv: 1803.03892 [astro-ph.SR].

Kimball, Chase et al. (July 2021). “Evidence for Hierarchical Black Hole Mergers in the Second LIGO-Virgo Gravitational Wave Catalog”. In: 915.2, L35, p. L35. DOI: 10.3847/2041-8213/ac0aef. arXiv: 2011.05332 [astro-ph.HE].

Kimball, Chase et al. (Aug. 2023). “A Black Hole Kicked at Birth: MAXI J1305-704”. In: 952.2, L34, p. L34. DOI: 10.3847/2041-8213/ace526. arXiv: 2211.02158 [astro-ph.HE].

King and Mitchell C. Begelman (July 1999). “Radiatively Driven Outflows and Avoidance of Common-Envelope Evolution in Close Binaries”. In: 519.2, pp. L169–L171. DOI: 10.1086/312126. arXiv: astro-ph/9904105 [astro-ph].

King et al. (May 2001). “Ultraluminous X-Ray Sources in External Galaxies”. In: 552.2, pp. L109–L112. DOI: 10.1086/320343. arXiv: astro-ph/0104333 [astro-ph].

Klencki, J. et al. (Nov. 2018). “Impact of inter-correlated initial binary parameters on double black hole and neutron star mergers”. In: 619, A77, A77. DOI: 10.1051/0004-6361/201833025. arXiv: 1808.07889 [astro-ph.HE].

Kojo, Toru, Gordon Baym, and Tetsuo Hatsuda (July 2022). "Implications of NICER for Neutron Star Matter: The QHC21 Equation of State". In: 934.1, 46, p. 46. DOI: 10.3847/1538-4357/ac7876. arXiv: 2111.11919 [astro-ph.HE].

Kolb, U. and H. Ritter (Sept. 1990). "A comparative study of the evolution of a close binary using a standard and an improved technique for computing mass transfer." In: 236, pp. 385–392.

Kretschmar, Peter et al. (Dec. 2019). "Advances in Understanding High-Mass X-ray Binaries with INTEGRALand Future Directions". In: 86, 101546, p. 101546. DOI: 10.1016/j.newar.2020.101546. arXiv: 2009.03244 [astro-ph.HE].

Kroupa, Pavel (Apr. 2001). "On the variation of the initial mass function". In: 322.2, pp. 231–246. DOI: 10.1046/j.1365-8711.2001.04022.x. arXiv: astro-ph/0009005 [astro-ph].

Kroupa, Pavel, Christopher A. Tout, and Gerard Gilmore (June 1993). "The Distribution of Low-Mass Stars in the Galactic Disc". In: 262, pp. 545–587. DOI: 10.1093/mnras/262.3.545.

Kruckow, Matthias U. (July 2020). "Masses of double neutron star mergers". In: 639, A123, A123. DOI: 10.1051/0004-6361/202037519. arXiv: 2002.08011 [astro-ph.SR].

Kruckow, Matthias U. et al. (Dec. 2018). "Progenitors of gravitational wave mergers: binary evolution with the stellar grid-based code COMBINE". In: 481.2, pp. 1908–1949. DOI: 10.1093/mnras/sty2190. arXiv: 1801.05433 [astro-ph.SR].

Kruckow, Matthias U. et al. (Dec. 2024). "The formation of black holes in non-interacting isolated binaries: Gaia black holes as calibrators of stellar winds from massive stars". In: 692, A141, A141. DOI: 10.1051/0004-6361/202452356. arXiv: 2410.18501 [astro-ph.SR].

Laor, Ari (July 1991). "Line Profiles from a Disk around a Rotating Black Hole". In: 376, p. 90. DOI: 10.1086/170257.

Laplace, E., F. R. N. Schneider, and Ph. Podsiadlowski (Sept. 2024). "It's written in the massive stars: The role of stellar physics in the formation of black holes". In: *arXiv e-prints*, arXiv:2409.02058, arXiv:2409.02058. DOI: 10.48550/arXiv.2409.02058. arXiv: 2409.02058 [astro-ph.SR].

Lattimer (Sept. 2021). "Neutron Stars and the Nuclear Matter Equation of State". In: *Annual Review of Nuclear and Particle Science* 71, pp. 433–464. DOI: 10.1146/annurev-nucl-102419-124827.

Lattimer and M. Prakash (Mar. 2001). "Neutron Star Structure and the Equation of State". In: 550.1, pp. 426–442. DOI: 10.1086/319702. arXiv: astro-ph/0002232 [astro-ph].

Lattimer and Madappa Prakash (Apr. 2007). "Neutron star observations: Prognosis for equation of state constraints". In: 442.1-6, pp. 109–165. DOI: 10.1016/j.physrep.2007.02.003. arXiv: astro-ph/0612440 [astro-ph].

Lehmer, Bret D. et al. (July 2019). "X-Ray Binary Luminosity Function Scaling Relations for Local Galaxies Based on Subgalactic Modeling". In: 243.1, 3, p. 3. DOI: 10.3847/1538-4365/ab22a8. arXiv: 1905.05197 [astro-ph.GA].

Leong, C. et al. (Dec. 1971). "X-Ray Emission from the Magellanic Clouds Observed by UHURU". In: 170, p. L67. DOI: 10.1086/180842.

Levermore, C. D. and G. C. Pomraning (Aug. 1981). "A flux-limited diffusion theory". In: 248, pp. 321–334. DOI: 10.1086/159157.

Li, Li-Xin and Bohdan Paczyński (Nov. 1998). "Transient Events from Neutron Star Mergers". In: 507.1, pp. L59–L62. DOI: 10.1086/311680. arXiv: astro-ph/9807272 [astro-ph].

LIGO Scientific Collaboration et al. (Apr. 2015). "Advanced LIGO". In: *Classical and Quantum Gravity* 32.7, 074001, p. 074001. DOI: 10.1088/0264-9381/32/7/074001. arXiv: 1411.4547 [gr-qc].

Liotine, Camille et al. (Dec. 2024). "Challenges in Forming Millisecond Pulsar-Black Holes from Isolated Binaries". In: *arXiv e-prints*, arXiv:2412.15521, arXiv:2412.15521. DOI: 10.48550/arXiv.2412.15521. arXiv: 2412.15521 [astro-ph.HE].

Livio, Mario and Noam Soker (June 1988). "The Common Envelope Phase in the Evolution of Binary Stars". In: 329, p. 764. DOI: 10.1086/166419.

Lopez, B. et al. (Mar. 2022). "MATISSE, the VLTI mid-infrared imaging spectro-interferometer". In: 659, A192, A192. DOI: 10.1051/0004-6361/202141785. arXiv: 2110.15556 [astro-ph.IM].

Lubow, S. H. and F. H. Shu (June 1975). "Gas dynamics of semidetached binaries." In: 198, pp. 383–405. DOI: 10.1086/153614.

Luo, Jun et al. (Feb. 2016). "TianQin: a space-borne gravitational wave detector". In: *Classical and Quantum Gravity* 33.3, 035010, p. 035010. DOI: 10.1088/0264-9381/33/3/035010. arXiv: 1512.02076 [astro-ph.IM].

Maccarone, Thomas J. et al. (Jan. 2007). "A black hole in a globular cluster". In: 445.7124, pp. 183–185. DOI: 10.1038/nature05434. arXiv: astro-ph/0701310 [astro-ph].

Maeder, A. (May 1987). "Evidences for a bifurcation in massive star evolution. The ON-blue stragglers." In: 178, pp. 159–169.

Majumder, Seshadri et al. (Jan. 2024). "First detection of X-ray polarization in thermal state of LMC X-3: spectro-polarimetric study with IXPE". In: 527.1, pp. L76–L81. DOI: 10.1093/mnrasl/slad148. arXiv: 2309.06845 [astro-ph.HE].

Mandel, Ilya (Feb. 2016). "Estimates of black hole natal kick velocities from observations of low-mass X-ray binaries". In: 456.1, pp. 578–581. DOI: 10.1093/mnras/stv2733. arXiv: 1510.03871 [astro-ph.HE].

Mandel, Ilya and Selma E. de Mink (May 2016). "Merging binary black holes formed through chemically homogeneous evolution in short-period stellar binaries". In: 458.3, pp. 2634–2647. DOI: 10.1093/mnras/stw379. arXiv: 1601.00007 [astro-ph.HE].

Mandel, Ilya and Tassos Fragos (June 2020a). "An Alternative Interpretation of GW190412 as a Binary Black Hole Merger with a Rapidly Spinning Secondary". In: 895.2, L28, p. L28. DOI: 10.3847/2041-8213/ab8e41. arXiv: 2004.09288 [astro-ph.HE].

Mandel, Ilya and Bernhard Müller (Dec. 2020b). "Simple recipes for compact remnant masses and natal kicks". In: 499.3, pp. 3214–3221. DOI: 10.1093/mnras/staa3043. arXiv: 2006.08360 [astro-ph.HE].

Mann, Christopher R. et al. (Apr. 2019). "A Multimass Velocity Dispersion Model of 47 Tucanae Indicates No Evidence for an Intermediate-mass Black Hole". In: 875.1, 1, p. 1. DOI: 10.3847/1538-4357/ab0e6d. arXiv: 1807.03307 [astro-ph.GA].

Marchant, Pablo et al. (Apr. 2016). "A new route towards merging massive black holes". In: 588, A50, A50. DOI: 10.1051/0004-6361/201628133. arXiv: 1601.03718 [astro-ph.SR].

Marín Pina, Daniel et al. (Aug. 2024). "Dynamical formation of Gaia BH3 in the progenitor globular cluster of the ED-2 stream". In: 688, L2, p. L2. DOI: 10.1051/0004-6361/202450460. arXiv: 2404.13036 [astro-ph.GA].

Mazeh, Tsevi et al. (Dec. 1992). "On the Mass-Ratio Distribution of Spectroscopic Binaries with Solar-Type Primaries". In: 401, p. 265. DOI: 10.1086/172058.

McKinney, Jonathan C. et al. (July 2014). "Three-dimensional general relativistic radiation magnetohydrodynamical simulation of super-Eddington accretion, using a new code HARMRAD with M1 closure". In: 441.4, pp. 3177–3208. DOI: 10.1093/mnras/stu762. arXiv: 1312.6127 [astro-ph.CO].

McLaughlin, M. A. et al. (Feb. 2006). "Transient radio bursts from rotating neutron stars". In: 439.7078, pp. 817–820. DOI: 10.1038/nature04440. arXiv: astro-ph/0511587 [astro-ph].

Mestel, L. (Jan. 1968). "Magnetic braking by a stellar wind-I". In: 138, p. 359. DOI: 10.1093/mnras/138.3.359.

Meynet, G. and A. Maeder (June 2003). "Stellar evolution with rotation. X. Wolf-Rayet star populations at solar metallicity". In: 404, pp. 975–990. DOI: 10.1051/0004-6361:20030512. arXiv: astro-ph/0304069 [astro-ph].

Miller et al. (May 2009). "Stellar-Mass Black Hole Spin Constraints from Disk Reflection and Continuum Modeling". In: 697.1, pp. 900–912. DOI: 10.1088/0004-637X/697/1/900. arXiv: 0902.2840 [astro-ph.HE].

Miller et al. (Dec. 2019). "PSR J0030+0451 Mass and Radius from NICER Data and Implications for the Properties of Neutron Star Matter". In: 887.1, L24, p. L24. DOI: 10.3847/2041-8213/ab50c5. arXiv: 1912.05705 [astro-ph.HE].

Miller-Jones et al. (Mar. 2021). "Cygnus X-1 contains a 21-solar mass black hole—Implications for massive star winds". In: *Science* 371.6533, pp. 1046–1049. DOI: 10.1126/science.abb3363. arXiv: 2102.09091 [astro-ph.HE].

Misra et al. (Oct. 2020). "The origin of pulsating ultra-luminous X-ray sources: Low- and intermediate-mass X-ray binaries containing neutron star accretors". In: 642, A174, A174. DOI: 10.1051/0004-6361/202038070. arXiv: 2004.01205 [astro-ph.HE].

Misra et al. (Apr. 2023). "X-ray luminosity function of high-mass X-ray binaries: Studying the signatures of different physical processes using detailed binary evolution calculations". In: 672, A99, A99. DOI: 10.1051/0004-6361/202244929. arXiv: 2209.05505 [astro-ph.HE].

Misra et al. (Feb. 2024). "Exploring the nature of ultra-luminous X-ray sources across stellar population ages using detailed binary evolution calculations". In: 682, A69, A69. DOI: 10.1051/0004-6361/202347880. arXiv: 2309.15904 [astro-ph.HE].

Miyaji, S. et al. (Jan. 1980). "Supernova triggered by electron captures." In: 32, pp. 303–329.

Moe, Maxwell and Rosanne Di Stefano (June 2017). "Mind Your Ps and Qs: The Interrelation between Period (P) and Mass-ratio (Q) Distributions of Binary Stars". In: 230.2, 15, p. 15. DOI: 10.3847/1538-4365/aa6fb6. arXiv: 1606.05347 [astro-ph.SR].

Mudambi, Sneha Prakash et al. (Nov. 2020). "Estimation of the black hole spin in LMC X-1 using AstroSat". In: 498.3, pp. 4404–4410. DOI: 10.1093/mnras/staa2656. arXiv: 2008.12588 [astro-ph.HE].

Nagarajan, Pranav and Kareem El-Badry (Nov. 2024). "Mixed origins: strong natal kicks for some black holes and none for others". In: *arXiv e-prints*, arXiv:2411.16847, arXiv:2411.16847. DOI: 10.48550/arXiv.2411.16847. arXiv: 2411.16847 [astro-ph.GA].

Nandez, J. L. A., N. Ivanova, and J. C. Lombardi Jr. (May 2014). "V1309 Sco—Understanding a Merger". In: 786.1, 39, p. 39. DOI: 10.1088/0004-637X/786/1/39. arXiv: 1311.6522 [astro-ph.SR].

Narayan, Ramesh, Igor V. Igumenshchev, and Marek A. Abramowicz (Dec. 2003). "Magnetically Arrested Disk: an Energetically Efficient Accretion Flow". In: 55, pp. L69–L72. DOI: 10.1093/pasj/55.6.L69. arXiv: astro-ph/0305029 [astro-ph].

Narayan, Ramesh et al. (Nov. 2012). "GRMHD simulations of magnetized advection-dominated accretion on a non-spinning black hole: role of outflows". In: 426.4, pp. 3241–3259. DOI: 10.1111/j.1365-2966.2012.22002.x. arXiv: 1206.1213 [astro-ph.HE].

Neijssel, Coenraad J. et al. (Dec. 2019). "The effect of the metallicity-specific star formation history on double compact object mergers". In: 490.3, pp. 3740–3759. DOI: 10.1093/mnras/stz2840. arXiv: 1906.08136 [astro-ph.SR].

Nelson, C. A. and P. P. Eggleton (May 2001). "A Complete Survey of Case A Binary Evolution with Comparison to Observed Algol-type Systems". In: 552.2, pp. 664–678. DOI: 10.1086/320560. arXiv: astro-ph/0009258 [astro-ph].

Neumann, M. et al. (Sept. 2023). "XRBcats: Galactic High Mass X-ray Binary Catalogue". In: 677, A134, A134. DOI: 10.1051/0004-6361/202245728. arXiv: 2303.16137 [astro-ph.HE].

Ng, C. et al. (June 2018). “PSR J1755-2550: a young radio pulsar with a massive, compact companion”. In: 476.4, pp. 4315–4326. DOI: 10.1093/mnras/sty482. arXiv: 1802.08248 [astro-ph.HE].

Nomoto, Ken’ichi and Yoji Kondo (Jan. 1991). “Conditions for Accretion-induced Collapse of White Dwarfs”. In: 367, p. L19. DOI: 10.1086/185922.

Novikov, I. D. and K. S. Thorne (Jan. 1973). “Astrophysics of black holes.” In: *Black Holes (Les Astres Occlus)*. Ed. by C. Dewitt and B. S. Dewitt, pp. 343–450.

Nugis, T. and H. J. G. L. M. Lamers (Aug. 2000). “Mass-loss rates of Wolf-Rayet stars as a function of stellar parameters”. In: 360, pp. 227–244.

O’Doherty, Tyrone N. et al. (May 2023). “An observationally derived kick distribution for neutron stars in binary systems”. In: 521.2, pp. 2504–2524. DOI: 10.1093/mnras/stad680. arXiv: 2303.01059 [astro-ph.HE].

Offner, S. S. R. et al. (July 2023). “The Origin and Evolution of Multiple Star Systems”. In: *Protostars and Planets VII*. Ed. by S. Inutsuka et al. Vol. 534. Astronomical Society of the Pacific Conference Series, p. 275. DOI: 10.48550/arXiv.2203.10066. arXiv: 2203.10066 [astro-ph.SR].

Ohsuga, K. et al. (July 2005). “Supercritical Accretion Flows around Black Holes: Two-dimensional, Radiation Pressure-dominated Disks with Photon Trapping”. In: 628, pp. 368–381. DOI: 10.1086/430728. eprint: astro-ph/0504168.

Olejak, A. et al. (June 2020). “Synthetic catalog of black holes in the Milky Way”. In: 638, A94, A94. DOI: 10.1051/0004-6361/201936557. arXiv: 1908.08775 [astro-ph.SR].

Oppenheimer, J. R. and G. M. Volkoff (Feb. 1939). “On Massive Neutron Cores”. In: *Physical Review* 55.4, pp. 374–381. DOI: 10.1103/PhysRev.55.374.

Orosz, Jerome A. et al. (May 2009). “A New Dynamical Model for the Black Hole Binary LMC X-1”. In: 697.1, pp. 573–591. DOI: 10.1088/0004-637X/697/1/573. arXiv: 0810.3447 [astro-ph].

Orosz, Jerome A. et al. (Dec. 2011). “The Mass of the Black Hole in Cygnus X-1”. In: 742.2, 84, p. 84. DOI: 10.1088/0004-637X/742/2/84. arXiv: 1106.3689 [astro-ph.HE].

Orosz, Jerome A. et al. (Oct. 2014). “The Mass of the Black Hole in LMC X-3”. In: 794.2, 154, p. 154. DOI: 10.1088/0004-637X/794/2/154. arXiv: 1402.0085 [astro-ph.SR].

Özel, Feryal et al. (Dec. 2010). “The Black Hole Mass Distribution in the Galaxy”. In: 725.2, pp. 1918–1927. DOI: 10.1088/0004-637X/725/2/1918. arXiv: 1006.2834 [astro-ph.GA].

Packet, W. (Sept. 1981). “On the spin-up of the mass accreting component in a close binary system”. In: 102.1, pp. 17–19.

Paczynski, Bohdan (Apr. 1991). “A Polytropic Model of an Accretion Disk, a Boundary Layer, and a Star”. In: 370, p. 597. DOI: 10.1086/169846.

Pang, Peter T. H. et al. (Nov. 2021). "Nuclear Physics Multimessenger Astrophysics Constraints on the Neutron Star Equation of State: Adding NICER's PSR J0740+6620 Measurement". In: 922.1, 14, p. 14. DOI: 10.3847/1538-4357/ac19ab. arXiv: 2105.08688 [astro-ph.HE].

Parker, M. L. et al. (July 2015). "NuSTAR and Suzaku Observations of the Hard State in Cygnus X-1: Locating the Inner Accretion Disk". In: 808.1, 9, p. 9. DOI: 10.1088/0004-637X/808/1/9. arXiv: 1506.00007 [astro-ph.HE].

Patruno, Alessandro and Anna L. Watts (Jan. 2021). "Accreting Millisecond X-ray Pulsars". In: *Timing Neutron Stars: Pulsations, Oscillations and Explosions*. Ed. by Tomaso M. Belloni, Mariano Méndez, and Chengmin Zhang. Vol. 461. Astrophysics and Space Science Library, pp. 143–208. DOI: 10.1007/978-3-662-62110-3_4. arXiv: 1206.2727 [astro-ph.HE].

Patton, Rachel A. and Tuguldur Sukhbold (Dec. 2020). "Towards a realistic explosion landscape for binary population synthesis". In: 499.2, pp. 2803–2816. DOI: 10.1093/mnras/staa3029. arXiv: 2005.03055 [astro-ph.SR].

Paxton, Bill et al. (Jan. 2011). "Modules for Experiments in Stellar Astrophysics (MESA)". In: 192.1, 3, p. 3. DOI: 10.1088/0067-0049/192/1/3. arXiv: 1009.1622 [astro-ph.SR].

Paxton, Bill et al. (Sept. 2013). "Modules for Experiments in Stellar Astrophysics (MESA): Planets, Oscillations, Rotation, and Massive Stars". In: 208.1, 4, p. 4. DOI: 10.1088/0067-0049/208/1/4. arXiv: 1301.0319 [astro-ph.SR].

Paxton, Bill et al. (Sept. 2015). "Modules for Experiments in Stellar Astrophysics (MESA): Binaries, Pulsations, and Explosions". In: 220.1, 15, p. 15. DOI: 10.1088/0067-0049/220/1/15. arXiv: 1506.03146 [astro-ph.SR].

Paxton, Bill et al. (Feb. 2018). "Modules for Experiments in Stellar Astrophysics (MESA): Convective Boundaries, Element Diffusion, and Massive Star Explosions". In: 234.2, 34, p. 34. DOI: 10.3847/1538-4365/aaa5a8. arXiv: 1710.08424 [astro-ph.SR].

Paxton, Bill et al. (July 2019). "Modules for Experiments in Stellar Astrophysics (MESA): Pulsating Variable Stars, Rotation, Convective Boundaries, and Energy Conservation". In: 243.1, 10, p. 10. DOI: 10.3847/1538-4365/ab2241. arXiv: 1903.01426 [astro-ph.SR].

Pietsch, W. et al. (July 2006). "M33 X-7: ChASeM33 Reveals the First Eclipsing Black Hole X-Ray Binary". In: 646.1, pp. 420–428. DOI: 10.1086/504704. arXiv: astro-ph/0603698 [astro-ph].

Podsiadlowski, Ph., S. Rappaport, and Z. Han (May 2003). "On the formation and evolution of black hole binaries". In: 341.2, pp. 385–404. DOI: 10.1046/j.1365-8711.2003.06464.x. arXiv: astro-ph/0207153 [astro-ph].

Podsiadlowski, Ph. et al. (Sept. 2004). "The Effects of Binary Evolution on the Dynamics of Core Collapse and Neutron Star Kicks". In: 612.2, pp. 1044–1051. DOI: 10.1086/421713. arXiv: astro-ph/0309588 [astro-ph].

Poelarends, Arend J. T. et al. (Dec. 2017). "Electron Capture Supernovae from Close Binary Systems". In: 850.2, 197, p. 197. DOI: 10.3847/1538-4357/aa988a. arXiv: 1710.11143 [astro-ph.HE].

Pols, Onno R. et al. (June 1995). "Approximate input physics for stellar modelling". In: 274.3, pp. 964–974. DOI: 10.1093/mnras/274.3.964. arXiv: astro-ph/9504025 [astro-ph].

Pols, Onno R. et al. (Aug. 1998). "Stellar evolution models for Z = 0.0001 to 0.03". In: 298.2, pp. 525–536. DOI: 10.1046/j.1365-8711.1998.01658.x.

Popham, Robert and Ramesh Narayan (Apr. 1991). "Does Accretion Cease When a Star Approaches Breakup?" In: 370, p. 604. DOI: 10.1086/169847.

Portegies Zwart, S. F. and F. Verbunt (May 1996). "Population synthesis of high-mass binaries." In: 309, pp. 179–196.

Qin, Ying et al. (Jan. 2019). "On the Origin of Black Hole Spin in High-mass X-Ray Binaries". In: 870.2, L18, p. L18. DOI: 10.3847/2041-8213/aaf97b. arXiv: 1810.13016 [astro-ph.SR].

Reitze, David et al. (Sept. 2019). "Cosmic Explorer: The U.S. Contribution to Gravitational-Wave Astronomy beyond LIGO". In: *Bulletin of the American Astronomical Society*. Vol. 51, 35, p. 35. DOI: 10.48550/arXiv.1907.04833. arXiv: 1907.04833 [astro-ph.IM].

Renzo, M. et al. (Jan. 2023). "Rejuvenated Accretors Have Less Bound Envelopes: Impact of Roche Lobe Overflow on Subsequent Common Envelope Events". In: 942.2, L32, p. L32. DOI: 10.3847/2041-8213/aca4d3. arXiv: 2206.15338 [astro-ph.SR].

Repetto, Serena, Melvyn B. Davies, and Steinn Sigurdsson (Oct. 2012). "Investigating stellar-mass black hole kicks". In: 425.4, pp. 2799–2809. DOI: 10.1111/j.1365-2966.2012.21549.x. arXiv: 1203.3077 [astro-ph.GA].

Repetto, Serena and Gijs Nelemans (Nov. 2015). "Constraining the formation of black holes in short-period black hole low-mass X-ray binaries". In: 453.3, pp. 3341–3355. DOI: 10.1093/mnras/stv1753. arXiv: 1507.08105 [astro-ph.HE].

Reynolds, Christopher S. (Sept. 2021). "Observational Constraints on Black Hole Spin". In: 59, pp. 117–154. DOI: 10.1146/annurev-astro-112420-035022. arXiv: 2011.08948 [astro-ph.HE].

Rhoades, Clifford E. and Remo Ruffini (Feb. 1974). "Maximum Mass of a Neutron Star". In: 32.6, pp. 324–327. DOI: 10.1103/PhysRevLett.32.324.

Riley et al. (Dec. 2019). "A NICER View of PSR J0030+0451: Millisecond Pulsar Parameter Estimation". In: 887.1, L21, p. L21. DOI: 10.3847/2041-8213/ab481c. arXiv: 1912.05702 [astro-ph.HE].

Riley et al. (Sept. 2021). "A NICER View of the Massive Pulsar PSR J0740+6620 Informed by Radio Timing and XMM-Newton Spectroscopy". In: 918.2, L27, p. L27. DOI: 10.3847/2041-8213/ac0a81. arXiv: 2105.06980 [astro-ph.HE].

Riley et al. (Feb. 2022). "Rapid Stellar and Binary Population Synthesis with COMPAS". In: 258.2, 34, p. 34. DOI: 10.3847/1538-4365/ac416c. arXiv: 2109.10352 [astro-ph.IM].

Ritter, H. (Aug. 1988). "Turning on and off mass transfer in cataclysmic binaries." In: 202, pp. 93–100.

Rivinius, Thomas, Alex C. Carciofi, and Christophe Martayan (Oct. 2013). "Classical Be stars. Rapidly rotating B stars with viscous Keplerian decretion disks". In: 21, 69, p. 69. DOI: 10.1007/s00159-013-0069-0. arXiv: 1310.3962 [astro-ph.SR].

Roberts, Mallory S. E. (Mar. 2013). "Surrounded by spiders! New black widows and redbacks in the Galactic field". In: *Neutron Stars and Pulsars: Challenges and Opportunities after 80 years*. Ed. by Joeri van Leeuwen. Vol. 291. IAU Symposium, pp. 127–132. DOI: 10.1017/S174392131202337X. arXiv: 1210.6903 [astro-ph.HE].

Rocha, Kyle Akira et al. (Aug. 2024). "To Be or Not To Be: The Role of Rotation in Modeling Galactic Be X-Ray Binaries". In: 971.2, 133, p. 133. DOI: 10.3847/1538-4357/ad5955. arXiv: 2403.07172 [astro-ph.HE].

Roman-Duval, Julia et al. (Nov. 2020). "Ultraviolet Legacy Library of Young Stars as Essential Standards (ULLYSES): Data Release I". In: *Research Notes of the American Astronomical Society* 4.11, 205, p. 205. DOI: 10.3847/2515-5172/abca2f.

Romani, Roger W. et al. (Aug. 2022). "PSR J0952-0607: The Fastest and Heaviest Known Galactic Neutron Star". In: 934.2, L17, p. L17. DOI: 10.3847/2041-8213/ac8007. arXiv: 2207.05124 [astro-ph.HE].

Romano, P. et al. (Apr. 2015). "Giant outburst from the supergiant fast X-ray transient IGR J17544-2619: accretion from a transient disc?" In: 576, L4, p. L4. DOI: 10.1051/0004-6361/201525749. arXiv: 1502.04717 [astro-ph.HE].

Romero-Shaw, Isobel et al. (Sept. 2023). "Rapid population synthesis of black hole high-mass X-ray binaries: implications for binary stellar evolution". In: 524.1, pp. 245–259. DOI: 10.1093/mnras/stad1732. arXiv: 2303.05375 [astro-ph.HE].

Sądowski, Aleksander et al. (Mar. 2013). "Semi-implicit scheme for treating radiation under M1 closure in general relativistic conservative fluid dynamics codes". In: 429.4, pp. 3533–3550. DOI: 10.1093/mnras/sts632. arXiv: 1212.5050 [astro-ph.HE].

Sądowski, Aleksander et al. (Mar. 2014). "Numerical simulations of super-critical black hole accretion flows in general relativity". In: 439.1, pp. 503–520. DOI: 10.1093/mnras/stt2479. arXiv: 1311.5900 [astro-ph.HE].

Sahu, Kailash C. et al. (July 2022). "An Isolated Stellar-mass Black Hole Detected through Astrometric Microlensing". In: 933.1, 83, p. 83. DOI: 10.3847/1538-4357/ac739e. arXiv: 2201.13296 [astro-ph.SR].

Salpeter, Edwin E. (Jan. 1955). "The Luminosity Function and Stellar Evolution." In: 121, p. 161. DOI: 10.1086/145971.

Sana, H. et al. (July 2012). “Binary Interaction Dominates the Evolution of Massive Stars”. In: *Science* 337.6093, p. 444. DOI: 10.1126/science.1223344. arXiv: 1207.6397 [astro-ph.SR].

Sana, H. et al. (Feb. 2013). “The VLT-FLAMES Tarantula Survey. VIII. Multiplicity properties of the O-type star population”. In: 550, A107, A107. DOI: 10.1051/0004-6361/201219621. arXiv: 1209.4638 [astro-ph.SR].

Sana, H. et al. (Aug. 2024). “X-Shooting ULLYSES: Massive stars at low metallicity. II. DR1: Advanced optical data products for the Magellanic Clouds”. In: 688, A104, A104. DOI: 10.1051/0004-6361/202347479. arXiv: 2402.16987 [astro-ph.SR].

Schaller, G. et al. (Dec. 1992). “New Grids of Stellar Models from 0.8-SOLAR-MASS to 120-SOLAR-MASSES at Z=0.020 and Z=0.001”. In: 96, p. 269.

Schrøder, Sophie L., Aldo Batta, and Enrico Ramirez-Ruiz (July 2018). “Black Hole Formation in Fallback Supernova and the Spins of LIGO Sources”. In: 862.1, L3, p. L3. DOI: 10.3847/2041-8213/aacf8d. arXiv: 1805.01269 [astro-ph.HE].

Sen, K. et al. (Aug. 2021). “X-ray emission from BH+O star binaries expected to descend from the observed galactic WR+O binaries”. In: 652, A138, A138. DOI: 10.1051/0004-6361/202141214. arXiv: 2106.01395 [astro-ph.SR].

Sepinsky, J. F. et al. (Nov. 2010). “Interacting Binaries with Eccentric Orbits. III. Orbital Evolution due to Direct Impact and Self-Accretion”. In: 724.1, pp. 546–558. DOI: 10.1088/0004-637X/724/1/546. arXiv: 1005.0625 [astro-ph.SR].

Shafee, Rebecca et al. (Jan. 2006). “Estimating the Spin of Stellar-Mass Black Holes by Spectral Fitting of the X-Ray Continuum”. In: 636.2, pp. L113–L116. DOI: 10.1086/498938. arXiv: astro-ph/0508302 [astro-ph].

Shakura, N. I. and R. A. Sunyaev (June 1973). “Reprint of 1973A&A....24..337S. Black holes in binary systems. Observational appearance.” In: 500, pp. 33–51.

Shao, Yong and Xiang-Dong Li (Nov. 2019). “Population Synthesis of Black Hole Binaries with Normal-star Companions. I. Detached Systems”. In: 885.2, 151, p. 151. DOI: 10.3847/1538-4357/ab4816. arXiv: 1909.11328 [astro-ph.SR].

– (Aug. 2020). “Population Synthesis of Black Hole X-Ray Binaries”. In: 898.2, 143, p. 143. DOI: 10.3847/1538-4357/aba118. arXiv: 2006.15961 [astro-ph.HE].

Sidoli, L. and A. Paizis (Dec. 2018). “An INTEGRAL overview of High-Mass X-ray Binaries: classes or transitions?” In: 481.2, pp. 2779–2803. DOI: 10.1093/mnras/sty2428. arXiv: 1809.00814 [astro-ph.HE].

Siegel, Jared C. et al. (Sept. 2023). “Investigating the Lower Mass Gap with Low-mass X-Ray Binary Population Synthesis”. In: 954.2, 212, p. 212. DOI: 10.3847/1538-4357/ace9d9. arXiv: 2209.06844 [astro-ph.HE].

Siess et al. (Feb. 2013). “BINSTAR: a new binary stellar evolution code. Tidal interactions”. In: 550, A100, A100. DOI: 10.1051/0004-6361/201220327.

Spera, Mario, Michela Mapelli, and Alessandro Bressan (Aug. 2015). "The mass spectrum of compact remnants from the PARSEC stellar evolution tracks". In: 451.4, pp. 4086–4103. DOI: 10.1093/mnras/stv1161. arXiv: 1505.05201 [astro-ph.SR].

Springel, Volker (Jan. 2010). "E pur si muove: Galilean-invariant cosmological hydrodynamical simulations on a moving mesh". In: 401.2, pp. 791–851. DOI: 10.1111/j.1365-2966.2009.15715.x. arXiv: 0901.4107 [astro-ph.CO].

Spruit, H. C. (Sept. 1999). "Differential rotation and magnetic fields in stellar interiors". In: 349, pp. 189–202. DOI: 10.48550/arXiv.astro-ph/9907138. arXiv: astro-ph/9907138 [astro-ph].

– (Jan. 2002). "Dynamo action by differential rotation in a stably stratified stellar interior". In: 381, pp. 923–932. DOI: 10.1051/0004-6361:20011465. arXiv: astro-ph/0108207 [astro-ph].

Stancliffe, Richard J. and John J. Eldridge (July 2009). "Modelling the binary progenitor of Supernova 1993J". In: 396.3, pp. 1699–1708. DOI: 10.1111/j.1365-2966.2009.14849.x. arXiv: 0904.0282 [astro-ph.SR].

Stevenson, Simon et al. (Apr. 2017). "Formation of the first three gravitational-wave observations through isolated binary evolution". In: *Nature Communications* 8, 14906, p. 14906. DOI: 10.1038/ncomms14906. arXiv: 1704.01352 [astro-ph.HE].

Stevenson, Simon et al. (Sept. 2019). "The Impact of Pair-instability Mass Loss on the Binary Black Hole Mass Distribution". In: 882.2, 121, p. 121. DOI: 10.3847/1538-4357/ab3981. arXiv: 1904.02821 [astro-ph.HE].

Stone, James M. et al. (July 2020). "The Athena++ Adaptive Mesh Refinement Framework: Design and Magnetohydrodynamic Solvers". In: 249.1, 4, p. 4. DOI: 10.3847/1538-4365/ab929b. arXiv: 2005.06651 [astro-ph.IM].

Sukhbold, Tuguldur et al. (Apr. 2016). "Core-collapse Supernovae from 9 to 120 Solar Masses Based on Neutrino-powered Explosions". In: 821.1, 38, p. 38. DOI: 10.3847/0004-637X/821/1/38. arXiv: 1510.04643 [astro-ph.HE].

Svoboda, Jiří et al. (Jan. 2024). "First X-Ray Polarization Measurement Confirms the Low Black Hole Spin in LMC X-3". In: 960.1, 3, p. 3. DOI: 10.3847/1538-4357/ad0842. arXiv: 2309.10813 [astro-ph.HE].

Sweeney, David et al. (Nov. 2022). "The Galactic underworld: the spatial distribution of compact remnants". In: 516.4, pp. 4971–4979. DOI: 10.1093/mnras/stac2092. arXiv: 2210.04241 [astro-ph.GA].

Tanikawa, Ataru et al. (Apr. 2023). "Search for a Black Hole Binary in Gaia DR3 Astrometric Binary Stars with Spectroscopic Data". In: 946.2, 79, p. 79. DOI: 10.3847/1538-4357/acbf36. arXiv: 2209.05632 [astro-ph.SR].

Tauris, Norbert Langer, and Philipp Podsiadlowski (Aug. 2015). "Ultra-stripped supernovae: progenitors and fate". In: 451.2, pp. 2123–2144. DOI: 10.1093/mnras/stv990. arXiv: 1505.00270 [astro-ph.SR].

Tauris and E. P. J. van den Heuvel (2006). "Formation and evolution of compact stellar X-ray sources". In: *Compact stellar X-ray sources*. Ed. by Walter H. G. Lewin and Michiel van der Klis. Vol. 39, pp. 623–665. DOI: 10.48550/arXiv.astro-ph/0303456.

Tauris et al. (Oct. 2013). "Evolution towards and beyond accretion-induced collapse of massive white dwarfs and formation of millisecond pulsars". In: 558, A39, A39. DOI: 10.1051/0004-6361/201321662. arXiv: 1308.4887 [astro-ph.SR].

Tauris et al. (Sept. 2017). "Formation of Double Neutron Star Systems". In: 846.2, 170, p. 170. DOI: 10.3847/1538-4357/aa7e89. arXiv: 1706.09438 [astro-ph.HE].

Tolman, Richard C. (Feb. 1939). "Static Solutions of Einstein's Field Equations for Spheres of Fluid". In: *Physical Review* 55.4, pp. 364–373. DOI: 10.1103/PhysRev.55.364.

Toonen, Adrian Hamers, and Simon Portegies Zwart (Dec. 2016). "The evolution of hierarchical triple star-systems". In: *Computational Astrophysics and Cosmology* 3.1, 6, p. 6. DOI: 10.1186/s40668-016-0019-0. arXiv: 1612.06172 [astro-ph.SR].

Toonen, G. Nelemans, and S. Portegies Zwart (Oct. 2012). "Supernova Type Ia progenitors from merging double white dwarfs. Using a new population synthesis model". In: 546, A70, A70. DOI: 10.1051/0004-6361/201218966. arXiv: 1208.6446 [astro-ph.HE].

Tylenda, R. et al. (Apr. 2011). "V1309 Scorpii: merger of a contact binary". In: 528, A114, A114. DOI: 10.1051/0004-6361/201016221. arXiv: 1012.0163 [astro-ph.SR].

van den Heuvel, E. P. J., S. F. Portegies Zwart, and S. E. de Mink (Nov. 2017). "Forming short-period Wolf-Rayet X-ray binaries and double black holes through stable mass transfer". In: 471.4, pp. 4256–4264. DOI: 10.1093/mnras/stx1430. arXiv: 1701.02355 [astro-ph.SR].

Verbunt, Andrei Igoshev, and Eric Cator (Dec. 2017). "The observed velocity distribution of young pulsars". In: 608, A57, A57. DOI: 10.1051/0004-6361/201731518. arXiv: 1708.08281 [astro-ph.HE].

Verbunt and C. Zwaan (July 1981). "Magnetic braking in low-mass X-ray binaries." In: 100, pp. L7–L9.

Vigna-Gómez, Alejandro et al. (Dec. 2018). "On the formation history of Galactic double neutron stars". In: 481.3, pp. 4009–4029. DOI: 10.1093/mnras/sty2463. arXiv: 1805.07974 [astro-ph.SR].

Vigna-Gómez, Alejandro et al. (Oct. 2021). "Fallback Supernova Assembly of Heavy Binary Neutron Stars and Light Black Hole-Neutron Star Pairs and the Common Stellar Ancestry of GW190425 and GW200115". In: 920.1, L17, p. L17. DOI: 10.3847/2041-8213/ac2903. arXiv: 2106.12381 [astro-ph.HE].

Vigna-Gómez, Alejandro et al. (May 2024). "Constraints on Neutrino Natal Kicks from Black-Hole Binary VFTS 243". In: 132.19, 191403, p. 191403. DOI: 10.1103/PhysRevLett.132.191403. arXiv: 2310.01509 [astro-ph.HE].

Vink, Jorick S., A. de Koter, and H. J. G. L. M. Lamers (Apr. 2001). "Mass-loss predictions for O and B stars as a function of metallicity". In: 369, pp. 574–588. DOI: 10.1051/0004-6361:20010127. arXiv: astro-ph/0101509 [astro-ph].

Walter, Roland et al. (Aug. 2015). "High-mass X-ray binaries in the Milky Way. A closer look with INTEGRAL". In: 23, 2, p. 2. DOI: 10.1007/s00159-015-0082-6. arXiv: 1505.03651 [astro-ph.HE].

Walton, D. J. et al. (Jan. 2022). "A multimission catalogue of ultraluminous X-ray source candidates". In: 509.2, pp. 1587–1604. DOI: 10.1093/mnras/stab3001. arXiv: 2110.07625 [astro-ph.HE].

Wang, Song et al. (Sept. 2024). "A potential mass-gap black hole in a wide binary with a circular orbit". In: *Nature Astronomy*. DOI: 10.1038/s41550-024-02359-9. arXiv: 2409.06352 [astro-ph.SR].

Webbink, R. F. (Feb. 1984). "Double white dwarfs as progenitors of R Coronae Borealis stars and type I supernovae." In: 277, pp. 355–360. DOI: 10.1086/161701.

Webster, B. Louise and Paul Murdin (Jan. 1972). "Cygnus X-1-a Spectroscopic Binary with a Heavy Companion ?" In: 235.5332, pp. 37–38. DOI: 10.1038/235037a0.

Weiss, Achim and Helmut Schlattl (Aug. 2008). "GARSTEC—the Garching Stellar Evolution Code. The direct descendant of the legendary Kippenhahn code". In: 316.1-4, pp. 99–106. DOI: 10.1007/s10509-007-9606-5.

White, N. E., J. H. Swank, and S. S. Holt (July 1983). "Accretion powered X-ray pulsars." In: 270, pp. 711–734. DOI: 10.1086/161162.

Willems, B. et al. (May 2005). "Understanding Compact Object Formation and Natal Kicks. I. Calculation Methods and the Case of GRO J1655-40". In: 625.1, pp. 324–346. DOI: 10.1086/429557. arXiv: astro-ph/0411423 [astro-ph].

Wojdowski, Patrick et al. (July 1998). "Quasi-periodic Occultation by a Precessing Accretion Disk and Other Variabilities of SMC X-1". In: 502.1, pp. 253–264. DOI: 10.1086/305893. arXiv: astro-ph/9801168 [astro-ph].

Wong, Tsing-Wai et al. (Aug. 2014). "Understanding Compact Object Formation and Natal Kicks. IV. The Case of IC 10 X-1". In: 790.2, 119, p. 119. DOI: 10.1088/0004-637X/790/2/119. arXiv: 1304.3756 [astro-ph.HE].

Woods, P. M. and C. Thompson (2006). "Soft gamma repeaters and anomalous X-ray pulsars: magnetar candidates". In: *Compact stellar X-ray sources*. Ed. by Walter H. G. Lewin and Michiel van der Klis. Vol. 39, pp. 547–586. DOI: 10.48550/arXiv.astro-ph/0406133.

Woosley, S. E. (Feb. 2017). "Pulsational Pair-instability Supernovae". In: 836.2, 244, p. 244. DOI: 10.3847/1538-4357/836/2/244. arXiv: 1608.08939 [astro-ph.HE].

Woosley, S. E. and E. Baron (May 1992). "The Collapse of White Dwarfs to Neutron Stars". In: 391, p. 228. DOI: 10.1086/171338.

Woosley, S. E., A. Heger, and T. A. Weaver (Nov. 2002). "The evolution and explosion of massive stars". In: *Reviews of Modern Physics* 74.4, pp. 1015–1071. DOI: 10.1103/RevModPhys.74.1015.

Woosley, S. E. and Alexander Heger (Sept. 2015). "The Remarkable Deaths of 9-11 Solar Mass Stars". In: 810.1, 34, p. 34. DOI: 10.1088/0004-637X/810/1/34. arXiv: 1505.06712 [astro-ph.SR].

– (May 2021). "The Pair-instability Mass Gap for Black Holes". In: 912.2, L31, p. L31. DOI: 10.3847/2041-8213/abf2c4. arXiv: 2103.07933 [astro-ph.SR].

Xing, Zepei et al. (Mar. 2024a). "From ZAMS to merger: Detailed binary evolution models of coalescing neutron star - black hole systems at solar metallicity". In: 683, A144, A144. DOI: 10.1051/0004-6361/202347971. arXiv: 2309.09600 [astro-ph.HE].

Xing, Zepei et al. (Oct. 2024b). "Mass-gap Black Holes in Coalescing Neutron Star Black Hole Binaries". In: *arXiv e-prints*, arXiv:2410.20415, arXiv:2410.20415. DOI: 10.48550/arXiv.2410.20415. arXiv: 2410.20415 [astro-ph.HE].

Xing, Zepei et al. (Feb. 2025a). "Combining REBOUND and MESA: dynamical evolution of planets orbiting interacting binaries". In: 537.1, pp. 285–292. DOI: 10.1093/mnras/stae2820. arXiv: 2410.19695 [astro-ph.EP].

Xing, Zepei et al. (Jan. 2025b). "Formation of wind-fed black hole high-mass X-ray binaries: The role of Roche-lobe-overflow post black hole formation". In: 693, A27, A27. DOI: 10.1051/0004-6361/202451275. arXiv: 2407.00200 [astro-ph.HE].

Xu, Xiao-Jie and Xiang-Dong Li (June 2010). "On the Binding Energy Parameter λ of Common Envelope Evolution". In: 716.1, pp. 114–121. DOI: 10.1088/0004-637X/716/1/114. arXiv: 1004.4957 [astro-ph.SR].

Zahn, J. -P. (May 1977). "Tidal friction in close binary systems." In: 57, pp. 383–394.

Zajacek, M. and A. Tursunov (Dec. 2019). "The Electric Charge of Black Holes: Is It Really Always Negligible". In: *The Observatory* 139, pp. 231–236. DOI: 10.48550/arXiv.1904.04654. arXiv: 1904.04654 [astro-ph.GA].

Zapartas, E. et al. (Dec. 2021). "Revisiting the explodability of single massive star progenitors of stripped-envelope supernovae". In: 656, L19, p. L19. DOI: 10.1051/0004-6361/202141506. arXiv: 2106.05228 [astro-ph.HE].

Zdziarski, Andrzej A. et al. (Feb. 2024a). "Black Hole Spin Measurements in LMC X-1 and Cyg X-1 Are Highly Model Dependent". In: 962.2, 101, p. 101. DOI: 10.3847/1538-4357/ad1b60. arXiv: 2308.06167 [astro-ph.HE].

Zdziarski, Andrzej A. et al. (May 2024b). "What Is the Black Hole Spin in Cyg X-1?" In: 967.1, L9, p. L9. DOI: 10.3847/2041-8213/ad43ed. arXiv: 2402.12325 [astro-ph.HE].

Zorec, J. et al. (Nov. 2016). "Critical study of the distribution of rotational velocities of Be stars. I. Deconvolution methods, effects due to gravity darkening, macroturbulence, and binarity". In: 595, A132, A132. DOI: 10.1051/0004-6361/201628760.